DEVELOPMENT OF ANCHORAGE SYSTEM FOR FRP STRENGTHENING APPLICATIONS USING INTEGRATED FRP COMPOSITE ANCHORS

by

Geoffrey N. McGuirk and Sergio F. Breña

Department of Civil and Environmental Engineering
University of Massachusetts Amherst

Report submitted to the
Concrete Research Council of the
ACI Foundation

Ocotober 2012

ACKNOWLEDGMENT

Funding for this research project was provided by the Concrete Research Council of the ACI Foundation. This support is greatly appreciated. The first author would like to express gratitude for the additional support provided by the University of Massachusetts Amherst, which enabled him to complete his MS Degree. In-kind material donations to construct the laboratory specimens needed for the project were received by various individuals and companies. Barker Steel provided the reinforcement needed to fabricate the reinforced concrete blocks, and Sika Corporation and Fyfe Co. provided the carbon fiber-reinforced materials needed to conduct this research. Without the support from these companies this research project would not have been possible.

.

ABSTRACT

Over the past three decades the use of externally bonded fiber-reinforced polymer (FRP) materials for structural strengthening applications has become an accepted and widely used method. A primary concern of FRP structural strengthening systems is that FRP sheets may debonds from the concrete surface at a force significantly lower than the strength of the FRP material. Debonding failures are often brittle and occur with little warning, therefore making them an undesirable failure mode. Past research studies have concluded that fastening FRP sheets with FRP anchors is an effective method for delaying or preventing debonding failures. There is, however, sparcity of research pertaining to fastening FRP sheets with FRP anchors, and a corresponding lack of design guidance. The primary objective of this research program was to better understand the behavior of bonded FRP sheets that include FRP anchors as a supplemental system to prevent debonding. The outcome of this research project will provide data for future development of design recommendations of this type of anchorage system of FRP sheets.

This report concentrates on carbon fiber unidirectional sheets applied using a wet layup approach. Test variables that were investigated include: type of the FRP sheet by including two different FRP material manufacturers, bonded sheets without supplemental FRP anchors, bonded sheets with supplemental FRP anchors, number of anchor rows and spacing between rows, number of sheet plies (single or double), and length of bonded sheet behind the anchors.

Sixteen laboratory specimens were fabricated and tested. Experimental results show that FRP anchorage systems are very effective in increasing load capacity by delaying debonding. Finite element models of anchored and unanchored FRP sheets were

developed to provide a methodology that can be used to expand the laboratory results to elements where anchors are applied using other configurations. In combination with the laboratory results, the finite element models provided a better understanding of the stress distribution within the FRP sheet as affected by the presence of FRP anchors.

TABLE OF CONTENTS

Page

LIST OF TABLES

Table Page

LIST OF FIGURES

Figure Page

CHAPTER 1

INTRODUCTION

1.1 Introduction to using FRP materials for structural strengthening applications

Over the past three decades the use of externally bonded FRP materials for structural strengthening applications has become an accepted and widely used alternative to traditional methods such as bonded steel plates, steel or concrete jackets, and external post-tensioning. The use of FRP materials for strengthening concrete structures was developed in Europe and Japan in the 1980s, and since then several thousand projects have utilized FRP systems worldwide. FRP strengthening systems are typically designed for existing concrete structures that are deemed structurally deficient due to deterioration, inadequate design, construction errors, increased loads due to new use of the structure, or for structures that need increased ductility or seismic capacity. In addition to structural applications, FRP materials can be used to reduce service load deflections, increase resistance to environmental factors, and even increase waterproofing in large pipes. ACI 440 2R-08 "Guide for the Design and Construction of Externally Bonded FRP Systems for Strengthening Concrete Structures" is one of the few guides for the design of FRP strengthening application available to engineers (ACI 440 2R-08).

1.2 FRP Structural Strengthening Applications

FRP can be used in a wide range of structural strengthening applications, and offers several advantages over traditional strengthening techniques. FRP materials are

significantly lighter than steel plates or concrete jackets. This makes them easier to install, requires less heavy equipment and results in reduced labor costs, which often makes up for increased material costs. FRP materials can also be easily adapted for a specific application. For instance, when using the wet layup process, the desired size FRP sheet is simply cut from the role, and the sheet is easily conformed to the surface of the concrete element, whether it is a circular column or a T-beam. FRP materials are also more resistance to corrosion than steel. This makes it particularly suitable for applications near, or even in, salt water. The relatively thin profile of FRP materials often makes it an aesthetically pleasing option.

Since FRP materials have very high tensile strength in the direction of the fibers, and essentially zero strength in compression and bending, they are most efficient when installed on structural elements such that the fibers are loaded primarily in tension. Below is a summary of FRP structural strengthening applications.

Columns: FRP materials can increase confinement in columns, especially those with circular cross sections, by wrapping the FRP around the column (Tan, 2002). By increasing confinement, the axial and flexural capacity and the ductility of the column can also be increased (Teng, 2002).

Beams: FRP materials can be applied to the tension side of beams to increase flexural capacity, and on the sides of beams to increase shear capacity (Teng, 2002; Smith and Teng, 2002; Aram et al., 2008). A specific example of flexural strengthening is applying FRP materials to the tension side of a beam to provide continuity in a beam that does not have continuous tensile reinforcement where it ties into a column (Kim, 2006). A specific example of shear strengthening is in reinforcing the ends of dapped end

prestressed beams, where shear cracks can develop from shear stress concentrations (Huang et al. 2000). It can also be applied to the sides of beams in expected yield locations, to stabilize the beam after yielding, and therefore increase ductility and capacity. Another example is in torsional strengthening of spandrel beams (Salom et al. 2004).

Slabs: FRP materials can be used to strengthen the positive and negative flexural capacity of slabs, as with beams. It can also be used to resist punching shear, and add strength around openings in slabs (Maaddawy and Soudki, 2008; Smith et al., 2010). Since FRP composites have negligible thickness, it will not reduce overhead clearance when applied to ceilings.

Walls: FRP materials can be used to increase ductility, in-plane shear capacity and in-plane and out-of-plane flexural capacity, and add strength around openings in walls (Antoniades et al., 2005; El Gawady et al., 2005; Binici et al., 2006). It can also be used to turn unreinforced masonry walls into shear walls (Binici et al., 2006).

1.3 Types of FRP systems

There are several materials commonly used in FRP systems, and they come in several different forms. ACI 440.2R-08 recognizes three common types of fibers used for FRP systems; continuous glass, aramid, and carbon fibers. Glass is currently the most common material used in FRP systems. However, despite its higher cost, carbon is gaining popularity since it has higher strength and tensile modulus. Table 1-1 shows typical tensile properties of the different types of fibers used in FRP systems.

Table 1-1 Tensile properties of fibers (ACI 4402R-08)

Table A1.1—Typical tensile properties of fibers used in FRP systems

Fiber Type	Elastic Modulus		Ultimate Strength		Rupture strain, Minimum, %
	102 ksi	GPa	ksi	MPa	
Carbon					
General	32 to 34	220 to 240	300 to 550	2050 to 3790	1.2
High-strength	33 to 34	221 to 240	550 to 700	3790 to 4820	1.4
Ultra-high-strength	34 to 34	222 to 240	700 to 900	4820 to 6200	1.5
High-modulus	50 to 75	340 to 520	250 to 450	1720 to 3100	0.5
Ultra-high-modulus	75-100	520 to 690	200 to 350	1380 to 2400	0.2
Glass					
E-glass	10 to 10.5	69 to 72	270 to 390	1860 to 2680	4.5
S-glass	12.5 to 13	86 to 90	500 to 700	3440 to 4140	5.4
Aramid					
General	10 to 12	69 to 83	500 to 600	3440 to 4140	2.5
High-performance	16 to 18	110 to 124	500 to 600	3440 to 4140	1.6

ACI 440.2R-08 recognizes four forms of FRP systems: wet layup systems, prepreg systems, precured systems and near-surface-mounted systems. With wet layup systems dry sheets of fibers are impregnated with resin on-site and then cured in place. The sheets are either saturated with resin and then applied shortly after to the concrete surface, or are applied first and then saturated with resin. With prepreg systems the FRP sheets are saturated with resin off-site, and then cured in place. Sometimes additional resin is required to adhere the sheet to the concrete surface, and often additional heating is required for curing. Precured systems are impregnated with resin and cured offsite, and then typically applied to the concrete with adhesive. Near-surface-mounted systems are precured FRP bars or plates that are bonded into premade grooves on the surface of the concrete. FRP sheets consist of either unidirectional or multidirectional fibers.

All materials are often purchased from one manufacturer and include the FRP sheet and necessary impregnating resins, surface primers and putties, etc. as part of a system. Manufactures offer a range of primers and impregnating resins depending on the application. For instance, when applying sheets overhead, some manufactures will offer

impregnating resins that are more viscous for ease of application. Some systems use one adhesive for both priming the surface and impregnating the fibers, and others use separate adhesives.

1.4 Failure Modes of Structures Strengthened with FRP Materials

This section discusses common failure modes of FRP strengthened structural members, with an emphasis on those that can be delayed or prevented with FRP anchors. Reinforced concrete elements strengthened with FRP systems have several additional failure modes compared with reinforced concrete elements that are not strengthened with FRP systems. It is essential that the engineer accounts for all relevant failure modes, as they can have very different failure loads, and behaviors. Since carbon fibers have very high strength in tension relative to the concrete and to the adhesive that binds them to the concrete, the common failure mode of bonded FRP sheets is debonding, and not rupture of the sheets. Debonding failures are typically sudden and brittle, and occur before the full strength of the FRP sheet has been reached, so require increased attention by structural engineers. For this reason, it is important to understand and be able to accurately predict the behavior of bonded FRP sheets.

The most heavily researched FRP application is flexural strengthening of reinforced concrete beams. Through extensive laboratory testing, researchers have defined several distinct failure modes for flexural strengthened beams. It is worth noting that the terminology used to describe the various failure modes varies within the literature. (Smith and Teng, 2001) lists six failure modes, which are shown in Figure 1.1: FRP rupture, concrete cover separation, crushing of compressive concrete, plate end

interfacial debonding, shear failure, and intermediate crack induced interfacial debonding.

The three failure modes on the right side of Figure 1.1 are generally termed debonding failures, and involve the beam failing before the strength of the FRP sheet is reached. Debonding failures are the most common type of failures, and are particularly troublesome because they are generally non ductile failures, that occur with little warning. Debonding failures can be further grouped into two categories; plate end interfacial debonding (plate end debonding) and intermediate crack induced debonding (IC debonding). In IC debonding, debonding initiates at the location of an intermediate flexural or flexural-shear crack and then propagates away from the crack towards one of the ends of the beam. In plate end debonding, failure initiates near the end of the beam, often at the termination of the FRP sheet, and then propagates towards the middle of the beam. The failure can either travel up to the tensile reinforcement and then along the reinforcement, so that the concrete cover debonds, which is termed concrete cover separation, or it can propagate near the FRP-concrete interface, which is termed plate end interfacial debonding. What is common among the debonding failures is that they initiate at stress concentrations; at the termination of the FRP in plate end failures, and at a cracks in interfacial debonding failures. Once failure initiates, it usually progresses very quickly, with little or any increase in load capacity of the member (S.T. Smith and J.G. Teng, 2001). IC debonding and plate end debonding are the most common failure modes of beams flexurally strengthened with FRP.

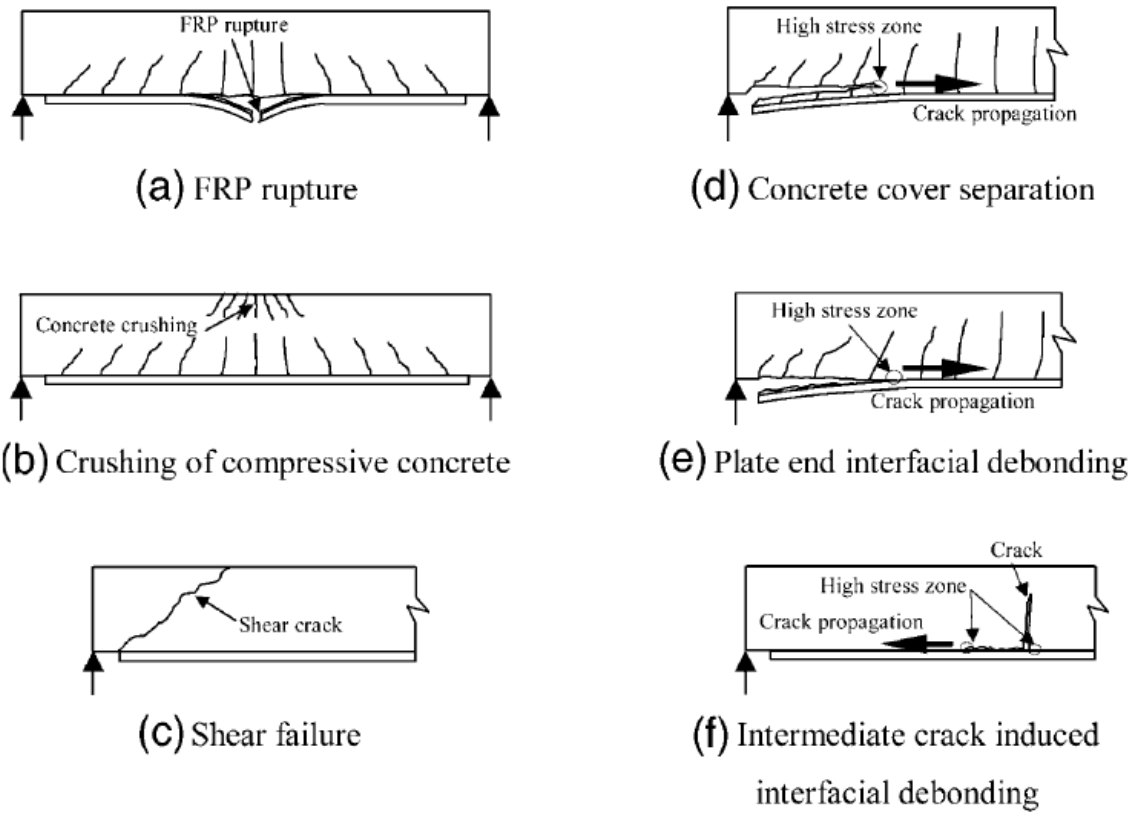

Figure 1.1 Failure modes of FRP-strengthened RC beams (S.T. Smith and J.G. Teng, 2001)

The use of FRP for shear strengthening is less researched than for flexural strengthening; however there are common failure modes for both strengthening applications. In shear strengthening applications, interfacial debonding and FRP rupture are the most common failure modes. Interfacial debonding can be difficult to design against in shear strengthening systems, since the space on the side of a beam where the FRP sheet is applied often limits the length of the sheet that can be applied; this is in contrast to FRP that is applied along the length of a flexurally strengthened beam, in which there is usually enough space to develop the strength of the bonded sheet.

1.5 Failure Prevention Methods

This section presents methods to prevent or delay the debonding failure modes discussed in section 1.4. Usually the preferred failure mode is rupture of the FRP laminate, which occurs when the strain induced in the laminate exceeds the strain capacity of the laminate. This is preferred because it means the full strength of the sheet was utilized. It is also easier to accurately predict ultimate capacity when the failure mode is FRP rupture, compared to debonding failure. Unfortunately, debonding is the most common failure mode in shear and flexural strengthening applications.

Debonding can be delayed or prevented by anchoring the FRP sheet where debonding is expected to initiate. ACI 440.2R-08 mentions the use of mechanical anchors and transversely placed FRP sheets, or U-wraps, to delay debonding. However, it does not give any details into mechanical anchor design, and does not mention the use of FRP anchors. Research has shown that FRP anchors are effective in delaying or preventing debonding failures (Niemitz, 2008; Orton et al., 2008; Anil and Belgin, 2009; Ceroni and Pecce, 2009; Smith et al., 2010). They are particularly useful in shear strengthening applications, in which space on the side of a beam where the FRP sheet is applied often limits the length of the sheet that can be applied

Figure 1.2 shows how FRP sheets can be positioned for flexural and shear strengthening applications. It also shows where intermediate cracks commonly form, which is where debonding failures often initiate due to high stress concentrations. For FRP that is placed on the tensile side of a beam or slab, FRP anchors can be placed at the end of the sheet to delay or prevent plate end debonding, and at multiple locations along the length of the sheet to delay or prevent intermediate crack induced debonding. For

shear strengthening applications the FRP is placed on the sides of the beam. Often it is not practical to have the FRP sheet wrap around the top of the beam, for instance, with T-beams and beams that are integral with a slab, which is the preferred wrapping scheme. When the sheet cannot be wrapped around all four sides of the beam, FRP anchors placed at the sheet ends can delay or prevent debonding, as show in Figure 1.2.

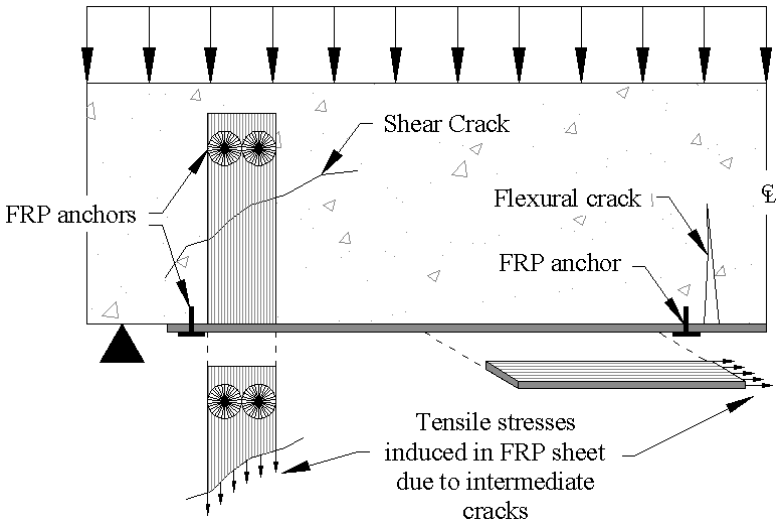

Figure 1.2 Tensile stresses induced in the FRP at intermediate cracks, and common FRP anchor locations.

FRP anchors are commonly composed of carbon or glass fibers. Often the same fibers used in the FRP sheets are used to fabricate the anchors. There are several anchor fabrication techniques, as discussed in section 0. The fibers are saturated with epoxy like the FRP sheets. The FRP anchors consist of a roll of fibers, as shown in Figure 1.3. The embedded portion of the anchor is inserted into a predrilled hole in the concrete. The anchor passes through the FRP sheet, usually by spreading apart longitudinal fibers, and the splayed end is spread over the FRP sheet.

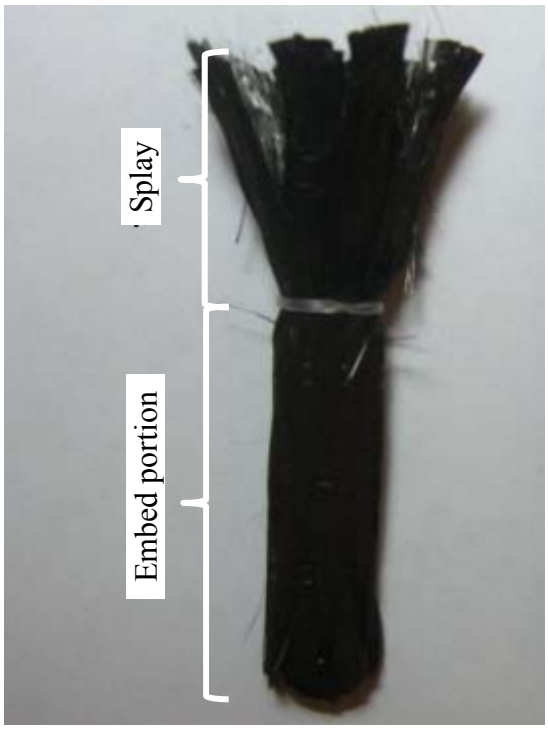

Figure 1.3 Example of an FRP anchor

In addition to mechanical and FRP anchors, there has been some research on the use of near surface mounted FRP bars to anchor the ends of sheets (Eshwar et al., 2008). This method works by wrapping the end of the FRP sheet around an FRP bar which is which is held in place with epoxy in a precut groove in the surface of the concrete.

To reduce stress in the sheet, ACI 440.2R-08 recommends terminating the sheet as close to areas of zero stress as possible. It also recommends making the distance from the end of the sheet to the expected point of maximum stress in the sheet longer than the development length, or the length required to reach the necessary stress in the sheet, similar to development length requirements for internal steel reinforcement. For multiple plies it is recommended to stager the termination points of the sheets, to reduce stress concentrations at the sheet ends.

1.6 Research Program

The primary objective of this research program is to better understand the behavior of bonded CFRP sheets that are secured with FRP anchors. While there are design guidelines for using unanchored FRP sheets for structural strengthening applications, most notably ACI 440.2R-08, which are backed by an abundance of research, there is a clear lack of research pertaining to anchored FRP sheets. ACI 440.2R-08 does not even mention the use of FRP anchors, which leaves engineers with little guidance if they choose to use FRP anchors in a design. ACI 440.2R-08 states that the performance of any anchorage system design should be backed by testing. The general consensus of the research already completed on anchored FRP sheets, is that FRP anchors can be used to increase capacity of bonded FRP sheets used in a wide variety of strengthening applications, and sometimes enough to develop the full strength of the sheets.

CHAPTER 2

LITERATURE REVIEW

2.1 Introduction

This chapter summarizes research on externally bonded FRP structural strengthening systems, with an emphasis on anchored FRP sheets. An overview of the guidance given for shear and flexural strengthening design with FRP materials by ACI 440.2R-02 *Guide for the Design and Construction of Externally FRP Systems for Strengthening Concrete Structure*, is also given.

2.2 Test Setups used in Past Research Studies

Chen et al. (2001) performed a large survey of existing test setups used to determine FRP-to-concrete bond behavior and strength. An accurate bond strength model is necessary to accurately predict failures of FRP shear and flexurally strengthened RC beams, since failure is very often due to debonding. Chen et al. (2001) grouped existing experimental test setups into five types: (a) double-shear pull tests; (b) double-shear push tests; (c) single-shear pull tests; (d) single-shear push tests; and (e) beam (or bending) tests. Yao et al. (2005) renamed these test setups (a) far end supported (FES) double-shear tests; (b) near end supported (NES) double-shear tests; (c) far end supported (FES) single-shear tests; and (d) near end supported (NES) single-shear tests, which are illustrated in Figure 2.1.

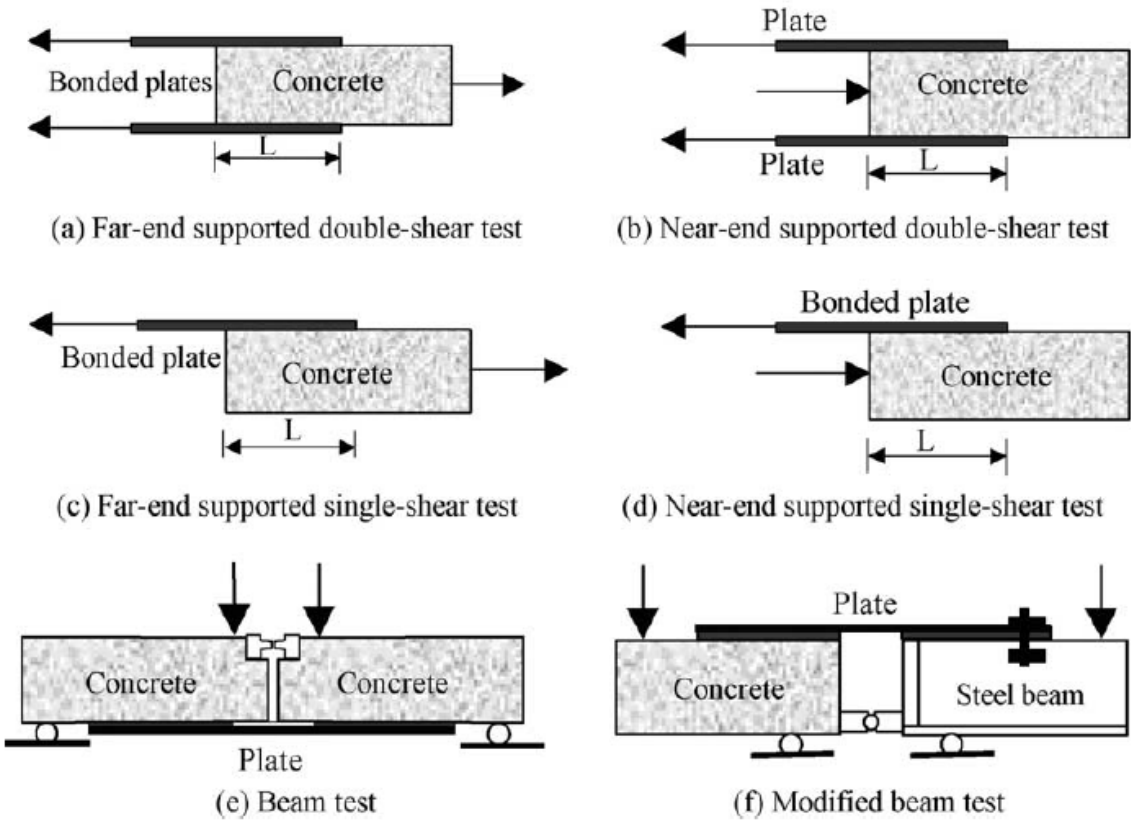

Figure 2.1 Classification of common test setups used (Chen et al. 2001), renamed by Yao et al. (2005).

According to Chen et al. (2001) double and single shear tests are the most popular, due to the simplicity of the test set-up. The near-end supported (NES) single-shear test setup was used in this research program. Numerical and experimental studies indicate that different test setups can influence bond strength. Even for a given setup results can be affected by small changes in the geometry of the FRP or the concrete block. Yao et al. (2005) examined the validity of the NES single-shear pull tests for determining bond strength, and also how bond strength is effected by variations in the test setup, by performing a large number of NES single-shear tests, and comparing results to the Chen and Teng, (2001) model. According to Yao et al. (2005) the stress states in a

beam that fails due to intermediate crack-induced debonding can be closely mimicked by the stress states in the concrete block in NES single-shear tests.

Test results show that increasing the free concrete edge (distance from the top surface of the concrete to the top of the support) increases the load capacity slightly. The specimens with 120 mm [4.7 in.] free edge had approximately 10% more capacity than those with a 5mm [0.2 in.] free edge. The author believes that this is because the local stiffness near the loaded end increases the closer the support is to the FRP sheet, which causes this area to assume more load and leads to premature debonding. Yao et al. (2005) concluded that the height of the free concrete edge should be around 50 mm [2 in.] for a concrete block 150 mm [6 in.] high.

It is important to understand the effect of loading angle since it may generate out of plane stresses during testing. Additionally FRP sheets spanning a flexural crack with a slight offset may be subjected to out of plane loading. Results show that an angle of more than +/- 1.7 degrees has a significant effect on the capacity when the bond length is small (100 mm [4 in.]), but negligible effect when the bond length is long (190 mm [7.5 in.]). For a positive angle, as failure propagates along the sheet the angle reduces, and therefore the effects of the angle become less pronounced. Yao et al. (2005) concluded that the bond length should be approximately twice as long as the effective bond length to avoid problems with load angle.

Test results from Yao et al. (2005) were close to the bond strength model presented by Chen and Teng, (2001), with the model slightly under predicting capacity when the sheet width to block width ratio was either close to one or zero. The specimens

for which this ratio was close to 1.0 caused failure of the concrete block instead of debonding. Therefore the author advises to avoid either of the two extremes.

2.3 Bond Strength and Behavior of Un-Anchored FRP Sheets

To accurately predict failure, it is imperative to have an accurate FRP-to-concrete bond strength model. Extensive research has been conducted to develop bond models, including a range of experimental tests, theoretical studies based on finite element analysis and fracture mechanics, and creation of empirical and semi-empirical models. An assessment of these studies as well as a proposed model can be found in Chen and Teng (2001). No known models currently exist that include the effect of FRP anchorage systems.

2.4 Chen and Teng Bond Model

Chen and Teng (2001) proposed the following bond strength model, which is widely cited in literature and has been verified by other researchers:

$$P_u = 0.427\beta_p\beta_L\sqrt{f_c'}b_pL_e \quad \text{[SI]} \qquad \textbf{[2.1]}$$

Where,

$$L_e = \sqrt{\frac{E_p t_p}{\sqrt{f_c'}}} \qquad \textbf{[2.2]}$$

$$\beta_p = \sqrt{\frac{2-b_p/b_c}{1+b_p/b_c}} \qquad \textbf{[2.3]}$$

$$\beta_L = \begin{cases} 1 & if \;\; L \geq L_e \\ \sin\dfrac{\pi L}{2L_e} & if \;\; L < L_e \end{cases} \qquad \textbf{[2.4]}$$

P_u = ultimate bond strength [kN]

b_p = bonded width of the FRP [mm]

b_c = width of the concrete member [mm]

f_c = cylinder concrete compressive strength [MPa]

L_e = Effective length [mm]

E_p = Modulus of elasticity of the FRP laminate [MPa]

t_p = thickness of the FRP laminate [mm]

L = bonded length of the FRP [mm]

It was the goal of the researchers to create an accurate, simple to use and rationally based model. The model is applicable to FRP sheets (including wet lay-up, prepreg and precured systems) or steel plates bonded to concrete surfaces, in which the dominant failure mode is debonding. The model is compared to results from a large number of single and double shear tests of bonded FRP and steel plates collected in literature. Research has shown that FRP and steel plates bonded to concrete behave similarly, and there is an abundance of research on bonded steel plates. The average experimental FRP-to-concrete bond strength was 1.05 times that predicted by the proposed model, with a standard deviation of 0.18. It is worth noting that the average experimental steel-to-concrete bond strength was 0.94 times that predicted by the proposed model, with a standard deviation of 0.11, which demonstrates the robustness of the model. The model includes two important parameters that are essential for accurately predicting failure load: the ratio of sheet or plate width to concrete width, and the effective bonded length. The effective length is the length of the stress transfer zone (STZ), which is discussed in section 2.5. The interfacial shear stresses are typically not

constant across the width of the bonded sheet. The distribution is affected by the ratio of the width of the FRP sheet to the width of the concrete member, as discussed in section 2.5. Yao et al. (2005) performed a large number of single-shear tests and found that the Chen and Teng (2001) model closely agreed with experimental bond strengths. The model underestimated the bond strength by an average of 4% when debonding occurred within a thin layer of the concrete, and overestimated by 4% when debonding occurred in the adhesive layer. This indicates that the model is applicable when debonding occurs within the adhesive or the concrete.

2.5 FRP Length and Width Effects

The width and length of bonded FRP sheets affect the load-carrying capacity and interfacial shear stress distribution. Many researchers have shown the existence of a stress transfer zone (STZ), which is length of bonded sheet that is effectively engaged in the stress transfer to the concrete surface. Bonded lengths beyond the STZ allow the debonded region to propagate along the length of the sheet at an approximately constant force. Figure 2.2 shows the strain distribution along the length of a bonded FRP sheet, from a test performed by Subramaniam et al. (2007). This is an important distinction from internal reinforcement, in which the full capacity of the reinforcement can always be reached with sufficient embedment length. There are several equations given in literature that estimate the length of the STZ, such as Eq. 2.2 (Chen and Teng, 2001).

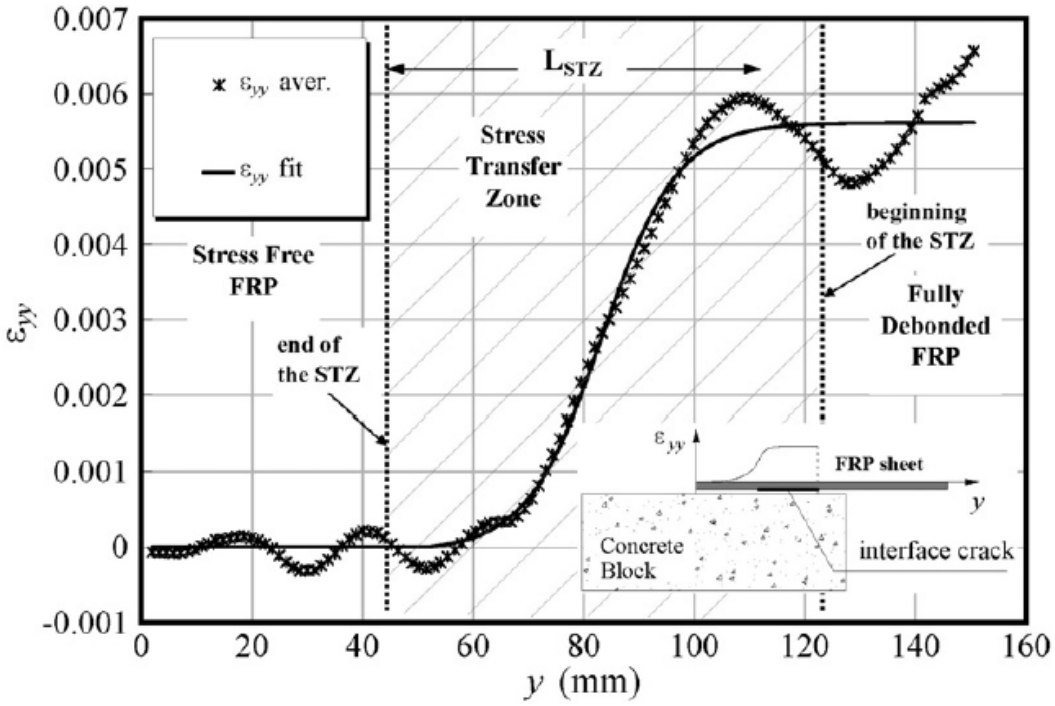

Figure 2.2 Longitudinal strain distribution of FRP sheet (Subramaniam et al., 2007)

There is a complicated relationship between load-carrying capacity and FRP width. Subramaniam et al. (2007) investigated the effect of width by performing single-shear tests. The sheet length was kept constant and longer than the STZ, and the width was varied. Displacements were measured using an optical technique known as digital image correlation. The study concluded that the sheet width and the ratio of sheet width to concrete member width both affect bond strength. The sheet width had negligible effect on the length of the STZ. Figure 2.3 and Figure 2.4 show shear strain and axial strain distributions, respectively, across the width of an FRP sheet and in the concrete member to the right and left of the sheet. In these figures b_l is the sheet width, b_s is the width of the central region and b_d is the width of concrete that is strained. It is clear from these graphs that there are two distinct regions across the width of the sheet where different strain fields are developed: (1) a central region which has nearly zero shear

strain and, correspondingly, a constant axial strain; and (2) an edge region on either side of the sheet, which has a high shear and axial strain gradient. Comparing the strain distributions of sheets with different widths, it was concluded that the width of the edge region remains nearly constant. If the sheet is narrow enough the central region disappears and there is then no width with constant axial strain and zero shear strain. When the sheet width is increased the width of the central region increases, which is a likely explanation for why ultimate shear stress increases when width increases. As the width of the FRP increases the ratio of b_s/b_1 approaches one, and thus the ultimate shear stress increases up to an asymptotic value. If the ratio of the width of the FRP sheet to the concrete member (b_1/b) is large enough the edge regions will not be able to fully develop. In such a case an increase in width of sheet results in less restraint from the concrete, and potentially a loss in load capacity.

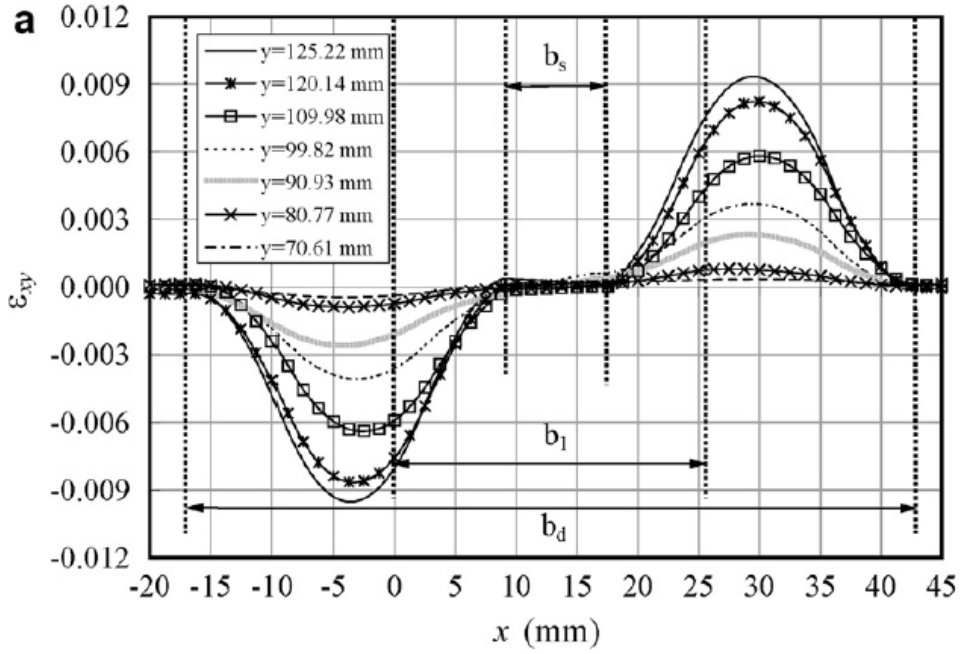

Figure 2.3 Shear strain distribution across the width of the FRP sheet (Subramaniam et al., 2007)

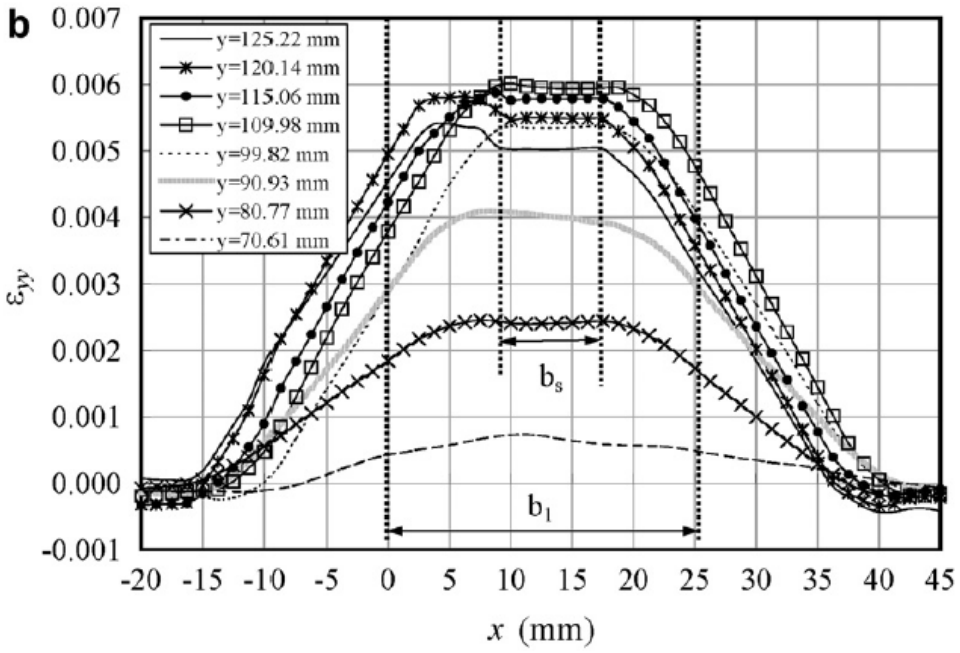

Figure 2.4 Axial strain distribution across the width of the FRP sheet (Subramaniam et al., 2007)

2.6 Summary of Research on FRP Sheets Anchored with FRP Anchors

This section reviews recent research on anchored FRP sheets. Limited experimental research has shown that fastening FRP sheets with FRP anchors can be a very effective method to delay or prevent debonding failures and to increase the failure load. However, there are no known bond strength models which include the capacity gained by anchoring the FRP in shear applications. ACI 440.2R-08 does not give any guidance in designing anchorage systems for FRP sheets, besides stating that any anchoring design should be validated with experimental testing. In addition, ACI 440.2R-08 mentions the use of mechanical anchors to fasten FRP sheets, but not the use of FRP anchors.

Section 2.6.1 summarizes each of the research programs, including the test setup, the FRP materials used, the anchor design parameters investigated, and the specimens tested. Findings from each of these research programs are presented in sections 2.6.4 and 2.6.5. A more detailed description of the FRP anchor properties and fabrication techniques used in these research programs is given in section 0. Section 2.6.3 discusses the experimental performance of FRP sheets fastened with FRP anchors. Sections 2.6.4 and 2.6.5 discuss the effect of anchor placement and anchor design parameters, respectively, on the performance of anchored FRP sheets. Section 2.7 discusses experimental testing of alternative methods of anchoring FRP sheets and section 2.8 discusses experimental testing of structural members strengthened with anchored FRP sheets.

2.6.1 Background Summary of Research Programs on Anchored FRP Sheets

Niemitz (2008) tested the behavior of FRP sheets fastened with FRP anchors, using a single-shear test setup, as shown in Figure 2.1. The experimental test program included two unanchored control specimens, nine anchored and bonded specimens, and one specimen which was anchored, and only bonded behind the anchors. Experimental parameters that were tested include anchor diameter, anchor splay diameter, anchor arrangement on the FRP sheet (transverse or longitudinal), and length and width of the FRP sheet. Mbrace CF 130 unidirectional FRP sheets were applied by hand using the wet layup process, with the properties shown in Table 2-1, and anchors were fabricated by hand from the same material as the FRP sheet. The anchor splays formed a full circle.

Anil and Belgin (2010) performed an experimental investigation of FRP sheets fastened with FRP anchors and steel mechanical anchors. SikaWrap230C was used, which is unidirectional CFRP. The design parameters investigated included the number of anchors, the arrangement of the anchors (in a single row along the centerline of the sheet or staggered, as shown in Figure 2.5) and type of anchors (CFRP or steel mechanical anchors). Twelve anchored sheets and two non-anchored control specimens were tested using a beam test setup, as shown in Figure 2.1. Nine specimens were fastened with mechanical steel anchors, and three were fastened with CFRP anchors. The CFRP anchor splays were fabricated by splitting the width of the sheet into 4 strips which were then laid out in a cross pattern. The steel anchors were 8 mm [0.3 in.] in diameter and the CFRP anchors were 10 mm [0.4 in.] in diameter, and were fabricated from a 50 mm [2 in.] width of sheet.

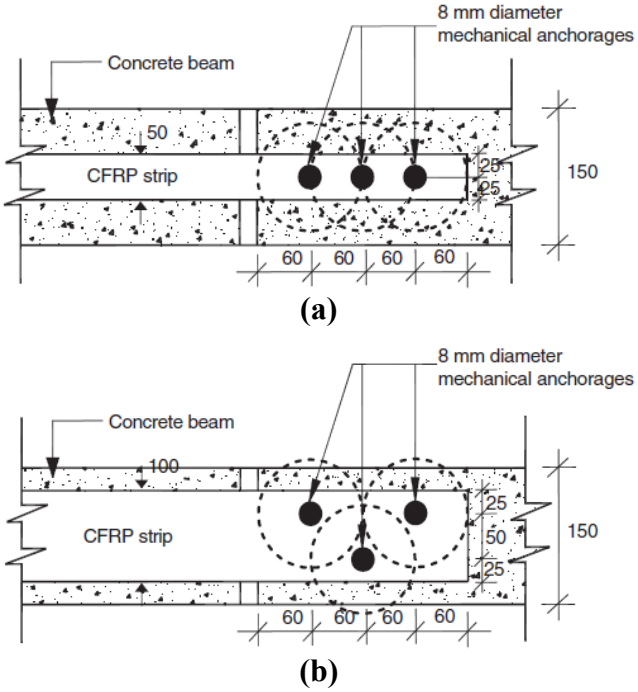

Figure 2.5 Single row (a) versus staggered (b) Anchor arrangements (Anil and Belgin, 2010).

Eshwar (2008) tested six CFRP sheets fastened with GFRP anchors using the near-end supported double-shear test setup shown in Figure 2.1. Mbrace CF 130 unidirectional FRP sheets were tested, with the properties shown in Table 2-1. All anchors were 10 mm [0.4 in.] in diameter. Anchor embedment depths of 50 and 75 mm [2 and 3 in.] were investigated. The anchors were constructed by the researchers and were composed of glass fibers, which have a significantly lower elastic modulus and a significantly higher rupture strain, as shown in Table 1-1.The anchors were fabricated by bundling loose dry fibers together to a desired anchor diameter. The FRP sheet was applied by hand to the concrete using the wet layup process; the same process used in this research program. All anchors were 10 mm [0.4 in.] in diameter. The anchor splays formed a full circle.

Kim and Smith (2009) experimentally investigated FRP sheets fastened with anchors using the single shear test setup, as shown in Figure 2.1. The main variable investigated was the effect of crack location relative to anchor location. This variable is important because in beams that are initially uncracked it is not known where cracks will form relative to the anchors, as shown in Figure 2.6. There were three unanchored specimens and three specimens each with anchors located 50, 75 and 100 mm [2, 3 and 4 in.] from the unbonded zone (analogous to an intermediate crack). All specimens had three plies that were 50 mm [2in.] wide and 150 mm [6 in.] long and were applied using the wet layup process. All anchors had an embedment depth of 40 mm [1.6 in.], and were fabricated by hand from a 40 mm [1.6 in.] wide CFRP sheet. The anchor splays had a fan shape that covered an angle of 60 degrees (instead of a full circle) and a length of 50 mm

[2 in.] and oriented in the direction of the load. It appears from test pictures that the splay covered the full width of the sheet.

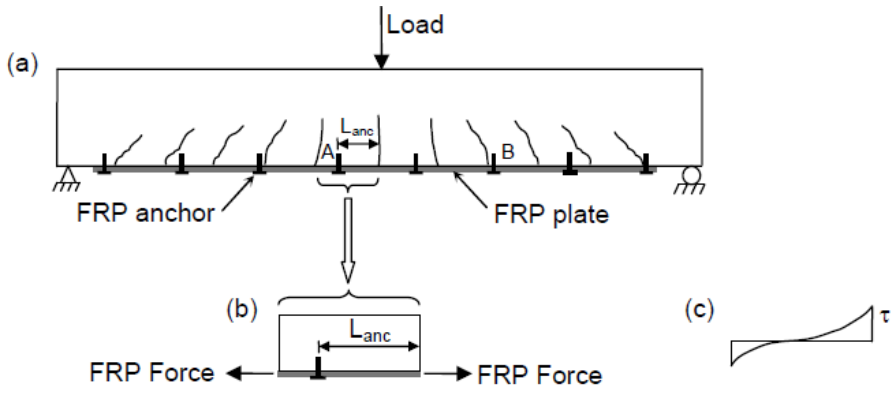

Figure 2.6 (a) Cracked and anchored FRP-strengthened RC beam, (b) Idealized FRP-to-concrete joint with anchor, and (c) Idealized elastic interfacial shear stress distribution (pre-debonding) (Kim and Smith, 2009)

2.6.2 FRP Anchor Fabrication Techniques

There are many different FRP anchor fabrication methods found in the literature. Figure 2.7 illustrates different FRP anchors used in research programs. Niemitz, (2008) fabricated anchors by cutting a desired size rectangular piece from the same FRP material used for the sheets. The dry FRP piece was then rolled into a cylinder and held together by two zip ties. On one end the transverse fibers were cut so that the fibers could be spread out into a circle to form a splay. The FRP sheet was then bonded to the concrete and the anchor was passed between sheet fibers. The anchor was inserted into a pre-drilled hole in the concrete surface that was halfway filled with epoxy. The exposed end was splayed out onto the surface of the FRP sheet and a layer of epoxy was applied.

Table 2-1 Comparison of material properties of the different CFRP materials

	Sika Composite Gross Laminate				Fyfe Composite Gross Laminate				Mbrace Composite Gross Laminate Properties			
	Average Value*		Design Value**		Average Value*		Design Value**		Average Value*		Design Value**	
	Psi	GPa	Psi	GPa	Psi	GPa	Psi	GPa	Psi	GPa	Psi	GPa
Tensile Strength in primary fiber direction	123,200	0.849	104,000	0.651	127,000	0.876	107,950	0.745				
Tensile Strength per inch width	4,298 lbs	21.9 kN	4,160 lbs.	18.5 kN	5,100 lbs	-	4,300 lbs	-				
Tensile Modulus in primary fiber direction	10,239,800	70.552	9,446,600	65.087	10,500,000	72.4	8,900,000	61.5				
Tensile Elongation at break	1.12%	-	0.98%	-	1.20%	-	1.00%	-				
Laminate Thickness	0.04 in	1.016 mm	-	-	0.04 in	1.0 mm	-	-				

*ASTM test method D-3039

** Average value minus 2 stnd deviations as recommended by ACI 440

	Sikadur 300 (Fabric Saturant/ surface	Ffye (Fabric Saturant/ surface	Ffye (Fabric Saturant/
Tensile Strength	8,000 psi	10,500 psi	10,500 psi
Tensile Modulus	250,000psi	461,000 psi	461,000 psi
Elongation at Break	0.03	0.05	0.05
Flexural Strength	11,500 psi	17,900 psi	17,900 psi
Flexural Modulus	500,000psi	452,000 psi	452,000 psi

Eshwar (2008) fabricated anchors by hand that were composed of glass fibers. The anchors were fabricated by bundling loose dry fibers together to a diameter of approximately 70% of the desired anchor diameter. One end of the fibers was saturated with epoxy and then passed through a hole in plate to achieve the desired anchor diameter. The other end of the fibers was kept dry by wrapping it in plastic. The FRP sheet was applied manually to the concrete using the wet layup process. Then the precured end of the anchor was inserted into a predrilled hole, which was filled halfway with epoxy, and the dry end was splayed out into a circular pattern and epoxy was applied to the splay. An FRP patch was placed over the splays.

Smith (2011) used an interesting method to construct the FRP anchors. As with Niemitz (2008) and Anil and Belgin (2010), a desired size rectangular piece was cut from the same FRP material used for the sheets. Epoxy was applied only to the end that later becomes the embedded part of the anchor. The sheet was rolled from both sides, so that there were two rolls of fibers. The epoxied end was then inserted into a polystyrene mold which was pre-filled with epoxy. After one day the mold was removed and the anchor was inserted into a predrilled hole in the concrete and allowed to cure for half a day. Fibers in the FRP sheets were pre-split at anchor locations to allow passing the anchors prior to bonding to the concrete surface using the wet-layup method. The dry portion of the anchors sticking up through the sheet were then splayed out on top of the FRP sheet into a bow-tie shape, and epoxy was used to saturate the anchor splays and the top surface of the bonded sheets. Smith (2011) advised against impregnating the anchor fibers with epoxy in the bend region between the splay and embedded part of the anchor.

This allows greater slips of the sheet relative to the concrete surface, which assists in avoiding brittle FRP anchor rupture failure. Smith (2011) also reported greater slip capacity of the "bow-tie" splay design compared to a single fan design.

Anil and Belgin (2010) fabricated anchors by cutting a desired size rectangular piece from the same FRP material used for the sheets. The sheet was wrapped around a plastic rod, with a diameter of 8 mm [0.3 in.], which made it easier to insert the anchors without distorting the fibers. One end of the anchor was inserted into a predrilled hole that was filled with epoxy. The exposed end of the anchor was divided into 4 equal strips, which were splayed onto the FRP sheet in an X-shape pattern, with two of the four strips facing forward and two facing backward. Epoxy was applied to the splay at the time of the FRP sheet final saturation.

2.6.3 Experimental Performance of FRP Sheets Fastened with FRP Anchors

Although there is a limited amount of experimental testing of anchored FRP sheets, there is a clear consensus among researches that FRP anchors can significantly improve performance, by delaying or preventing debonding failures which occur before the capacity of the FRP is reached (Niemitz, 2008; Eshwar, 2008; Anil and Belgin, 2010; Smith, 2011; Kim and Smith, 2009). However, these researchers report a wide range of increases in load capacity compared to unanchored sheets. Several experimental researchers were able to achieve full or close to the full capacity of the FRP sheets by preventing debonding failure. The effectiveness of the anchors depends on several anchor design parameters, which are discussed in section 2.6.5.

(a) (b)

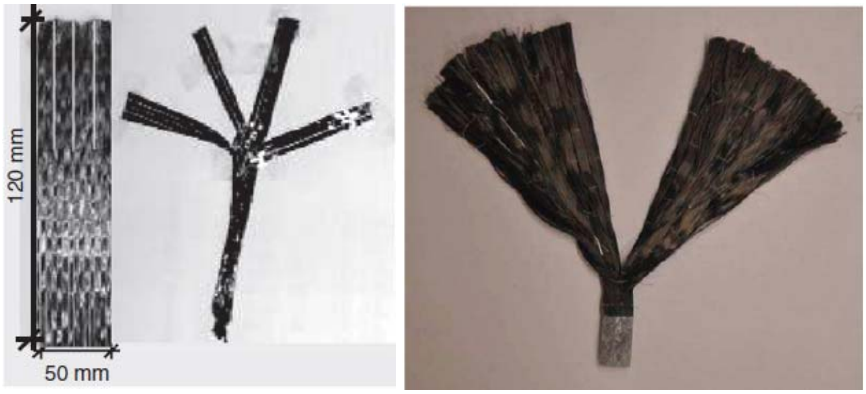

(c) (d)

Figure 2.7 (a) GFRP anchors from (Eshwar, 2008); (b) CFRP anchor from (Niemitz, 2008), (c) CFRP anchor from (Anil and Belgin, 2010), and (d) CFRP anchor from (Smith, 2011)

In unanchored sheets, debonding failures usually occur well before the capacity of the FRP sheet is reached, which results in inefficient use of the FRP material. This creates a particular concern because high material costs are one of the primary drawbacks of using FRP systems. Unfortunately, increasing the length of the sheet beyond the STZ increases the ductility, but results in negligible change in load carrying capacity (Chen and Teng, 2001). Therefore, supplemental anchorage is almost always required to develop the full capacity of the sheet. In some instances space limitations prevent the FRP sheet from being as long as the STZ, which results in even lower debonding failure

loads. This can occur in shear strengthening applications, and especially with beams that are integral with a slab.

Debonding was greatly delayed in all of the anchored specimens from Niemitz (2008) compared to the unanchored specimens, and in some anchored specimens debonding failure was prevented. Although all of the sheets fastened with FRP anchors from Anil and Belgin, (2010), Kim and Smith (2009) and Eshwar et al. (2008) failed at least partially by debonding, it appears that the anchors at least delayed debonding, since they failed by debonding at a higher load than the unanchored specimens in all cases.

Unanchored sheets give little warning of impending failure. Once debonding initiates in unanchored sheets, the debonding front quickly propagates along the length of the sheet, with little change in load capacity. In contrast, for anchored specimens there is often a significant reserve capacity after the initiation of debonding in front of the anchors, since the anchors also resist part of the total applied load (Niemitz, 2008). This adds a large amount of robustness to anchored sheets. The load capacities of anchored FRP sheets are also less reliant on the surface conditions of the concrete. This is especially advantageous when applying FRP to existing concrete structures that have poor surface conditions, or where the strength of the surface of concrete is not well known.

(Anil and Belgin, 2010) tested the performance of anchored FRP sheets using the beam test setup, as shown in Figure 2.1, while (Niemitz, 2008), (Eshwar, 2008) and (Kim and Smith, 2009) used either the single or double shear test setups, also as shown in Figure 2.1. It is difficult to compare failure loads measured using different test configurations such as the shear and beam test setups.

Table 2-2 compares results from tests conducted by Niemitz (2008) and Eshwar (2008). Both researTable 2-1chers conveniently used the same FRP system (Mbrace CF 130 unidirectional FRP sheets), which has the properties shown in Table 2-1. As can be seen, tests conducted by Niemitz (2008) reached significantly higher percentages of the sheet capacity than did those of Eshwar (2008). The two unbonded specimens tested by Niemitz (2008) failed at 45% and 33% of the capacity of the sheet, while the best performing anchored sheet from Eshwar (2008) failed at only 32% of the capacity of the sheet. This means that all of the anchored specimens from Eshwar (2008) failed at a lower percentage of the capacity than the unanchored specimens from Niemitz (2008). This is likely largely due to the fact that Eshwar (2008) tested double ply specimens and Niemitz (2008) tested single ply specimens. Unanchored double ply specimens tend to fail at a lower percentage of the capacity of the sheet than unanchored single ply specimens, because the double ply specimens have twice the load capacity but the same bonded area on the concrete. The sheet capacity to anchor capacity ratio was also significantly higher for the Eshwar (2008) specimens compared to the Niemitz (2008) specimens for three reasons: (1) Eshwar (2008) used two plies instead of one, (2) Eshwar (2008) used 10 mm [0.4 in.] diameter anchors while Niemitz (2008) used mostly 13 mm [0.5 in.] diameter anchors, and (3) Eshwar (2008) used GFRP anchors which have a significantly lower stiffness than the CFRP anchors used by Niemitz (2008). It is believed that the specimens from Eshwar (2008) would have performed better if a more substantial anchorage system was used (either more anchors, or larger and stiffer anchors, and possibly larger anchor splays).

Eshwar (2008) calculated an experimental bond reduction coefficient (κ_{exp}) which equaled the maximum measured strain from each test specimen divided by the strain capacity, which was determined from FRP coupon tests. The values of (κ_{exp}) for the anchored specimens ranged from 0.23 to 0.50. As discussed in section **Error! Reference source not found.**, ACI 440.2R-08 recommends limiting (κ_v) to a maximum value of 0.75 when designing FRP shear strengthening systems. Eshwar (2008) recommends significantly reducing (κ_v) to 0.25. It is believed that this is unreasonable, since some researchers were able to reach nearly the full capacity of sheets that were anchored. In addition, this would discourage the use of anchors, since (κ_v) would often be higher for unanchored sheets.

As discussed in section 2.6.1, Kim and Smith (2009) experimentally tested the effect of anchor location relative to intermediate crack location. The average increase in load capacity compared to the unanchored specimens for specimens with anchors located 50, 75 and 100 mm [2, 3 and 4 in.] from the unbonded zone (analogous to an intermediate crack), was 68.7%, 56.3% and 18.6%, respectively. These results are in closer agreement to those reported by Niemitz (2008) than to those by Eshwar (2008). The unanchored specimens failed by debonding. Eight of the nine anchored specimens failed by debonding of the sheet followed by either anchor shear failure or anchor splay delamination, and one specimen failed by simultaneous debonding of the sheet and splay delamination. Specimens that failed by anchor splay delamination failed at a lower load than those that failed by anchor shearing. It was noted that specimens that failed by complete debonding of the sheet first, followed by anchor failure, had a reserve strength

of up to half of the peak load, while specimens that failed by debonding and shear failure simultaneously obviously had no reserve strength after debonding of the sheet.

Table 2-2 Comparison of Test Results from Niemitz (2008) and Eshwar (2008)

	Sheet Properties			Anchor Properties					Performance		
Specimen	# of Plys	Width [mm]	Bonded Length [mm]	# of Anchors	Placement	Diam. [mm]	Splay Diam. [mm]	Embedment [mm]	Failure Load [kN]	Ptest/ Pult	Failure Mode
A-0-0-5-0	1	127	762	None	-	-	-	-	35.6	**0.45**	Debonding
A-0-0-10-0	1	254	762	None	-	-	-	-	50.9	**0.33**	Debonding
B-Z-2-5-2	1	127	762	2	Longitudinal (254 mm apart)	6	51	51	45.4	**0.58**	Anchor Shear, sheet debonding
B-Z-2-5-4	1	127	762	2	Longitudinal (254 mm apart)	13	51	51	53	**0.68**	FRP rupture, sheet debonding
B-W-2-5-4	1	127	318	2	Longitudinal (254 mm apart)	13	51	51	41.3	**0.53**	FRP rupture, sheet debonding
B-Z-4-5-4	1	127	762	2	Longitudinal (254 mm apart)	13	102	51	49	**0.63**	Anchor Shear, sheet debonding
B-Z-4-5-6	1	127	762	2	Longitudinal (254 mm apart)	19	102	51	58.2	**0.74**	FRP rupture, sheet debonding
B-Y-2-5-4	1	127	762	2	Transverse	13	51	51	55.3	**0.71**	FRP rupture, sheet debonding
B-X-2-5-4	1	127	381	2	Transverse	13	51	51	60.6	**0.77**	FRP rupture, splay delamination, debonding
C-Y-4-10-6	1	254	762	2	Transverse	19	102	51	96.6	**0.62**	FRP rupture, sheet debonding, splay delamination
C-X-4-10-6	1	254	381	2	Transverse	19	102	51	87.6	**0.56**	FRP rupture, sheet debonding, anchor pullout, splay delamination
C-U-2-10-4	1	254	762	4	Transverse	13	51	51	129.1	**0.83**	FRP rupture
(Niemitz, 2008)											
T-1	2	102	250	None	-	-	-	-	53.4	**0.21**	Sheet debonding
T-2	2	102	250	1	Longitudinal	10	unkown	50	66.7	**0.26**	Sheet debonding
T-2	2	102	250	1	Longitudinal	10	unkown	75	66.7	**0.26**	Sheet debonding
T-3u	2	102	0	1	Longitudinal	10	unkown	50	16.5	**0.06**	Failure of anchor
T-3u	2	102	0	1	Longitudinal	10	unkown	75	14.7	**0.06**	Failure of anchor
T-4	2	102	250	2	Longitudinal (102 mm apart)	10	unkown	75	124.5	**0.49**	Sheet debonding
T-5u	2	102	0	2	Longitudinal (102 mm apart)	10	unkown	75	40	**0.16**	Failure of anchor
(Eshwar et al., 2008)											

The reported loads from Anil and Belgin (2010) refer to the load applied to the beam, and not the force on the sheet, so the loads cannot be directly compared to those of

Niemitz (2008), Eshwar (2008) and Kim and Smith (2009). The test results are given in Table 2-3. The specimens fastened with two, three and four CFRP anchors failed at 45%, 76% and 95% higher loads, respectively, compared to the unanchored specimen. These increases in load capacity are relatively close to those reported by Niemitz (2008) and Kim and Smith (2009). All of the specimens failed by debonding. The initial stiffnesses of the anchored specimens were greater than for the unanchored specimen, and the displacement at failure was greater for the anchored specimens except for the specimen with four anchors.

Table 2-3 Test results from Anil and Belgin (2010)

Number of Anchors	Failure Load [kN]	Failure Load/ Unachored Failure Load	Displacement at Ultimate Load [mm]	Initial Stiffness [kN/mm]	Failure Mode
None	9.32	-	2.74	4000	Debonding
2	13.47	1.45	3.56	4900	Debonding
3	16.37	1.76	2.98	5670	Debonding
4	18.16	1.95	2.74	6040	Debonding

2.6.4 Anchor Placement

The number of anchors and the placement of the anchors are both important parameters that affect load capacity. Niemitz (2008) found that the ultimate load capacity of bonded and anchored FRP sheets is largely dependent on the ability of the leading anchors (anchors closest to the loaded end) to delay debonding from progressing through the sheet. In general, the specimens that did not fully debond performed better than the specimens that failed by debonding. It was concluded that the anchors splays are most effective when they cover the full width of the sheet, or else debonding progressed past the anchors in the gap between the anchor splays, and resulted in premature failure of the

specimen. Niemitz (2008) tested two general anchor arrangements; anchors placed across the width of the sheet, and along the centerline of the sheet. In general, the specimens with anchors across the width of the sheet better delayed debonding, and therefore had higher failure loads. Anil and Belgin (2010) also tested two general anchor arrangements: along the centerline of the sheet, like Niemitz (2008), and a staggered anchor arrangement (Figure 2.5). Although mechanical anchors were used instead of FRP anchors, it is believed that these findings still apply to FRP anchors as well. The mechanical anchors in one row were more effective than a staggered anchor arrangement. The three specimens with a staggered anchored pattern had an average failure load 20% lower than that of the sheets with the same number of anchors aligned in a single row. This is displayed graphically in Figure 2.8. Anil and Belgin (2010) believes this is partly because the stresses are highest along the centerline of the sheet, so it is more efficient to place all of the anchors there. It is believed that this observation is correct but would be dependent on the ability of the single row of anchors to prevent debonding across the full width of the sheet. Also, as is explained later in this section, Niemitz (2008) found that anchors can alter the transverse distribution of stresses in the FRP sheet, causing peak strains (stresses) to occur in front of the anchors, and not necessarily along the centerline of the sheet. Another plausible explanation for the single row arrangement performing better is that staggered anchor arrangements were not symmetric about the longitudinal axis, which can cause uneven loading across the width of the sheet and result in a reduction in the load capacity of the sheet.

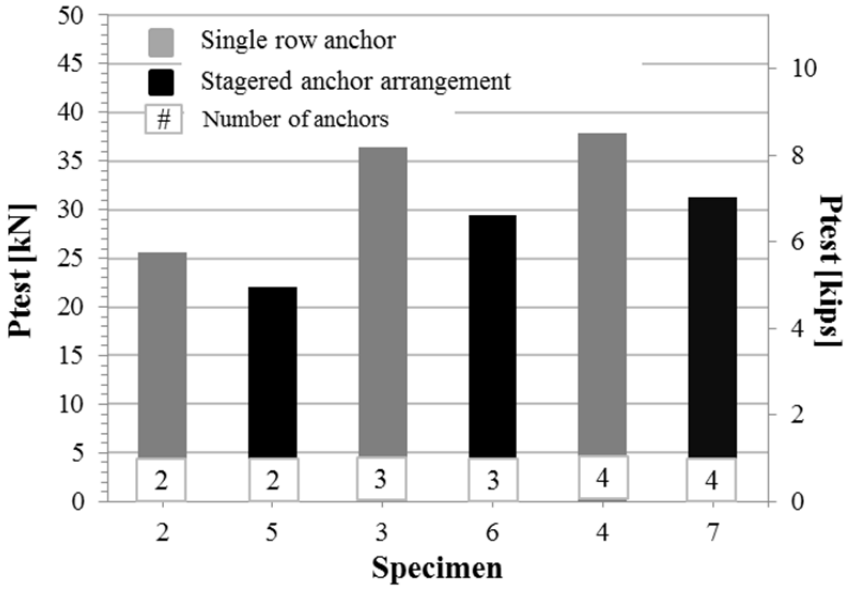

*CFRP sheet is 100 mm by 240 mm [4 in. by 9.4 in.]

Figure 2.8 Load capacity results of staggered and single row anchor arrangements (Anil and Belgin, 2010)

Niemitz (2008) found that in the specimens with anchors along the length of the sheet the front anchor appeared to resist most of the load, and the trailing anchor added ductility but little load capacity. This is evident from strains recorded at discrete locations along the length of the sheet. Figure 2.9 shows the longitudinal strain distribution of a sheet with two anchors spaced along the length of the sheet. As can be seen, there was negligible strain in the sheet in front of the trailing anchor, until a load of 48.3 kN [10.9 kips], which was approximately 83% of the peak load. The change in strain in sections located in front of the anchors and behind the anchors is related to the amount of load that the anchors and bond resist. At the peak load in Figure 2.9, there was a greater drop in strain at the front anchor than at the trailing anchor indicating that the front anchor resisted a larger fraction of the total load. It also appears that the debonding front passed the front anchor, but not the trailing anchor, which suggests that the drop in strain at the

trailing anchor was partly due to the load transferred by the bond into the concrete substrate.

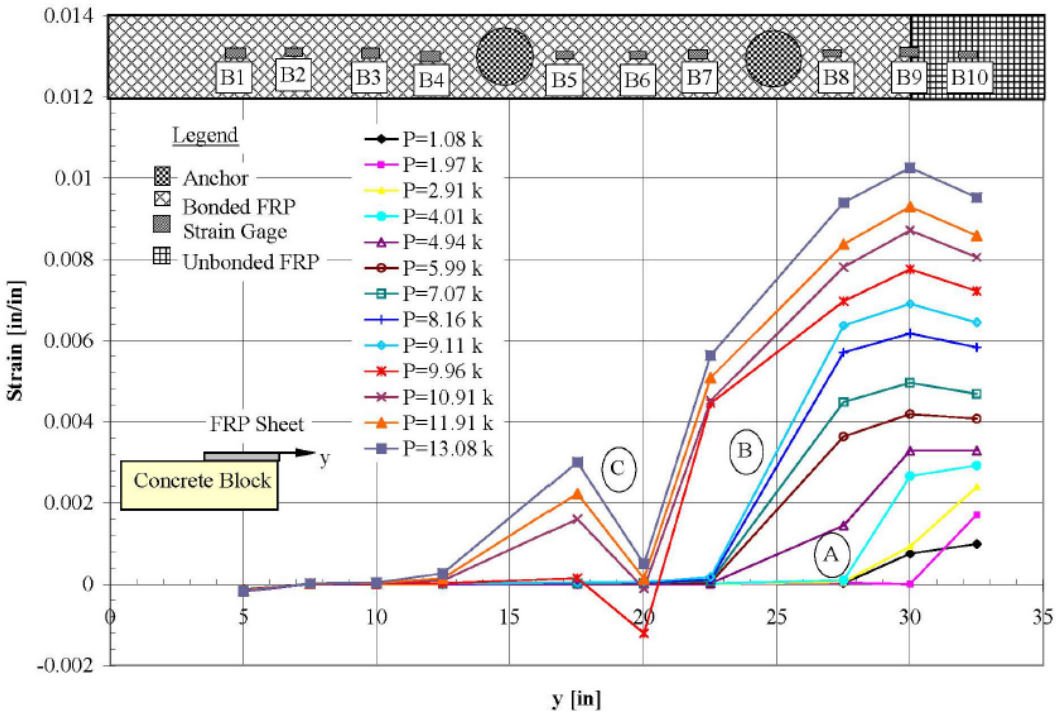

Figure 2.9 Longitudinal strain distribution of anchored FRP sheet (Niemitz, 2008)

In contrast, Anil and Belgin (2010) found that there was a positive correlation between number of anchors along the centerline of the sheet and load capacity. With each additional anchor, however, there was a smaller increase in capacity. The specimen with three FRP anchors along the centerline of the sheet failed at a 22% higher load than the specimen with two anchors, and the specimen with four anchors failed at only an 11% higher load than the specimen with three anchors. This is displayed graphically in Figure 2.13. The longitudinal spacing between anchors may affect their efficiency since it may determine whether an anchor lies within the STZ. The anchors tested by Niemitz (2008) had a 250 mm [10 in.] spacing, whereas the anchors in specimens with two, three and four anchors tested by Anil and Belgin (2010) were spaced only 80, 60 and 48 mm [3.1,

2.4 and 1.9 in] apart, respectively. If the back row or rows of anchors are beyond the STZ then they may not assume appreciable load until after the debonding front has progressed passed the first row of anchors. Eshwar (2008) tested specimens with two anchors spaced 100 mm [4 in.] apart, and also found that the trailing anchors increased load capacity. The average failure load of the six (T-2) specimens from Eshwar (2008), which were fastened with one anchor, was 25% greater than the average failure load of the three unanchored (T-1) specimens. The three (T-4) specimens, fastened with two anchors, failed at an average load 233% higher than the average load in unanchored (T-1) specimens. Specimen (T-5U), which was unbonded and was fastened with two anchors, failed at a 270% higher load than the average failure load of the three (T-3U) specimens, which were unbonded and fastened with one anchor. It was expected that specimen (T-5U) would fail at less than double the failure load of the (T-3U) specimens, since it was expected that for specimen (T-5U) the front anchor would resist more load than the back anchor. For the specimens tested by Eshwar (2008) the stiffness of the sheet compared to the stiffness of the anchors was likely significantly greater than for the Niemitz (2008) specimens, since Eshwar (2008) used two plies instead of one and used GFRP anchors instead of CFRP anchors. A higher stiffness sheet with lower stiffness anchors encourages a better distribution of force to the front and back anchors.

Past researchers have documented that for unanchored sheets the strain tends to be highest along the centerline of the sheet, and decreases toward the edges of the FRP sheet (Subramaniam et al., 2007). Niemitz (2008) showed that anchors affect the transverse strain distribution. The portion of the sheet in front of and in line with the FRP anchors tends to attract more force, and therefore experiences higher strains. This can be observed

by comparing Figure 2.10 with Figure 2.11. Figure 2.10 shows the transverse strain profile for a sheet with a single anchor in the center. As expected, the strains are significantly higher in front of the anchor. Figure 2.11 shows the strain profile for a sheet with two transversely spaced anchors. Contrary to the sheet with one anchor in the middle, the strain is lowest in the center of the sheet; but like the sheet with one anchor, the strain is highest in line with the anchors.

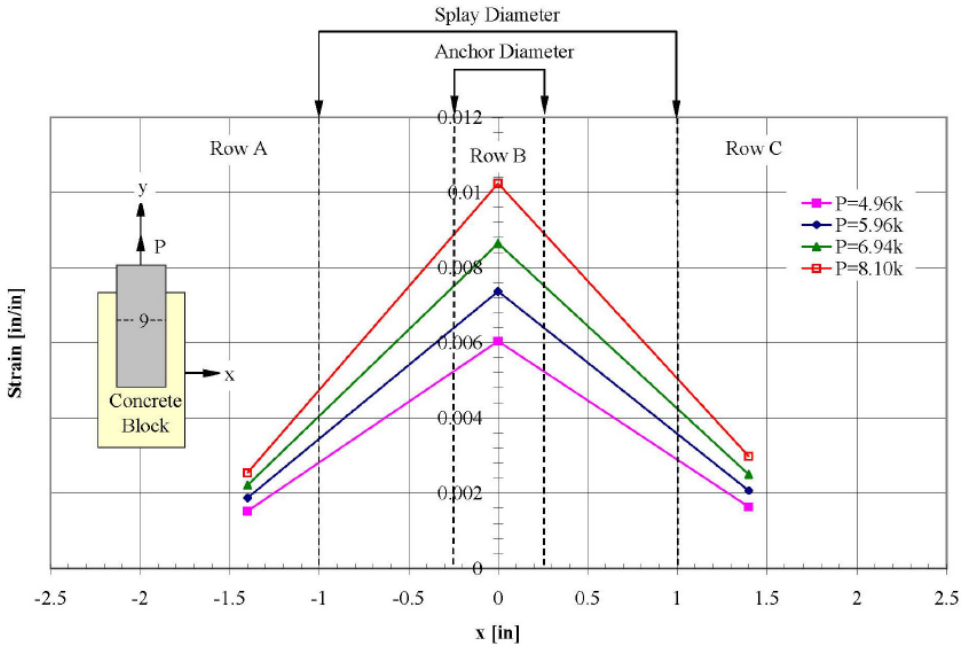

Figure 2.10 Transverse Distribution of Strain Across FRP Sheet Width (Specimen B-W-2-5-4, Niemitz, 2008)

As discussed in section 2.6.1, Kim and Smith (2009) experimentally tested the effect of anchor location relative to intermediate crack location. It was concluded that the distance from the crack to the anchors significantly affected load capacity. The average increase in load capacity compared to the unanchored specimens for specimens with anchors located 50, 75 and 100 mm [2, 3 and 4 in.] from the unbonded zone (analogous to a crack), was 68.7%, 56.3% and 18.6% respectively. The authors attribute this finding to the fact that the stresses are highest at the start of the bonded zone and reduce away

from the loaded end, so the anchors would be able to assume more load and therefore be more effective in the proximity to the unbonded zone.

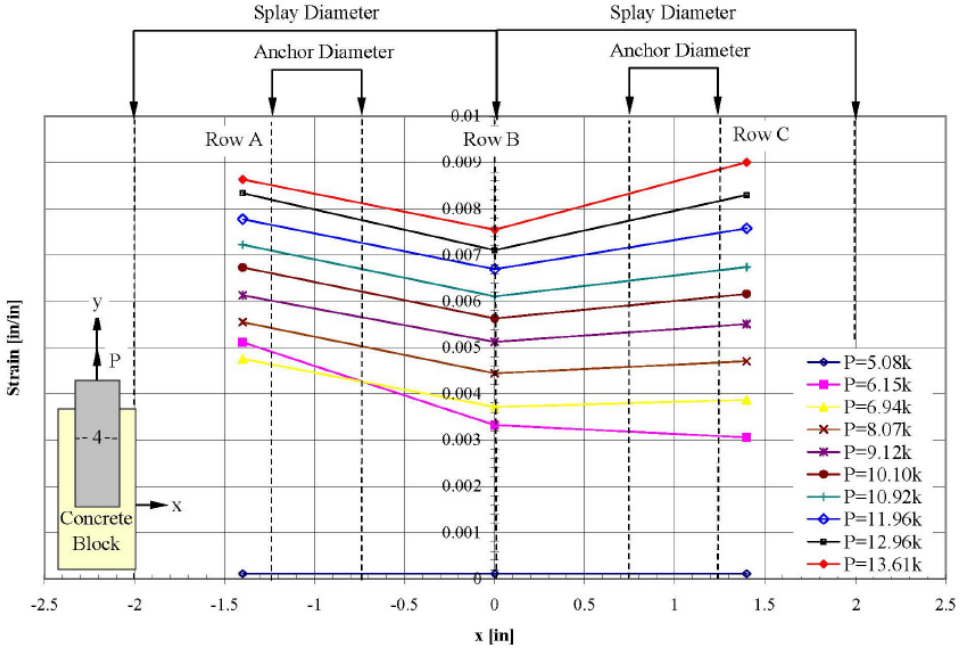

Figure 2.11 Transverse Distribution of Strain Across FRP Sheet Width (Specimen B-X-2-5-4, Niemitz, 2008)

Findings from Niemitz (2008) appear to contradict these findings. In all of the tests completed by Niemitz (2008) anchors were placed 125 mm [5 in.] from the unbonded region. The length of the anchors from unbonded region appeared to have negligible effect on ultimate capacity, but rather only affected the initial stiffness of the FRP sheet. Strain readings along the length of the sheet show that the anchors initially resisted little load because they were either outside or near the end the stress transfer zone (STZ). After the initiation of debonding the STZ translated along the sheet and the anchors rapidly assumed more load. It is believed that if the anchors were placed very far from the unbonded edge that it would simply take longer for the STZ to reach the

anchors, at which point the sheet would behave the same as a specimen with anchors placed close to the unbonded edge, and the peak load capacities would be the same.

The bonded length of sheet behind the anchors appears to be of greater importance than the length of sheet in front of the anchors. In several of the tests performed by (Niemitz, 2008), the load increased after the debonding front passed the anchor location. A bonded region behind the anchor location allows the development of axial strains in the FRP sheet thereby generating higher stresses. The effect of bonded length behind anchor sections appeared to have little or no effect in tests in which the anchors were able to develop the full strength of the FRP sheet before the debonding front had passed behind them.

2.6.5 FRP Anchor Design Parameters

The effectiveness of FRP anchors depends on several anchor design parameters such as number and placement of the anchors, type of FRP material, anchor diameter, anchor splay diameter, ratio of splay diameter to anchor diameter, splay shape, and anchor embedment depth.

Niemitz (2008) found that anchor splays are effective in securing only a width of sheet fibers approximately equal to the splay diameter, and therefore it is most effective to have the anchors splays placed such that they cover the entire width of the FRP sheet. For specimens that had an open space between anchor splays, the sheet between the splays debonded prematurely.

Niemitz (2008) tested anchors with diameters of 6, 13 and 19 mm [0.25, 0.5 and 0.75 in.] and a constant embedment depth of 50 mm [2 in.]. Since some anchors failed by anchor shear, and not anchor pullout, it was concluded that embedment depth had a

negligible effect on capacity for the range of anchor and sheet parameters tested. Eshwar (2008) tested anchors installed at embedment depths of 50 and 75 mm [2 and 3 in.]. He also concluded that embedment depth had negligible effect on load capacity. From these two sources, it appears that a 50 mm [2 in.] embedment depth is sufficient for CFRP anchors with diameters of up to 75 mm [3 in.]. In addition to anchor diameter, anchor fabrication technique affects the shear capacity of anchors because of the maximum fiber content that can effectively be placed by hand. It may be advantageous to have the anchors extend into the rebar cage in flexural strengthening applications, to discourage failure by separation of the concrete cover.

The size of the anchor splay, which determines the width of the sheet engaged by the anchors, relative to the anchor diameter is important. Niemitz (2008) empirically derived Equation 2.5 to determine the required anchor diameter for a chosen anchor splay diameter. Equation 2.5 is only valid for FRP anchors ranging from 6.4 mm to 19.1 mm [0.25 in. to 0.75 in.] in diameter, since those were the FRP anchor diameters tested.

$$D_A = \sqrt{\frac{4(S_A)(f_{fu})(t_p)(n_p)}{\pi(35.8)}} \qquad \textbf{[2.5]}$$

Where:

D_A = FRP anchor diameter [in.]

S_A = anchor splay diameter [in.]

f_{fu} = FRP ultimate tensile strength [ksi]

t_p = nominal thickness of FRP sheet [ksi]

n_p = number of FRP plies

2.7 Alternative Methods of Anchoring FRP Sheets

2.7.1 Near Surface Mounted End Anchors

Khalifa et al. (1999) stated that anchoring the end of FRP sheets in grooves, with and without near surface mounted (NSM) bars, can prevent debonding failures and allow for the development of the ultimate strength of FRP sheets. This anchorage method can be used to secure FRP sheets used for flexural and shear strengthening of beams. Eshwar (2008) completed an experimental investigation of FRP sheets secured with NSM end anchors, using the beam test setup, as shown in Figure 2.1 (e). A sketch of a near surface mounted end anchor is shown in Figure 2.12. The end anchorage system works by wrapping the end of the FRP sheet around an FRP bar that is subsequently embedded into a precut groove. The groove is filled with epoxy to bond the bar to the concrete element. This anchoring system works for FRP sheets that are applied using the wet-layup application.

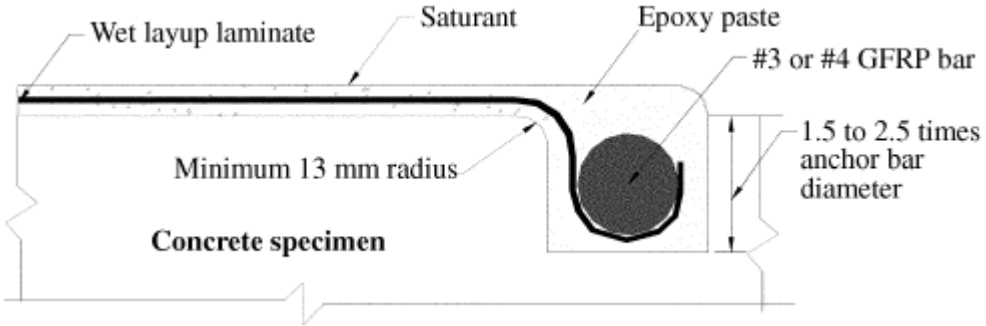

Figure 2.12 Near surface mounted end anchor

In agreement with Khalifa et al., (1999), Eshwar (2008) concluded that anchoring sheets with NSM end anchors can significantly increase the capacity beyond that of unanchored sheets. Eshwar (2008) found that the groove size, bar size, radius of the corners of the groove, and location of the bars are all important design parameters, and

can significantly affect load capacity. The increase in capacity of the sixteen specimens where FRP sheets were fastened with NSM end anchors compared to the unanchored specimens ranged from 7 to 51%. The unanchored specimen failed by debonding, while seven of the anchored specimens failed by FRP rupture.

2.7.2 Steel Mechanical Anchors

As mentioned in section 2.6.1, Anil and Belgin (2010) compared the performance of FRP sheets fastened with CFRP anchors and steel mechanical anchors. Both types of anchors successfully increased load capacity and stiffness compared to the unanchored control specimens, but the mechanical anchors performed significantly better than the CFRP anchors. The mechanically anchored specimens were stiffer and had a higher load capacity than the specimens with CFRP anchors, as shown in Figure 2.13. On average the mechanically anchored specimens failed at a 70% higher load than the CFRP anchored specimens. All of the mechanically anchored specimens failed by FRP rupture and all of the CFRP anchored specimens failed by debonding. The initial stiffness of specimens with two, three and four mechanical anchors in a row were 18, 60 and 176% higher than in specimens with two, three and four CFRP anchors in a row. Anil and Belgin (2010) believe this is because the steel anchors had significantly greater shear stiffness and load capacity, and the mechanical anchors provided a greater normal force that maintained the sheet in contact with the concrete surface. The steel anchors were 8 mm [0.3 in.] in diameter and the CFRP anchors were 10 mm [0.4 in.] in diameter, but were fabricated by rolling only a [2 in.] width of CFRP sheet into a cylinder.

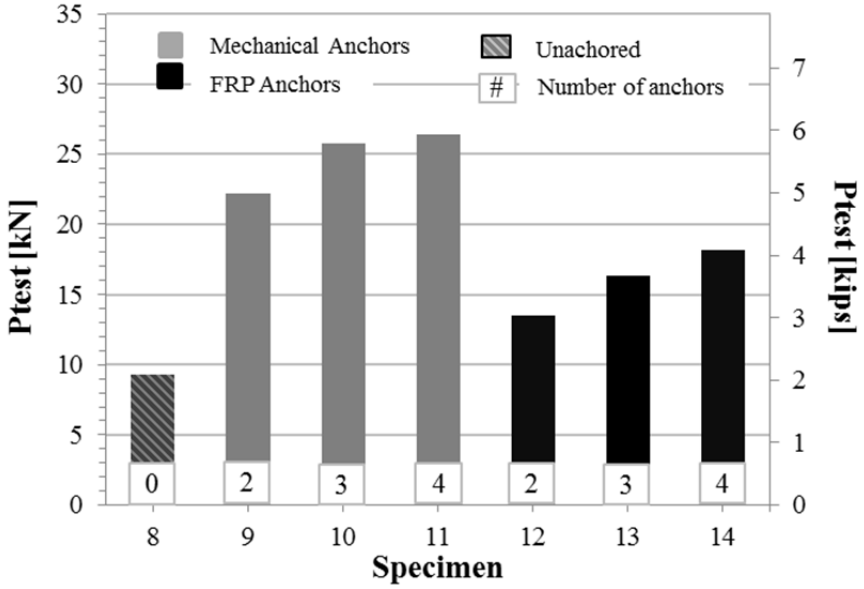

*CFRP sheet was 50 mm by 240 mm [2 in. by 9.4 in.]

Figure 2.13 Load capacity results of mechanical anchors and FRP anchors (Anil and Belgin, 2010)

2.8 Experimental Tests on Structural Members Strengthened with Anchored FRP Sheets

Smith (2011) tested RC slabs with no FRP strengthening, unanchored FRP sheets, and anchored FRP sheets. This study is one of the few studies to test RC members strengthened with anchored FRP sheets. Eight tests were completed, all on one-way simply supported RC slabs. One test had no FRP strengthening, one test had 3-plies of FRP sheets on the tensile side of the slab, and the other six tests had 3-plies of FRP sheets with varying anchor designs. The key design parameters were type and position of anchors. The anchors were handmade, and were fabricated by rolling a piece of CFRP sheet into a cylinder. Details of the anchors are discussed in section 2.6.5.

Several important observations were made. An important general observation was that the anchored FRP sheets increased the strength and robustness of the slab

significantly compared with the slabs strengthened with unanchored FRP sheets, by delaying and controlling crack growth. Even after complete debonding of the FRP sheet, the anchors maintained enough force in the FRP that the load capacity was still greater than that of the unstrengthened slab. Anchors placed in the constant moment region in the center of the span had little effect on performance. In contrast, anchors on the ends of the span were the most effective. The highest strength and deflection capacity was obtained by placing anchors with higher fiber content near the peak bending moment region, and placing closely spaced anchors with lower fiber content near the ends. Results show that closely spacing anchors at the ends of the slab delayed debonding and enabled larger deflections to be sustained.

CHAPTER 3

EXPERIMENTAL PROGRAM

3.1 Introduction

This research program consists of a series of single shear tests (see Figure 2.1 for an illustration of a single shear test) in which a tensile load is applied to a FRP sheet bonded to a concrete block. This test setup is similar to other common setups used by researchers in the past to test bonded FRP sheets. Results from previous research indicate that it successfully mimics the loading and stress condition on FRP sheets used for strengthening of existing concrete elements that span an intermediate crack.

This research program deals with carbon fiber unidirectional sheets applied using the wet layup system. Several design parameters were investigated, the primary ones being longitudinal spacing between anchors, length of sheet behind trailing anchor, CFRP sheets from different manufacturers, and single vs. double ply specimens. The influence of the spacing between rows of anchors is important to understand. Depending on sheet and anchor geometry a single row of anchors may not be adequate in developing the full capacity of a sheet, and therefore more than one row may be necessary. Previous tests show that when a second anchor is added 250 mm [10 in.] behind the first row, the additional anchor has negligible effect on the ultimate load capacity of the sheet. Two different manufacturers of CFRP sheets, Fyfe (www.fyfeco.com) and Sika (www.sikacorp.com), were tested using identical configurations for comparison. Results were also compared to similar tests previously completed at UMass Amherst using FRP materials from MBrace (www.basf.com).

3.2 Test setup

3.2.1 Experimental Setup

A diagram of the test setup is shown in Figure 3.1. The test setup consisted of a CFRP sheet adhered to the surface of a concrete block. The concrete block was secured to the test frame and the CFRP sheets were loaded in tension to develop interface shear stresses between the concrete block and attached sheet. The block rests on top of 2 w-sections, which served only to align the top surface of the block with the loading ram. Longitudinal movement of the block was resisted by a steel buttress made from a stiffened W-section located on the right end of the concrete block. Prior to each test the block was positioned against the buttress while filling any gaps with thin sheet metal. Overturning of the block was restrained by a W-section laid transversely on top of the unloaded (left) end of the block. This section was tied to the reaction frame using four 3/4 in. diameter threaded rods.

The CFRP sheet extended 300 mm [13 in.] beyond then edge of the block to minimize variations in stress across the sheet from the loading apparatus. Two steel plates 75 mm [3 in.] long by 250 mm [10 in.] wide by 6 mm [0.25 in.] thick were bonded on the last 75 mm of sheet to transfer force between the loading ram and FRP sheet. These plates were then placed between two large steel grips. The grips have a lipped edge which the plates bear against. Slip critical bolts sandwich the plates between the grips as well as secure the grips to a steel piece which screws into the load cell. The loading apparatus is similar to the one used by (Niemitz, 2008)

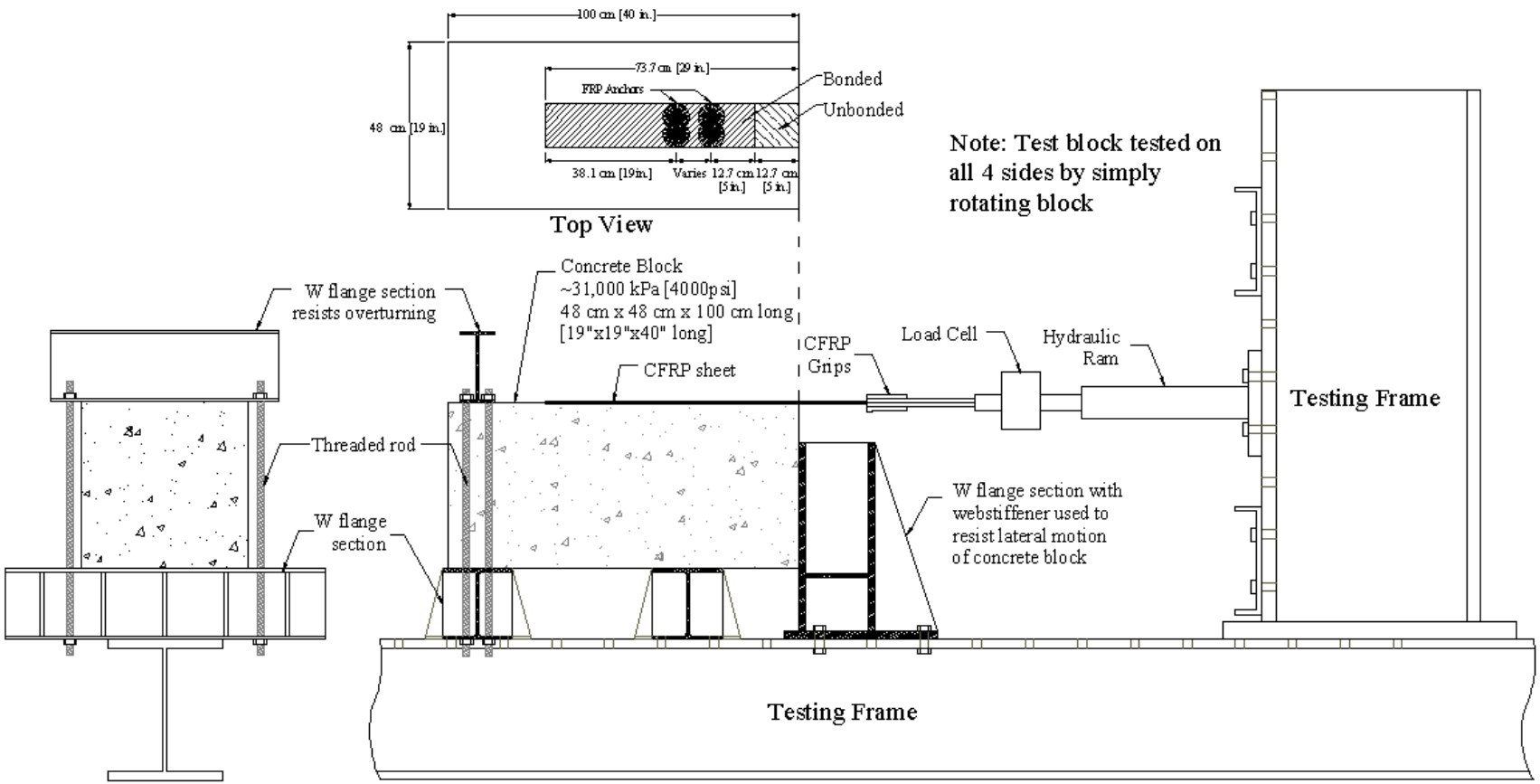

Figure 3.1 Test set up

3.2.2 Concrete Block Geometry and Internal Reinforcement

A total of four concrete blocks were fabricated in the Structural Engineering Laboratory at UMass Amherst. All concrete blocks are identical in dimension and internal reinforcement and were made using a commercially available bagged concrete mix (*High Strength Sakrete)*, with a reported 28-day compressive strength of 28 MPa (4000 psi). The blocks were symmetric on all four sides, which allowed each block to be used in four tests. The blocks were 1020 mm [40 in.] long by 480 mm [19 in.] square. The blocks were left in the formwork for roughly two days while covered with an inner layer of wet burlap and an outer layer of plastic sheathing to retain moisture. The formwork was then removed and the blocks were left to cure in air for at least 28 days before testing.

The blocks were designed such that the tensile forces in the block would not exceed the tensile strength of the concrete during testing or during block handling in the laboratory, so that the concrete would remain uncracked. The block width was selected to prevent a reduction in sheet bonding capacity. (Subramaniam et al., 2006) reports that when the width ratio between the sheet and the block is low, the capacity of the sheet can be significantly reduced. Longitudinal reinforcement in the blocks was designed according to ACI 318-08, where minimum area of steel requirement governed the design. Flexural steel consists of two No. 5 Grade 60 reinforcing bars along the four corners of the block. Transverse reinforcement design was also governed by minimum steel requirements in ACI 318-08 and consists of six No. 3 Grade 60 hoops. The longitudinal spacing of the shear reinforcement is such that it would not interfere with the FRP anchors, nor influence the test results by affecting the potential formation of a concrete

pullout cone. All blocks were provided with a 32 mm [1.25 in.] clear cover above the transverse steel. Figure 3.2 and Figure 3.3 give reinforcement details of a typical concrete block used for the laboratory tests.

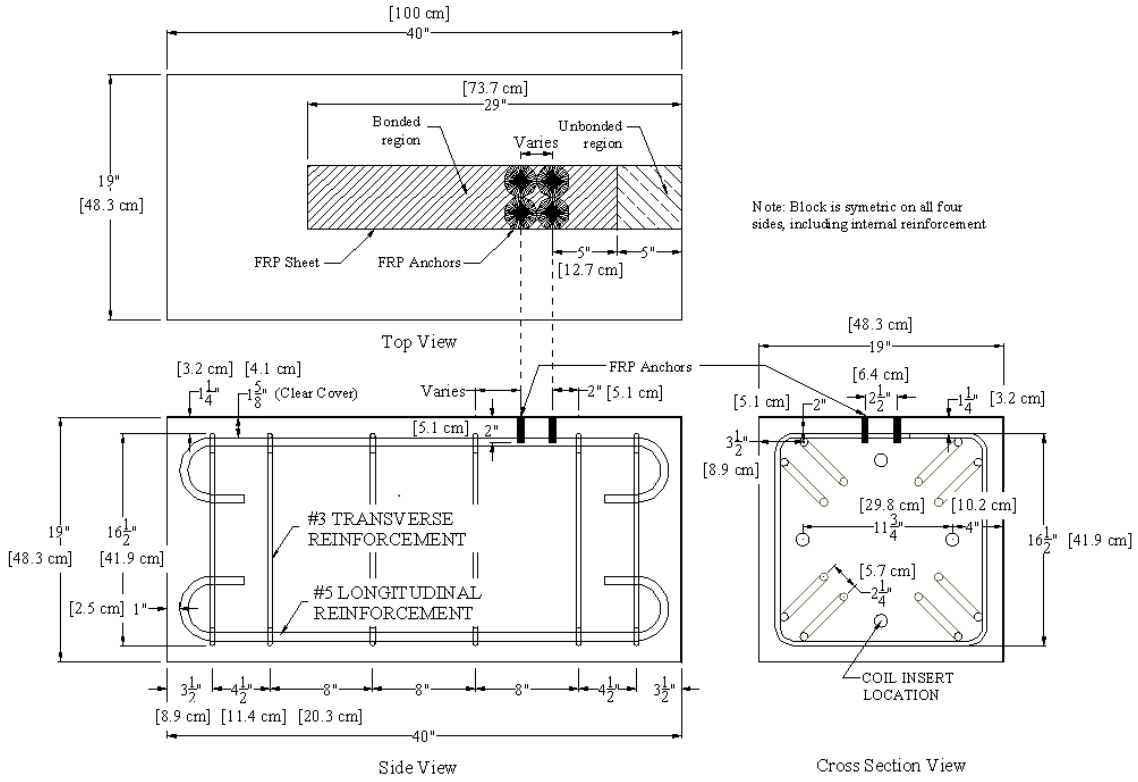

Figure 3.2 Concrete block geometry and internal reinforcement, and anchor location

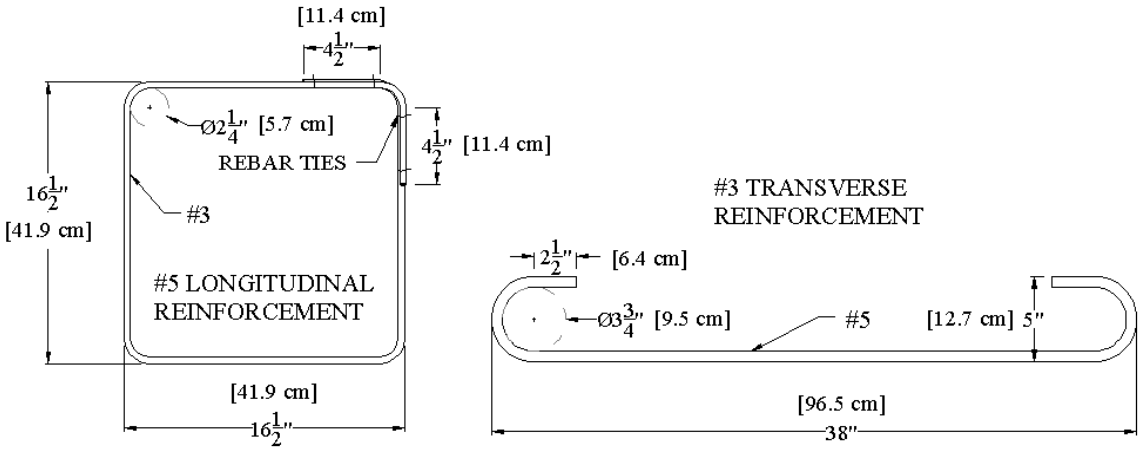

Figure 3.3 Internal reinforcement

3.3 FRP Strengthening Configurations

This section describes the strengthening configurations that were tested in this research project. All tests were on unidirectional CFRP sheets installed using the wet layup process. Baseline tests were performed on unanchored single ply specimens using both Fyfe and Sika systems. A series of anchored single ply tests were then completed to determine the effect of anchoring the sheets. Tests of anchored and unanchored double ply specimens were performed to compare the performance of double ply and single ply specimens. Finally, unbonded specimens were tested to isolate the behavior of the anchors. The test identification key below illustrates the how specimens were identified for this research project, while the test matrix is presented in Figure 3.4.

Test Identification Key:

AB-C-D-E

A= Manufacturer: (S=Sika, F=Fyfe)

B = Number of plies

C = Number of anchors ("a" stands for anchor; 2a = one row of two anchors, 4a = two rows of two anchors)

D = Spacing between rows of anchors in terms of anchor splay diameters (this number is excluded from the test identification if there are more than one row of anchors)

E = Length of bonded portion of the sheet in inches

Test Category	Test	Manufacturer	Bond Length	Bond Width	Anchor Pattern	Anchor Longitudinal Spacing	Anchor Transverse Spacing	Purpose of Test
Unanchored Baseline Tests	*S1-0a-24*	Sika	61 cm [24 in]	12.7 cm [5 in]	No Anchor	--	--	Baseline Test for Anchored Specimens, Double Ply Specimens and Comparison of Manufacturers
	F1-0a-24	Fyfe				--	--	
Anchored Single Ply tests	*S1-2a-24*	Sika			1 row of 2	--	1 d_b	Baseline for Specimens with Two Rows of Anchors
	F1-2a-24	Fyfe						
	S1-4a-1-24	Sika			2 rows of 2	1 d_b		Second Row of Anchors and Longitudinal Spacing of Anchors
	F1-4a-1-24	Fyfe						
	S1-4a-2-24	Sika				2 d_b		
	F1-4a-2-24	Fyfe						
	S1-4a-1-12.5	Sika	32 cm [12.5 in]			1 d_b		Length of Sheet Behind anchors
Double Ply Tests	*F2-0a-24*	Fyfe	61 cm [24 in]		No Anchor	--	--	Unanchored Double Ply
	F2-2a-24				1 row of 2		1 d_b	Anchored Double Ply
	S2-2a-24	Sika						
	F2-4a-1-24	Fyfe			2 rows of 2	1 d_b		
	S2-4a-1-24	Sika						
Unbonded Tests	F2-2a-24U	Fyfe	0 cm	0 cm	1 row of 2	--		Unbonded, Anchored Sheets
	F2-4a-1-24U				2 rows of 2	1 d_b		

Note: All anchors 1.3 cm [1/2 in] Diameter with 5.1 cm [2 in] embedment depth
All anchor splays 6.4 cm [2 1/2 in] Diameter

Figure 3.4 Test Matrix

3.3.1 Unanchored Baseline Tests

There are two unanchored baseline tests; S1-0a-24 and F1-0a-24. Test S1-0a-24 was on an unanchored sheet supplied by Sika, and was 127 mm [5 in.] wide with a bonded length of 610 mm [24 in.]. Test F1-0a-24 was on an unanchored sheet from Fyfe, with the same dimensions. These tests serve as baseline tests for the anchored specimens as well as the double ply specimens. They also serve to compare the performance of carbon fiber unidirectional sheets provided by different manufacturers. The Fyfe and Sika tests are also compared to a similar test completed by (Niemitz, 2008) on a FRP sheet from Mbrace, 760 mm [30 in.] long and 127 mm [5 in.] wide. It is believed that the difference in length between the two specimens had negligible effect on the ultimate capacity, since the transfer length for both sheets is much less than 610 mm [24 in.].

3.3.2 Anchored Single Ply Tests

There are seven tests within this category; S1-2a-24, S1-4a-1-24, S1-4a-2-24, F1-2a-24, F1-4a-1-24, F1-4a-2-24 and S1-4a-1-12.5. The primary goals of these tests were to determine the increase in capacity gained by anchoring the FRP sheets, and to determine the possibility of having two rows of anchors in close proximity such that they can be treated as an anchor group and increase capacity beyond sheets with only one row or anchors. Previous tests at UMass (Niemitz 2008) showed that sheets with two anchors spaced 255 mm [10 in.] apart longitudinally did not have increased capacity over identical sheets with only one anchor. It was believed that if the two rows of anchors were placed close enough they would act as a group and increased capacity would be possible.

In tests S1-2a-24 and F1-2a-24 the same sheet dimensions were used as in specimens S1-0a-24 and F1-0a-24, except two anchors were placed transversely 125 mm [5 in.] within the bonded section from the loaded end. The anchors were 12.7 mm [½" in.] diameter with an embedment depth of 25 mm [2 in.]. The anchor splay diameters were 65 mm [2.5 in.], which was chosen so that two anchors could fully cover the width of the sheet. Previous research showed that it is important that the full width of sheet is engaged by the anchors to reach full capacity of the sheet (Niemitz, 2008).

In tests S1-4a-1-24 and F1-4a-1-24 the same sheet dimensions were used again and a second row of anchors was added 65 mm [2.5 in.], or one splay diameter, behind the first row such that the anchor splays of the two rows just touched at the edges. This distance was mostly arbitrary as there is very limited research to use as guidance.

In test S1-4a-1-12.5 everything was identical to test S1-4a-1-24 except that the length of bonded sheet behind the trailing anchor was shortened from 445 mm [17.5 in.] to 125 mm [5 in.]. This test investigated the effect of bond length behind the anchors. The shorter bond length behind the anchors is also more typical of FRP sheet used in shear applications.

In tests S1-4a-2-24 and F1-4a-2-24 everything was identical to specimens S1-4a-1-24 and F1-4a-1-24 except that the spacing between the two rows of anchors was increased from 65 mm [2.5 in.]to 125 mm [5 in.], or equivalently, 1 anchor splay diameter to 2 splay diameters.

3.3.3 Double Ply Tests

There are four tests within this category; S2-0a-24, F2-0a-24, S2-4a-1-24, F2-4a-1-24. The main purpose of these tests is to determine the increase in capacity of double

ply specimens over single ply specimens, and to compare the behavior of anchored and unanchored double ply specimens.

3.3.4 Anchored-Unbonded Tests

There are two tests within this category. The purpose of these tests is to isolate the behavior of the anchors by leaving the FRP sheets unbonded, except for a small bonded section behind the anchors. The details of the setup of these tests are not worked out. The results from these tests were used to determine anchor properties for the finite element models presented in Chapter 6.

3.4 Test Specimen Preparation

3.4.1 Application of CFRP Sheets

3.4.1.1 Surface Preparation

Before applying the CFRP sheets, the surface of the concrete block was prepared by grinding it using an angle grinder until the aggregate was visible and the surface was smooth and as level as possible. The surface integrity was inspected for voids, cracks, or loose particles. After grinding the surface, dust was removed using pressurized air. An example of the surface of the concrete before and after preparation is shown in Figure 3.6.

3.4.1.2 Sheet Application

Following manufacturer's directions the surface was primed using the same epoxy used to impregnate the sheets. An epoxy primer was applied using a paint roller, as shown in Figure 3.9. Small voids in the concrete surface were filled with epoxy. The impregnated sheet was applied to the concrete within 15 minutes, but not less than 5 minutes, of applying the primer. Both Sika and Fyfe lists several ways to impregnate the

sheet. For larger jobs, the sheets are typically impregnated using impregnation devices, and for smaller projects, the sheets can be impregnated by hand. In either method it is critical to fully impregnate the sheet. In this research the sheets were impregnated by hand using a paint roller as shown in Figure 3.10. The sheet was cut to the desired size and laid out on plastic sheets as shown in Figure 3.7. Epoxy was applied to one side at a time using an epoxy roller. The epoxy was applied liberally at first, and then excess was removed by applying light to moderate pressure to the roller to assist in air bubble removal. The impregnated sheet was rolled onto the concrete surface, starting from the end corresponding to the loading steel grips, while applying minimal tension to the sheet. The sheet was left unbonded within the first 125 mm [5 in.] of the concrete block to eliminate any edge effects and to prevent wedge failures at the edge of the block. The portion of sheet extending past the concrete block was supported by plywood formwork covered in plastic sheathing. Plastic sheathing was also placed on the concrete block in the unbonded portion of the sheet.

3.4.1.3 Anchor Fabrication and Installation

Prior to applying the CFRP sheets, holes were drilled in the concrete blocks to insert the FRP anchors as shown in Figure 3.8. FRP manufacturers typically advise drilling holes slightly larger in diameter than the anchors, so that the anchor can be easily slid into the hole. All FRP anchors used in this research program were 12.7 mm [0.5 in.] diameter and were inserted into 15.9 mm [0.625 in.] diameter holes. Holes were drilled to a depth of 50 mm [2 in.] (+- 3 mm [1/8 in.]). It is believed this depth range had negligible effect on results, since failure never occurred by anchor pullout. After applying the FRP sheet the longitudinal fibers were spread to allow passage of fibers forming the FRP

anchors. This was accomplished by cutting the transverse stitches on either side of the hole. After inserting the anchors attention was given to minimize the gap in fibers in front of and behind the anchors, while at the same time keeping the longitudinal fibers at an angle of no more than about 20 degrees. The anchor holes were filled halfway with epoxy prior to inserting the anchors. This epoxy filled any gap between the anchor and the concrete. The exposed anchor fibers were then splayed as evenly as possible into a circular pattern. An extra epoxy layer was then carefully applied over top of the splays. The splays were covered with plastic sheathing and a short wood block was placed on top to keep them flat on top of the FRP sheet during the curing process.

The Sika anchors were fabricated by cutting a desired sized rectangular piece from the FRP sheet, as shown in Figure 3.7. The anchors were then formed by applying epoxy to both sides of the FRP piece and then rolling the sheet into a cylinder. Applying epoxy to the FRP before rolling it ensured full impregnation of the anchor. (Niemitz, 2008) rolled anchors prior to saturating with epoxy, and noted that in one specimen anchor shear occurred due to the epoxy not fully impregnating the embedded portion of the anchors. The length of the sheet is equal to the embedment depth of the anchor plus roughly half the splay diameter; which equaled 83 mm [3.25 in.] for the anchors , since the embedment depth was 50 mm [2 in.] and the splay diameter was 65 mm [2.5 in.]. To ensure that the anchor splay diameters were consistent, the anchors were rolled and inserted into the predrilled holes before applying epoxy, and trimmed until the desired splay diameter was obtained, as shown in Figure 3.8. There is limited guidance on what width of sheet to use for a given anchor diameter. It was decided to use a 102 mm [4 mm] width sheet for 12.7 mm [0.5 in.] diameter anchors. This is the same width of sheet used

by (Niemitz, 2008). The Fyfe system uses a unique approach for anchor fabrication. For a given anchor diameter and length, the necessary weight of fibers is calculated. The anchors are then fabricated by bundling an amount of individual fibers that equals this weight, unlike the Sika anchors, that were fabricated by rolling a certain width of FRP sheet. The bundle of anchors is then folded in half and secured with rubber bands at both ends. The bent end is the end that is inserted into the anchor hole. The anchors were cut to a desired length like the Sika anchors, and then saturated with epoxy by immersing the anchor in epoxy until the anchors were fully saturated, as shown in Figure 3.10. The epoxy was also gently rubbed into the anchor by hand. The epoxy impregnation process was approximately 15 minutes long. Figure 3.5 compares an unsaturated Fyfe anchor with an unsaturated Sika anchor.

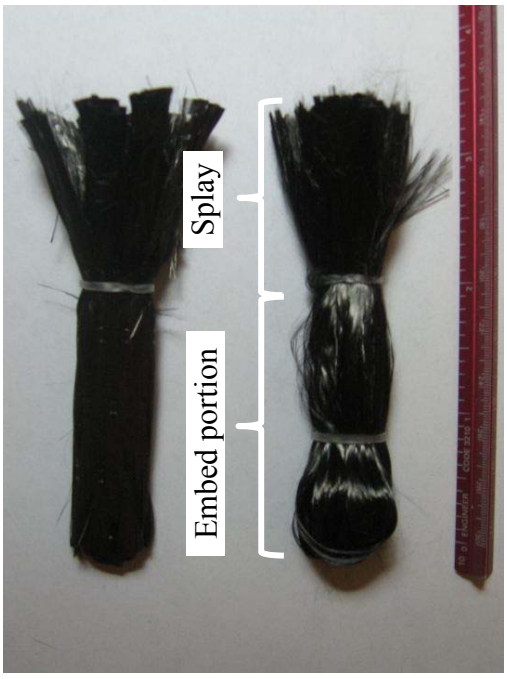

Figure 3.5 Handmade Sika anchor (Left), Fyfe anchor (Tyfo® SCH Fibr™ Anchors) (Right)

(a) **(b)**

Figure 3.6 Concrete surface before grinding (a) and after grinding (b)

(a) **(b)**

Figure 3.7 Prepared concrete surface, with anchor holes (a) and FRP pieces cut from the roll for the sheet and anchors (b)

Figure 3.8 FRP anchors are trimmed, prior to applying epoxy, to ensure correct splay diameters

(a) **(b)**

Figure 3.9 (a) The two component epoxy is mixed with a mixing paddle attached to a drill and (b) epoxy is applied to the surface as a surface primer

(a) **(b)**

Figure 3.10 Left: Epoxy is applied two both sides of FRP sheet to ensure complete impregnation. Right: FRP anchors are soaked in a bag of epoxy.

Figure 3.11 FRP sheet is laid onto concrete surface starting from one end. A paint roller is used to eliminate trapped air. A second layer of epoxy is applied to the sheet.

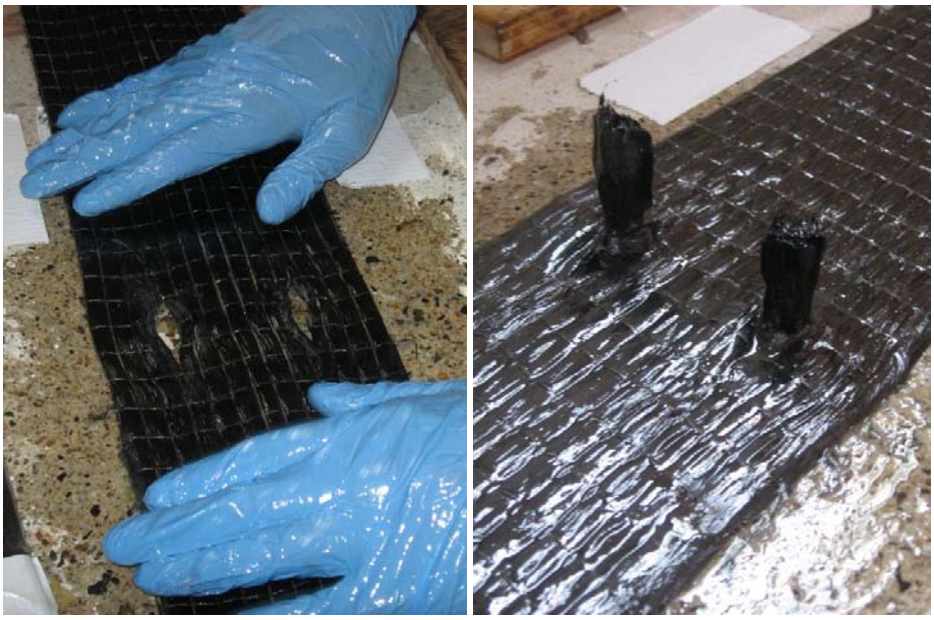

(a) (b)

Figure 3.12 (a) Fiber bundles of the FRP sheet are spread at the anchor holes, to allow for insertion of the anchor. This requires the transverse fibers to be cut. (b) FRP anchors inserted into the anchor holes, prior to forming splay.

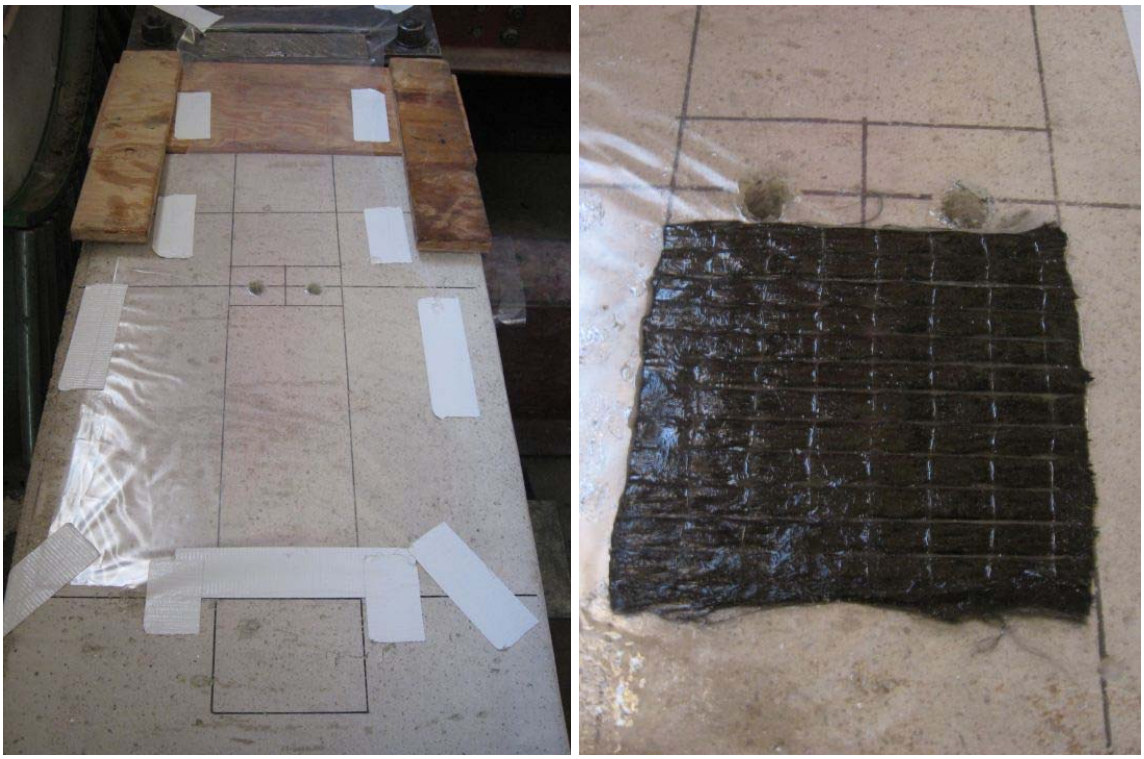

(a) (b)

Figure 3.13 (a) Setup for specimens F1-2a-24U and F4a-1-24U. (b) Prior to application of FRP sheet a transverse sheet was placed under specimen to prevent anchors from splitting the specimen.

3.5 Instrumentation and Data Acquisition

Load was recorded using a 50-kip (222.4 kN) load cell attached to a hydraulic ram. Strain distribution in the sheets was measured with transversely and longitudinally spaced strain gauges, with 119.5 ± 0.5 Ω electrical resistance and a gage length of 3 mm. Strain gauge and load cell data were recorded using a Hewlett Packard 3852 data acquisition system. The focus of the strain instrumentation was on capturing the longitudinal and transverse distribution of strain on the FRP sheet. Previous research at UMass Amherst has shown that strain tends to vary erratically across the width of the sheet, making it difficult to draw meaningful conclusions from strain readings. This is partly because the debonding front often propagates at an angle, rather than perpendicular to the length of the sheet. Transverse strain recordings, however, allow identifying the effect of FRP anchors on strain distribution compared with sheets without anchors. Strain readings along the centerline of the sheet will typically give a better idea of the location of the debonding front, and how strain varies along the length of the sheet, since they are less affected by the variable angle of the debonding front. Longitudinal strain distribution is also useful in determining the effectiveness of anchors. An ideal anchor configuration would have peak strains in front of the anchors and zero strain behind the anchor. Strain gauge locations and instrument notation as well as sheet dimensions and anchor locations are shown for each test in Figure 3.14 through Figure 3.18.

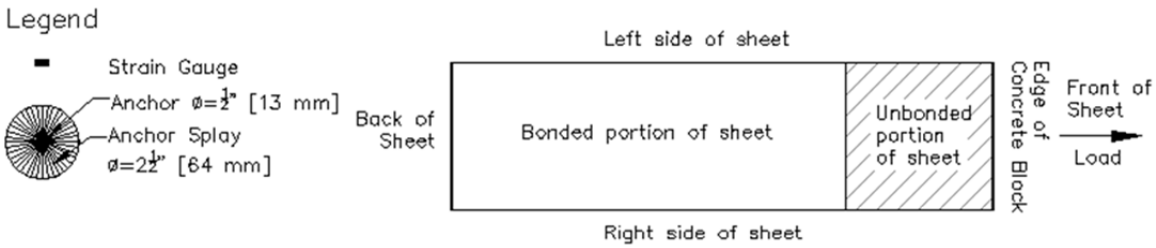

Figure 3.14 Strain gauge identification

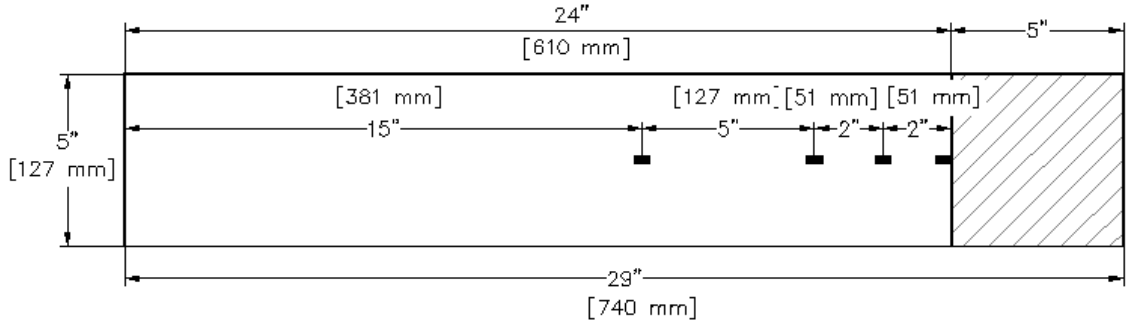

Figure 3.15 Strain gauge locations for specimens S1-0a-24, F1-0a-24, and F2-0a-24

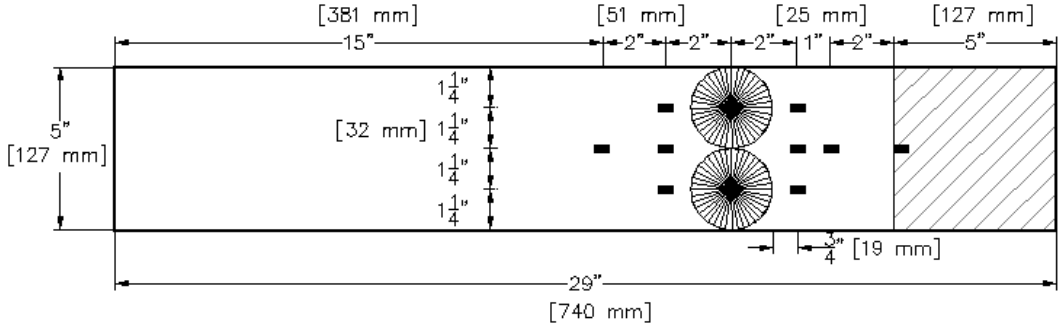

Figure 3.16 Strain gauge locations for specimens S1-2a-24, F1-2a-24, S2-2a-24, and F2-2a-24

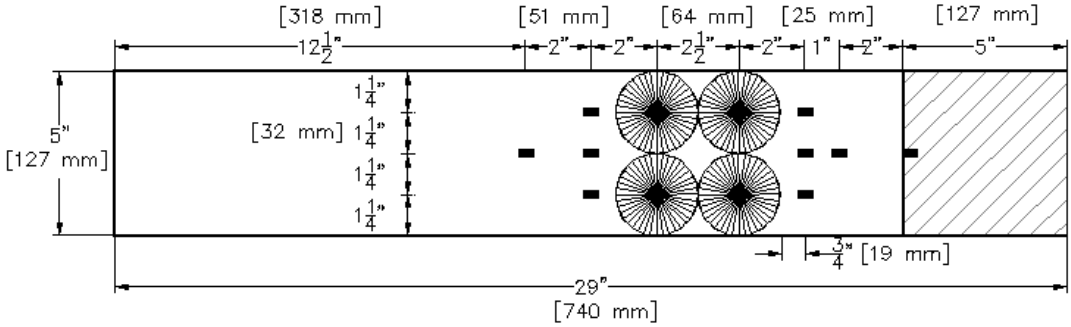

Figure 3.17 Strain gauge locations for specimens S1-4a-1-24, F1-4a-1-24, S2-4a-1-24, and F2-4a-1-24

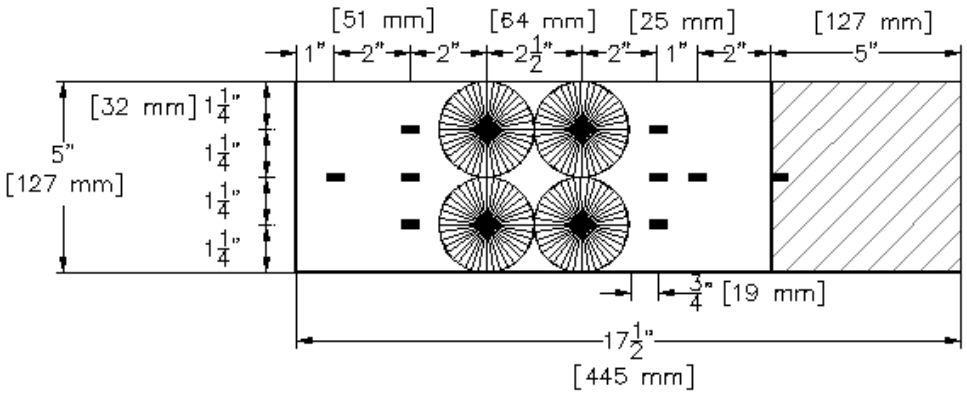

Figure 3.18 Strain gauge locations for specimen S1-4a-1-12.5

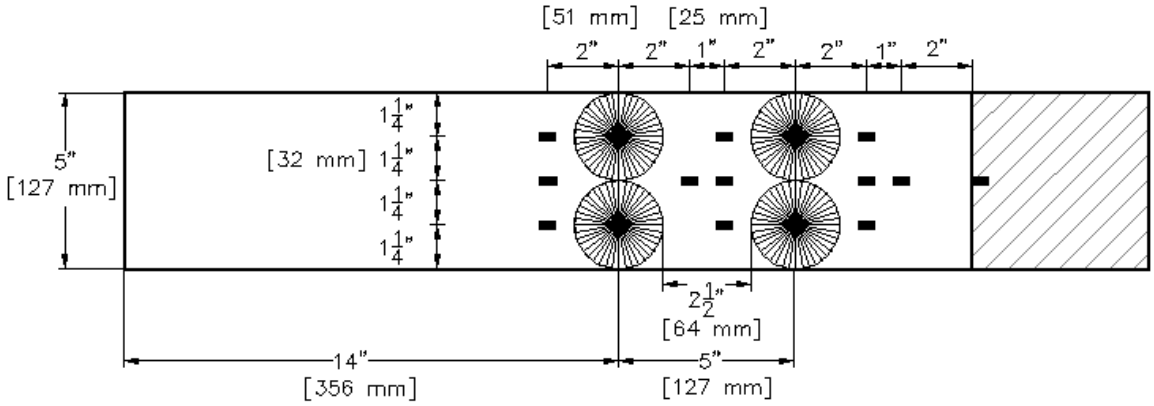

Figure 3.19 Strain gauge locations for specimens S1-4a-2-12.5 and F1-4a-2-12.5

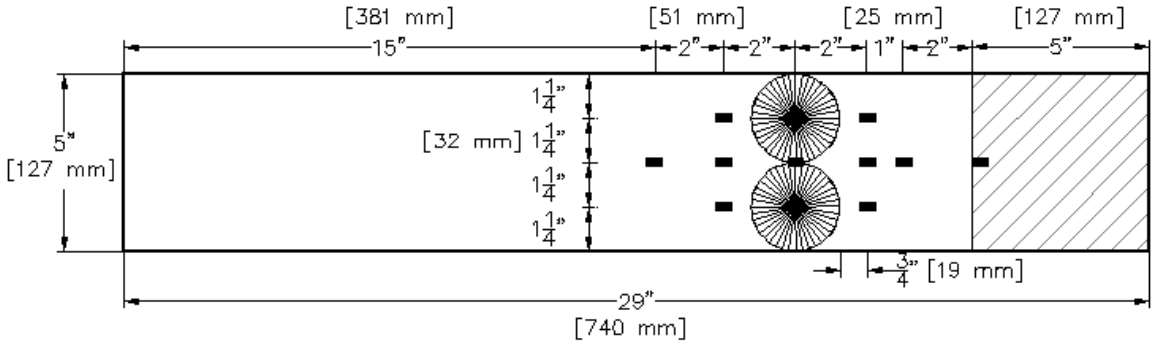

Figure 3.20 Strain gauge locations for specimen F1-2a-24U

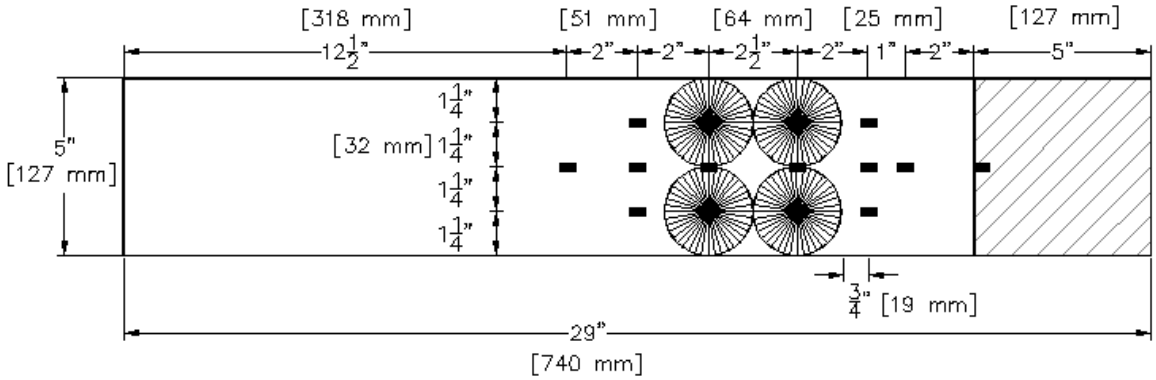

Figure 3.21 Strain gauge locations for specimen F1-4a-1-24U

The sheet dimensions and anchor locations for the Mbrace specimens tested by (Niemitz, 2008) that are similar to specimens from this research program are shown in

Figure 3.22 Specimen A-0-0-5-0 (Niemitz, 2008)

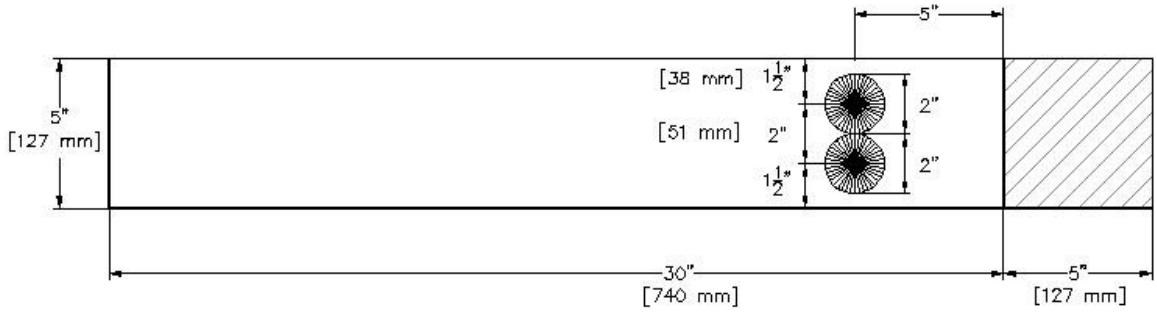

Figure 3.23 Specimen B-Y-2-5-4 (Niemitz, 2008)

through Figure 3.24. The performance of the Mbrace specimens is compared to the Sika and Fyfe specimens in section 5.2.

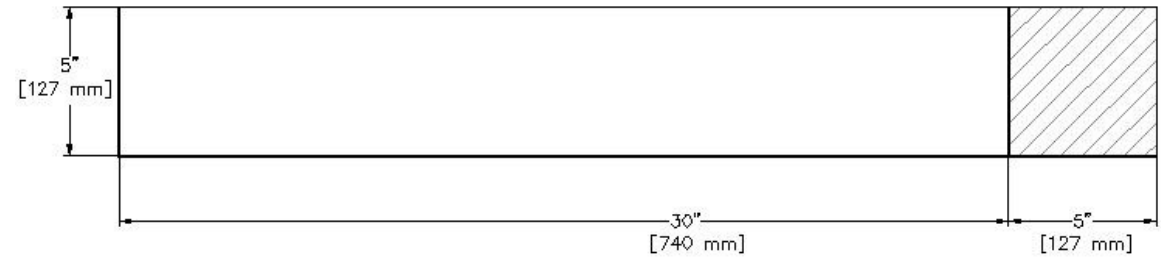

Figure 3.22 Specimen A-0-0-5-0 (Niemitz, 2008)

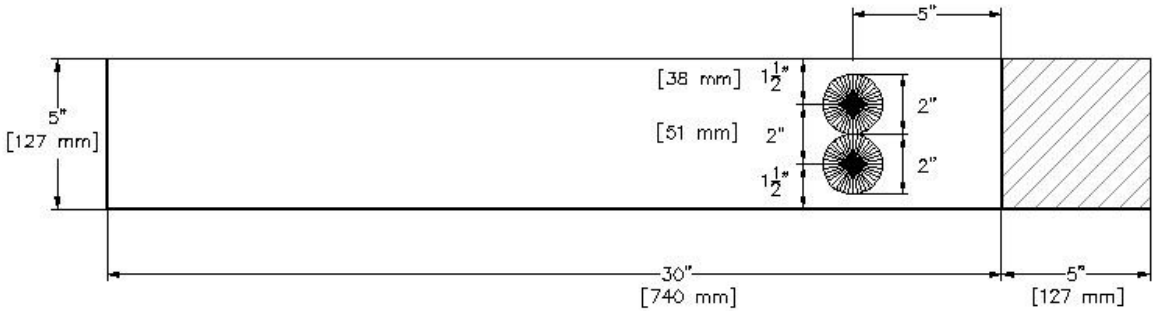

Figure 3.23 Specimen B-Y-2-5-4 (Niemitz, 2008)

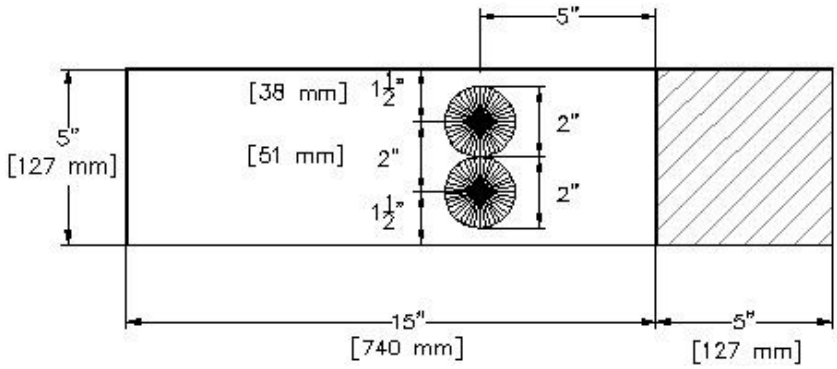

Figure 3.24 Specimen B-X-2-5-4 (Niemitz, 2008)

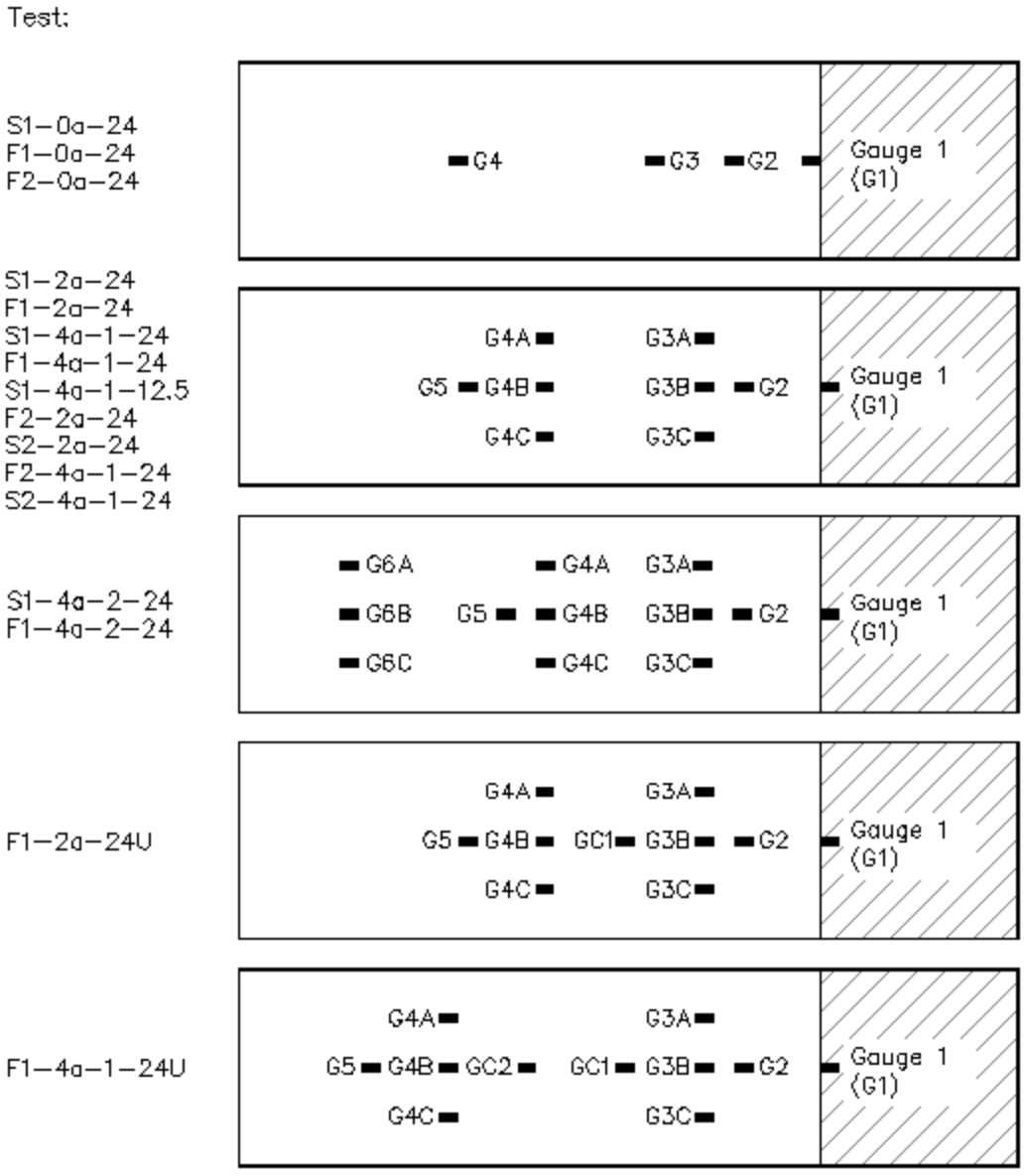

Figure 3.25 Strain gauge identification

In addition to strain gauges, specimens F1-2a-24U and F1-4a-24U were instrumented with two and four displacement gauges, respectively. Figure 3.26shows how the four displacement gauges of specimen F1-4a-24U are set up. The displacement gauges are held in place by clamping the gauge to a block of wood, which is attached to the concrete block with adhesive. The gauges measure displacement of the steel instrumentation angles which are adhered to the anchor splays, as shown in Figure 3.26. This setup allows the overall load on the FRP sheet to be directly compared to the displacement of the anchors.

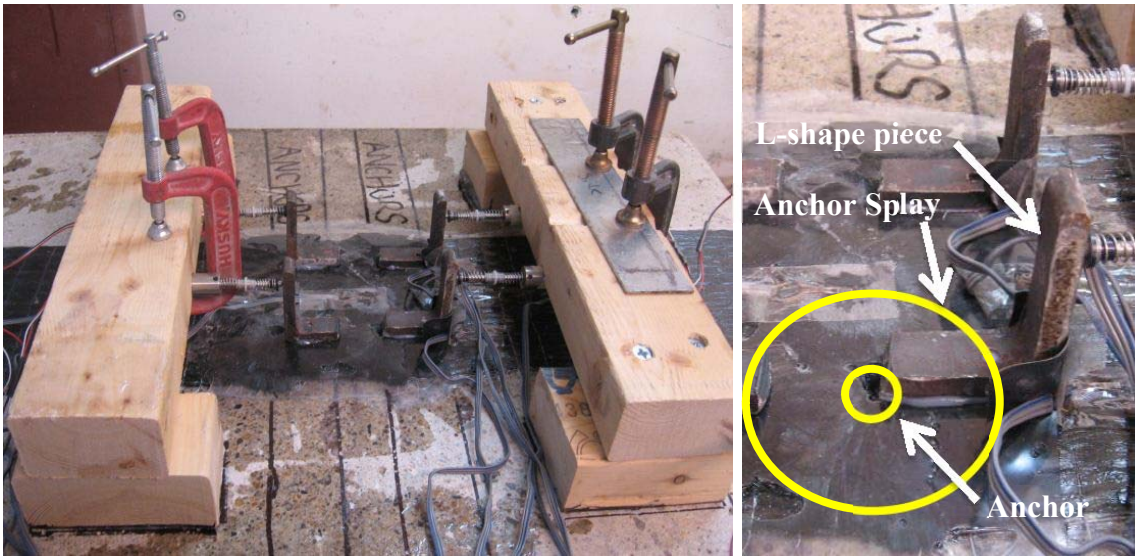

Figure 3.26 Left: Four displacement gauges for specimen F1-4a-1-24U are shown. Right: Displacement gauges measure displacement of steel instrumentation angles, which are epoxied to the anchor splays.

CHAPTER 4

OBSERVED SPECIMEN RESPONSE

4.1 Concrete Cylinder Tests

Each concrete block was poured separately. Each block required approximately eighteen 36.2 kg [80lb] bags of prepackaged concrete mix (Sakrete®) and four pours. Approximately 3.8L [4 qts.] of water were added to each bag of concrete, as directed by the manufacturer. In some cases slightly more water (not more than about 4.7 L [5 qts]) was added until the desired workability of the concrete was achieved.

Each block was used for four tests; one on each side. After the first and fourth tests on a block were conducted, three standard 4 in. diameter [102 mm] by 8 in. [203 mm] height cylinders were tested in compression and two 6 in. [153 mm] diameter by 12 in. [305 mm] high cylinders were tested to determine tensile strength (split cylinder tests). The only exception was that only two compression tests were completed for the first test of block 1 by mistake. The third compression cylinder was instead completed after the second test. After the second and third tests using a specific block, one compression test and one split cylinder test were conducted. The compression tests were performed in conformance with ASTM C39 and split cylinder tests were performed in conformance with ASTM C496. Concrete cylinder test results are summarized in

Table 4-1 and displayed graphically in Figure 4.1. In general the compressive and tensile strengths of blocks 1 and 2 were higher than the strengths of blocks 3 and 4.

Table 4-1 Concrete strength tests

Block #	Test #	# Days Cured	Cylinder #	Compressive Strength		Cylinder #	Tensile Strength	
				f'_c [MPa]	f'_c [psi]		f'_t [MPa]	f'_t [psi]
1	S1-0a-24	30	C1	34.5	5005	T1	2.3	331
			C2	33.6	4868	T2	3.4	492
			Average	34.0	4937	Average	2.8	411.3
	S1-2a-24	44	C1	33.9	4916	T1	3.5	501
			C2	31.8	4605			
			Average	32.8	4761	Average	3.5	501.4
	S1-4a-1-24	56	C1	29.9	4332	T1	3.3	479
			Average	29.9	4332	Average	3.3	479
	S1-4a-1-12.5	64	C1	34.5	5003	T1	3.5	505
			C2	34.4	4984	T2	3.3	475
			C3	32.5	4711			
			Average	33.8	4899	Average	3.4	490.3
2	S1-4a-2-24	28	C1	35.7	5184	T1	3.2	465
			C2	35.5	5155	T2	3.1	443
			C3	33.0	4793			
			Average	34.8	5044	Average	3.1	454.2
	F1-0a-24	36	C1	35.2	5112	T1	3.4	494
			Average	35.2	5112	Average	3.4	493.7
	F1-4a-1-24	47	C1	35.2	5101	T1	3.0	436
			Average	35.2	5101	Average	3.0	435.7
	F2-2a-24	91	C1	33.6	4875	T1	2.9	420
			C2	37.2	5390	T2	3.0	435
			C3	36.1	5235			
			Average	35.6	5166	Average	2.9	427.4
3	F1-2a-24	42	C1	32.7	4739	T1	3.1	451
			C2	31.1	4516	T2	2.8	401
			C3	30.5	4419			
			Average	31.4	4558	Average	2.9	426.0
	F1-4a-2-24	50	C1	29.2	4235	T1	2.3	341
			Average	29.2	4235	Average	2.3	340.5
	F2-0a-24	57	C1	31.5	4562	T1	2.9	419
			Average	31.5	4562	Average	2.9	418.5
	F2-4a-1-24	65	C1	34.4	4989	T1	2.3	338
			C2	29.4	4263	T2	3.3	481
			C3	31.5	4574			
			Average	31.8	4609	Average	2.8	409.1
4	S2-4a-1-24	28	C1	25.6	3710	T1	2.4	352
			C2	29.7	4313	T2	2.7	387
			C3	34.7	5031			
			Average	30.0	4351	Average	2.5	369.1
	S2-2a-24	34	C1	25.7	3728	T1	2.0	288
			Average	25.7	3728	Average	2.0	288.3
	F1-2a-24U	43	C1	28.7	4165	T1	2.5	368
			Average	28.7	4165	Average	2.5	367.6
	F1-4a-1-24U	56	C1	30.4	4410	T1	3.2	469
			C2	28.0	4061	T2	2.0	297
			C3	29.5	4273			
			Average	29.3	4248	Average	2.6	383.2

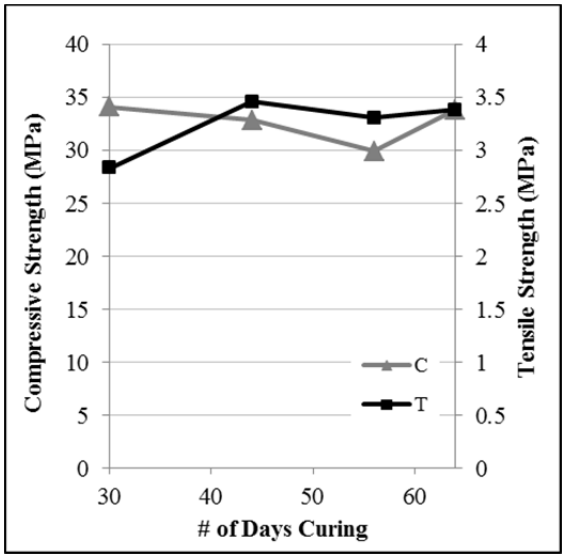

(a)

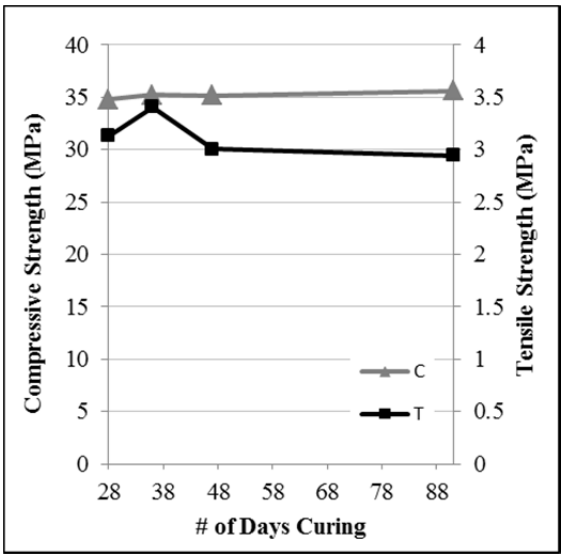

(b)

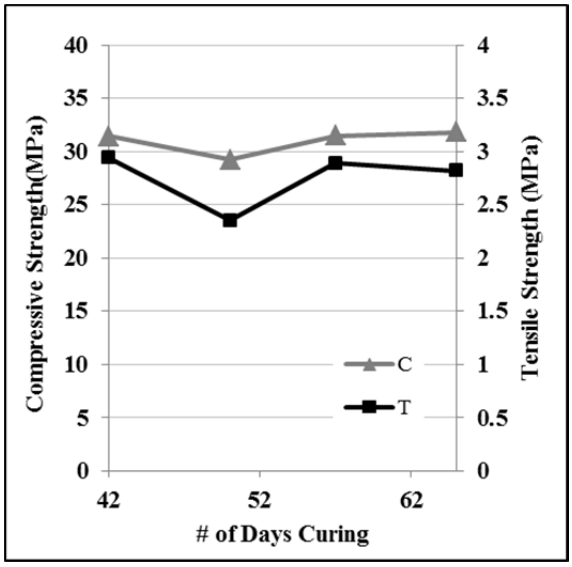

(c)

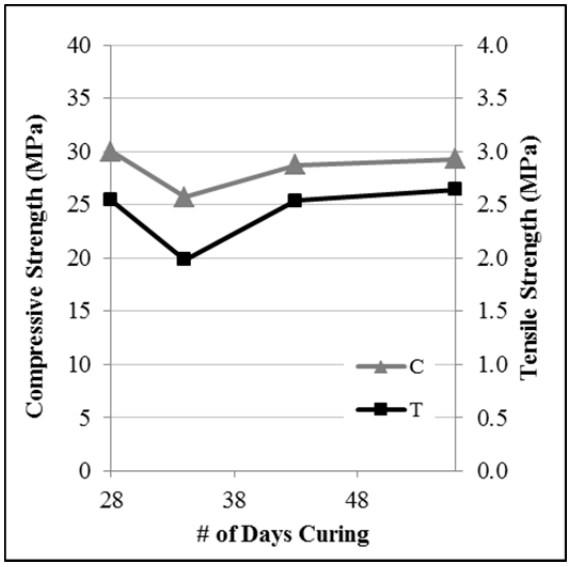

(d)

Figure 4.1 Concrete cylinder results for Block 1 (a), Block 2 (b), Block 3 (c) and Block 4 (d)

4.2 Observed Behavior of Specimens

This section gives a detailed description of each of the sixteen tests performed as part of this research program. The sequence of events leading to total failure of the specimen, the maximum load achieved, and the condition after failure of each specimen are discussed. The specimens are grouped according to the test categories shown in the

test matrix in Figure 3.4; unanchored baseline tests, anchored single ply tests, double ply tests, and unbonded tests. The following sections summarize test observations. Subsequent sections primarily discuss the strain and displacement results of each test.

Included in each test description are pictures of the state of the specimen and concrete surface after failure. A video was taken of every test except S1-0a-24 and S1-4a-1-12.5. The depth of the concrete failure was measured by laying a level across the surface of the concrete, and measuring with a thin ruler the distance from the level to the damaged surface. The thickness of concrete attached to the sheet was measured using a caliper and subtracting the thickness of the sheet. The front, back, left and right sides of the FRP sheet are defined in Figure 4.2. The same orientation is used when describing the concrete block. All pictures, unless otherwise noted, are aligned such that the top of the picture corresponds to the loading end of the sheet. In the pictures, the extent of debonding is marked with a solid line. FRP failure, either by sheet rupture or anchor splay rupture is shown with a dotted line, and splay delamination is shown with a dashed line.

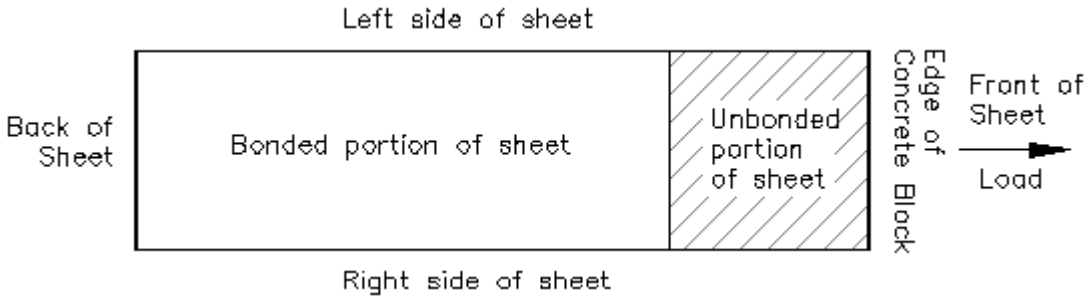

Figure 4.2 Reference orientation of the sheet

Table 4-2 presents the failure modes and loads of all of the specimens, including three Mbrace specimens tested by (Niemitz, Carl, 2008). The failure modes are listed in order of prominence. For instance, if debonding is listed before FRP rupture, than failure was due primarily to debonding, although FRP rupture also occurred.

Table 4-2 Summary of Specimen Failure Modes and Loads

Test Specimen	Bond Length	Bond Width	Concrete f'_c	Concrete f'_t	Capacity of the Sheet P_{ult}	Failure Load P_{test}	P_{test}/P_{ult}	Failure Mode
S1-0a-24	24”	5”	34	2.8	24,640	9,750	39.6%	Debonding
F1-0a-24			35.2	3.4	25,500	11,200	43.9%	Debonding
S1-2a-24			32.8	3.5	24,640	17,500	71%	Debonding,Anchor splay rupture and delamnination
F1-2a-24			31.4	2.9	25,500	18,120	71.1%	FRP Rupture
S1-4a-1-24			29.9	3.3	24,640	21,060	85.5%	FRP debonding and rupture, and anchor splay rupture and delamination
F1-4a-1-24			35.2	3	25,500	23,970	94%	FRP Rupture
S1-4a-2-24			34.8	3.1	24,640	14,140	57.4%	FRP debonding, FRP rupture, splay delamination and splay rupture
F1-4a-2-24			29.2	2.3	25,500	25,100	98.4%	FRP Rupture, minor splay delamination
S1-4a-1-12.5	12.5"		33.8	3.4	24,640	20,600	83.6%	Anchor splay delamination, FRP rupture and debonding
F2-0a-24	24”		31.5	2.9	51,000	15,700	30.8%	FRP debonding
F2-2a-24			35.6	2.9	51,000	33,830	66.3%	FRP debonding and splay delamination and
S2-2a-24			25.7	2	49280	26,300	53.4%	Debonding and anchor splay delamination
F2-4a-1-24			31.8	2.8	51,000	41,000	80.4%	Debonding, FRP rupture and splay delamination
S2-4a-1-24			30	2.5	49280	35,200	71.4%	Splay delamination, FRP debonding
F1-2a-24U	-	-	28.7	2.5	25,500	13,900	54.5%	Splay delamination
F1-4a-1-24U	-	-	29.3	2.6	25,500	14,000	54.9%	Anchor splay delamination and FRP rupture
Mbrace Specimens (Niemitz, 2008)								
A-0-0-5-0	30"	5"	28.6	-	17,600	8,000	45.5%	Debonding
B-Y-2-5-4			35.4	-	17,600	12,420	70.6%	FRP Rupture, Debonding
B-X-2-5-4	15"		35.9	-	17,600	13,610	77.3%	FRP Rupture, Delamination, Debonding

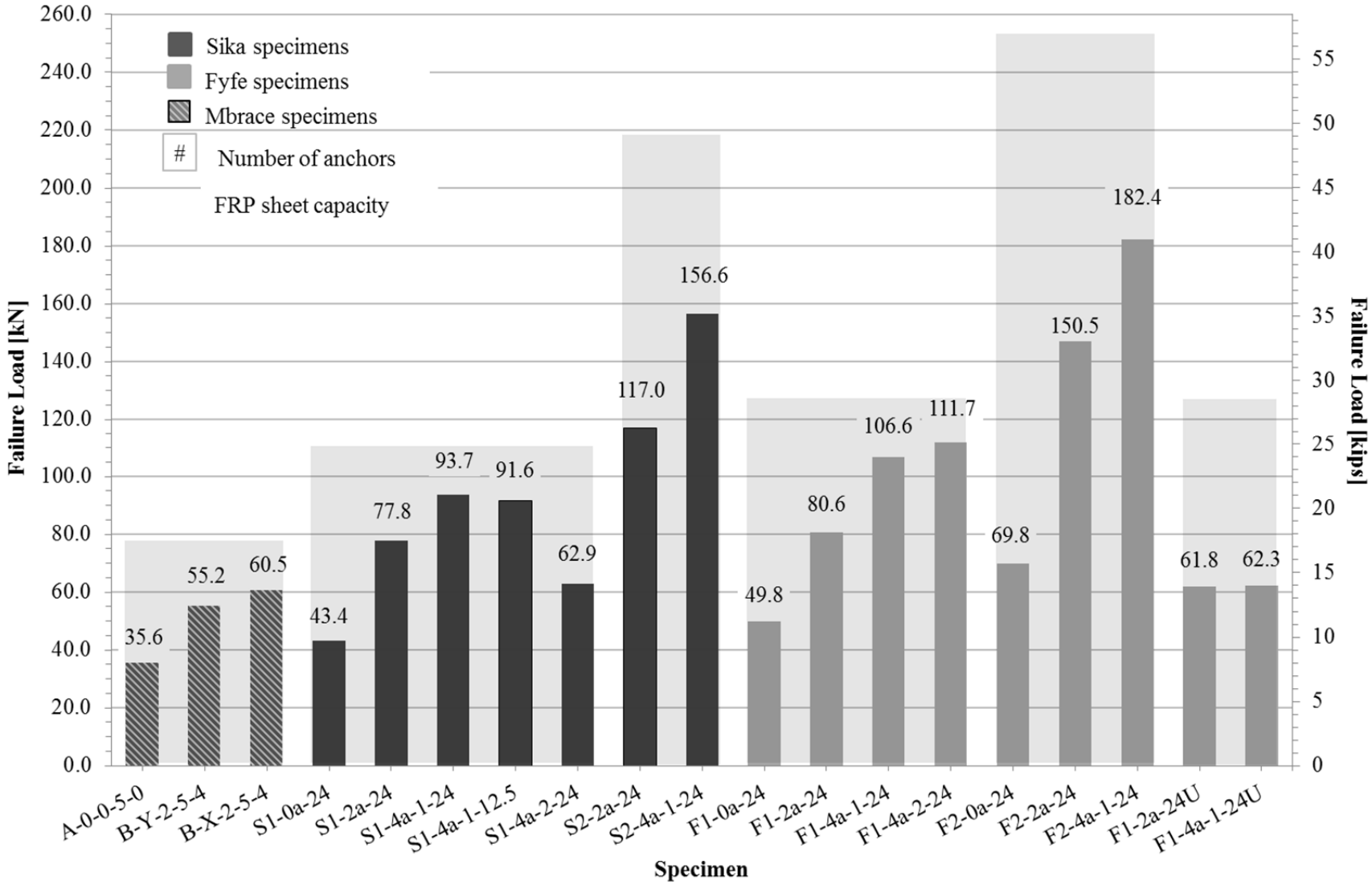

Figure 4.3 Specimen failure loads

4.2.1 Unanchored Baseline Tests

This section presents test observations for specimens S1-0a-24 and F1-0a-24. These specimens were single ply and were bonded to the concrete blocks but did not contain any anchors.

4.2.1.1 Specimen S1-0a-24

Specimen S1-0a-24 failed by debonding. A layer of concrete between 0 to 4 mm [0-0.16 in.] thick remained attached to the sheet as shown in Figure 4.4 (a). The surface of the concrete had scattered pieces missing, most 4 to 5 mm [0.16 to 0.2 in.] deep. In the last 50 to 75 mm [2 to 3 in.] of the FRP sheet on the unloaded end, concrete failure was more substantial, with a denser cluster of pieces missing around 9 mm [0.35 in.] in depth. Figure 4.4 (a) shows randomly distributed patches where the adhesive is visible, indicating that debonding occurred within the adhesive layer. However, the Figure 4.4 (b) shows that in many of these places there are diagonal cracks that extend into the concrete several millimeters, indicating that failure occurred in both the adhesive layer and within a shallow layer of concrete.

Cracking noises were audible at around 11.1 to 13.3 kN [2,500 to 3,000 lbs] during testing of this specimen. With increased load debonding progressed towards the unloaded end of the sheet. When debonding had progressed to a certain distance from the unloaded end there was a debonding failure at 43.4 kN [9,750 lbs], in which the rest of the sheet suddenly debonded. The highest measured load corresponds to approximately 45% of the manufacturer's published average strength of the FRP sheet (95.6 kN [21,490 lbs]). A few seconds prior to failure there was a noticeable increase in cracking noises, indicating that failure was imminent.

(a) **(b)**

Figure 4.4 Specimen S1-0a-24 after failure

4.2.1.2 Specimen F1-0a-24

Specimen F1-0a-24 failed by debonding like specimen S1-0a-24. A layer of concrete remained attached to nearly the entire sheet, as shown in

Figure 4.5, indicating that failure occurred almost entirely within a shallow layer of concrete, and not within the adhesive layer. The layer of concrete attached to the sheet was roughly uniform across the width and length of the sheet, and ranged from approximately 1 to 3 mm [0.039 to 0.12 in.] in thickness, except in the last 50 to 75 mm [2 to 3 in.] of the bonded part of the sheet. Here, as with specimen S1-0a-24, failure in the concrete failure extended deeper into the block, with a denser cluster of concrete pieces missing around 9 mm [0.35 in.] in depth.

Very faint cracking noises were first audible around a load of 17.8 kN [4,000 lbs]. Then almost no cracking noises were heard until a load of approximately 40.0 kN [9000 lbs]. It is believed that debonding initiated around this load. At a load of 48.9 kN [11,000 lbs] debonding progressed from approximately 130 mm to 300 mm [5 in. to 12 in.] from the loaded end in approximately two seconds. There was a 5 second period with no debonding noises, likely caused by stress redistribution within the debonded region, followed by another period of rapid debonding from approximately 300 mm to 430 mm [12 in. to 17 in.] from the loaded end. Again debonding stopped for a couple of seconds, then progressed to approximately 500 mm [20 in.] from the loaded end, or 100 mm [4 in.] from the unloaded end, followed by sudden debonding of the remainder of the sheet at a load of 49.8 kN [11,200 lbs]. The peak load corresponds to approximately 44% of the manufacturer's published average strength of the FRP sheet (113.4 kN [25,500 lbs]). The similar behavior and loads to failure of the two bonded specimens (S1-0a-24 and F1-0a-24) clearly show that they were governed by the concrete surface tensile strength. The concrete tensile strength of the block for specimen F1-0a-24 was higher than for S1-0a-24 (see Table 4-1).

(a) **(b)**

Figure 4.5 Specimen F1-0a-24 after failure (a) and a close up of the concrete attached to the FRP sheet after failure (b)

4.2.2 Anchored Single Ply Tests

This section presents test observations for specimens S1-2a-24, F1-2a-24, S1-4a-1-24, F1-4a-1-24, S1-4a-2-24, F1-4a-2-24, and S1-4a-1-12.5. These specimens were single ply and were attached to the concrete blocks through bonding and FRP anchors.

4.2.2.1 Specimen S1-2a-24

Failure of S1-2a-24 occurred by debonding, as with all four of the unanchored specimens. The failure load was 77.8 kN [17,500 lbs], which is approximately 80% more than the failure load of S1-0a-24 of 43.4 kN [9,750 lbs].Concrete remained attached to the sheet, however, unlike the unanchored specimens, there was significantly more concrete damage in the back half of the sheet than in the front half, as observed in Figure 4.7. In the front 250 mm [10 in.] of the bonded portion of the sheet the concrete damage

was 0 mm to 3 mm [0.12 in.] deep, and in the back 350 mm [14 in.] damage was 75 mm to 125 mm [3 in. to 5 in.] deep. As with most specimens that failed by debonding, damage in the concrete extended deeper into the surface in the last 25 mm [1" in.] of the bonded section.

Faint cracking noises were audible at around 8.9 to 13.3 kN [2,000 to 3,000 lbs], becoming noticeably louder around 22.2 to 26.7 [5,000 to 6,000 lbs] and at 31.3 kN [7,000 lbs] the nearly constant cracking noises indicated that the debonding front was clearly progressing along the sheet towards the unloaded end. At 44.5 kN [10,000 lbs], the load at which specimen S1-0a-24 failed, the debonding front had just progressed to the front of the anchors. This could be observed during the test, and is consistent with negligible strain readings measured in the gauges behind anchors at this load (discussed in section 4.3.4.3.1, Figure 4.67). The anchors were successful in delaying the progression of the debonding front towards the unloaded end.

Louder and more frequent cracking noises were heard starting at a load of approximately 75.6 kN [17,000 lbs], indicating that failure was imminent. Several frames from the test video can be seen in Figure 4.6. The series of pictures in Figure 4.6 occurs in approximately one second. The video clearly shows the debonding front, which is noticeable as a change in the reflection of the light, as it propagates through the sheet. When debonding had progressed to approximately 125 mm [5 in.] from the unloaded end a sudden debonding failure occurred at a load of 77.8 kN [17,500 lbs]. At the same time both anchors fail by a combination of anchor shearing and splay delamination. Although it is difficult to say with certainty, it is believed that failure was initiated by sudden

debonding, which subsequently caused load to be transferred to the anchors and led to anchor failure.

Figure 4.8 shows the portion of the two anchor splays that delaminated from the FRP sheet (Figure 4.8 (a)) and the portions that sheared from the embedded part of the anchor and still remain attached to the FRP sheet (Figure 4.8 (b)).

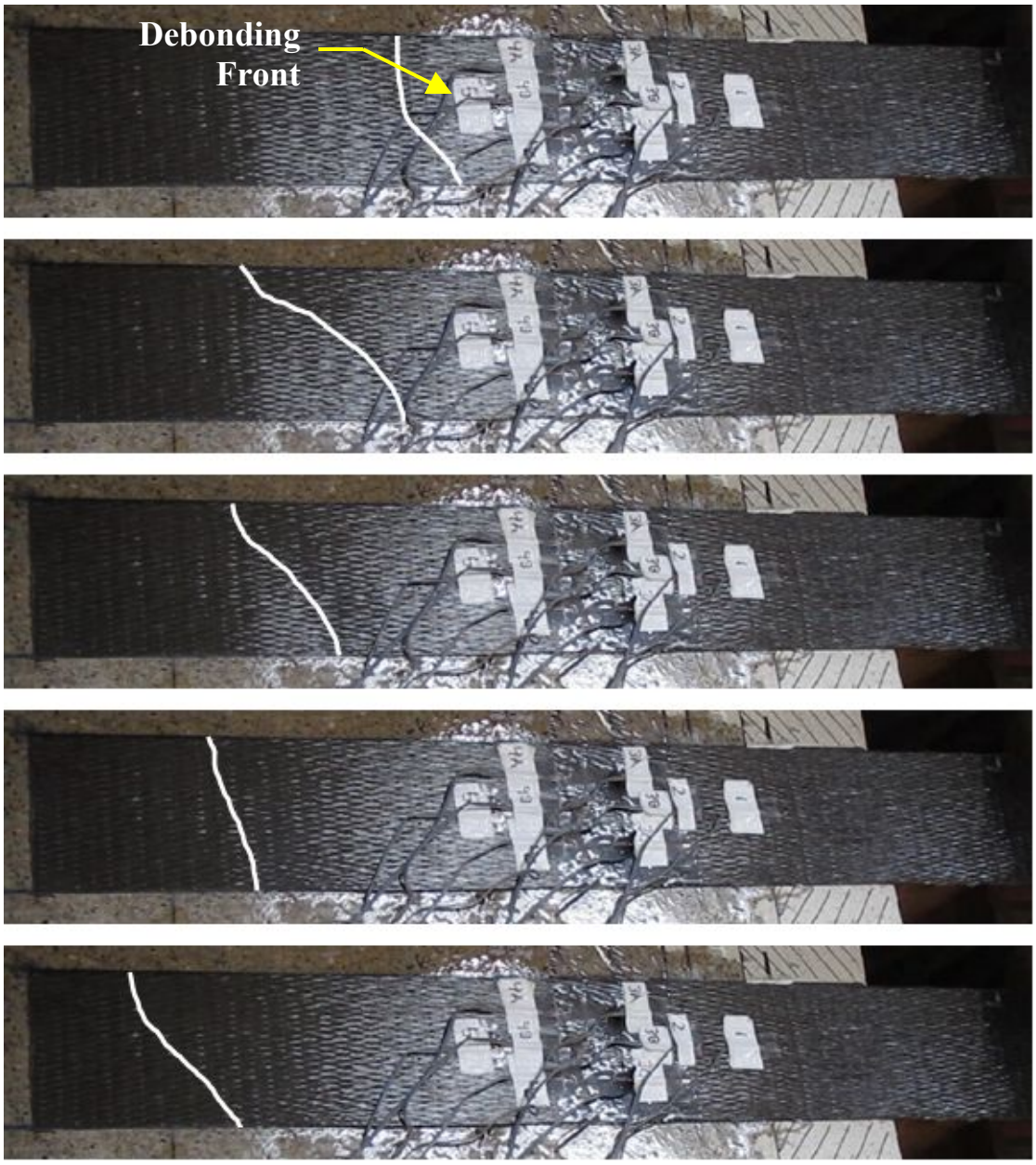

Figure 4.6 Approximate debonding front in specimen S1-2a-24

(a) (b)

Figure 4.7 Specimen S1-2a-24 after failure

(a) (b)

Figure 4.8Specimen S1-2a-24 after failure (a) and after removal of the FRP sheet to show the portion of the anchor not ruptured (b).

4.2.2.2 Specimen S1-4a-1-24

Failure of specimen S1-4a-1-24 occurred at a load of 93.7 kN [21,060 lbs]. This is 15.8 kN [3,560 lbs], or 20.3%, more than specimen S1-2a-24, which was identical except was fastened with two anchors instead of four. Failure was due to a combination FRP rupture and debonding, and anchor splay rupture and delamination, but the failure sequence could not be determined. The surface of the concrete was noticeably more damaged in front of the anchors than with specimens S1-2a-24 and 21-0a-24, with damage extending into the concrete block between 1 to 8mm [0.04 in. to 0.3 in.] deep. Behind the anchors there was minimal concrete damage, indicating that debonding occurred primarily in the adhesive layer.

Initial cracking noises were audible at around 24.5 kN [5,500 lbs]. During the test it appeared that the debonding front began progressing along the sheet at around 35.6 kN [8,000 lbs], which is supported by a jump in strain in Figure 4.69 (discussed in section 4.3.4.3.3). Leading up to failure, cracking noises slowly increased in intensity and frequency. Debonding progressed towards the unloaded end of the sheet until it reached the trailing anchors at a load of approximately 53.4 kN [12,000 lbs], where it stopped until failure. Load increased to the failure load of 93.7 kN [21,060 lbs], followed by a sudden violent failure.

It is difficult to tell from the test video how failure initiated. Figure 4.9 shows the first frame of the test video showing failure. It appears that 25 mm [1 in.] widths of sheet between the anchors and on the left edge of the sheet debond from the concrete, delaminate from the anchor splays and/or rupture the anchor splays, at the same instance that there is rupture across the rest of the sheet in front of the anchors, as shown in Figure

4.10 (b). The extent of debonding after failure is shown in Figure 4.10 (a) by a solid yellow line. 25 mm [1 in.] width strips in the center and on the left side of the sheet completely debonded. As with specimen S1-2a-1-24 the FRP anchors failed by a combination of FRP rupture and splay delamination, as shown in Figure 4.10 (b).

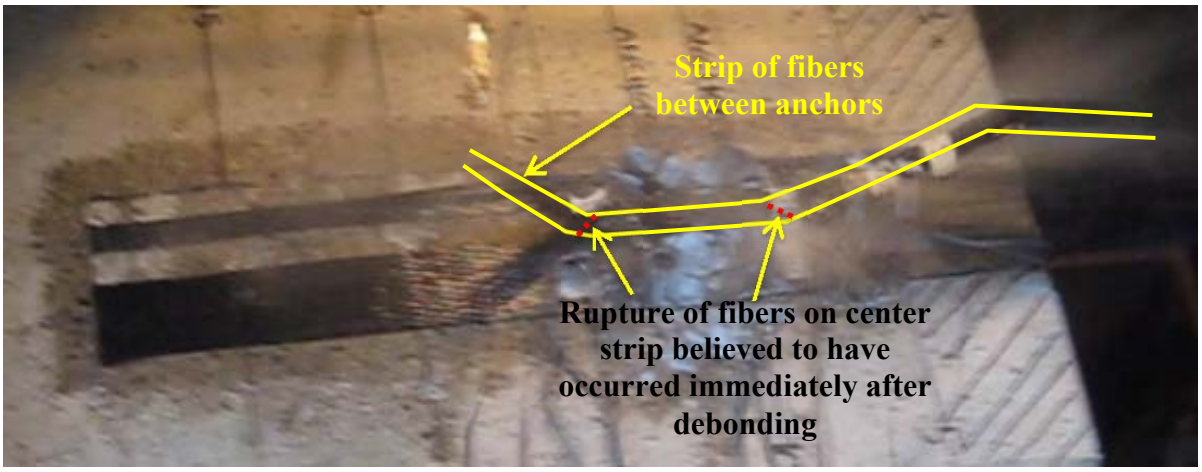

Figure 4.9 First frame from test video of specimen S1-4a-1-24 showing failure

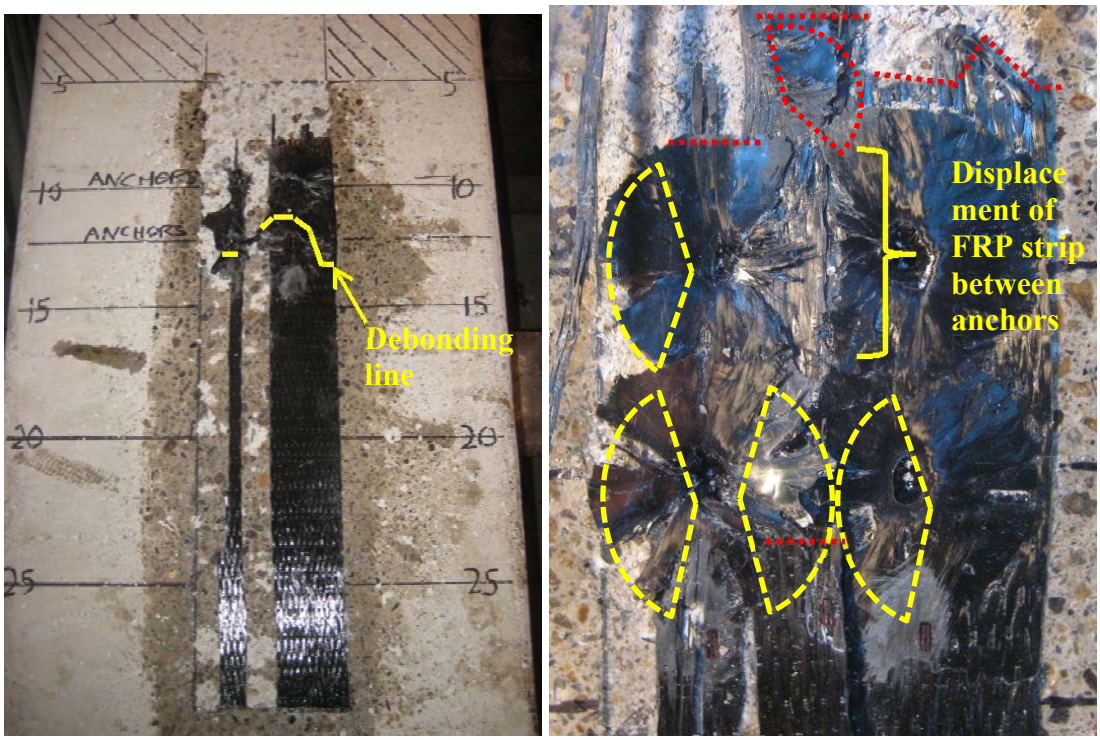

(a) **(b)**

Figure 4.10 Specimen S1-4a-1-24 after failure

4.2.2.3 Specimen S1-4a-1-12.5

Failure of test S1-4a-1-12.5 occurred at a load of 91.7 kN [20,600 lbs], compared to specimen S1-4a-1-24 which failed at 93.7 kN [21,059 lbs], or only 2% more. This indicates that the length of sheet behind the trailing anchor had practically no effect on capacity. The failure mode also appeared to be very similar in the two specimens, and consisted of FRP rupture and debonding, and anchor splay rupture and delamination. Again the failure sequence could not be determined during the test.

Initial cracking noises were audible at around 15.6 kN [3,500 lbs]. At a load of around 40.0 kN [9,000 lbs], there was an increase in cracking noises, indicating the initiation of debonding, consistent with an increase in measured strains in Figure 4.71 (discussed in section 4.3.3.2.7). At 44.5 kN [10,000 lbs] the debonding front was approximately 65 mm [2.5 in.] in front the leading anchor, and at 57.8 kN [13,000 lbs] it had moved to approximately 25 mm [1 in.] in front of the anchors. Debonding continued progressing towards the unloaded end of the sheet until it reached the trailing anchors, where it stopped, as in specimen S1-4a-1-24, until the failure load of 91.7 kN [20,600 lbs] was reached.

At a load of 80 kN [18,000 lb] a 6mm [0.25 in.] width of sheet on the right edge of the sheet ruptured. This could be caused by uneven loading of the sheet across its width, with higher load being applied on the right side. Although this was not visually obvious during the test, Figure 4.49 (discussed in section 4.3.3.2.7) concurs with this assumption because of higher strains measured on the right side of the sheet than on the left side. Also, Figure 4.11 (b) shows that the right half of the sheet slipped on the loading

grips, which could be due to the load exceeding the friction of the grips, or could have simply slipped after the sudden violent failure.

As with specimen S1-4a-1-24, at the same instance that FRP rupture occurred, the anchor splays delaminated, and there was complete debonding of the left half of the sheet. Minimal strain readings in gauges G4 and G5 in Figure 4.71(discussed in 4.3.4.3.5) indicate that there was a relatively small load in the FRP sheet behind the anchors just prior to failure, which indicates that failure was likely not initiated by debonding. It is possible that failure initiated by delamination of the anchor splays, which would have transferred a large amount of load to the bonded region of the sheet, causing the 25 mm [1 in.] widths of sheet in the center and on the left edge of the sheet to debond. This would then have caused a sudden transfer of load to the rest of the sheet, and would likely lead to failure of the specimen.

The majority of the sheet in front of the right anchor splay ruptured, as shown in Figure 4.11 (b). Rupture also occurred across most of the rest of the width of the sheet, however, it is believed that this occurred as a result of the sudden movement of the sheet after debonding, as with specimen S1-4a-1-24. The surface of the concrete was very similar to specimen S1-2a-1-24 with the most significant damage in front of the anchors and minimal concrete damage behind the anchors.

4.2.2.4 Specimen S1-4a-2-24

Failure of test S1-4a-2-24 occurred by a combination of FRP rupture, FRP debonding, splay delamination and splay rupture. It is believed that failure was primarily due to FRP debonding, which then triggered the other failure modes due to a sudden transfer of forces. Initial cracking noises were audible at around 24.5 kN [5,500 lbs]. At a

load of approximately 53.4 kN [12,000 lbs] a 6 mm [0.25 in.] width of sheet on the right edge ruptured, which caused a small loss in load. Two seconds later a 40 mm [1.5 in.] width of sheet adjacent to the previously ruptured sheet, slipped from the loading plates (see Figure 4.13), which caused the load to reduce approximately 6.7 kN [1,500 lbs]. Figure 4.43 (discussed in 4.3.3.2.5) shows a corresponding sudden drop in strain in gauge G3C (the gauge on the right side of the sheet in front of the anchors) at a load around 53.4 kN [12,000 lbs]. Load increased until the peak load of 62.9 kN [14,140 lbs] was reached. A few seconds prior to reaching the peak load there was visible debonding behind the first row of anchors, but still negligible strain behind the second row of anchors, as shown in Figure 4.72 and in Figure 4.45 (discussed in 4.3.3.2.5). A few seconds after debonding could be seen behind the first row of anchors, a 20 mm [0.75 in.] width of sheet, adjacent to the fibers that slipped on the plates, ruptured causing the load to drop almost 11.1 kN [2,500 lbs], and the sheet to debond past the back row of anchors. Debonding was then clearly seen progressing towards the unloaded end, with minimal increase in load, until the debonding front reached approximately 125 mm [5 in.] from the unloaded end, at which point the rest of the sheet suddenly debonded. It is believed that the left anchor splays delaminated at approximately the same time that the rest of the sheet suddenly debonded. Figure 4.12 (a) shows the extent of debonding after failure. Notice that the right side of the sheet is still bonded, since that side of the sheet slipped from the loading plates. Unfortunately the ultimate load capacity was very likely affected by this, since it prevented the full width of sheet from carrying load.

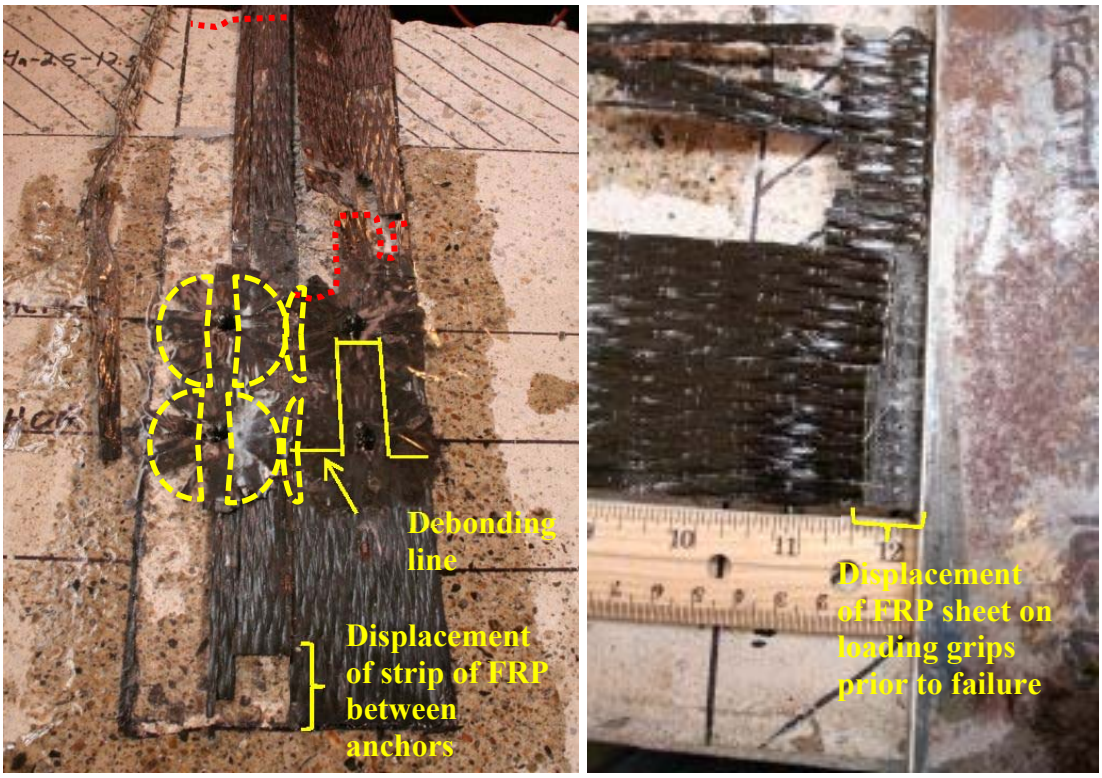

(a) (b)

Figure 4.11 Specimen S1-4a-1-12.5

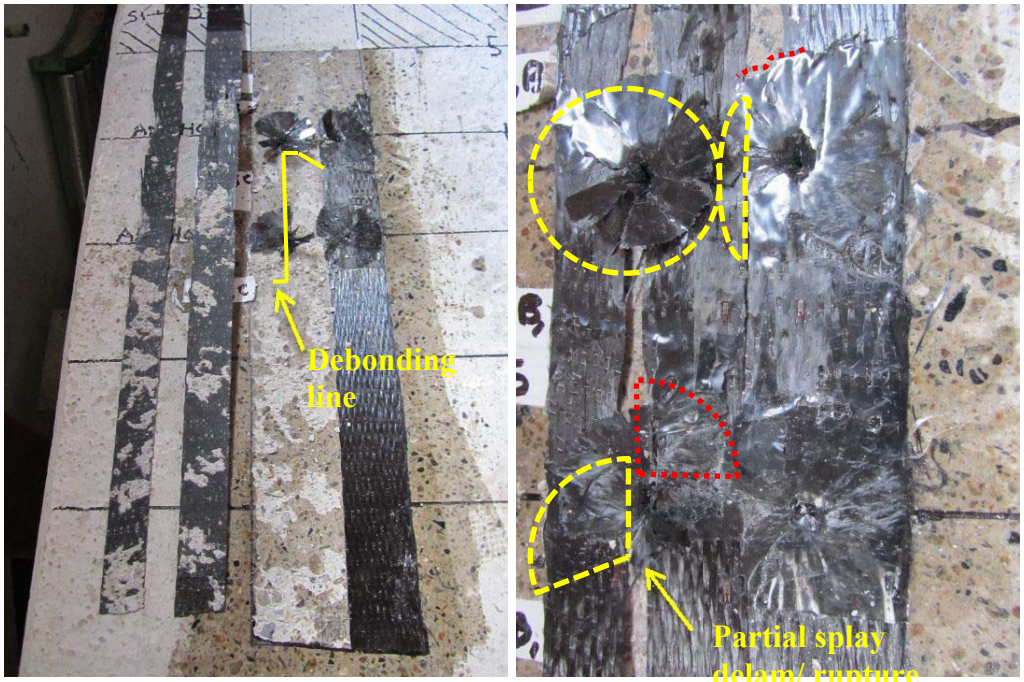

(a) (b)

Figure 4.12 Specimen S1-4a-2-24 after failure

Figure 4.13 Fibers on right side of specimen S1-4a-2-24 slipped on loading plates prior to failure (note picture is after failure)

4.2.2.5 Specimen F1-2a-24

Failure of test F1-2a-24 occurred by FRP rupture of the full width of the sheet at load of 80.6 kN [18,120 lbs], as shown in Figure 4.14. This is approximately 60% more than the failure load of specimen F1-0a-24 of 49.8 kN [11,200 lbs]. However, this load is significantly less than the manufacturer's published average strength of the FRP sheet (95.6 kN [25,500 lbs]). A possible cause for this was a slight inclination of the sheet during the test. The loading apparatus was approximately 3 mm [1/8th in.] higher than the surface of the concrete, which could have caused stress concentrations in the sheet at the location of the anchor splays when the debonding front was behind the anchors.

Initial faint cracking noises were audible at around 27 kN [6,000 lbs]. At a load of approximately 40 kN [9,000 lbs] there was suddenly more frequent cracking noises,

indicating that the debonding front was progressing towards the anchors, which is supported by a rapid increase in strain in front of the anchors in Figure 4.68 (discussed in 4.3.4.3.2) from a load of 40.39 kN to 44.75 kN [9,080 lbs to 10,060 lbs]. At a load of approximately 71.2 kN [16,000 lbs] a 12 mm [0.5 in.] width of fibers on the right side of the sheet ruptured. Figure 4.37 (discussed in 4.3.3.2.2) shows that strain was still nearly symmetric across the width of the sheet in front of the anchors at this load. Figure 4.14 shows that after failure of the specimen there was minimal anchor damage and the debonding front progressed had passed the anchors across most of the width of the sheet.

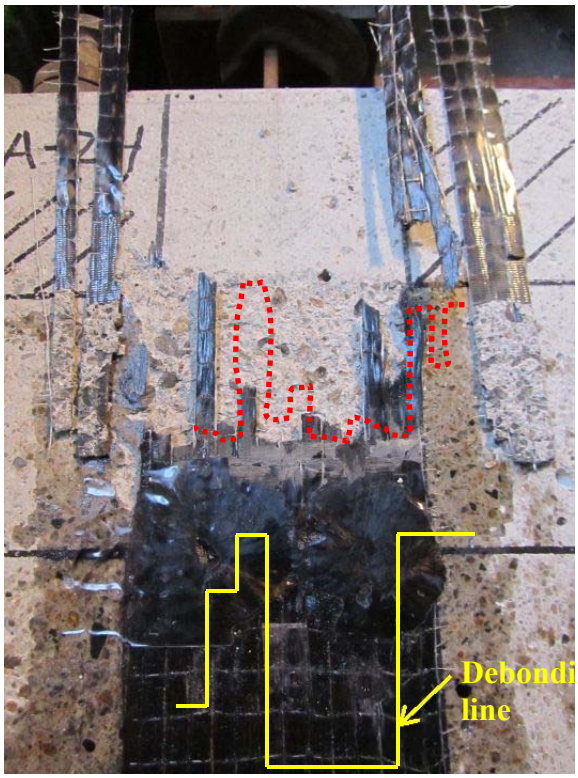

Figure 4.14 Specimen F1-2a-24 after failure

4.2.2.6 Specimen F1-4a-1-24

Failure of test F1-4a-1-24 occurred by FRP rupture at load of 106.6 kN [23,970 lbs]. This load is approximately 32% greater than the failure load of specimen F1-2a-24 of 80.6 kN [18,120 lbs]. It is also 94% of the manufacturer's published average FRP

sheet strength of 113.4 kN [25,500 lbs]. Despite nearly reaching the FRP sheet strength, Figure 4.41 and Figure 4.42 show that there was significantly more strain on the left side of the sheet than on the right, which is likely due to uneven loading across the width of the sheet. This is discussed further in Section 4.3.3.2.4. Initial faint cracking noises were audible at around 28.9 kN [6,500 lbs]. At a load of 10,000 lbs there was suddenly more frequent cracking noises, indicating that the debonding front was progressing towards the anchors, which is supported by a jump in strain in Figure 4.70 (discussed in 4.3.4.3.4). The debonding front stopped at the anchors, and cracking noises subsided, until the sudden failure due to FRP rupture across the full width of the sheet, as shown in Figure 4.15 (a). The extent of debonding is shown in Figure 4.15 (b). As can be seen, the debonding front progressed to the front of the first row of anchors, except on the edges of the sheet, where it progressed to the second row of anchors.

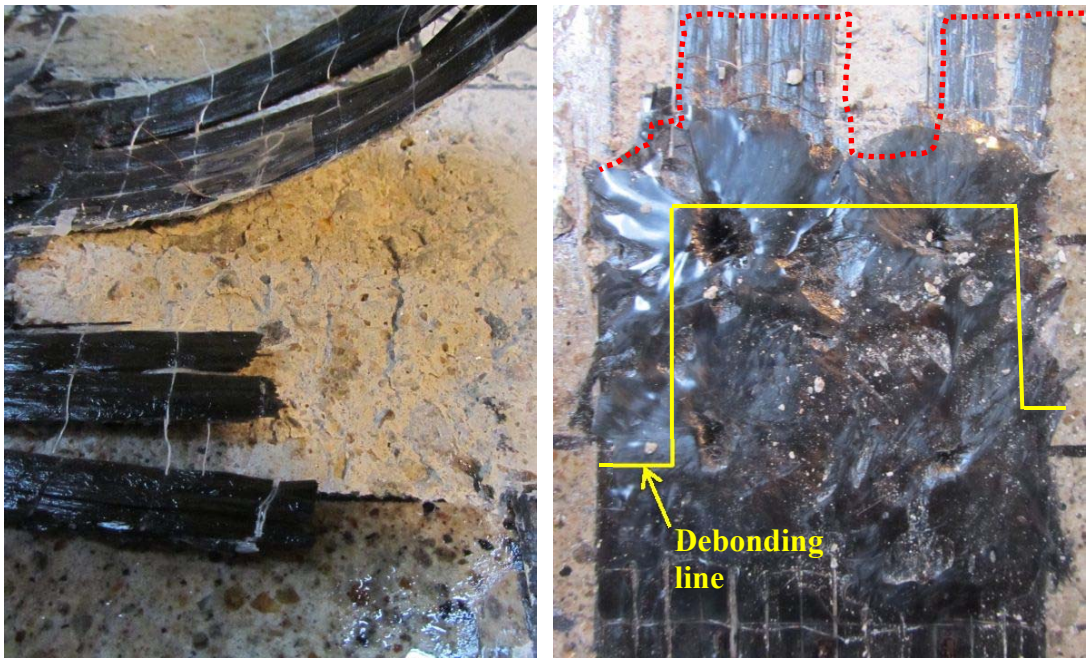

(a) **(b)**

Figure 4.15 Specimen F1-4a-1-24 after failure

4.2.2.7 Specimen F1-4a-2-24

Failure of test F1-4a-2-24 occurred by FRP rupture at a load of 111.6 kN [25,100 lbs]. This is slightly greater than the manufacturer's published average FRP sheet strength of 113.4 [kN] 25,500 lbs. This load is approximately 5% more than the failure load of specimen F1-4a-1-24 of 106.6 kN [23,970 lbs].

Initial faint cracking noises were audible at around 13.3 kN [3,000 lbs]. At a load of approximately 31.1 kN [7,000 lbs] there was suddenly louder and more frequent cracking noises, indicating that the debonding front was progressing towards the anchors, which is supported by a jump in strain in Figure 4.73 (discussed in 4.3.4.3.7). Debonding progressed to approximately 50 mm [2 in.] behind the trailing anchors, except for a 25 mm [1 in.] width of sheet in line with each of the trailing anchors, as shown in Figure 4.16 (a). The sheet ruptured across its full width in front of the front anchors. There was also rupture of two bundles of fibers in the center of the sheet, as shown in Figure 4.16 (b).

4.2.3 Double Ply Tests

This section presents test observations for specimens F2-0a-24, S2-2a-24, F2-2a-24, S2-4a-1-24, F2-4a-1-24. These specimens were double ply. The main purpose of this group of specimens was to determine the performance of double ply specimens compared to single ply specimens. For each double ply specimen there was a single ply specimen with the same dimensions and anchor arrangement. As discussed in section 5.6, interesting comparisons can also be made between the performances of anchored single ply specimens with unanchored double ply specimens, which further highlight the efficiency of using anchors. Details of each specimen, including sheet width, bonded

length and anchor locations, and strain gauge locations are given in section 3.5. As a reminder, the number of anchors used in a specimen is indicated in the specimen names by either 0a, 2a or 4a, for zero, two and four anchors, respectively.

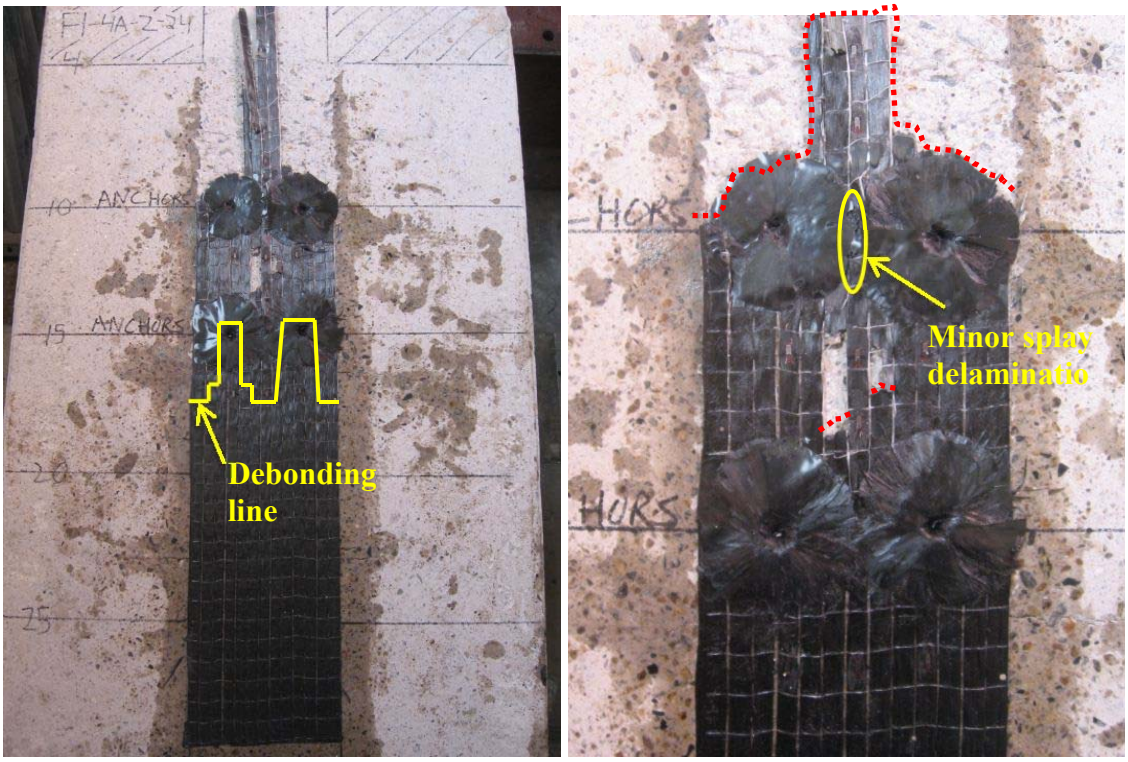

(a) **(b)**

Figure 4.16 Failure of specimen F1-4a-2-24

4.2.3.1 Specimen F2-0a-24

Failure of test F2-0a-24 occurred by FRP debonding at a load of 69.8 kN [15,700 lbs]. Figure 4.74 (discussed in 4.3.4.4.1) indicates that after reaching the peak load there was a sudden increase in the rate of debonding and the debonding front past gauge G3. This was evident during the test, and in the video, by a sudden increase in cracking noises. After reaching the peak load the load dropped approximately 1.5 kN [0.3 k]. As the applied load increased debonding continued progressing along the sheet with little change in load, and then failed suddenly by debonding of the rest of the sheet at a load of

67.0 kN [15.06 k]. This is 34% more than the failure load of the single ply specimen (F1-0a-24) of 49.8 kN [11,200 lbs]. This load is also approximately 30% of the manufacturer's published FRP sheet strength of 226.9 kN [51,000 lbs]. It was not clear during the test or in the video how far the debonding front had propagated prior to failure of the specimen.

Figure 4.17 Failure of specimen F2-0a-24

4.2.3.2 Specimen F2-2a-24

Failure of test F2-2a-24 occurred by FRP debonding and splay delamination and rupture at a load of 150.5 kN [33,830 lbs]. This is 115% more than the failure load of specimen F2-0a-24 of 69.8 kN [15,700 lbs]. This load is also approximately 66% of the manufacturer's published FRP sheet strength of 226.9 kN [51,000 lbs].

It took three attempts to fail specimen F2-2a-24. Fortunately the strain results from the first, second and final attempt converge relatively closely at higher loads, as seen in Figure 4.53 (discussed in section 4.3.3.3.2). In the first attempt to test specimen F2-2a-24 the sheet slipped from the loading grips at a load of 130.0 kN [29,300 lbs]. The only noticeable damage after the first test attempt was debonding of the sheet to the location shown in Figure 4.18 (a). For the second attempt the sheet again slipped prior to failure, at a load of 99.2 kN [22,300 lbs]. There was no noticeable change in the extent of debonding from the first attempt. A 20 mm [0.75 in] width of fibers on the left edge of the sheet ruptured during the second attempt.

For the third attempt a FRP sheet was wrapped around the top and bottom of the sheet in an attempt to repair the broken fibers as shown in Figure 4.19 (b). This sheet delaminated prior to failure, causing the applied load to drop from 139.3 kN to 132.1 kN [31,300 lbs to 29700 lbs]. Also, the strain in gauges G3A, G3B and G3C all increased suddenly by a small amount, as discussed in section (4.3.3.3.2). Unfortunately the 20 mm [0.75 in] width of fibers on the left edge were no longer loaded after the delamination of the sheet.

Failure consisted of a combination FRP debonding and anchor splay rupture and delamination, as shown in Figure 4.19 (a). The sequence of failures could not be determined during the test. However, it is believed that failure initiated by debonding, and that the sudden transfer of force to the anchors caused anchor splay failure, as shown in Figure 4.20 (a). One reason this is believed, is because there is no evidence of anchor splay damage prior to failure in the test video. Also debonding progressed past the anchors prior to failure. It is not known how far debonding progressed prior to failure,

however in the test video it appears that there was debonding 230 mm [9 in.] from the unloaded end on the right side of the sheet in approximately one second before failure. Also strain readings from Figure 4.76 (discussed in section 4.3.4.4.3) indicate that there was a relatively large amount of force in the sheet behind the anchors, which further indicates that debonding progressed past the anchors.

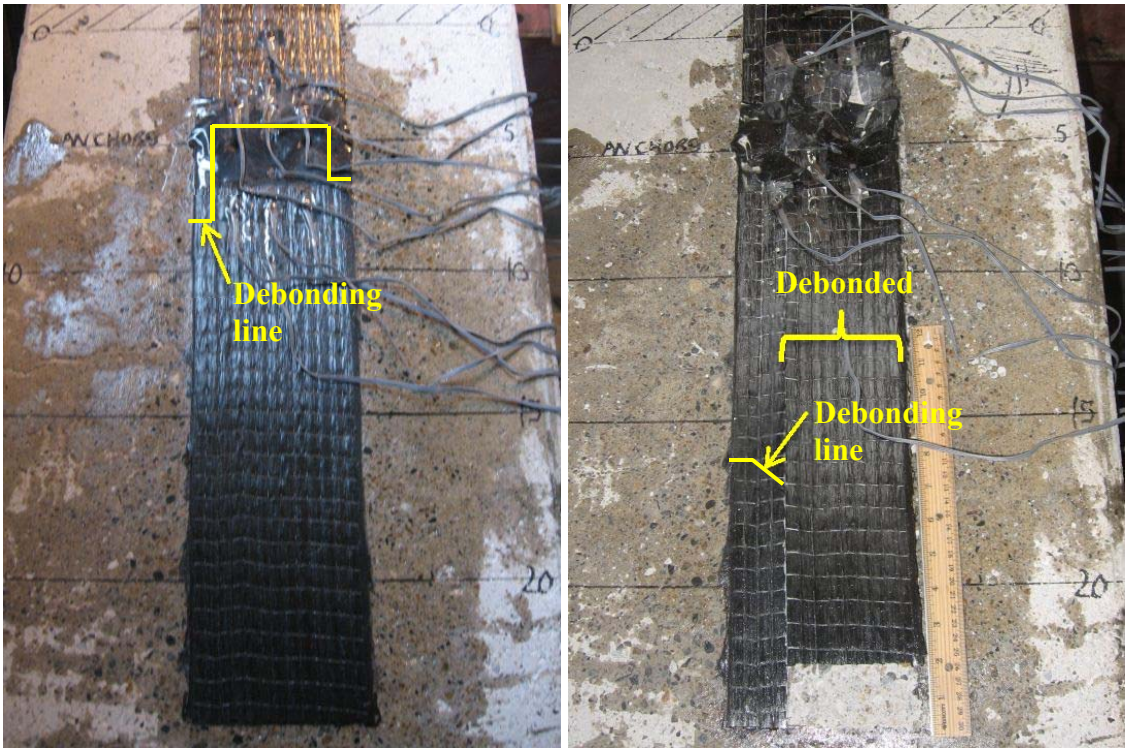

(a) **(b)**

Figure 4.18 Approximate location of the debonding front of Specimen F2-2a-24 after the first and second attempts (a). Specimen F2-2a-24 after failure (b)

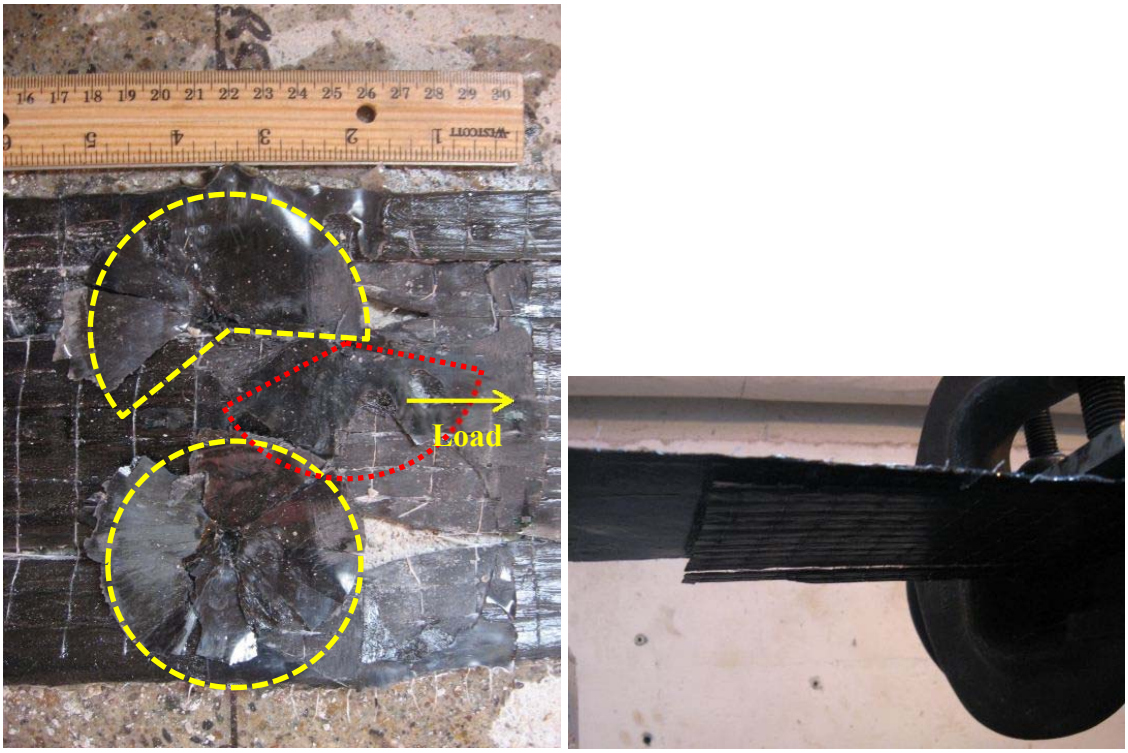

(a) (b)

Figure 4.19 Specimen F2-2a-24 after failure (a), transverse sheet wrapped around sheet to repair broken fibers (b)

Figure 4.20 1st frame from test video of specimen F2-2a-24 showing failure

4.2.3.3 Specimen F2-4a-1-24

Failure of test F2-4a-1-24 occurred at a load of 182.4 kN [41,000 lbs]. This is 160% more than the failure load of specimen F2-0a-24 of 69.8 kN [15,700 lbs]. This load is also approximately 80% of the manufacturer's published strength of the FRP sheet

equal to 226.9 kN [51,000 lbs]. It appears that failure was caused by debonding, followed almost instantly by FRP rupture, across the width of the sheet, as well as splay delamination. The specimen after failure is shown in Figure 4.21. At a load of 62 kN [14,000 lbs] an increase in cracking noises indicated that the sheet was debonding in front of the anchors, which agrees with strain readings for gauge G3B in Figure 4.78 (discussed in section 4.3.4.4.5). With increased load cracking noises subsided, indicating that the debonding front had stopped progressing at the anchors, which also agrees with Figure 4.78. At a load of about 164.6 kN [37,000 lbs] cracking noises again became noticeable more frequent and it was apparent that failure was imminent. The test video showed that at a load of 177.9 kN [40,000 lbs] debonding progressed to approximately 250 mm [10 in.] from the unloaded end, or 420 mm [16.5 in.] behind the trailing anchors, on the right side of the sheet. Two seconds later the entire sheet suddenly debonded, except for a 40 mm by 100 mm [1.5 in. wide by 4 in.] long section in the back left corner of the sheet, as shown in Figure 4.21 (a). The same frame from the test video shows the sheet ruptured and the front two anchor splays delaminated at this time.

4.2.3.4 Specimen S2-2a-24

Failure of test S2-2a-24 occurred at a load of 7.2 kN [26,300 lbs] due to debonding and anchor splay delamination. This is 50% more than the failure load of specimen S1-2a-24 of 77.8 kN [17,500 lbs]. This load is also about 61% of the manufacturer's published average FRP sheet strength of 191.2 kN [42,980 lbs]. The test video shows that at around five seconds prior to failure the anchor splays began to delaminate, with splay areas detaching from the FRP sheet. As the splays delaminated from the sheet, the sheet behind the anchors carried more load and debonding accelerated

until the sheet suddenly debonded completely. It is not clear from the test video how far debonding progressed before the sudden debonding failure of the entire sheet. However, Figure 4.75 (discussed in section 4.3.4.4.2) shows a rapid increase in strain in the gauges behind the anchors shortly before failure, clearly indicating the debonding front passing the anchors before failure.

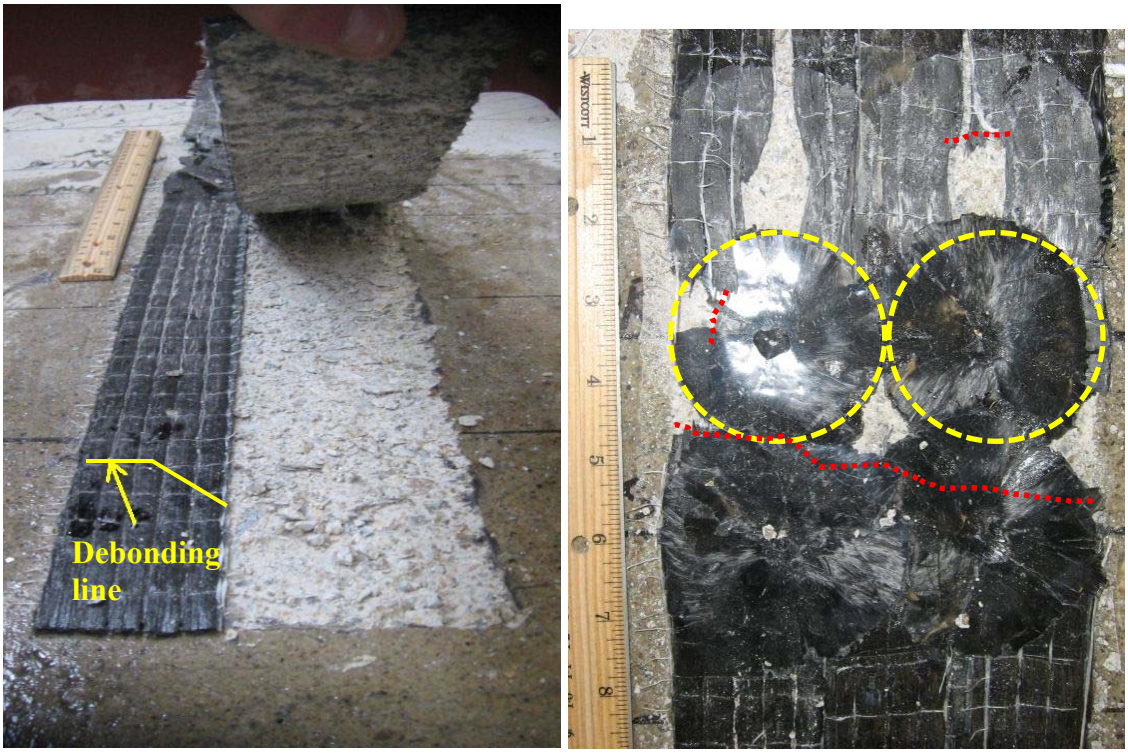

(a) **(b)**

Figure 4.21 Specimen F2-4a-1-24 after failure

Figure 4.22 (a) shows that greater concrete damage was generated and that more concrete adhered to the sheet on the left side than on the right side. Figure 4.52 (discussed in section 4.3.3.3.1) shows that behind the anchors at a load of 106.79 kN [24.01 k] the strain in gauge G4A is slightly smaller than the strain in gauge G4C, and then at a load of 115.88 kN [26.05 k] the strain in gauge G4A drops by approximately 50% while there is negligible change in strain in gauge G4C. This indicates that the left side of the sheet

debonded further than the right side prior to failure. The suddenness of the debonding at failure could have resulted in less damage on the right side.

(a)

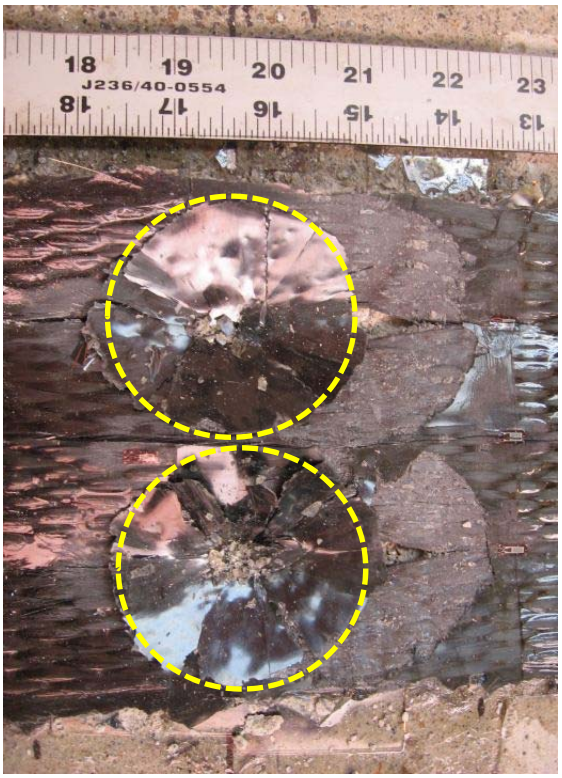

(b)

(c)

Figure 4.22 Specimen S2-2a-24 after failure (a), (b) and (c)

4.2.3.5 Specimen S2-4a-1-24

Failure of test S2-4a-1-24 occurred at a load of 156.7 kN [35,200 lbs], at which point the sheet completely debonded. This is 34% more than the failure load of specimen S2-2a-24 of 17.2 kN [26,300 lbs]. This load is also approximately 82% of the manufacturer's published average FRP sheet strength of 191.2 kN [42,980 lbs]. Initial cracking noises were heard around 20 kN [4,500 lbs].The anchor splays were almost entirely delaminated from the sheet after failure, as shown in Figure 4.23 (b). It is believed that the anchor splays delaminated prior to failure of the sheet, as with specimen S2-2a-24, except that the splays delaminated longer before failure. This would explain the uncharacteristically long period of cracking noises usually heard only shortly before debonding failure of most other specimens. From a load of about 70 kN [16000 lbs], until failure, there was nearly continuous cracking noises. Figure 4.75 (discussed in section 4.3.4.4.4) shows that there is no sudden increase of strain in the gauges behind the anchors, but strains increased approximately linearly with load until failure.

A layer of concrete remained attached to nearly the entire sheet, and had a constant thickness along the length and width of the sheet, as shown in Figure 4.23 (a). Damage to the surface of the concrete was approximately 1-3 mm [0.04 in to 0.12 in.] deep, with no increase in the damage depth at the unloaded end of the sheet, as was common with most of the tests. It is not clear from the test video how far debonding progressed before the sudden debonding failure of the entire sheet. However, as discussed in section 4.3.4.4.4, longitudinal strain gauges indicate that debonding had progressed to gauge G5 (100 mm [4 in.] behind the trailing anchors) at approximately 107 kN [24,000 lbs], which is long before the failure of the sheet.

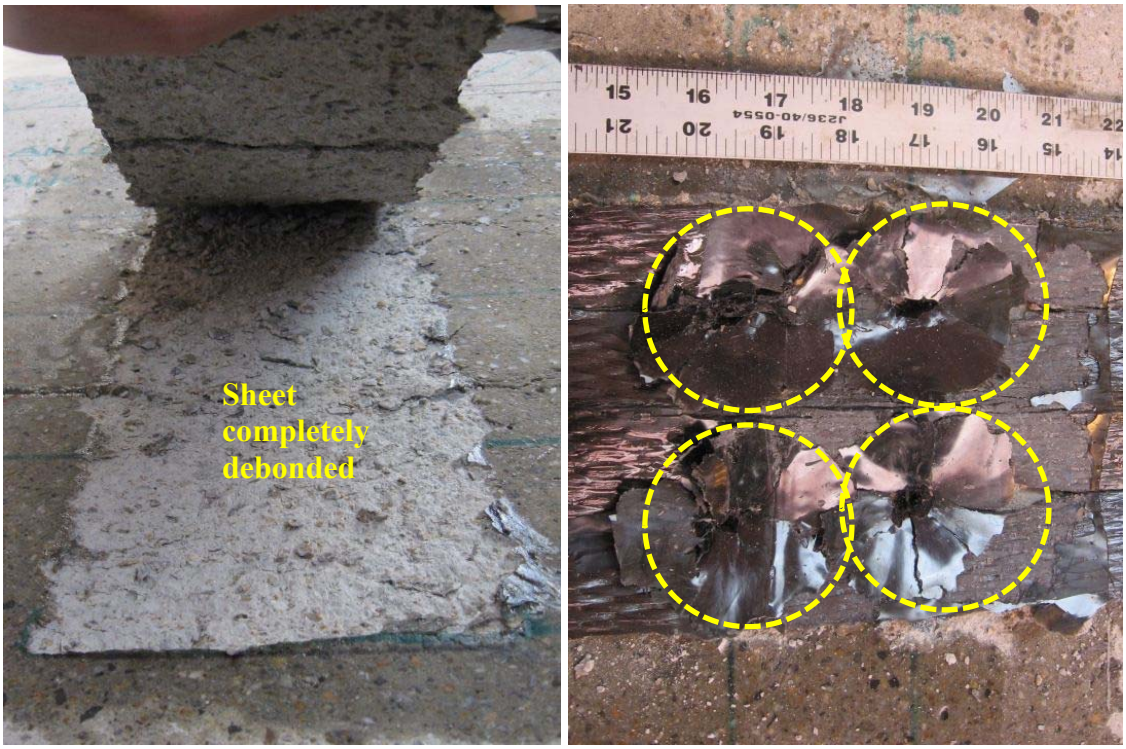

(a) (b)

Figure 4.23 Failure of specimen S2-4a-1-24

4.2.4 Unbonded Single Ply Tests

This section presents test observations for specimens F1-2a-24U and F1-4a-1-24U. These specimens were singly ply and were anchored and only bonded behind the anchors, as described in section 3.3.4

4.2.4.1 Specimen F1-2a-24U

Failure of specimen F1-2a-24U occurred at a load of 61.8 kN [13,900 lbs]. This load is about 77% of the failure load of the bonded specimen F1-2a-24 of 80.6 kN [18,120 lbs]. This load is also approximately 55% of the manufacturer's published average FRP sheet strength of 95.6 kN [25,500 lbs]. It is likely that stress concentrations around the anchors caused the sheet to rupture well below the average FRP sheet

strength. Also Figure 4.63 (discussed in section 4.3.3.4.1) shows that the strain distribution across the width of the sheet was not constant.

It is believed that failure occurred by anchor splay delamination, followed shortly by debonding of the bonded section. Figure 4.24 shows the specimen after failure. At around 35.6 kN [8,000 lbs] the edges of the right anchor splay could be seen detaching from the sheet in the test video. At a load of 43.6 kN [9,800 lbs] both instrumentation angles detached from the anchor splays, which was likely due to the deformation of the splays breaking the adhesive bond holding those pieces on, and the applied load dropped about 1.3 kN [300 lbs]. The strain gauges behind the anchors show a sudden increase in strain around 43.6 kN [9,800 lbs]. Figure 4.79 (discussed in section 4.3.4.5.1) also shows a rapid increase in strain in the gauges behind the anchors between loads 40.06 kN and 45.05 k [9,010 lbs and 10,120 lbs]. This would only be possible if the anchors carried less load because of slippage. In Figure 4.62 (discussed in section 4.3.3.4.1) gauge G3A, located in front of the left anchor, shows a sudden drop in strain around a load of 43.6 kN [9,800 lbs]. With increasing load gauges G3A and G3C showed approximately equal strain, indicating that the left anchor likely slipped more than the right anchor so that the load was distributed more evenly to the two anchors. One second prior to failure there was a sudden increase in cracking noises, indicating that the bonded zone was debonding.

4.2.4.2 Specimen F1-4a-1-24U

Failure of test F1-4a-1-24U occurred at a load of 62.1 kN [14,000 lbs]. This load is about 58% of the failure load of the bonded specimen F1-4a-1-24 of 106.6 kN [23,970 lbs]. It is also approximately 55% of the manufacturer's published average FRP sheet strength of 95.6 kN [25,500 lbs]. Since the strain behind the anchors was significantly

lower at failure for specimen F1-4a-1-24U than for F1-2a-24U, it can be assumed that the bonded section in specimen F1-2a-24U carried more load than in specimen F1-4a-1-24U, therefore the failure loads of the two specimens cannot be directly compared.

(a) **(b)**

(c)

Figure 4.24 Failure of specimen F1-2a-24U after failure

Failure occurred suddenly by anchor splay delamination and FRP rupture. The sheet remained bonded in the bonded section unlike in specimen F1-2a-24U. FRP sheet ruptured across the width of the sheet around the location of the anchors, as shown in

Figure 4.25. At a load of about 35 kN [8,000 lbs], the front left anchor gauge detached from the sheet. Around 49 kN [11,000 lbs] the edges of the right front anchor splay can be seen in the test video detaching from the FRP sheet. Gauges 4A, 4B and 4C (the row of gauges 50 mm [2 in.] behind the trailing anchors) show a small jump in strain around this load. The longitudinal strain profile of specimen F1-4a-1-24U (Figure 4.80, and discussed in section 4.3.4.5.2) does not show any sudden large increases in strain behind the anchors like the strain profile for specimen F1-2a-24U (Figure 4.79).

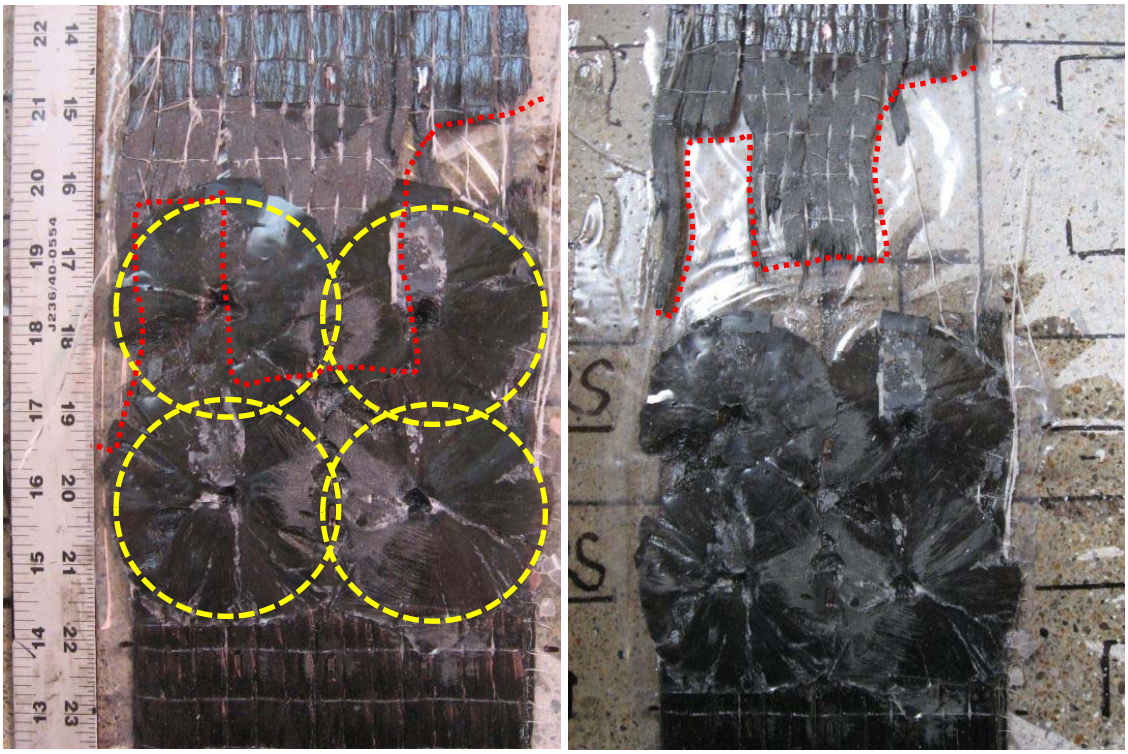

(a) **(b)**

Figure 4.25 Failure of specimen F1-4a-1-24U

4.3 Measured Test Results

4.3.1 FRP Strain Measurements

This section discusses the recorded strain data. As explained in section 3.5, strain was measured in the direction of loading on the surface of the FRP for each specimen.

Section 4.3.2 presents an overview of strain vs. applied load behavior; section 4.3.3 discusses the transverse strain distributions and section 4.3.4 discusses the longitudinal strain distributions.

The locations of the strain gauges for each specimen were shown in Figure 3.15 through Figure 3.21. The placement of the gauges was kept as consistent as possible between specimens so that results could easily be compared between specimens. In general, for unanchored specimens four strain gauges were placed along the centerline of the specimen, and for anchored specimens five gauges were placed along the centerline and two gauges were placed in front and behind the anchors aligned with the two columns of anchors. For specimens S1-4a-2-24 and F1-4a-2-24, which had a space between the anchor splays, additional gauges were placed between the two rows of anchors. For the unbonded specimens, an additional gauge was placed along the centerline of the sheet at each anchor row.

4.3.2 Load-Strain Behavior of FRP Sheets

This section discusses the observed load-strain relationships measured during the tests. The specimens are grouped into three categories depending on their strain-load characteristics: unanchored-bonded, anchored-bonded, and anchored-unbonded.

4.3.2.1 Unanchored-Bonded Specimens

All unanchored specimens demonstrated similar strain behavior. Figure 4.26 presents the load-strain data for the strain gauges of specimen F2-0a-24, which serves as an example for the behavior of the other unanchored specimens.

Unanchored specimens exhibit two regions of strain behavior that correspond to loading before and after the initiation of debonding. From initial loading to the initiation

of debonding strain increased within the stress transfer zone (STZ). The STZ is the length of bonded sheet that is effectively engaged in the stress transfer to the concrete surface. Therefore stresses increase within this portion of the sheet but remain relatively constant outside of this region. The concept of a STZ was discussed earlier in section 2.4 and section 2.5. The load capacity of the sheet is governed by the shorter of the length of the STZ and the overall length of the sheet. In all of the specimens, the STZ was significantly shorter than the length of the sheet so the capacity of the sheet was controlled by the capacity developed within the STZ. The portion of the sheet extending beyond the STZ had negligible impact on increased load capacity. Within the STZ strain decreases exponentially at distances away from the loaded end in the sheet prior to debonding. For instance, in Figure 4.26, gauge G5 recorded very low strain until the initiation of debonding, which indicates that, prior to debonding, gauges G2 and G3 were within the STZ, and gauge G5 was not.

The initiation of debonding at a gauge is easily recognized by a sudden rapid increase in strain at the gauge. Figure 4.26 clearly shows the initiation of debonding in specimen F2-0a-24 at a load of approximately 69 kN [15,500 lbs]. Once debonding initiated, the STZ traveled along the sheet until reaching a region near the end of the sheet, at which point the rest of the sheet suddenly debonded. Figure 4.26 shows that gauges G2, G3 and G4 indicate debonding at approximately the same load. After the initiation of debonding the maximum measured load changed little until failure of the specimen. Gauge G1, which was located in the unbonded section on the loaded end of the sheet, recorded linear behavior, which is consistent with the linear elastic properties of the FRP material.

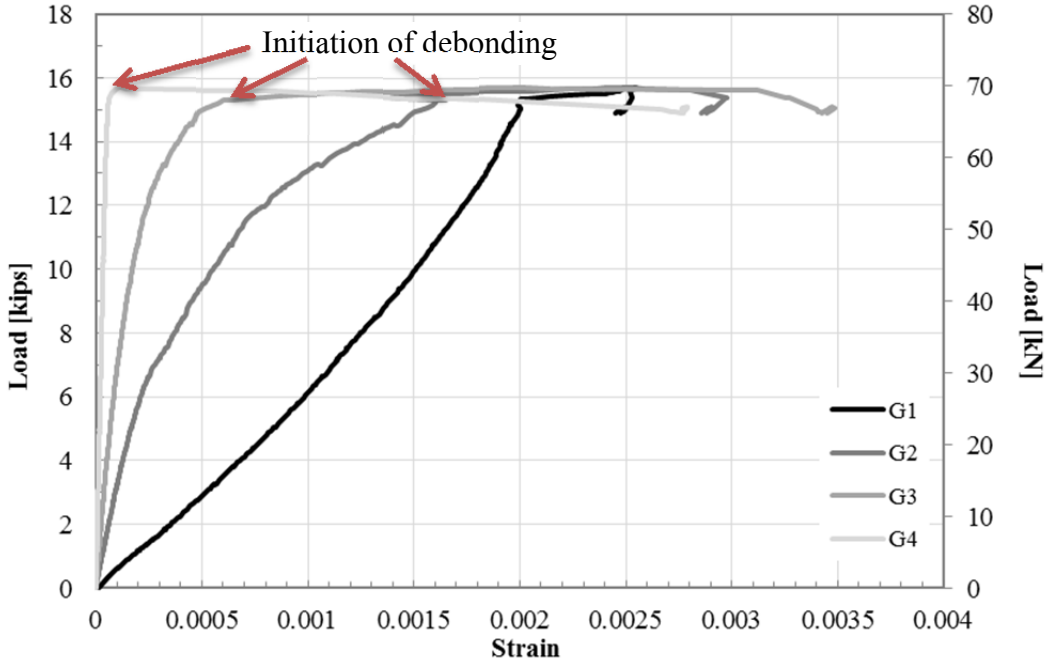

Figure 4.26 Typical load-strain relationship for an anchored-bonded specimen (specimen F2-0a-24)

4.3.2.2 Anchored-bonded specimens

All anchored-bonded specimens, including single and double ply specimens, demonstrated similar load-strain behavior. Figure 4.27 shows the load-strain relationships of the longitudinal gauges (gauges along the centerline of the sheet) for specimen F2-4a-1-24, and serves as an example for the behavior of the other anchored specimens. The gauges in line with the anchors recorded similar strain behavior as those along the centerline.

Gauges G2, G3A, G3B and G3C, located in front of the anchors, typically recorded three distinct regions of behavior; a nonlinear increase of strain prior to debonding, a sudden increase in strain at initiation of debonding, and an approximately linear increase in strain until failure of the specimen. The three regions are identified in the load-strain plots for specimen F2-4a-1-24 in Figure 4.27. Strain gauges from the

unanchored specimens also exhibited the first two regions described above, but as discussed in section 4.3.2.1, the load capacity changed little after the initiation of debonding. Anchored specimens generally resisted significantly more load after the initiation of debonding in contrast with unanchored specimens. For example, for specimen F2-4a-1-24, the peak load was 290% higher than the load at which debonding initiated. This was possible because the anchors resisted a significant amount of load after debonding initiated.

Figure 4.28 compares the strain behavior of specimens F2-0a-24 and F2-4a-1-24. The two specimens were identical except specimen F2-4a-1-24 had four anchors, and F2-0a-24 had no anchors. Gauges G2 and G3B in specimen F2-4a-1-24, showed remarkably similar behavior compared to gauges G2 and G3 from specimen F2-0a-24, from initial loading until the initiation of debonding. Notice that the peak strain reached in specimen F2-0a-24 was approximately 0.003, which is approximately the strain recorded by gauges G2 and G3B in specimen F2-4a-1-24 after the debonding front had propagated behind these gauges. This likely results from the anchors in specimen F2-4a-1-24 resisting little load prior to the initiation of debonding, and therefore strains in specimen F2-4a-1-24 were initially similar to the companion unanchored specimen.

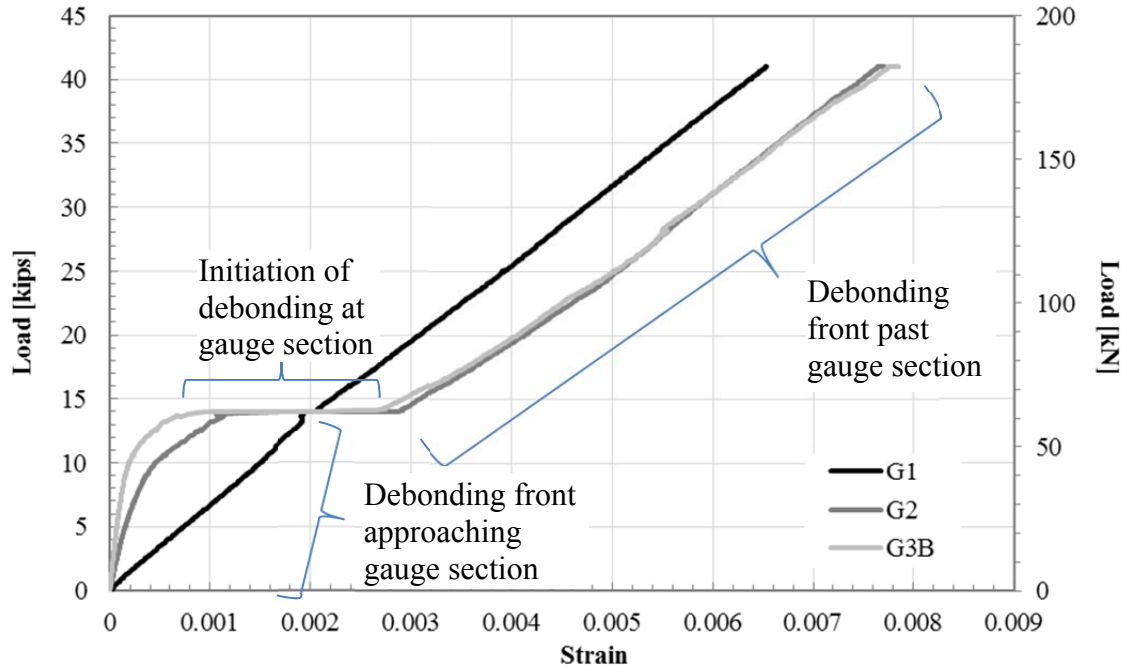

Figure 4.27 Typical load-strain relationships of the gauges located in front of the anchors (specimen F2-4a-1-24)

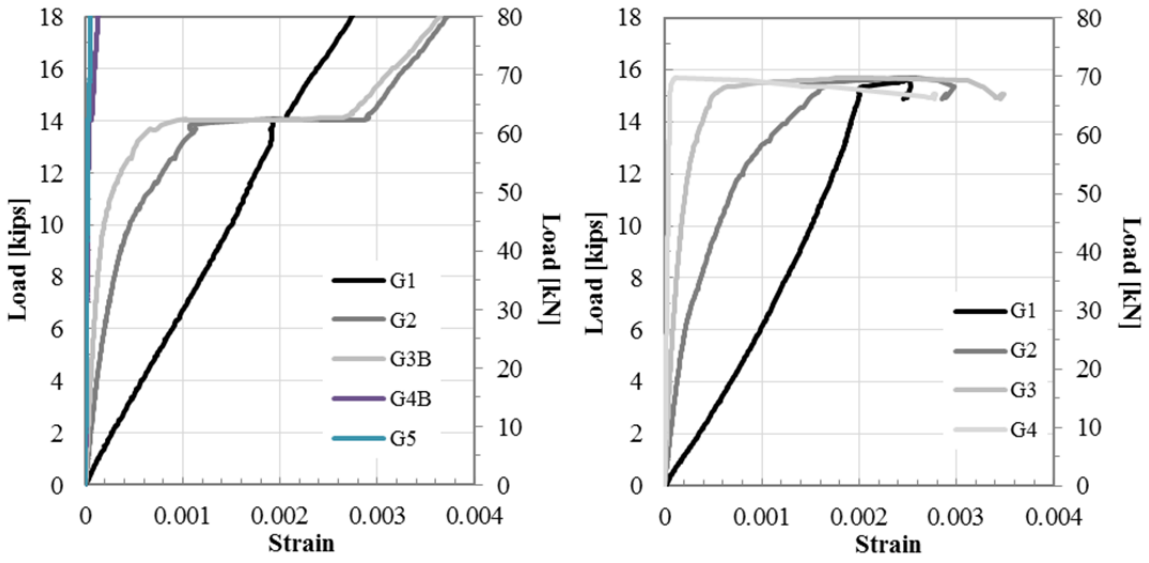

(a) **(b)**

Figure 4.28 Comparison of strain behavior of (a) an anchored specimen (specimen F2-4a-1-24) and with (b) an unanchored specimen (specimen F2-0a-24)

With several of the anchored specimens, gauge G2 recorded a reduction in strain shortly after, or before, the initiation of debonding. This occurred in specimen F1-4a-1-

24, for instance, as is shown in Figure 4.29. It is believed that this reduction in strain in gauge G2 was due to the effect of anchors on the distribution of strain transversely along the sheet. Figure 4.29 also shows that gauge G3B recorded a larger increase in strain than gauge G2 at the initiation of debonding. This occurred with several specimens, and is also believed to be due to the effect of anchors on the distribution of strain in the sheet.

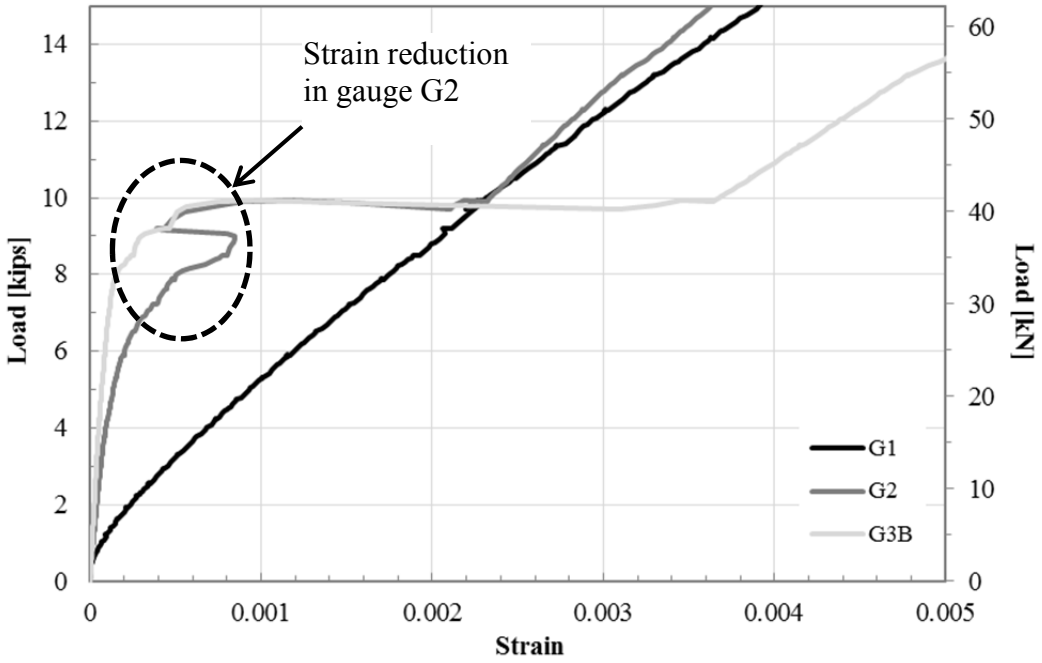

Figure 4.29 Strain behavior of specimen F1-4a-1-24

The gauges located behind the anchors generally recorded very low strains until debonding occurred in front of the anchors. This is shown in Figure 4.30 at a load of approximately 62.3 kN [14,000 lbs]. After the initiation of debonding, strain gauges behind the anchors recorded a nonlinear increase in strain, as shown in Figure 4.30 from loads of 62.3 kN [14,000 lbs] to 151 kN [34,000 lbs]. Points of anchor damage caused sudden increases in strain. For instance, damage to the anchor splays caused sudden jumps in strain behind the anchors because less load was transferred from the sheet into the anchors. In specimens that debonded past gauges G4B and G5, the initiation of

debonding at these gauges was generally apparent by a large increase in the rate of strain. However, gauges G4B and G5 almost always recorded a lower rate of strain increase than the gauges in front of the anchors at the initiation of debonding, since the anchors resisted load.

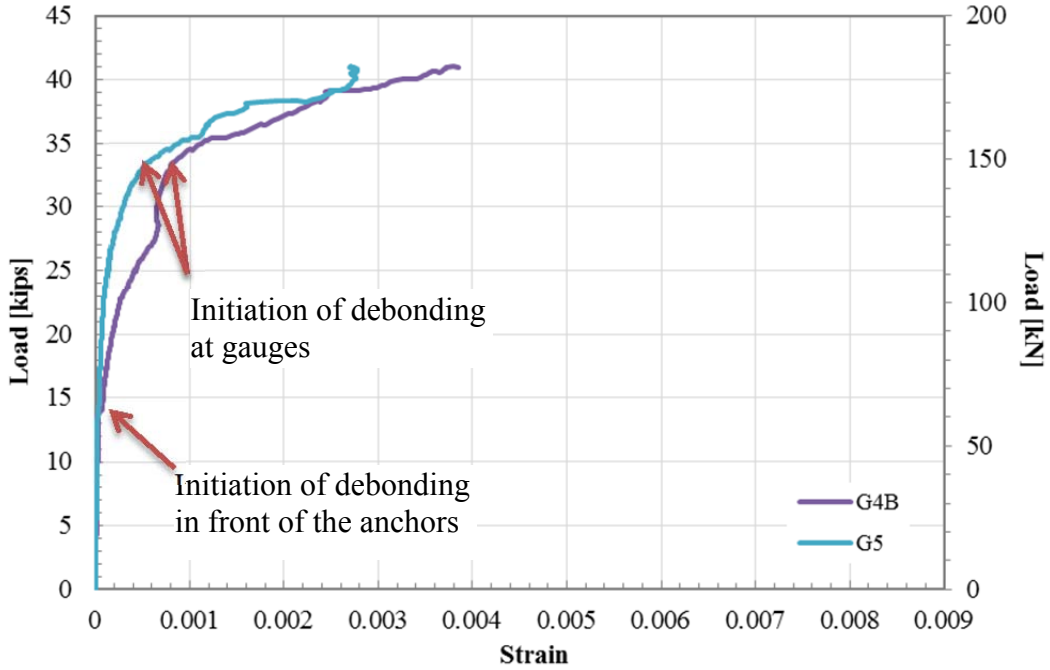

Figure 4.30 Typical load vs. strain relationships of the gauges located behind the anchors, for an anchored and bonded specimen (specimen F2-4a-1-24)

4.3.2.3 Anchored-unbonded specimens

Specimens F1-2a-24U and F1-4a-1-24U differed from the other anchored specimens in that they were unbonded, except for the last 125 mm [5 in] of the sheet. An additional strain gauge was placed between each of the two columns of anchor splays, as shown in Figure 3.20 and Figure 3.21.

For both unbonded specimens, all of the gauges in front of the anchors recorded linear increases in strain, except for a few instances where there were sudden changes in strain due to anchor damage, as shown in Figure 4.31 and Figure 4.32. Strains in gauges

G3A and G3C, located in line with the anchors, increased at a higher rate than in gauge G3B, located along the centerline of the sheet. This behavior was also observed for most anchored-bonded specimens, as discussed in section 4.3.2.2.

The difference in strain measured in front and behind the anchors seemed to relate to the magnitude of load resisted by the anchors. Load was only transferred to the region of the sheet behind anchors after anchors deformed significantly or when the anchor splays delaminated from the sheet. Perfectly rigid anchors would not allow load to be transferred to the sheet behind the anchors. Figure 4.31 and Figure 4.32 exemplify the load magnitude that the anchors in both specimens resisted, since there was greater strain in front of the anchors than behind the anchors. The initial rate of strain in gauges G4A and G5 was less in specimen F1-4a-1-24 than in F1-2a-24, which seems reasonable since there were half as many anchors in the latter specimen. For both specimens, gauge G4B showed higher strain than gauges G4A and G4C, which was also true for most bonded specimens. The gauges behind the anchors recorded an increasing rate of strain with increasing load, as was typical of the anchored and bonded specimens. It is believed that the sudden increases in strain or increases in rate of strain, as identified in Figure 4.31 and Figure 4.32, correspond to either instances of anchor deflection caused by anchor pullout or anchor splay damage.

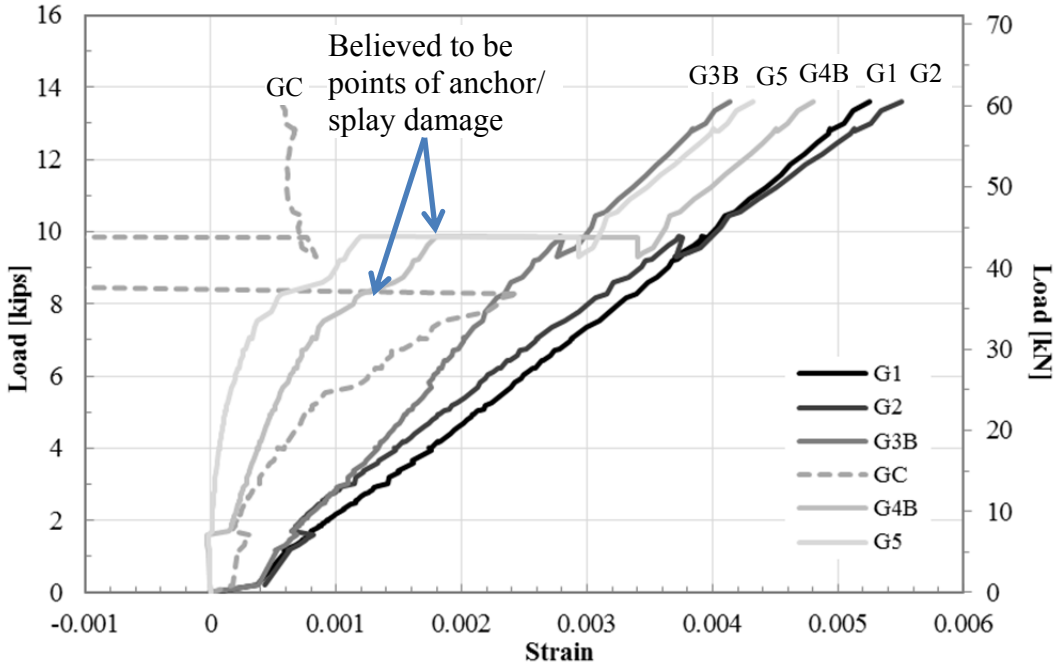

Figure 4.31 Load-strain relationship for specimen F1-2a-24U (negative strains correspond to compression)

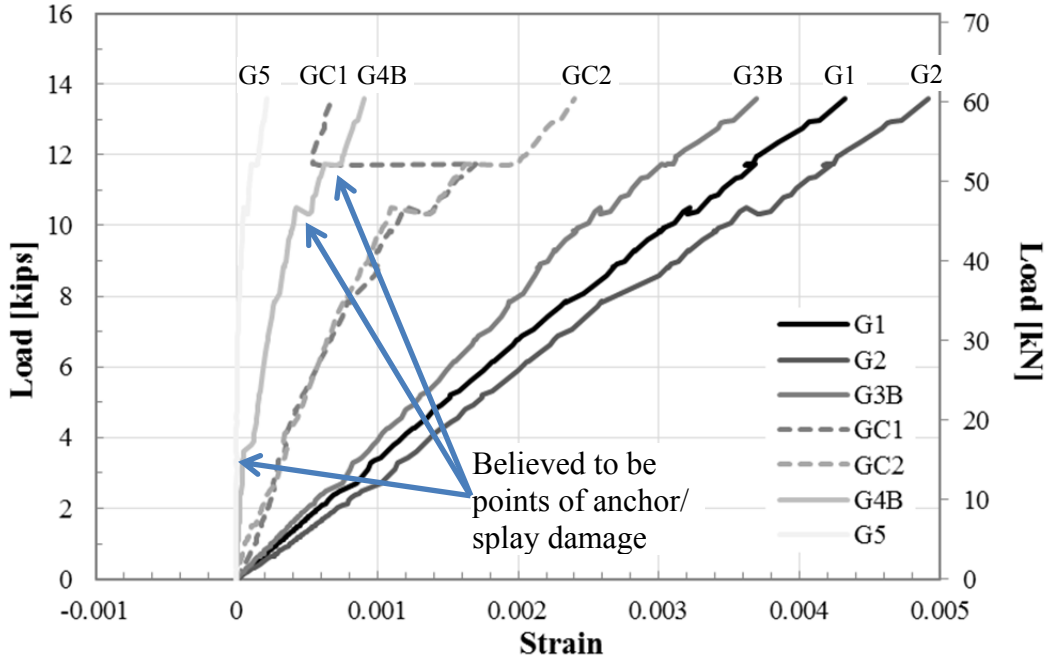

Figure 4.32 Load-strain relationship for specimen F1-4a-1-24U (negative strains correspond to compression)

4.3.3 Strain Distribution across FRP Laminate

This section presents data for the transverse distribution of strain for the anchored specimens only. Unanchored specimens were instrumented with gauges only placed along the centerline of the sheet, since the transverse strain distribution of unanchored sheets has already been studied extensively (Subramaniam et al., 2007; Niemitz, 2008). To capture the transverse distribution of strain, a row of three strain gauges was placed in sections located in front and behind the anchors; one gauge in-line with each anchor, and one on the centerline of the sheet as shown in Figure 3.15 through Figure 3.21. Strain measurements are plotted at selected loads to show the variation in transverse distribution of strains with increasing load. All strain profiles are plotted at the same scale so that different specimens can be easily compared. (x=0 mm) corresponds to the left edge of the sheet and (x=127 mm) corresponds to the right edge of the sheet.

4.3.3.1 General Observations on Strain Distribution across FRP Laminate

This section discusses overall trends in the recorded strain distributions across the FRP sheets. Detailed descriptions of the strain distributions across the FRP sheets for each specimen are given in sections 4.3.3.2 (anchored single ply specimens), 4.3.3.3 (anchored double ply specimens) and 0 (unbonded specimens).

Figure 4.33 presents a compilation of strain distributions from each anchored specimen at a transverse section located 50 mm [2 in.] in front of the anchors at approximately the peak load. It seems that sheet fibers located in line with the anchors were generally more effectively restrained from slippage by the anchor splays, so higher load and strains were developed than in fibers along the centerline of the FRP sheet. This

agrees with the finite element model, as discussed in section 6.5.8. Figure 4.34 presents a compilation of strain distributions from each specimen 50 mm [2 in.] behind the anchors at approximately the peak load. Results from two specimens (S1-4a-2-24 and F1-4a-2-24) were excluded from the compilation because they had a unique strain gauge and anchor arrangement. The strains were generally higher in the center of the sheet than in fibers lining up with the anchors. This also agrees with the finite element model, as discussed in section 6.5.8. A likely explanation for this is that the anchors resisted the major portion of the total load in the sheet, and prevented stress from generating in fibers in line with the anchors

Localized FRP anchor effects, local variations in bond strength, and skewed debonding fronts contributed largely to the large variations observed in transverse strain distributions in different specimens as well as the asymmetry in the strain distributions in many of the specimens. Strains rapidly vary across the width and length of anchored FRP sheets, especially near the location of the anchors, so the recorded strains are very sensitive to gauge location. It is clear from the transverse strain data that debonding of the FRP sheets often did not occur perpendicular to the direction of the applied load, but rather at an angle. Assuming equal displacement along the loaded edge of the sheet a skewed debonding front causes uneven loading and strain distribution in the sheet. In several specimens, as will be mentioned in the subsequent sections, there was fiber rupture across a partial width of the sheet prior to failure, which effected the transverse strain distributions.

The strains behind the anchors were generally significantly lower than in front of the anchors. The drop in strain from in front to behind the anchors is related to the load that is resisted by the anchors. This is discussed further in section 5.3.

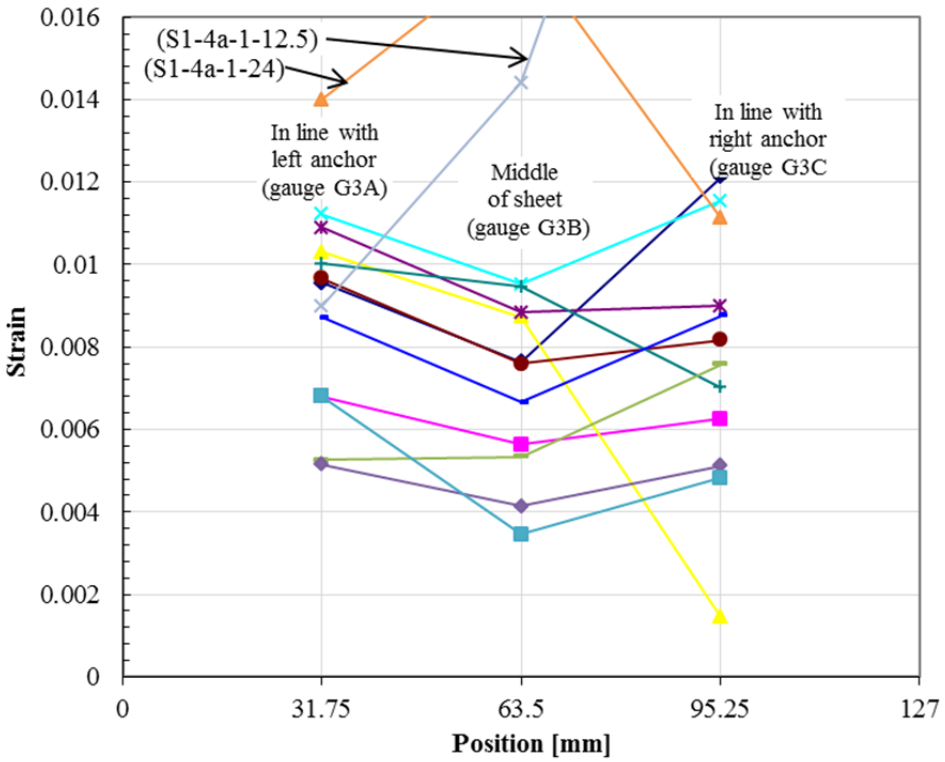

Figure 4.33 Compilation of transverse strain distributions 50 mm [2 in.] in front of the anchors at approximately the peak load in anchored-bonded and anchored-unbonded specimens

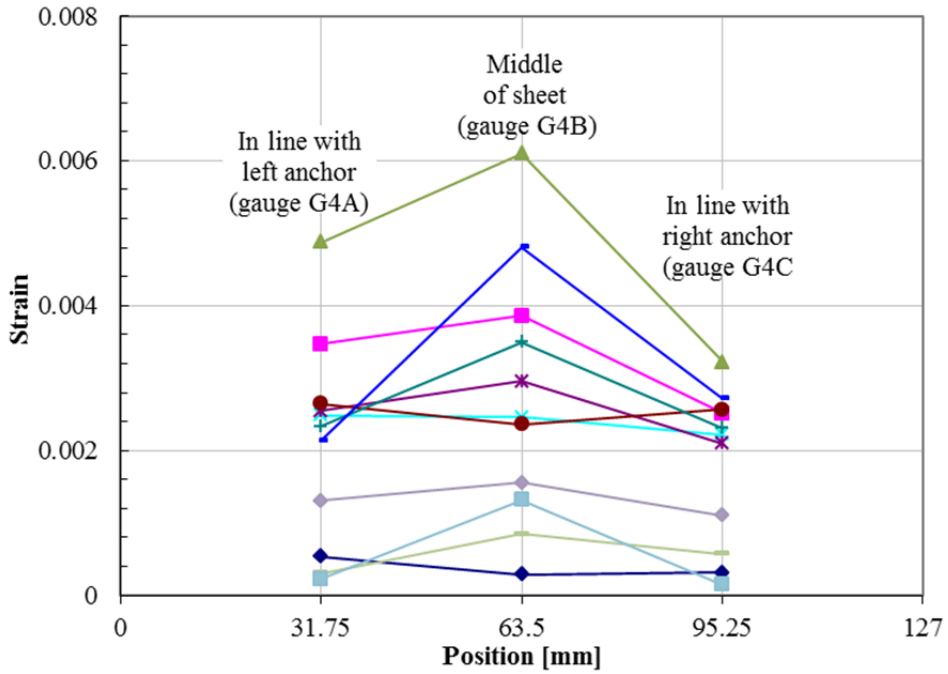

Figure 4.34 Compilation of transverse strain distributions 50 mm [2 in.] behind the anchors at approximately the peak load in anchored-bonded and anchored-unbonded specimens

4.3.3.2 Anchored Single Ply Specimens

4.3.3.2.1 Specimen S1-2a-24

Transverse strain plots for specimen S1-2a-24 are presented in Figure 4.35 and Figure 4.36. The shape of the strain plots were similar to most of the anchored specimens: in front of the anchors there were higher strains in line with the anchors than along the centerline of the sheet, and the opposite was true behind the anchors, where strains were higher along the centerline of the sheet. The three transverse gauges in front of the anchors recorded nearly zero strain until approximately 31 kN [7,000 lbs]. Strains suddenly increased at loads slightly exceeding 31 kN and up 33 kN [7,000 lbs to 7,500 lbs] indicating that initiation of FRP debonding at these gauges. From the transverse strain distribution at a load of 31.35 kN [7,050 lbs] in Figure 4.35 it appears that the debonding front reached gauge G3C before reaching the other two gauges. Following

debonding, the three gauges recorded a constant increase in strain until approximately 71 kN [16,000 lbs], at which point gauge G3A recorded a sudden decrease in strain, and gauge G3C recorded an increase in rate of strain. This could be due to an uneven debonding crack front, or the left anchor could have slipped, both of which would have caused load to be shifted to the right side of the sheet.

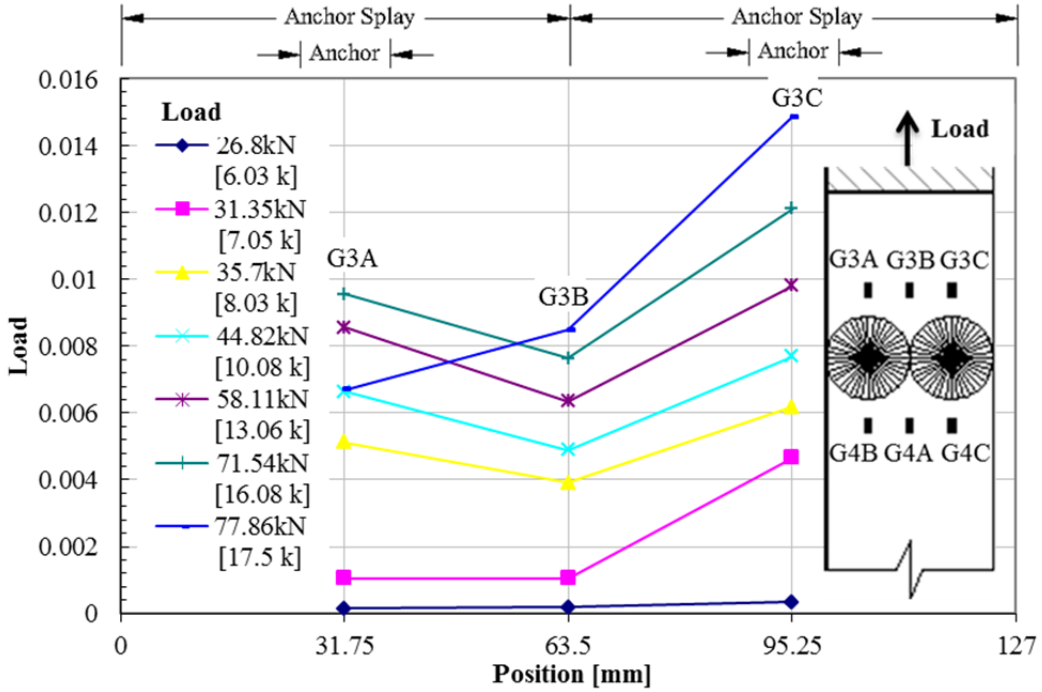

Figure 4.35 Transverse strain in Specimen S1-2a-24 in front of anchors

Figure 4.36 shows the transverse strain distribution at a section located 50 mm [2 in.] behind the anchors. There was very little increase in strain until approximately 31 kN [7,000 lbs], the load at which debonding initiated in front of the anchors. There was an increase in rate of strain at load of 49 kN [11,000 lbs] in gauge G4B and at 58 kN [13,000 lbs] in gauges G4A and G4C, indicating the initiation of debonding at these gauges.

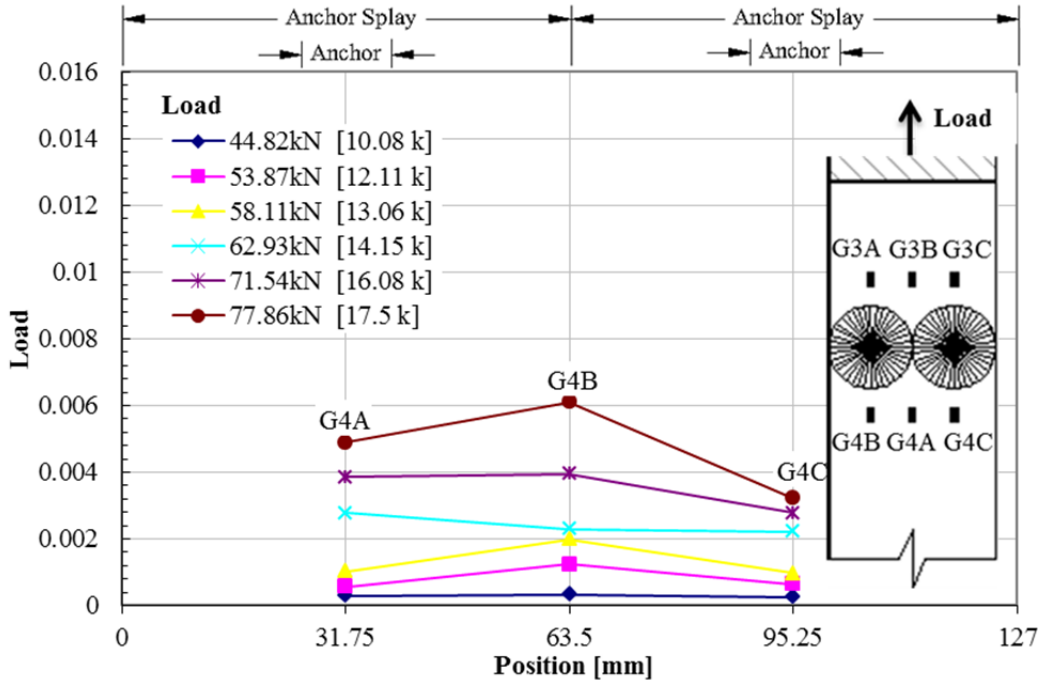

Figure 4.36 Transverse strain in specimen S1-2a-24 behind anchors

4.3.3.2.2 Specimen F1-2a-24

Transverse strain distributions at different loads in specimen F1-2a-24 are shown in Figure 4.37 and Figure 4.38. As with specimens S1-2a-24, Figure 4.37 shows that in front of the anchors there were higher strains in line with the anchors than along the centerline of the sheet. The opposite is true behind the anchors, where strains were higher along the centerline of the sheet than in line with the anchors, as shown in Figure 4.38. The strain recorded by the three gauges in front of the anchors was nearly zero until approximately 44.5 kN [9,000 lbs]. Strains rapidly increased from loads of approximately 40.0 kN to 44.5 kN [9,000 to 10,000 lbs] indicating the initiation of debonding of the FRP sheet from the concrete at these gauges. From a load of 44.5 kN [10,000 lbs] to failure, the three gauges recorded a constant rate of increase in strain.

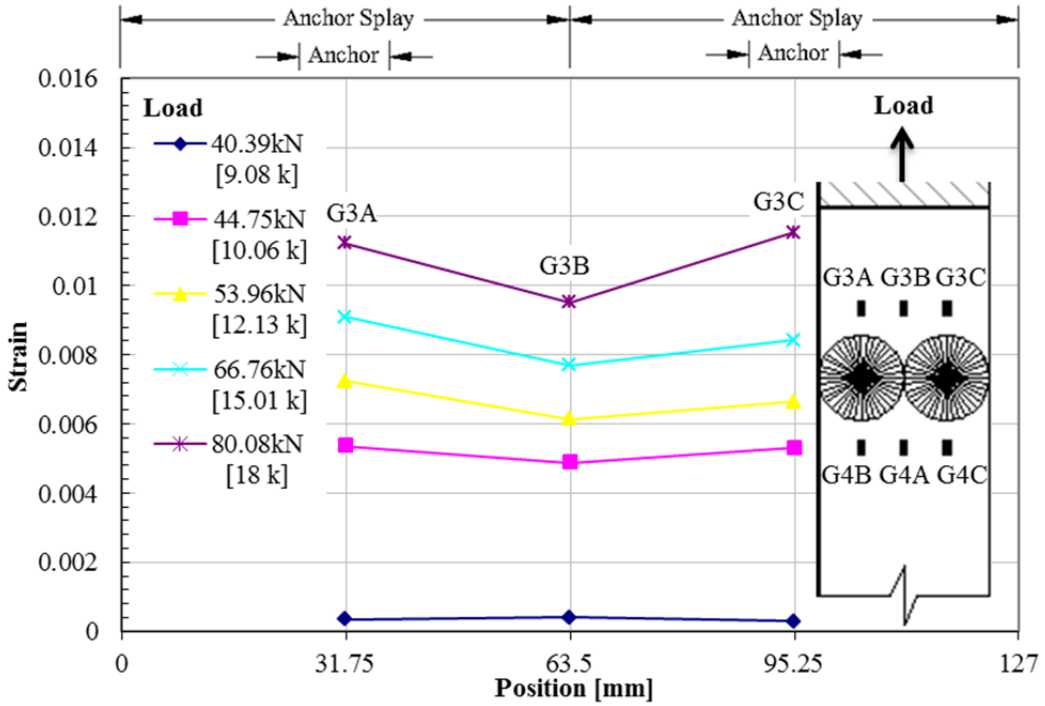

Figure 4.37 Transverse strain in specimen F1-2a-24 in front of the anchors

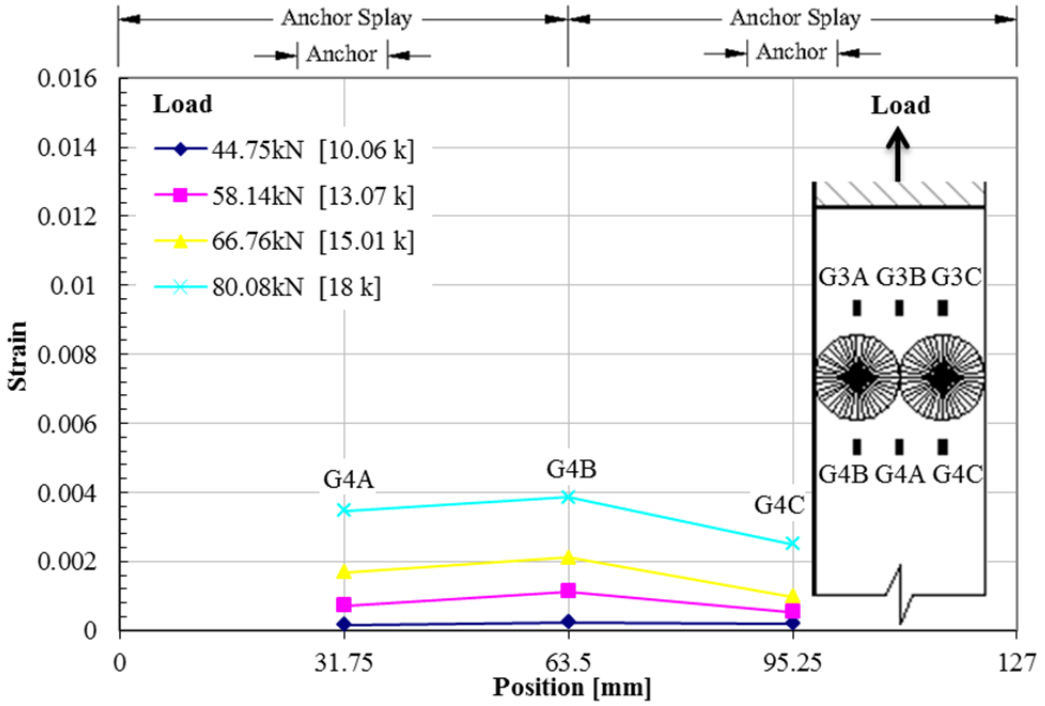

Figure 4.38 Transverse strain in specimen F1-2a-24 behind the anchors

There were very small strains behind the anchors until a load of approximately 40.0 kN [9,000 lbs], at which the debonding front passed the strain gauges in front of the

anchors. The strain profile was nearly symmetric about the centerline of the sheet in front of the anchors. Behind the anchors, the strain distribution was approximately symmetric. There was no discernible anchor damage, which could have contributed to the symmetry of the strain distribution

4.3.3.2.3 Specimen S1-4a-1-24

Transverse strain distributions for specimen S1-4a-1-24 are shown in Figure 4.39 and Figure 4.40. Unlike most other anchored specimens, higher strains were recorded along the center line of the FRP sheet than in line with the anchors at the section in front of the anchors. There were also significantly higher strains recorded compared to most other anchored specimens, including specimen F1-4a-1-24, which failed at a higher load. This indicates that the gauges were influenced more by stress concentrations within the sheet. Prior to a load of approximately 35.6 kN [8,000lbs] there was minimal strain in gauges located in front of the anchors. There was a rapid increase in strain in these gauges from loads of approximately 35.5 kN [8,000 lbs] to 44.5 kN [10,000lbs], indicating the initiation of debonding at these gauges. From a load of approximately 44.5 kN [10,000lbs] until failure, strain increased at a constant rate. At loads of 52.9 kN [11,890 lbs] and 78.7 kN [17,7000 lbs] gauges G3B and G3A, respectively malfunctioned.

The strain profile is nearly symmetric about the centerline of the sheet in front of the anchors until a load of approximately 49 kN [11,000 lbs]. At this load the strain recorded by gauge G3A slowly increased relative to gauge G3C. Gauge G3A measured a peak strain 40% higher than in G3C at a load of 78.7 kN [17,690 lbs].

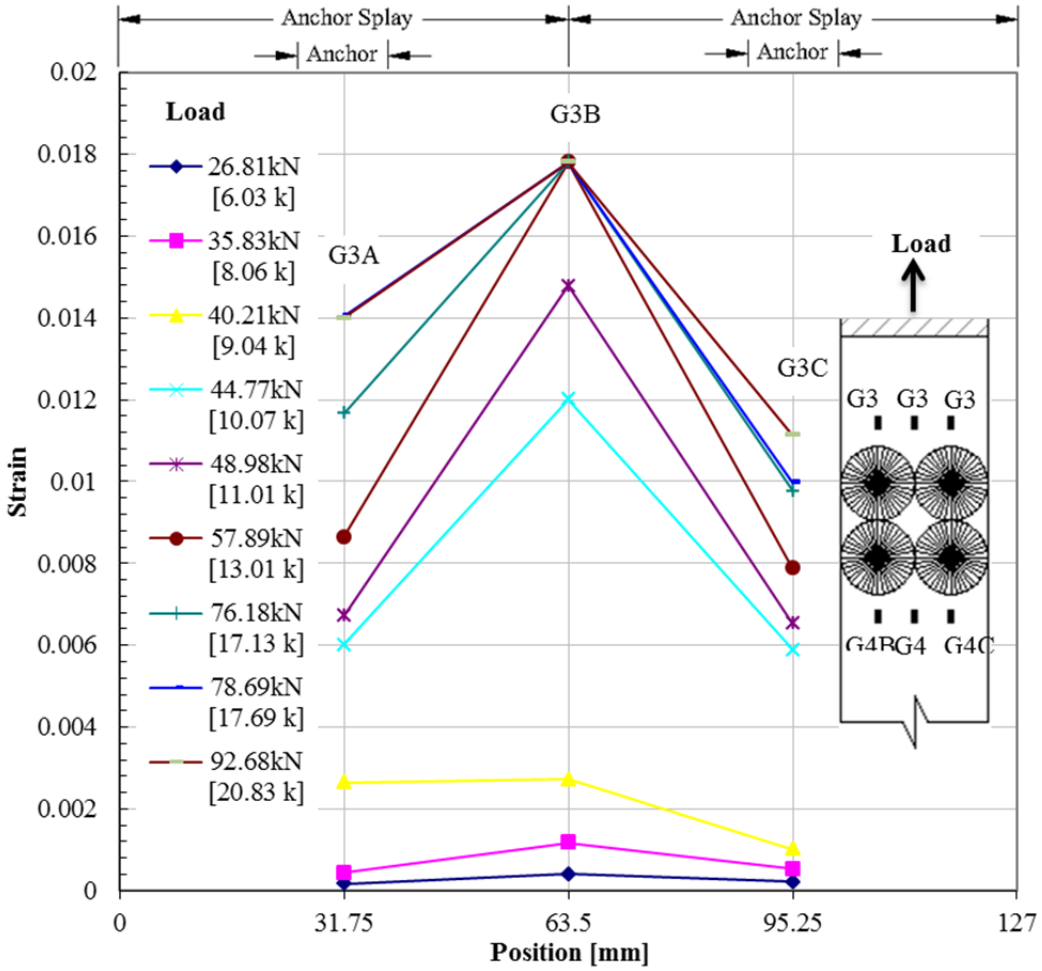

Figure 4.39 Transverse strain in specimen S1-4a-1-24 in front the anchors

Figure 4.40 shows the transverse strain profile behind the trailing anchor row in specimen S1-4a-1-24. Despite the larger strains in front of the anchors, the strains behind the anchors were smaller than in specimens S1-2a-24 and F1-2a-24, which had one row of two anchors instead of two rows of two anchors. This indicates that both rows of anchors resisted load. There was a very slow increase in strain until approximately 35.5 kN [8,000 lbs], which is the load at which the debonding front passed the strain gauges in front of the anchors. The measured strains behind the anchors were approximately constant, although were slightly higher for most loads in line with the anchors than along the centerline, which is in contrast to most anchored specimen.

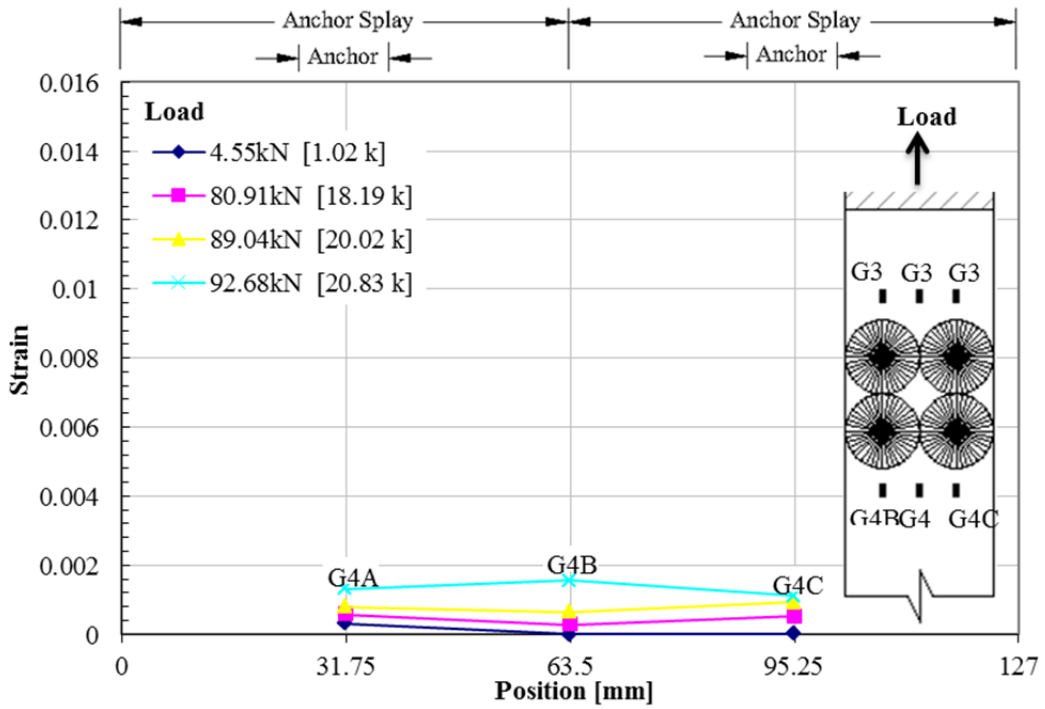

Figure 4.40 Transverse strain in specimen S1-4a-1-24 behind the anchors

4.3.3.2.4 Specimen F1-4a-1-24

Transverse strain distributions for specimen F1-4a-1-24 are shown in Figure 4.41 and Figure 4.42. At all loads, there was significantly higher strain on the left side of the sheet than on the right side, both in front of and behind the anchors. This may be indicative of uneven loading of the FRP sheet. The strains were approximately 70% higher in gauge G4A than in G4C at failure.

There was minimal strain in the transverse gauges located in front of the anchors until approximately 44.5 kN [9,000 lbs]. At approximately 44 kN [10,000 lbs] there was a rapid increase in strain in all the three gauges, indicating the initiation of debonding at these gauges. The greatest increase in strain occurred in gauge GA, followed by gauge G3B, which recorded approximately 25% less strain, followed by gauge G3C, which recorded significantly less strain than the other two gauges. Gauges G3B and G3A then

recorded a constant, and approximately equal, rate of strain. Gauge G3C recorded a much lower rate of strain until approximately 66.7 kN [15,000 lbs], after which it recorded negligible increase in strain until failure.

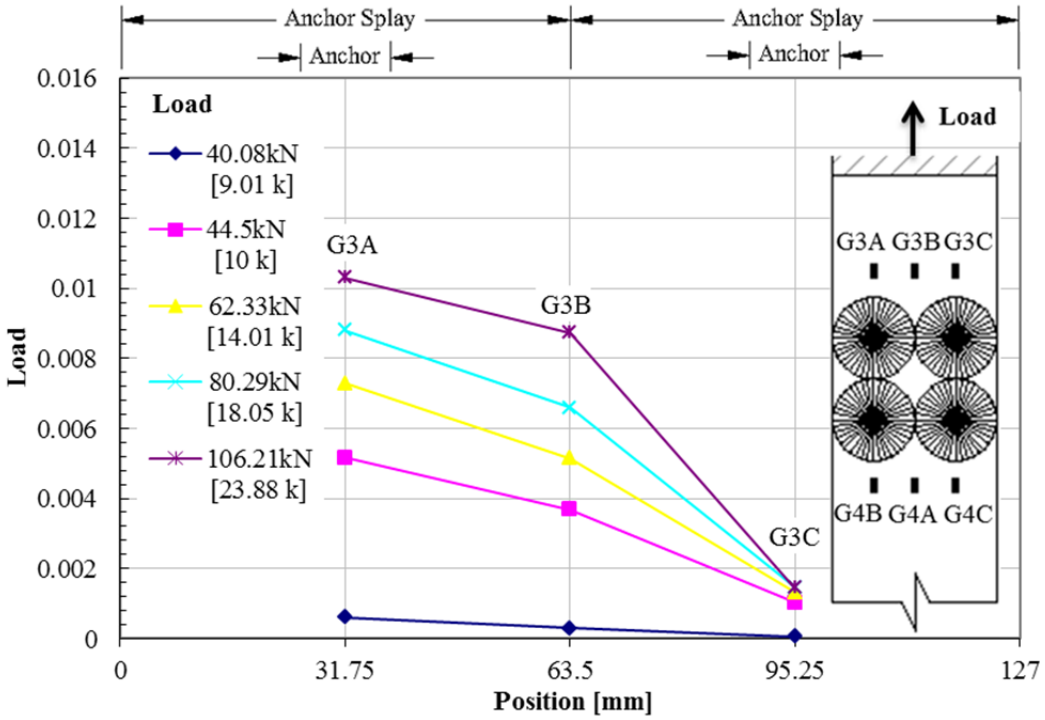

Figure 4.41 Transverse strain in specimen F1-4a-1-24 in front of the anchors

Figure 4.42 shows the transverse strain profile behind the trailing anchor in specimen F1-4a-1-24. Like in specimen S1-4a-1-24, there were small strains behind the anchors, which indicates that the anchors resisted a significant amount of load. There was an increase in rate of strain in all three transverse gauges located behind the anchors at a load of 44 kN [10,000 lbs], which is the load at which the debonding front passed the strain gauges in front of the anchors, although the magnitude of strain was still very low relative to the strain in front of the anchors.

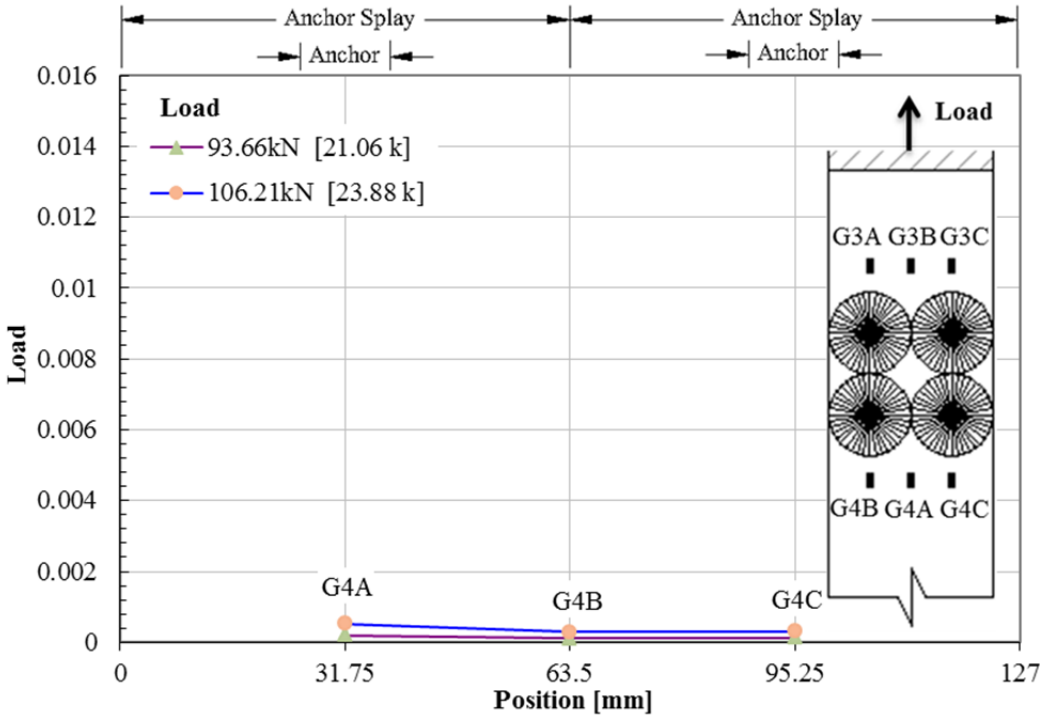

Figure 4.42 Transverse strain in specimen F1-4a-1-24 behind the anchors

4.3.3.2.5 Specimen S1-4a-2-24

Transverse strain distributions for specimen S1-4a-2-24 are presented in Figure 4.43, Figure 4.44 and Figure 4.45. From initial loading to a load of approximately 26.7 kN [6,000lbs] there was minimal strain in the gauges located in front of the anchors, followed by a rapid increase in strain from loads of approximately 28.9 kN [6,500 lbs] to 33.4 kN [7,500lbs], indicating the initiation of debonding at these gauges. From loads of 33.4 kN [7,500 lbs] to approximately 53.4 kN [12,000 lbs] strain increased in gauges G3A, G3B, and G3C at a constant rate. At a load of approximately 53.4 kN [12,000 lbs] fibers on the right side of the sheet ruptured and slipped from the loading plates, as discussed in section 4.2.2.4. At this load gauge G3B was damaged, the strain in gauge G3A dropped approximately 90% and gauge G3C recorded approximately a 25% increase in strain due to load redistribution. G3B subsequently recorded a constant

increase in strain until just prior to failure when there was another small sudden increase in strain. G3C showed little increase in strain until failure.

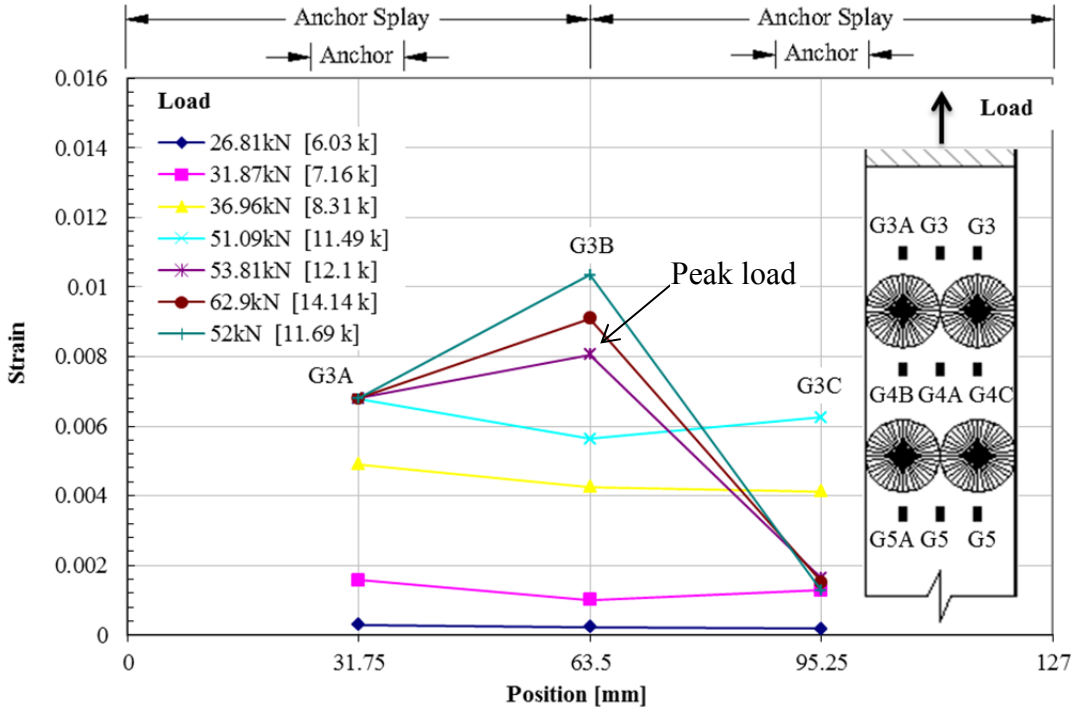

Figure 4.43 Transverse strain in specimen S1-4a-2-24 in front of the anchors

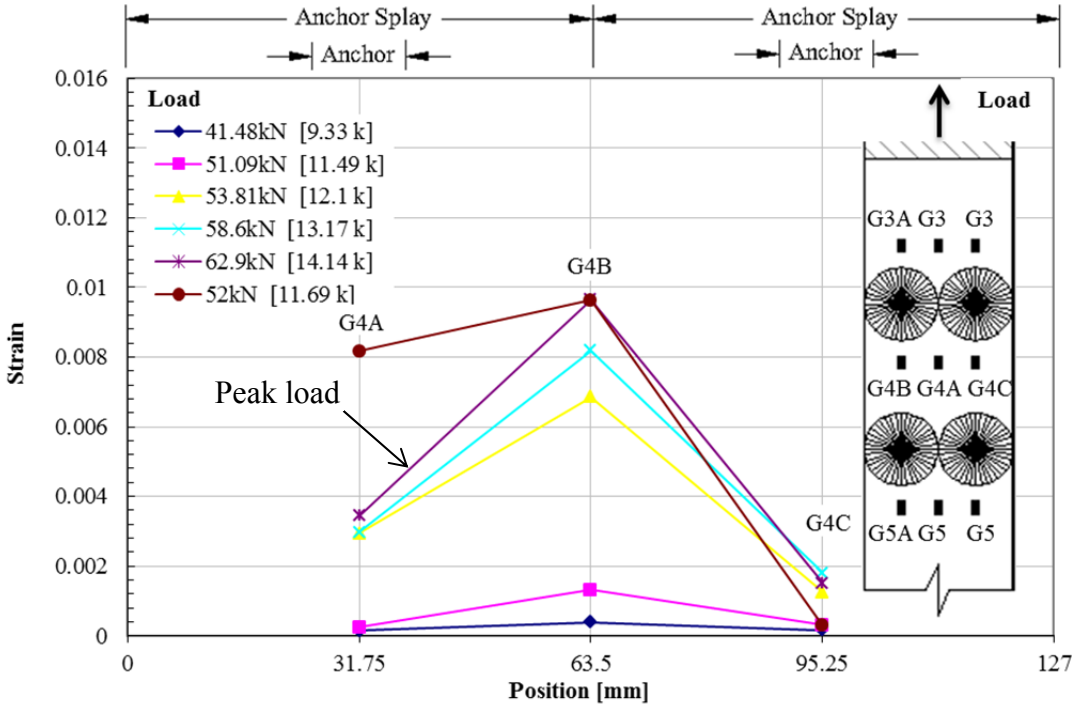

Figure 4.44 Transverse strain in specimen S1-4a-2-24 behind first row of anchors

Figure 4.44 shows that behind the first row of anchors strains were significantly higher along the centerline of the sheet than in line with the anchors. Shortly after the peak load of 62.9 kN [14.14 k] was reached a width of sheet, adjacent to the fibers that slipped on the plates, ruptured, as discussed in section 4.2.2.4. This caused load to be redistributed to the left side of the sheet, which is evident by large jump in strain in gauge G4A while gauge G4C recorded a decrease in strain to nearly zero strain.

Figure 4.45 shows that there was very low strain in gauges G6A, 6B, and 6C at the maximum recorded load. Seconds after the peak load was reached, there was a sudden increase in strain in gauges G6A and 6B, which indicates that the debonding front did not pass the second row of anchors until after the peak load was reached. Gauge G6C showed negligible strain throughout the entire test, which is logical, since the right side of the sheet slipped from the loading grips prior to the peak load.

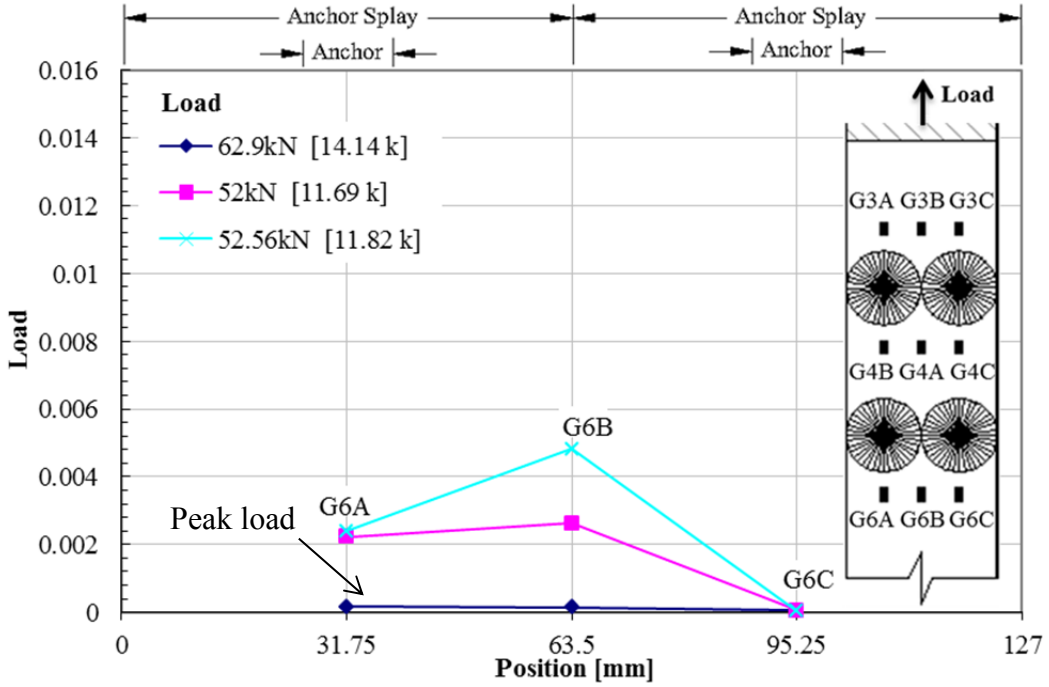

Figure 4.45 Transverse strain in specimen S1-4a-2-24 behind the second row of anchors

4.3.3.2.6 Specimen F1-4a-2-24

Transverse strain distributions for specimen F1-4a-2-24 are presented in Figure 4.46, Figure 4.47 and Figure 4.48. There were slightly higher strains on the left side of the sheet. Gauges G3A, 3B and 3C showed very little strain until a load of approximately 31 kN [7,000 lbs]. From loads of 31 to 42 kN [7,000 to 9,500 lbs] there was a rapid increase of strain in all three gauges, indicating the initiation of debonding at this row of gauges. All three gauges then recorded a constant increase in strain until failure. Strain increased at a slightly greater rate for gauge G3A than for the other two gauges, which recorded approximately the same rate of strain.

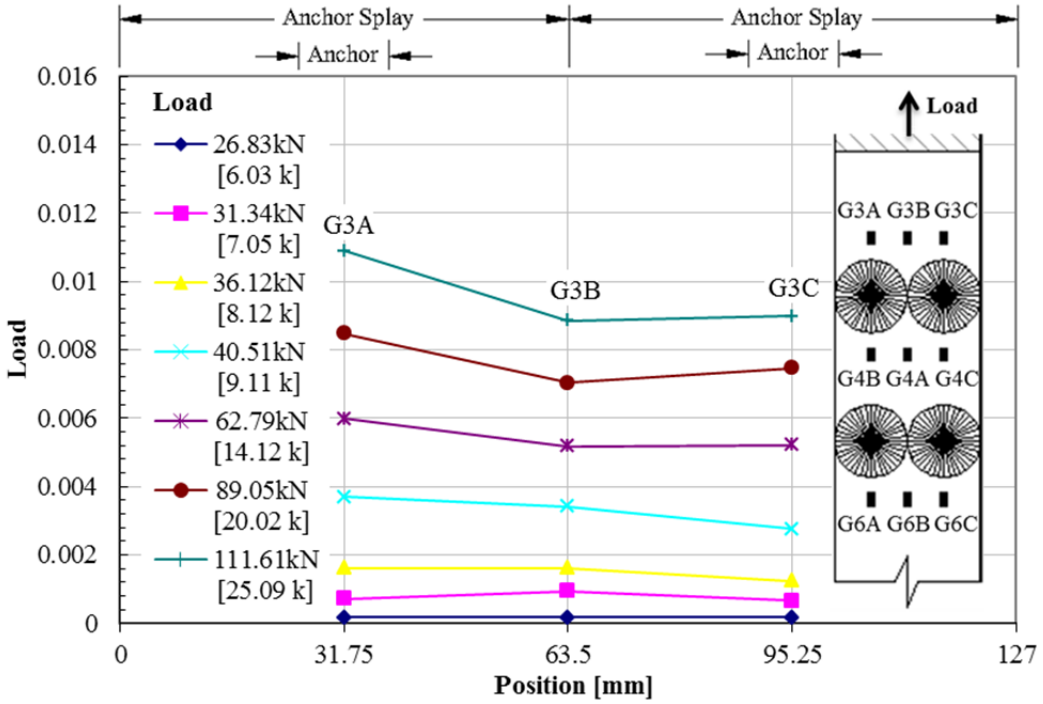

Figure 4.46 Transverse strain in specimen F1-4a-2-24 in front of the anchors

Gauges G4A, 4B and 4C showed negligible rate of strain increase until 35.6 kN [8,000 lbs]. From loads of 35.6 kN [8,000 lbs] to 55.6 kN [12,500 lbs] there is a significantly higher rate of strain increase in all three gauges, indicating that the

debonding front passed these gauges during this load interval. All three gauges then show a constant, and nearly equal, rate of strain increase until failure. It is interesting that the strain behind the first row of anchors resembles typical strain behavior found in front of the anchors, with three distinct periods of behavior that occur before debonding, when debonding initiates, and after debonding, as explained in section 4.3.2.2.

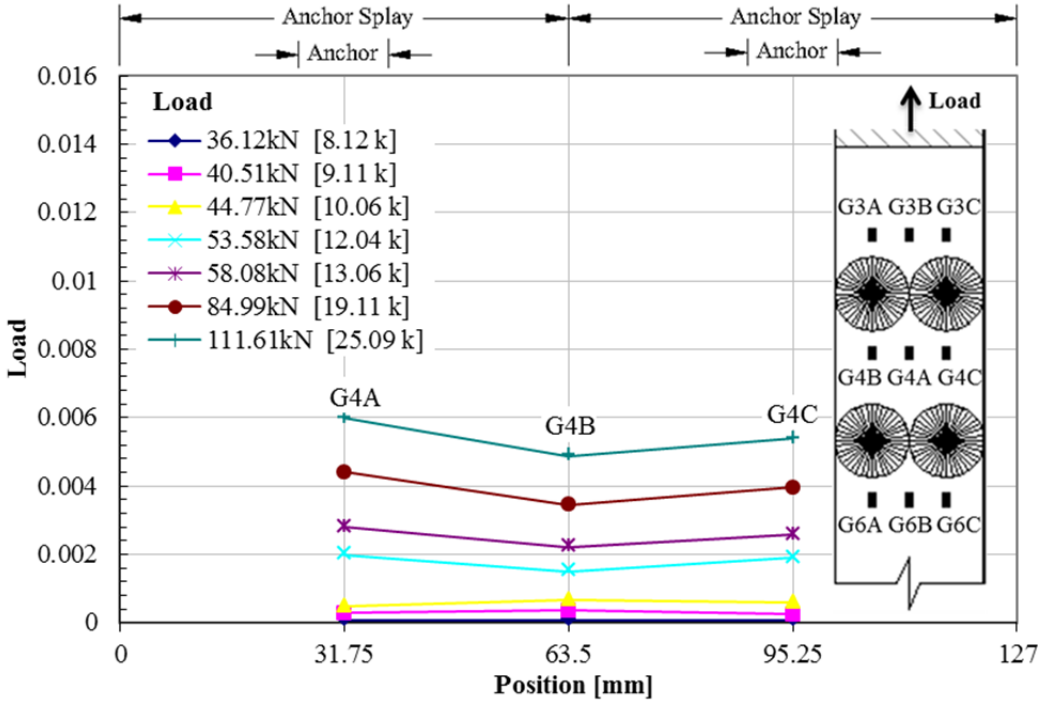

Figure 4.47 Transverse strain in specimen F1-4a-2-24 behind the first row of anchors

Figure 4.48 shows that there was very little strain in gauges G6A, G6B and G6C until a load of approximately 58 kN [13,000 lbs], around the load that the debonding front passed the gauges in between the rows of anchors. From 58 kN to 107 kN [13,000 lbs to 24,000 lbs] there is a clear increase in rate of strain. From 24,000 lbs until failure, there is sudden further increase in rate of strain in gauge G6B, indicating that the debonding front passed this gauge, but not G6A or G6C. This agrees with Figure 4.16.

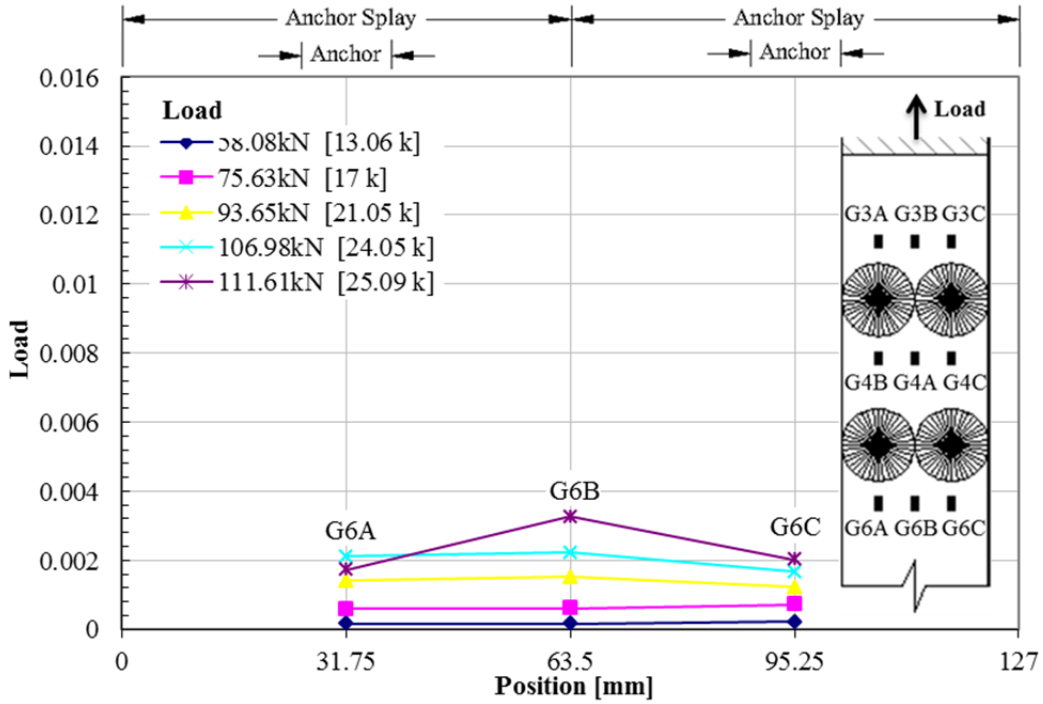

Figure 4.48 Transverse strain in specimen F1-4a-2-24 behind the second row of anchors

4.3.3.2.7 Specimen S1-4a-1-12.5

Transverse strain distributions for specimen S1-4a-1-12.5 are shown in Figure 4.49 and Figure 4.50. There were significantly higher strains on the right side of the sheet than the left side at failure, as shown in Figure 4.49. It is believed that uneven loading of the sheet was largely to blame for this. The strain profile behind the anchors was more symmetric, indicating that the anchors redistributed the load.

Gauges G3A, 3B and 3C showed negligible strain until a load of approximately 35.6 kN [8,000 lbs]. From loads of 42 kN to 47 kN [9,500 lbs to 10,500 lbs] there was a rapid increase in strain, indicating the initiation of debonding at these gauges. At 46.7 kN [10,500 lbs] the strain is nearly equal in all three gauges. From a load of 47 kN [10,500 lbs] to failure all three gauges showed a constant increase in strain until failure. Strain increased at a greater rate for gauge G3C than for G3B, and strain for G3B increased at a greater rate than for G3A.

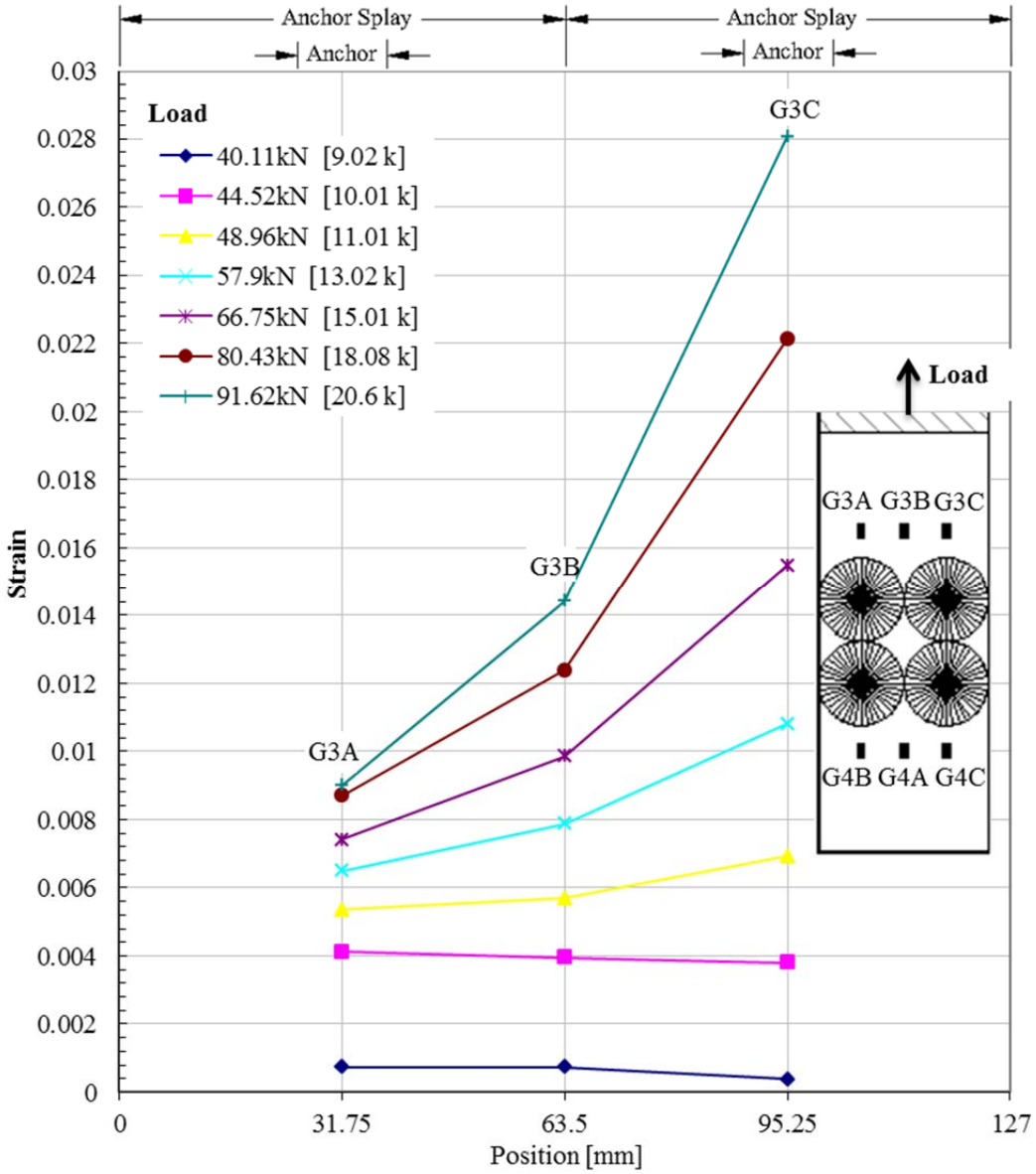

Figure 4.49 Transverse strain in specimen S1-4a-1-12.5 in front of the anchors

The low level of peak strain in Figure 4.50 indicates the debonding front did not reach this row of gauges prior to failure. Consistent with most anchored tests, behind the anchors the strain was greater along the centerline of the sheet behind the anchors.

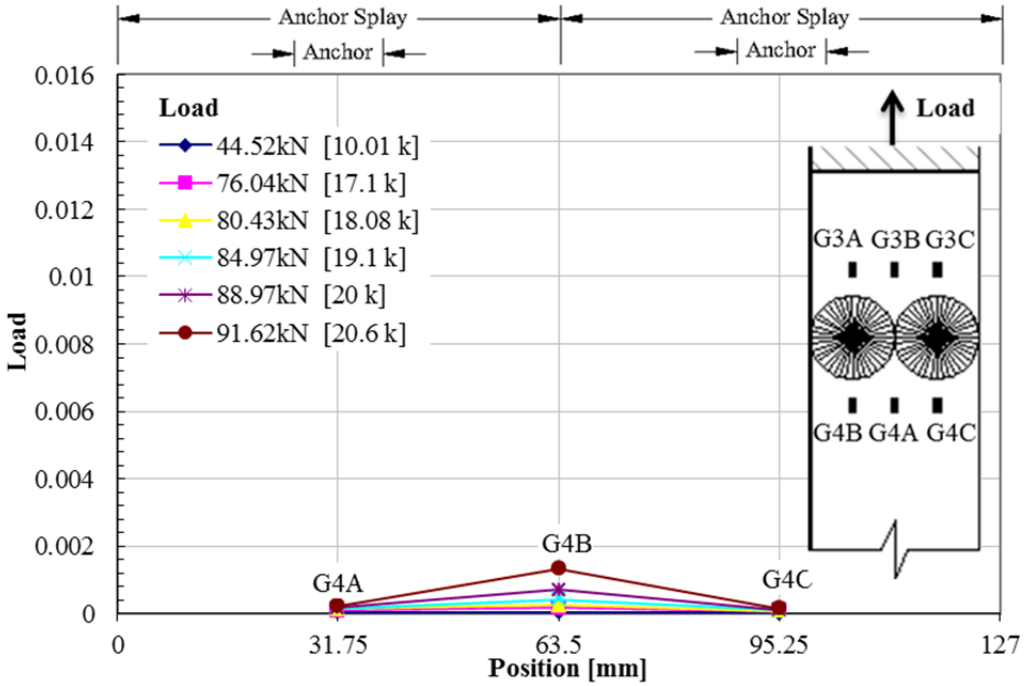

Figure 4.50 Transverse strain in specimen S1-4a-1-12.5 behind the anchors

4.3.3.3 Double Ply Specimens

4.3.3.3.1 Specimen S2-2a-24

Transverse strain distributions for specimen S2-2a-24 are shown in Figure 4.51 and Figure 4.52. Strain results from the single ply specimens indicated that anchors most efficiently secure the fibers in line with the anchors. It is believed that the additional ply helped distribute the load better across the width of the sheet. The variation in strain across the sheet is lower than in most other specimens. From initial loading until a load of approximately 62.5 kN [14,000 lbs] strain was almost constant across the width of the sheet.

There were significantly lower strains in specimen S2-2a-24 than in specimen S1-2a-24. This can be seen by comparing Figure 4.51 with Figure 4.35. In specimen S1-2a-24 at the failure load of approximately 77.8 kN [17,500 lbs] the strain in gauge G1 was

0.0061 compared to 0.0040, or approximately 30% less, at the same load in specimen S2-2a-24. Very low strains were measured in the three transverse gauges in front of the anchors until approximately 31.1 kN [12,500 lbs]. At this load all three gauges recorded a rapid increase in strain, indicating the initiation of debonding at these gauges. Gauges G3A and G3C then recorded an approximately constant rate of strain until failure. The rate of strain decreased in gauge G3B with increasing load. At the peak load there is a small increase in strain in gauge G3C and small decrease in G3A.

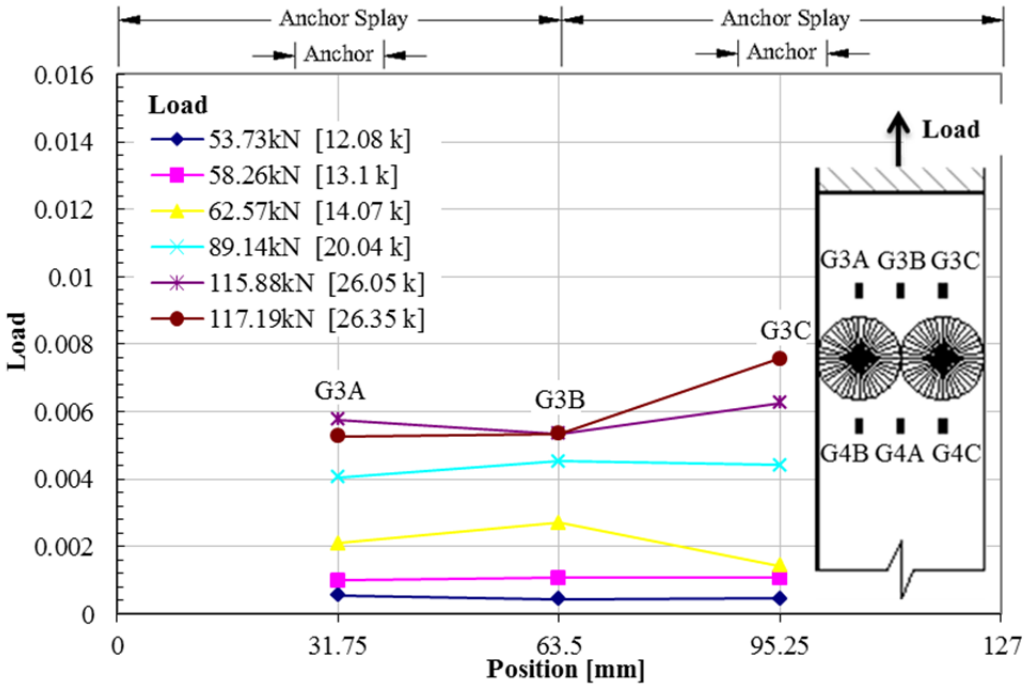

Figure 4.51 Transverse strain in specimen S2-2a-24 in front of the anchors

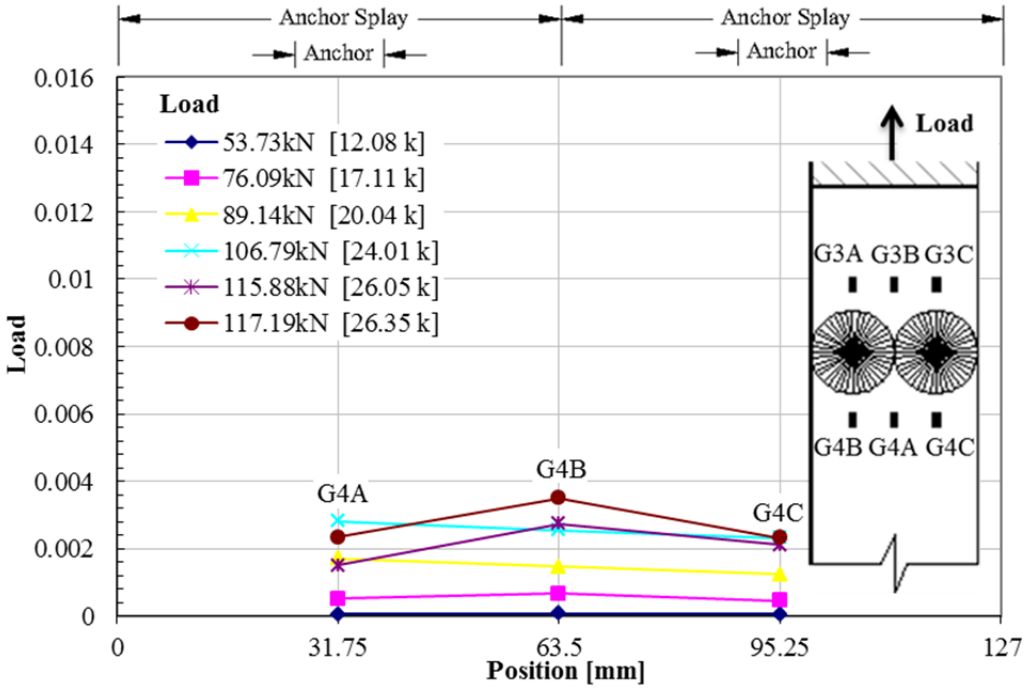

Figure 4.52 Transverse strain in specimen S2-2a-24 behind the anchors

Figure 4.52 shows that behind the anchors there were higher strains along the centerline of the sheet than in line with the anchors prior to failure. There was negligible rate of strain increase behind the anchors until approximately 62 kN [14,000 lbs]. From loads of 62 kN to 98 kN [14,000 lbs to 22,000 lbs] there was a significantly greater rate of strain, indicating the initiation of debonding at these gauges during this load interval. Several seconds prior to failure the anchor splays began to delaminate, as discussed in section 4.2.3.4. As the splays delaminated from the sheet, the sheet behind the anchors carried more load and there is a corresponding rapid increase in strain in all three gauges prior to failure.

4.3.3.3.2 Specimen F2-2a-24

Transverse strain distributions for specimen F2-2a-24 are presented in Figure 4.54 and Figure 4.55. It is difficult to describe the transverse strain for specimen F2-2a-24, since it took three test runs to fail the specimen, as discussed in section 4.2.3.2.

Fortunately the strain results from the first, second and final test runs in gauges G1, 2, 3A, 3B, and 3C converge very closely at higher loads. Gauge G4A shows slightly more strain in the third run than on the first, gauge G4B shows approximately the same, and gauge G4C shows slightly more. It appears that gauge G5 would have converged if the first run had reached a higher load.

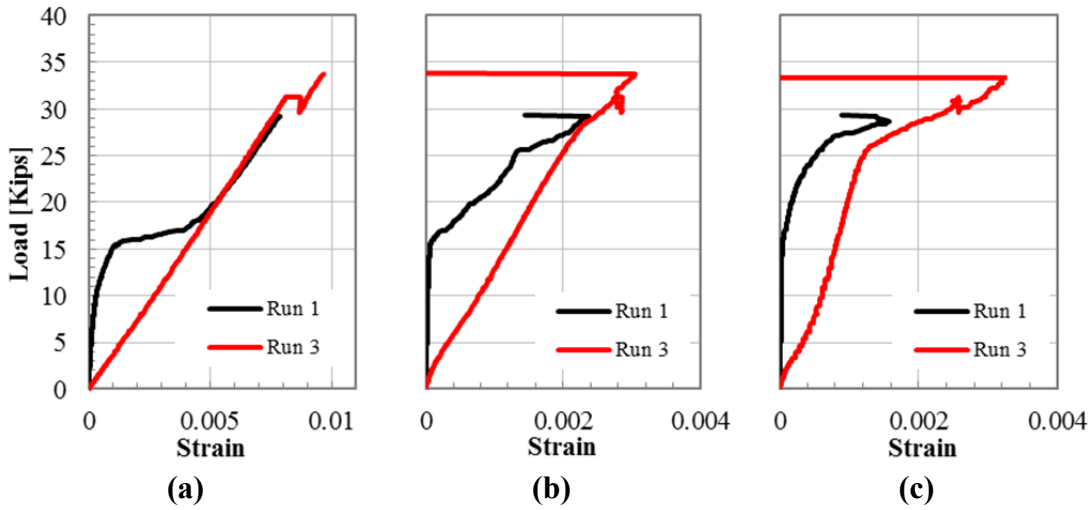

Figure 4.53 (a) Gauge G3B, (b) Gauge G4B, (c) Gauge G5 for test runs 1 and 3.

In the first test attempt, there was a low rate of strain increase in the three gauges in front of the anchors until approximately 53 kN [12,000 lbs]. From approximately 53 kN to 80 kN [12,000 lbs to 18,000 lbs] all three gauges recorded a rapid increase in strain, indicating the initiation of debonding at these gauges during this load interval. From approximately 80 kN [18,000 lbs] to failure, gauges G3A and G3B recorded the same constant rate of strain, and gauge G3C recorded a lower rate of strain, until the sheet slipped from the loading grips. It is believed that this is due to localized FRP anchor effects or a skewed debonding crack front.

In the third test run gauges G3A, G3B and G3C recorded a constant rate of strain increase from initial loading until the FRP patch delaminated on the left side of the sheet

at a load of 138 kN [31,000 lbs], as discussed in section 4.2.3.2. As with the first and second test runs, gauges G3A and G3B recorded a very close rate of strain, and gauge G3C recorded a lower rate of strain. As with specimen S2-2a-24, the variation in strain across the sheet is lower than in most other specimens, which again suggests that the additional ply helps better distribute the load across the width of the sheet. At a load of 138 kN [31,000 lbs], all three gauges recorded a sudden small increase in strain followed by a linear increase in strain until failure.

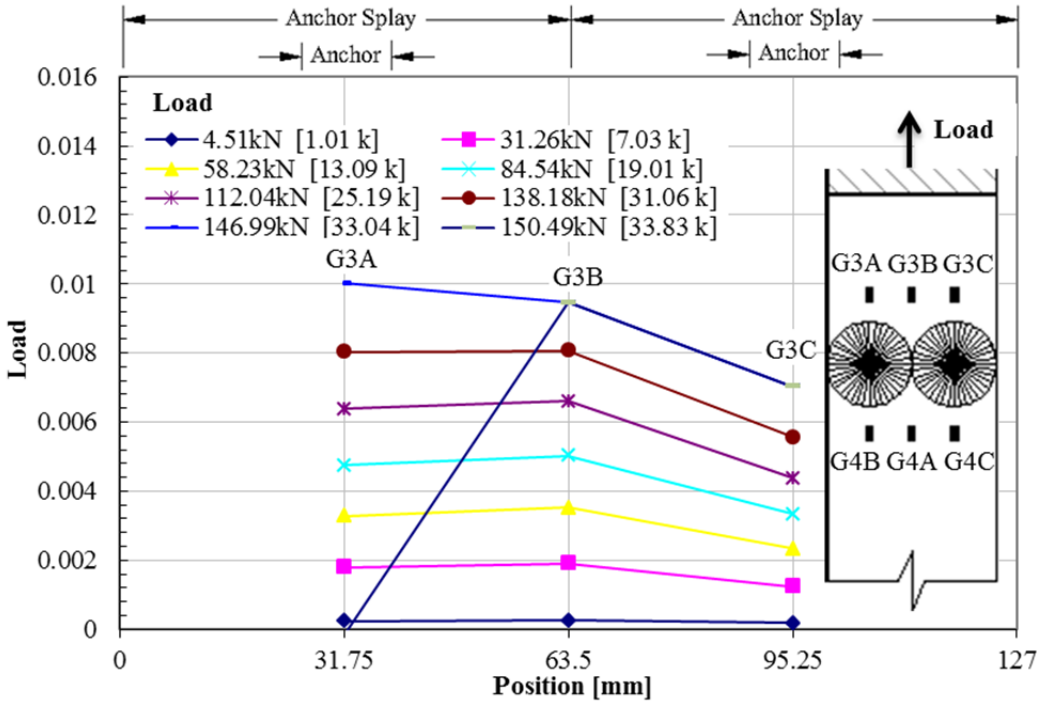

Figure 4.54 Transverse strain in specimen F2-2a-24 in front of the anchors

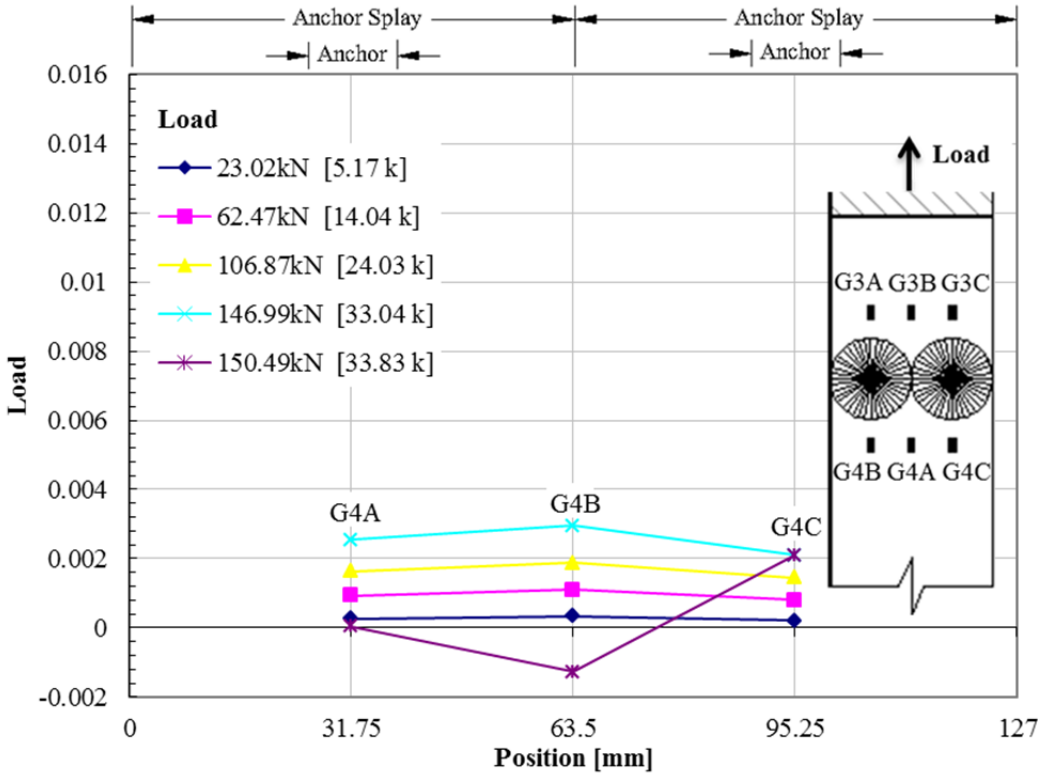

Figure 4.55Transverse strain in specimen F2-2a-24 behind the anchors

For the first test attempt, there was negligible strain in the transverse gauges located behind the anchors, until the debonding front passed the gauges in front of the anchors, at a load of approximately 71 kN [16,000 lbs]. From loads of 76 kN to 98 kN[17,000 lbs to 22,000 lbs] and from 98 kN to 116 kN [22,000 lbs to 26,000 lbs] gauges G4A and G4C, respectively, recorded a slight decrease in strain. These two gauges then recorded a rapid increase in strain until the sheet slipped from the loading plates. Gauge G4B recorded a constant rate of strain increase from 71 kN to 111 kN [16,000 lbs to 25,000 lbs] and then a greater rate of strain from a load of 111 kN [25,000 lbs] until the sheet slipped. For test attempt three, strain increased at a constant rate in gauges G4A, G4B, G4C from initial loading to a load of 129 kN [29,000 lbs], the peak load from the first test attempt, and then recorded an increased rate until 138 kN [31,000 lbs]. At a load of 138 kN [31,000 lbs], the load at which the FRP patch debonded, all three gauges

recorded erratic readings, and the sheet failed shortly after. Behind the anchors, there was only minimal variation in the three gauges, although there were slightly higher strains along the centerline of the sheet than in line with the anchors.

4.3.3.3.3 Specimen S2-4a-1-24

Transverse strain distributions for specimen S2-4a-1-24 are presented in Figure 4.56 and Figure 4.57. A comparison of Figure 4.56 with Figure 4.39 shows that the strains in specimen S2-4a-1-24 were significantly lower than the strains in specimen S1-4a-1-24. In specimen S1-4a-1-24 at the failure load of approximately 21,000 lbs the strain in G1 was 0.0066 compared to 0.0050 at the same load in specimen S2-4a-1-24.

There was negligible strain in the three transverse gauges in front of the anchors until a load of approximately 45 kN [10,000 lbs], at which point there was an increase in rate of strain in all three gauges. Gauges G3A and G3C then recorded a nearly equal constant rate of strain from 45 kN [10,000 lbs] until failure. This is unlike the strain readings from in front of the anchors of most specimens, in which there was three distinct periods of strain behavior, as discussed in section. From initial loading until approximately 90 kN [20,000 lbs] the recorded strain distribution across the sheet was nearly constant, which again suggests that the additional ply helps better distribute the load across the sheet. At loads greater than 90 kN [20,000 lbs] the shape of the transverse strain distribution in front of the anchors is typical of anchored specimens, with higher strains in line with the anchors, than along the centerline of the sheet. The strain distribution was nearly symmetric at all loads.

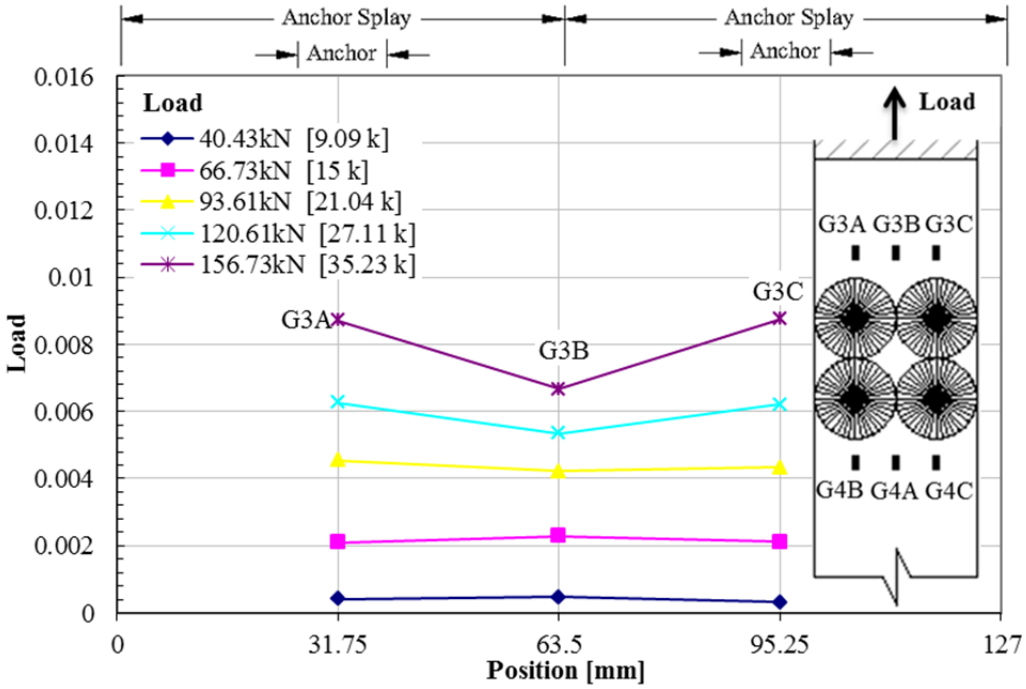

Figure 4.56Transverse strain in specimen S2-4a-1-24 in front of the anchors

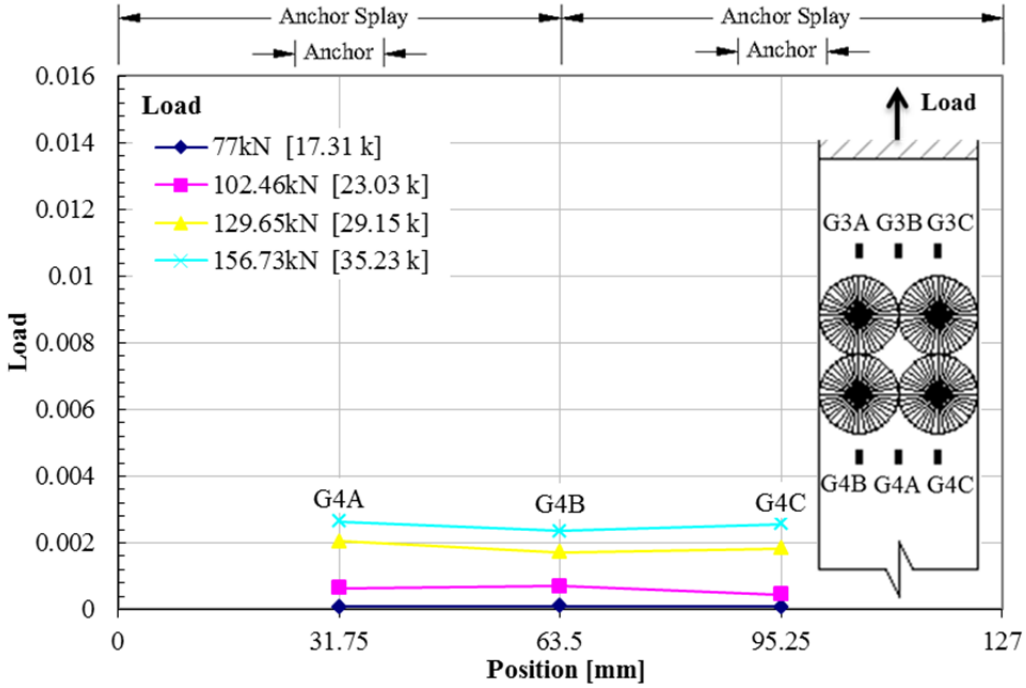

Figure 4.57 Transverse strain in specimen S2-4a-1-24 behind the anchors

There was a very low rate of strain behind the anchors until a load of approximately 80.1 kN [18,000 lbs]. From a load of 80.1 kN [18,000 lbs] to failure, there

was a significantly greater rate of strain, indicating the initiation of debonding at these strain gauges. The strain distribution behind the anchors was nearly constant throughout the entire test.

4.3.3.3.4 Specimen F2-4a-1-24

Transverse strain distributions for specimen F2-4a-1-24 are shown in Figure 4.58 and Figure 4.59. There were higher strains on the left side of the sheet as shown in Figure 4.58. Gauges G3A, 3B and 3C showed minimal strain until a load of approximately 62 kN [14,000 lbs], at which point all three gauges show a rapid increase in strain, indicating the initiation of debonding at these gauges. For the majority of loads there were greater strains in line with the anchors than along the centerline of the sheet, like most anchored specimens. Like other double ply specimens, there is a lower amount of variation across the width of sheet compared to most anchored single ply specimens.

There was very low strain in gauges G4A, G4B, and G4C, located behind the anchors, until the debonding front passed the gauges in front of the anchors, at a load of 62 kN [14,000 lbs]. From loads of 62 kN to 133 kN [14,000 lbs to 30,000 lbs] the rate of strain recorded by the three gauges increased slowly with increasing load. At a load of approximately 133 kN [30,000 lbs] there was a significant increase in load, indicating the initiation of debonding at these three gauges. From loads of 133 kN to 165 kN [30,000 lbs to 37,000 lbs] there was an approximately linear increase in strain in all three gauges. From 165 kN [37,000 lbs] to failure gauge G4C recorded an overall decrease in strain, while gauges G4A and G4B recorded increases in strain, which indicates an uneven debonding front.

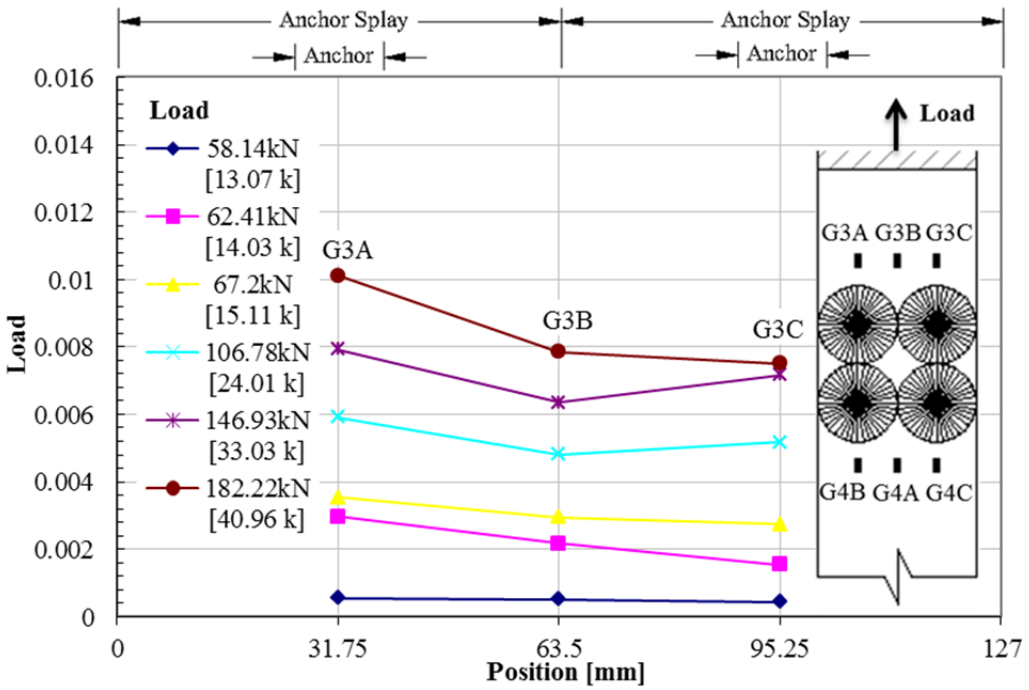

Figure 4.58 Transverse strain in specimen F2-4a-1-24 in front of the anchors

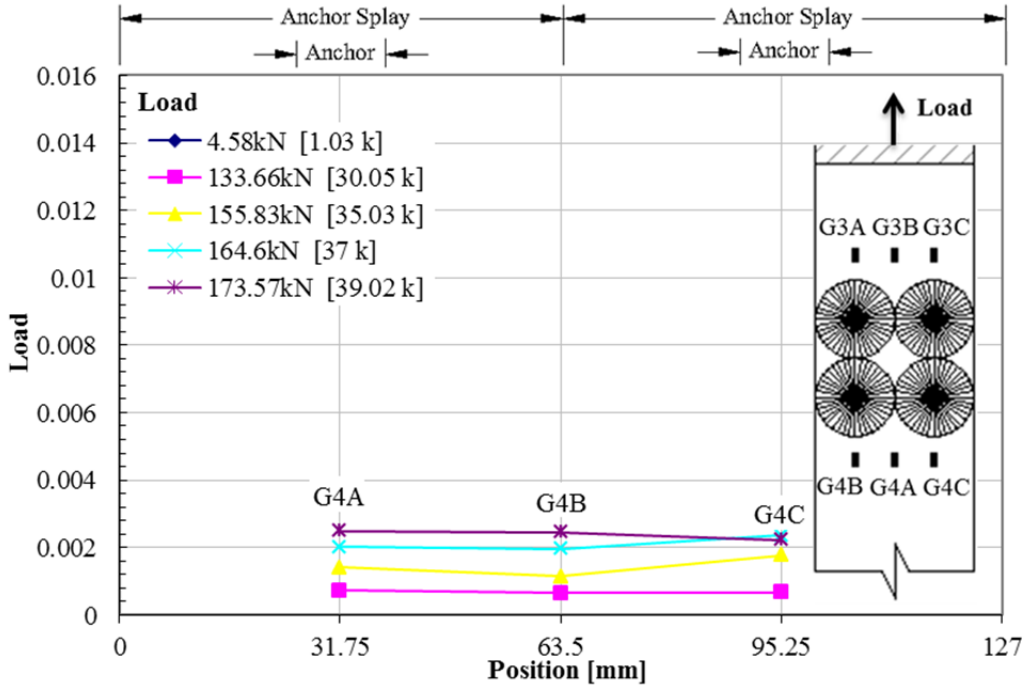

Figure 4.59 Transverse strain in specimen F2-4a-1-24 behind the anchors

4.3.3.4 Unbonded Specimens

4.3.3.4.1 Specimen F1-2a-24U

Transverse strain distributions for specimen F1-2a-24U are presented in Figure 4.60 and Figure 4.61. An important observation is that in front of the anchors the strain is greater in line with the anchors than along the center line, as was true for most of the bonded and anchored specimens. Since the specimen was unbonded in front of the anchors, and therefore the bond did not influence the stress distribution, this is further evidence that the anchor splays most effectively hold the sheet in line with the anchors.

Gauge G3B recorded a constant rate of strain increase from 4.4 kN [1,000 lbs] until failure. Gauges G3A and G3C recorded constant rate of strain increase from 4.4 kN [1,000 lbs] until [8,000 lbs]. G3A recorded a slightly greater rate of strain than G3C, indicating that the left anchor was attracting more load than the right anchor. A likely explanation for this is that the left anchor splay more effectively grasped the sheet than the right anchor. Around 35.6 kN [8,000 lbs] the edges of the right anchor splay could be seen detaching from the sheet in the test video, as discussed in section 4.2.4.1. From 35.6 kN to 43.6 [8,000 lbs to 9,800 lbs] there was a rapid increase in strain in G3A, while G3C recorded a reduction in rate of strain. It is possible that the anchor splays fully delaminated and the anchors were able to resist load by the anchor shaft bearing against the FRP sheet that placed behind the anchors to prevent splitting of the sheet. At a load of 43.6 kN [9,800 lbs] it is believed that anchor damage, or deflection of the anchors, caused load to transfer to the bonded section behind the anchors, as discussed in section 4.2.4.1. Gauges G3A and G3C showed approximately equal strain from a load of 43.6 kN [9,800 lbs] until failure, as shown in Figure 4.60 and Figure 4.62, indicating that the load

redistributed more evenly to the two anchors. From 43.6 kN [9,800 lbs] to failure, all three gauges showed approximately equal constant rate of strain.

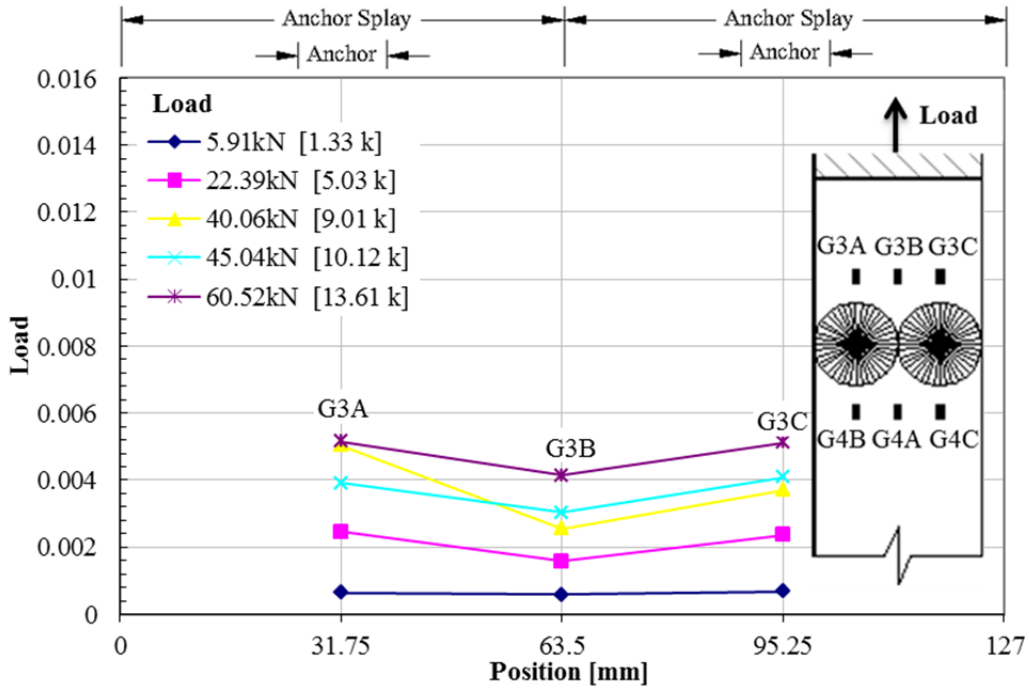

Figure 4.60 Transverse strain in specimen F1-2a-24U in front of the anchors

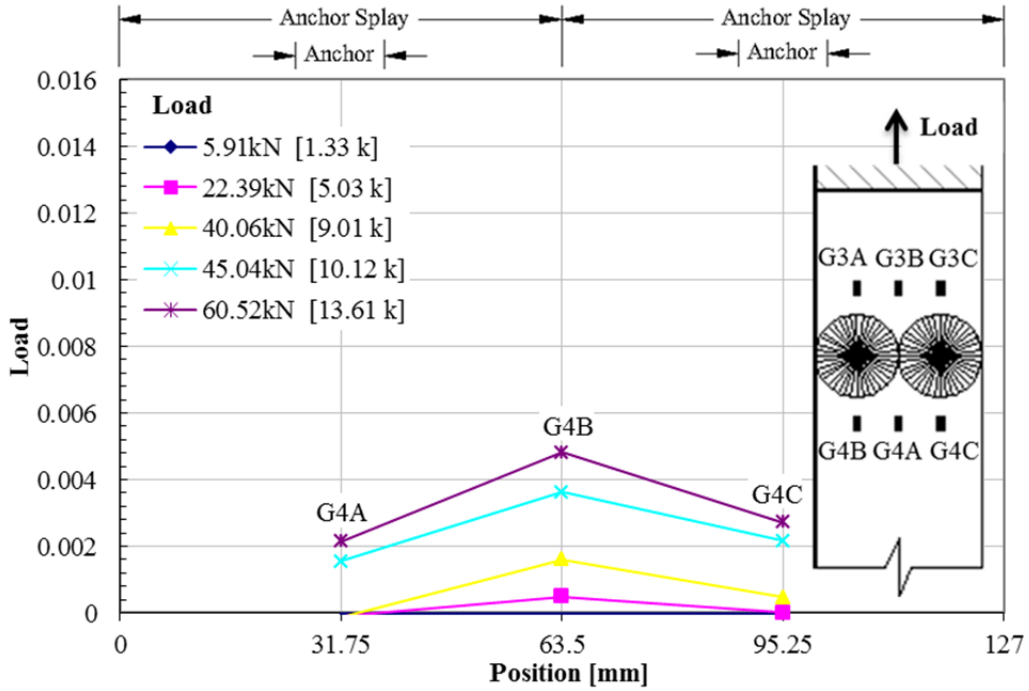

Figure 4.61 Transverse strain in specimen F1-2a-24U behind the anchors

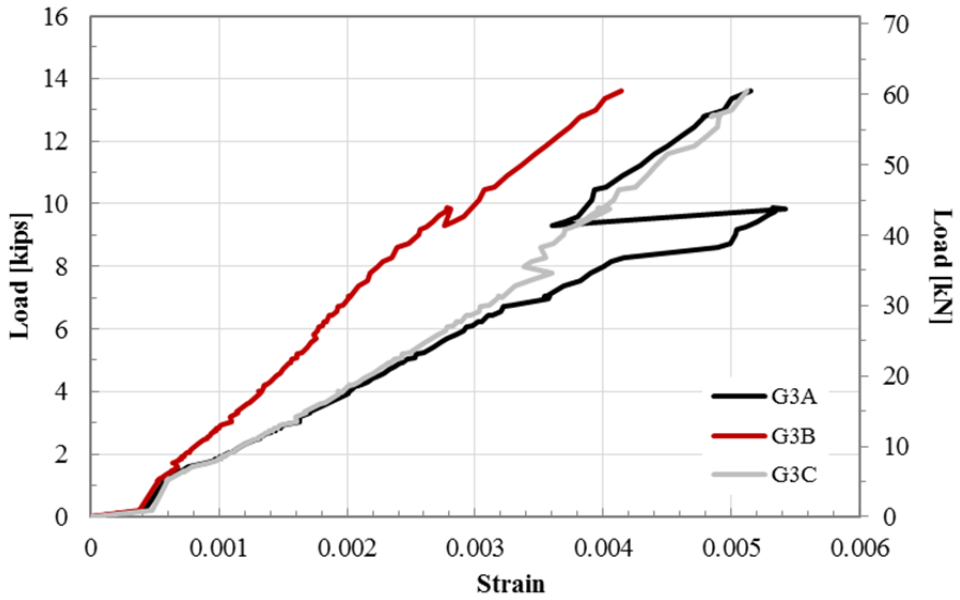

Figure 4.62 Specimen F1-2a-24U strain gauges G3A, G3B and G3C

The strain behind the anchors was greater along the centerline of the sheet than in line with the anchors, as with most of the anchored-bonded specimens. The drop in strain from in front to behind the anchors was not as significant as with the anchored-bonded specimens. From initial loading to approximately 35.6 kN [8,000 lbs] there is minimal strain in gauges G4A and G4C. Gauge G4A actually recorded negative strain from initial loading to 43.6 kN [9,800 lbs] and G4C recorded negative strain until approximately 20.0 kN [4,500 lbs]. At a load of approximately 35.6 kN [8,000 lbs], the load in which the anchors splays visibly began to delaminate from the sheet, as explained in section 4.2.4.1, there is an increase in rate of strain in gauges G4B and G4C, and gauge G4A records a small decrease in strain. At a load of 43.6 kN [9,800 lbs] there was a large jump in strain in all three gauges, indicating that the anchors suddenly resisted less load. It is likely that the anchors still resisted some load since the specimen reached a peak load of 61.8 kN [13,900 lbs], which is 24% higher than the failure load of the bonded but unanchored specimen, F1-0a-24. After the jump in strain, gauges G4A and G4C recorded an

approximately equal constant increase in strain until failure, while gauge G4B recorded a greater rate of strain, as expected.

4.3.3.4.2 Specimen F1-4a-1-24U

Transverse strain distributions for specimen F1-4a-1-24U are presented in Figure 4.63 and Figure 4.64. As with specimen F1-2a-24U, the strain in front of the anchors was greater in line with the anchors than along the center line of the sheet, as shown in Figure 4.63. All three transverse gauges in front of the anchors showed a constant rate of strain increase until failure. Gauge G3A recorded approximately a 40% higher rate of strain than G3C.

There was a much larger drop in strain from in front to behind the anchors in this specimen than in specimen F1-2a-24U, which indicates that the four anchors in this specimen resisted more load than the two anchors in specimen F1-2a-24U. The lower strains behind the anchors also indicates that the bonded zone in specimen F1-4a-1-24U resisted less load than in F1-2a-24U. As with specimen F1-2a-24U, there was initially negative strain behind, and in line with the anchors. All three gauges then show periods of constant increases in strain, separated by sudden small jumps in strain. These small increases in strain are likely due to the anchors suddenly resisting less load, either due to anchor deflection or anchor damage.

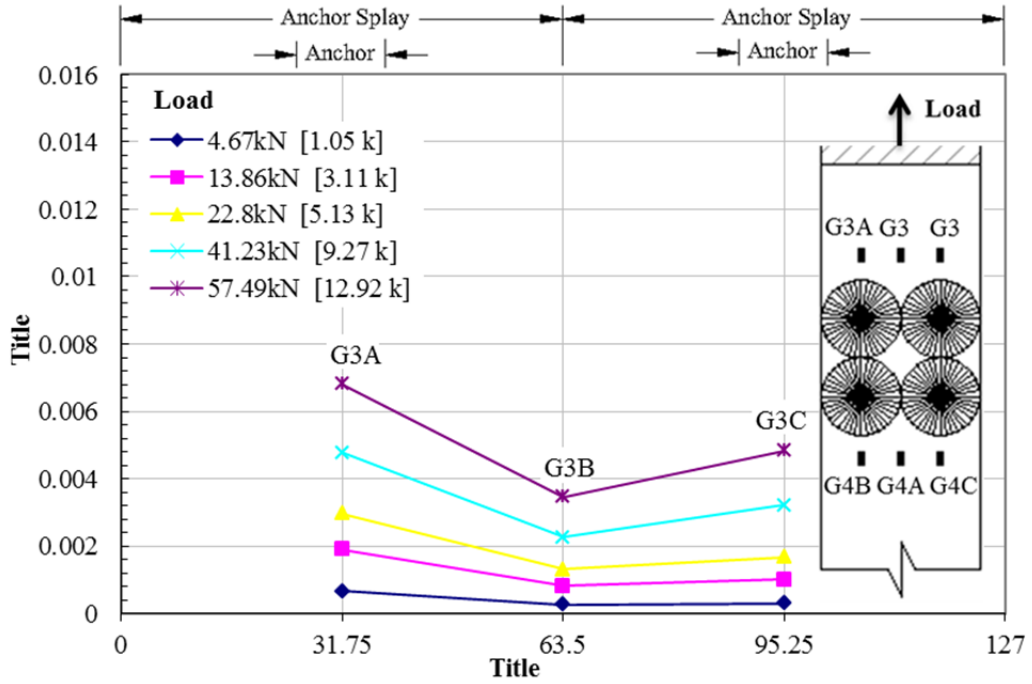

Figure 4.63 Transverse strain in specimen F1-4a-1-24U in front of the anchors

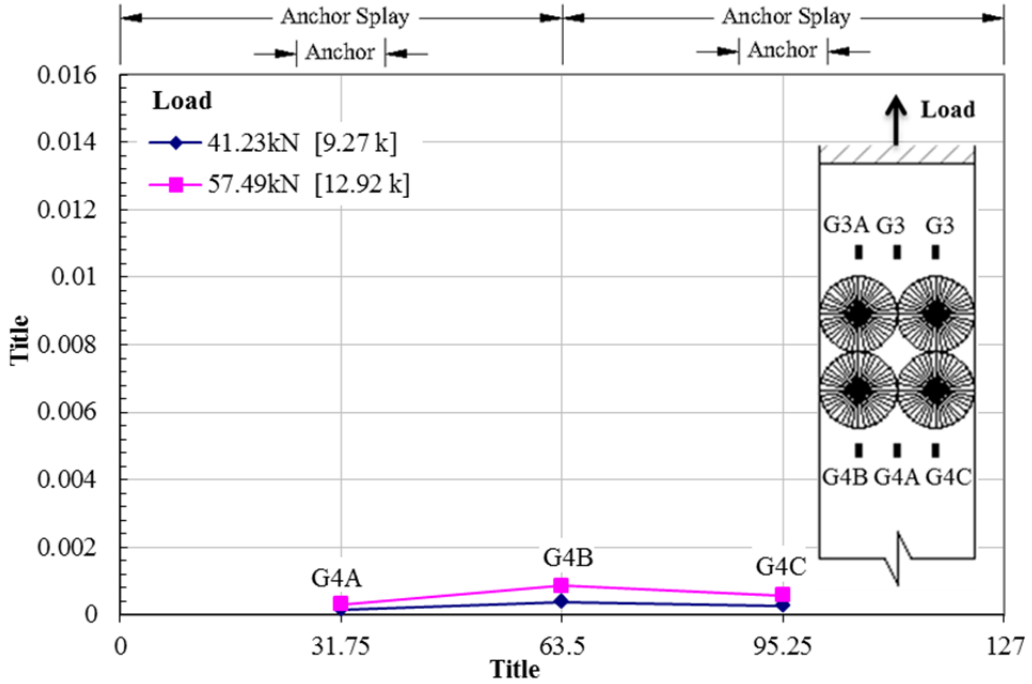

Figure 4.64 Transverse strain in specimen F1-4a-1-24U behind the anchors

4.3.4 Strain Distribution along FRP Laminate

This section presents the longitudinal strain distribution data for each specimen. To capture the longitudinal strain distribution, a column of gauges was placed along the center line of the FRP sheet. Strains were plotted at selected loads to show the variation of longitudinal strains distribution with increasing load. The locations of the strain gauges are given in Figure 3.15 through Figure 3.21. Strain gauge identification is given in Figure 3.25. All strain distributions are plotted at the same scale so that different specimens can be easily compared.

4.3.4.1 General Observations of Strain Distribution along FRP Laminate

This section discusses overall trends in the recorded strain distributions along the FRP sheets. Detailed descriptions of the strain distributions across the FRP sheets for each specimen are given in sections 4.3.4.2 (unanchored single ply specimens), 4.3.4.3 (anchored single ply specimens), 4.3.4.4 (double ply specimens) and 4.3.4.5 (anchored-unbonded specimens).

For unanchored-bonded specimens, from initial loading to the initiation of debonding, strain increased within the stress transfer zone (STZ), which is the length of bonded sheet that is effectively engaged in the stress transfer to the concrete surface. In all unanchored-bonded specimens, the strain decreased exponentially within the STZ and beyond the STZ there was negligible strain. When the capacity of the STZ was reached, debonding initiated, and the STZ progressed along the sheet towards the unloaded end of the FRP sheet with little change in load. The longitudinal strain distributions of the anchored-bonded and unanchored-bonded specimens were similar, or even

indistinguishable, prior to the initiation of debonding because the anchors were either outside or near the end of the STZ, and therefor assumed little load. The anchors allowed much higher strains to be developed in the sheet, and therefore increased load capacity. The increase in load compared to identical unanchored specimens is related to the amount of load resisted by the anchors, and the amount of load resisted by the anchors is related to the drop in strain from in front to behind the anchors. The level of strain behind the anchors indicates whether or not the debonding front passed the anchors. Typically there were significantly lower strains behind the anchors in specimens with four anchors than in identical specimens with two anchors at the same loads, which indicates that the additional row of anchors further discouraged the debonding front from passing the anchors.

In anchored and unanchored specimens the strains were not constant along the length of FRP sheet in the unbonded region. As discussed in section 6.5.8, finite element modeling showed that there is a complex stress distribution in the unbonded region. In anchored specimens there is an even larger variation in stresses in the unbonded region. In many of the anchored specimens there was a decrease in strain from gauge G1 to G2 and a large increase in strain from gauge G2 to G3B.

4.3.4.2 Unanchored Single Ply Specimens

4.3.4.2.1 Specimen S1-0a-24

The longitudinal strain distributions for specimen S1-0a-24 is presented in Figure 4.65. For an unknown reason there was greater noise in the strain data than for any other test. From initial loading to approximately 35.6 kN [8,000 lbs] strain increases within the STZ. Figure 4.65 shows a rapid increase in strain in gauges G2 and G3 from 35.95 kN to

40.34 kN [8,080 lbs to 9,070 lbs], which indicates the initiation of debonding at these gauges. The STZ appears to be approximately 100 mm [4 in.] long since there appears to be little strain beyond gauge G3 prior to the initiation of debonding. The maximum strain in the sheet changed little after debonding initiated.

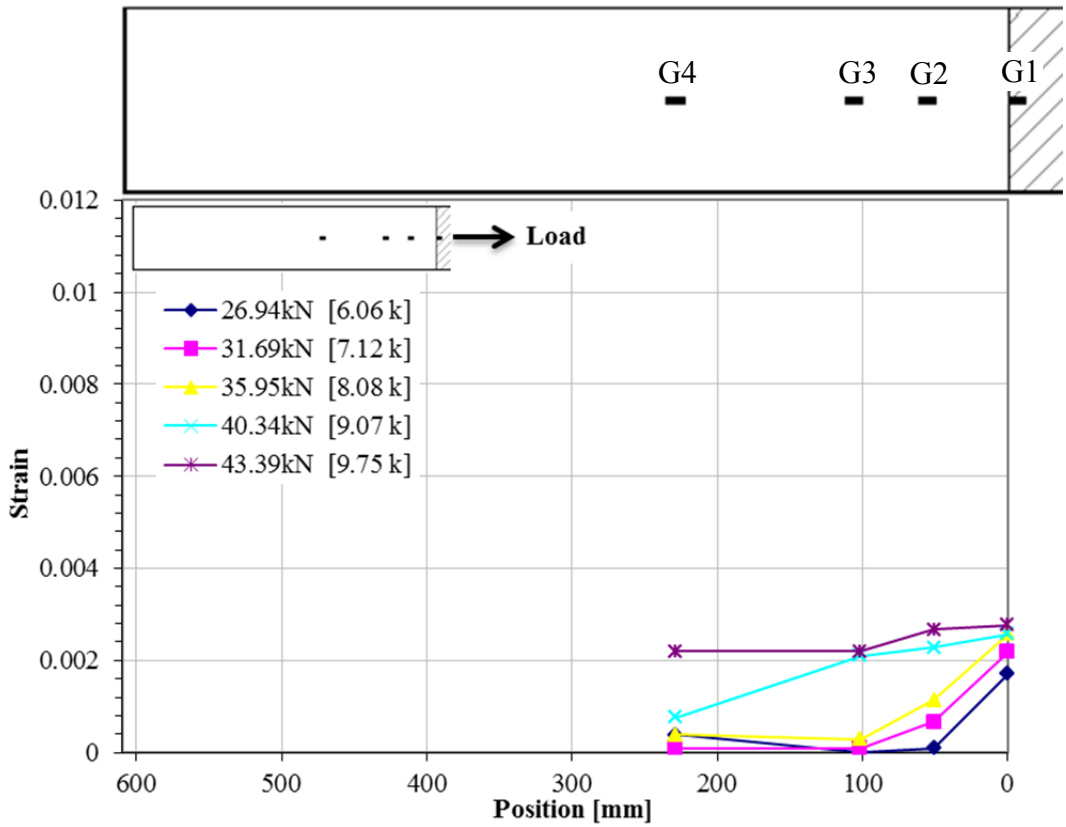

Figure 4.65 Longitudinal strain profile for specimen S1-0a-24

4.3.4.2.2 Specimen F1-0a-24

The longitudinal strain profile for specimen F1-0a-24 is presented in Figure 4.66. The strain profile matches the behavior of the other two unanchored specimens (S1-0a-24 and F2-0a-24). The STZ appears to be approximately 100 mm [4 in.] long, since there was negligible strain beyond gauge G3 prior to debonding at a load of approximately 44.5 kN [10,000 lbs]. From initial loading to a load of 44 kN [10,000 lbs] strain increased in the sheet within the STZ, and there was negligible strain beyond the STZ. Figure 4.66

shows a rapid increase in strain in gauges G2 and G3 from 44.58 kN to 49.05 kN [10,020 lbs to 11,030 lbs], which indicates the initiation of debonding at these gauges. Shortly after, the debonding front reaches gauge G4, which is evident by a rapid increase in strain from loads of 49.05 kN to 46.92 kN [11,030 lbs to 10,550 lbs]. There was minimal change in the maximum load/ strain after debonding initiated. As can been seen in Figure 4.66, at a load of 46.92 kN [10.55 k] the strain is not constant along the length of the sheet in the debonded region.

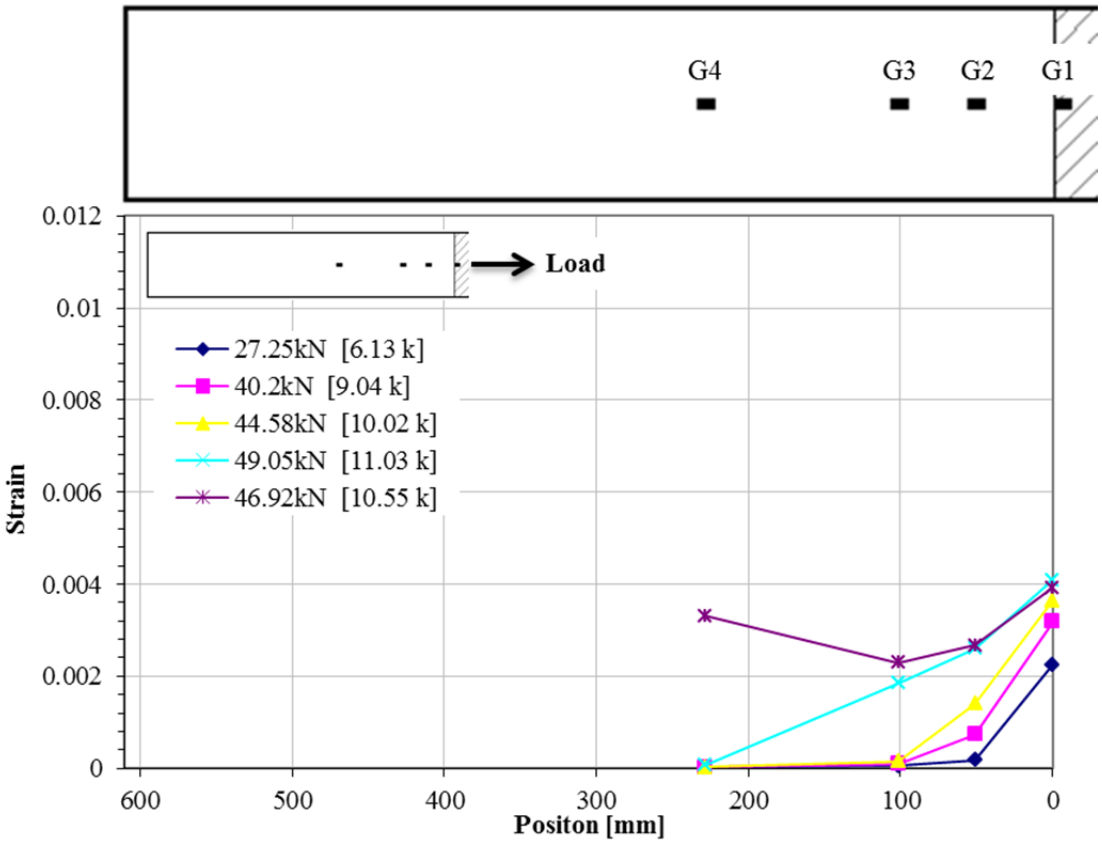

Figure 4.66 Longitudinal strain profile for specimen F1-0a-24

4.3.4.3 Anchored Single Ply Specimens

4.3.4.3.1 Specimen S1-2a-24

The longitudinal strain profile for specimen S1-2a-24 is presented in Figure 4.67. At a load of approximately 31 kN [7,000 lbs] there was a rapid increase in strain in gauges G2 and G3B, indicating that the initiation of debonding at these gauges. Unlike the unanchored specimens, the load increased significantly after the initiation of debonding, and the debonding front temporarily stopped in front of the anchors. This is very important, because it means the maximum attainable strain in the sheet is not limited by the capacity of the STZ. The peak load was 80% higher than that of specimen S1-0a-24.

There was negligible increase in strain in gauges G4B and G5, located behind the anchors, until a load of 31 kN [7,000 lbs], the load at which debonding initiated in front of the anchors. Gauge G4B recorded a slow increase in rate of strain from 31 kN to 49 kN [7,000 lbs to 11,000 lbs], and then a sudden increase in rate of strain at 49 kN [11,000 lbs], indicating the initiation of debonding at this gauge. From 49 kN to 71 kN [11,000 lbs to 16,000 lbs] gauge G4B recorded a linear increase in strain and then from 71 kN [16,000 lbs] until failure recorded a rapid increase in strain. Gauge G5 recorded a slow increase in rate of strain from 31 kN to 71 kN [7,000 lbs to 16,000 lbs], and then a rapid increase in strain from 71 kN [16,000 lbs] to failure, indicating the initiation of debonding at this gauge.

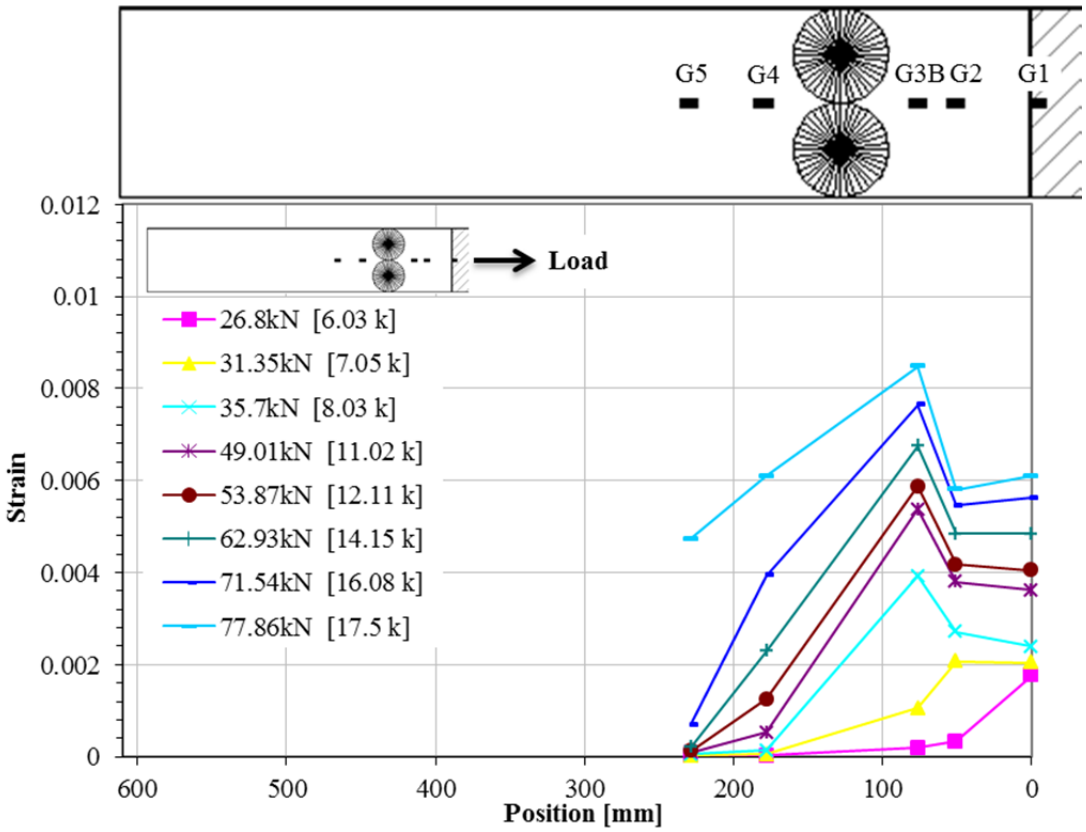

Figure 4.67 Longitudinal strain profile for specimen S1-2a-24

4.3.4.3.2 Specimen F1-2a-24

The longitudinal strain profile for specimen F1-2a-24 is presented in Figure 4.68. From loads of 40 kN to 44 kN [9,000 lbs to 10,000 lbs] there was a rapid increase in strain in gauges G2 and G3B, indicating the initiation of debonding at these gauges. The debonding front temporarily stopped at the anchors as strain continued to increase. The maximum strain achieved along the centerline of the sheet was 0.00952, which is approximately 230% more than in the unanchored Fyfe specimen (F1-0a-24). The peak recorded strain was very close to that from the identical Sika specimen (S1-2a-24), but the strains were significantly lower behind the anchors compared to the Sika specimen, which is logical because the Sika specimen failed by debonding.

There was negligible increase in strain in gauges G4B and G5, located behind the anchors, until a load of 40 kN [9,000 lbs], the load at which debonding initiated in front of the anchors. At a loads of 53 kN and 71 kN [12,000 lbs and 16,000 lbs] gauges G4B and G5, respectively, recorded an increase in rate of strain, and then an approximately constant increase in strain until failure of the specimen. Figure 4.14 shows that debonding did progress past the anchors across a portion of the width of the sheet, although it is not clear from the data when debonding initiated behind the anchors.

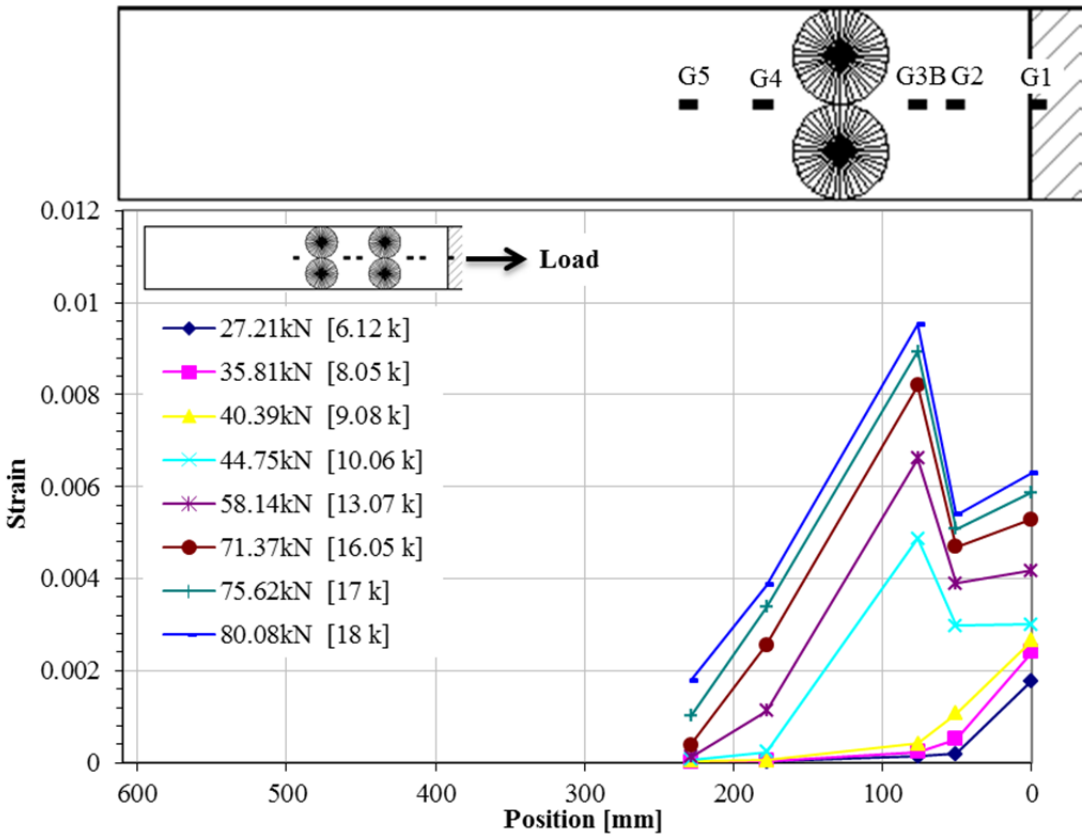

Figure 4.68 Longitudinal strain profile for specimen F1-2a-24

4.3.4.3.3 Specimen S1-4a-1-24

The longitudinal strain profile for specimen S1-4a-1-24 is presented in Figure 4.69. From loads of 36 kN to 44 kN [8,000 lbs to 10,000 lbs] there was a rapid increase in strain in gauges G2 and G3B, indicating that initiation of debonding at these gauges. At a

load of 40 kN [9,000 lbs] the strain was approximately equal in gauges G2 and G3B, however at a load of 44 kN [10,000 lbs], the strain in G3B was 67% greater than in G2. From a load of 44.5 kN [10,000 lbs] to failure of the specimen, gauges G1 and G2 recorded a constant increase in strain. However, gauge G3B continued to show a rapid increase in strain until 52.0 kN [11,700 lbs] at which point it recorded infinite strain, indicating local fiber rupture. This second row of anchors in specimen S1-4a-1-24 allowed higher strains to develop in front of the anchors compared to in specimen S1-2a-24, which resulted in a higher failure load. The additional anchor row also further delayed debonding. The very low strain in the gauges behind the anchors indicate that debonding did not initiate behind the anchors until shortly before failure, whereas specimen S1-2a-24 failed by debonding.

4.3.4.3.4 Specimen F1-4a-1-24

The longitudinal strain profile for specimen F1-4a-1-24 is presented in Figure 4.70. From loads of 40 kN to 44 kN [9,000 lbs to 10,000 lbs] there was a rapid increase in strain in gauges G2 and G3B, indicating the initiation of debonding at these gauges. From a load of 44.5 kN [10,000 lbs] to failure of the specimen, gauges G1, G2 and G3B recorded a constant rate of strain increase. Gauge G2 recorded a slightly lower rate of strain increase than gauges G1 and G3. The anchors successfully stopped the debonding front from progressing along the sheet, which is evident by the very low strain behind the anchors at failure in Figure 4.70.

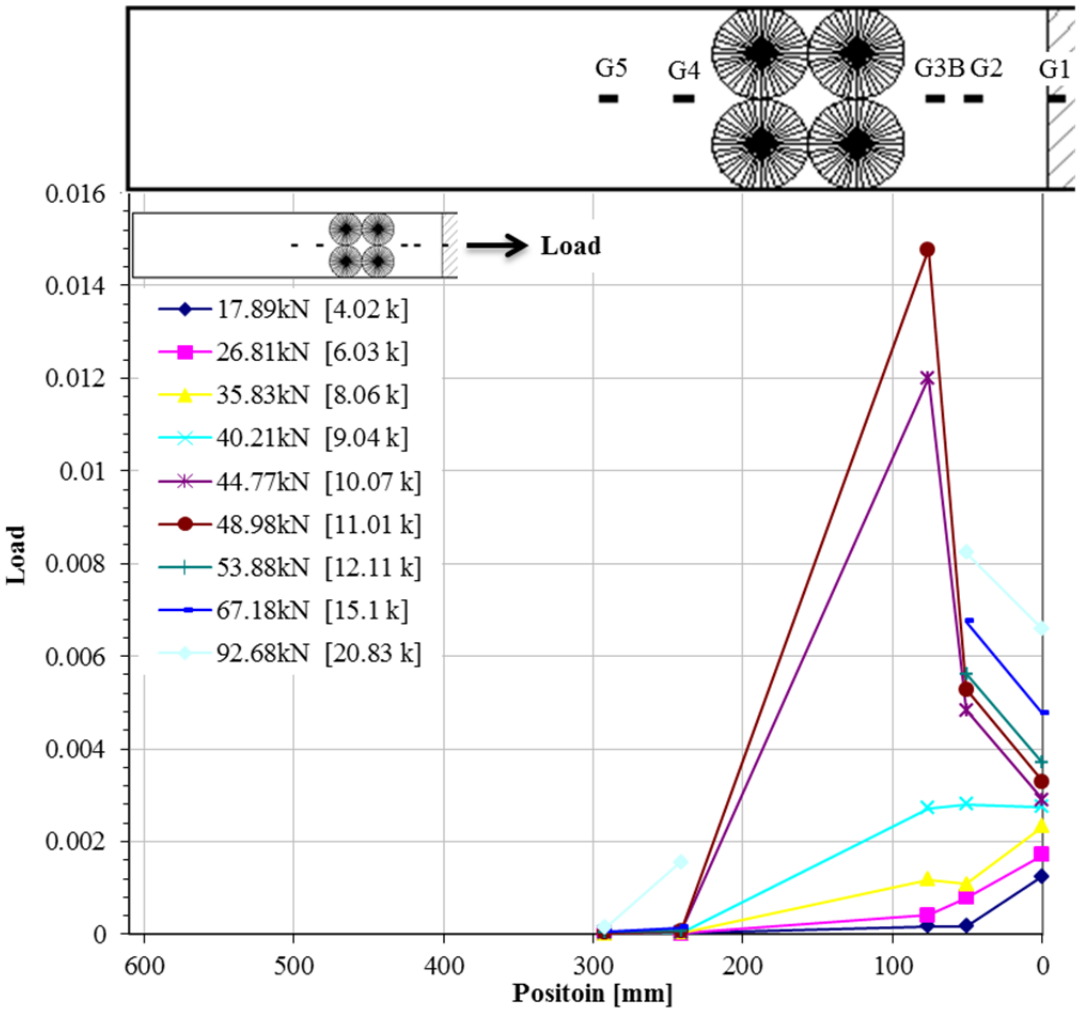

Figure 4.69 Longitudinal strain profile for specimen S1-4a-1-24

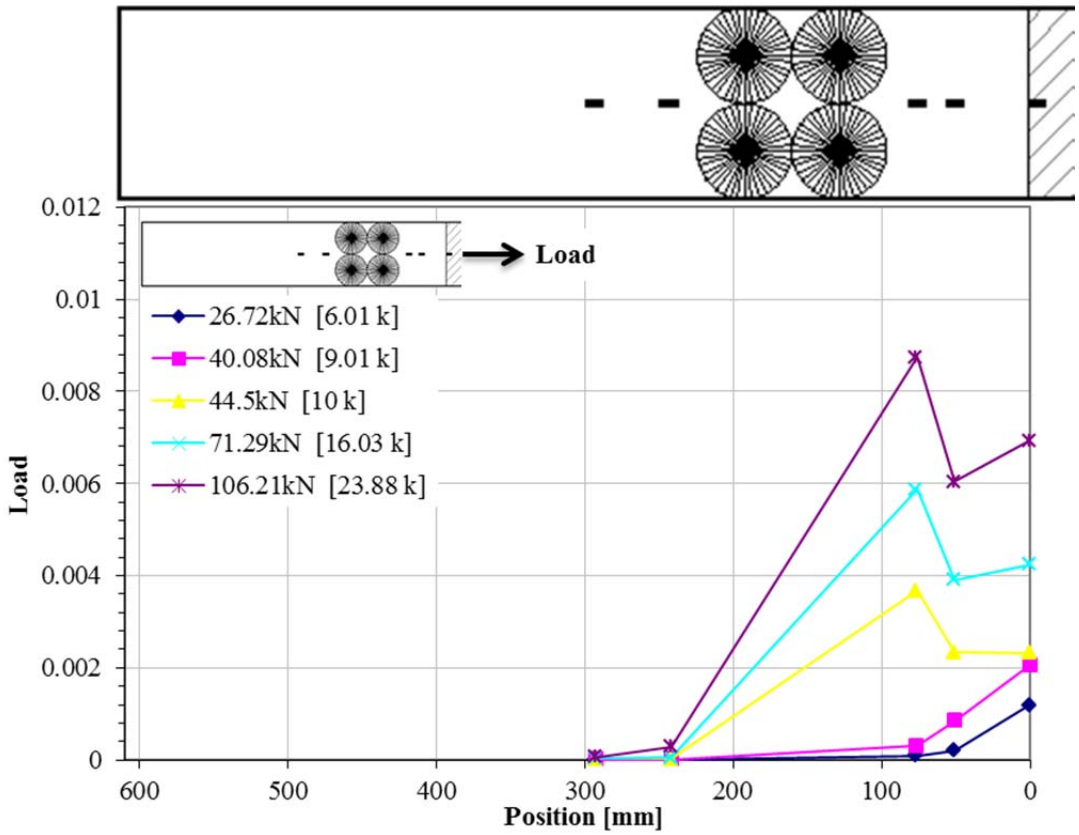

Figure 4.70 Longitudinal strain profile for specimen F1-4a-1-24

4.3.4.3.5 Specimen S1-4a-1-12.5

The longitudinal strain profile for specimen S1-4a-1-12.5 is presented in Figure 4.71. Specimen S1-4a-1-12.5 was identical to specimen S1-4a-1-24, except for length of bonded sheet behind the anchors, which was shortened from 610 mm to 320 mm [24 in to 12.5 in.].

From loads of 40 kN to 44 kN [9,000 lbs to 10,000 lbs] there was a rapid increase in strain in gauges G2 and G3B, indicating that the initiation of debonding at these gauges. The debonding front passed these gauges in specimen S1-4a-1-12 at approximately the same load. From 48.9 kN [11,000 lbs] until failure of the specimen gauges G1, G2 and G3B recorded an approximately constant rate of strain increase.

Gauge G1 recorded a slightly greater rate of strain than gauge G2, and gauge G3B recorded approximately twice the rate of strain of G2.

The low strain levels behind the anchors, indicate that the anchors stopped the debonding front until shortly before failure of the specimen. It appears from Figure 4.71, that the debonding front passed gauge G4B shortly before failure but did not reach gauge G5. The strain profile is very similar to that of specimen S1-4a-1-24. This is logical since in both specimens there was very low strains behind the anchors, which indicates that the additional length of sheet in specimen S1-4a-1-24 resisted little load.

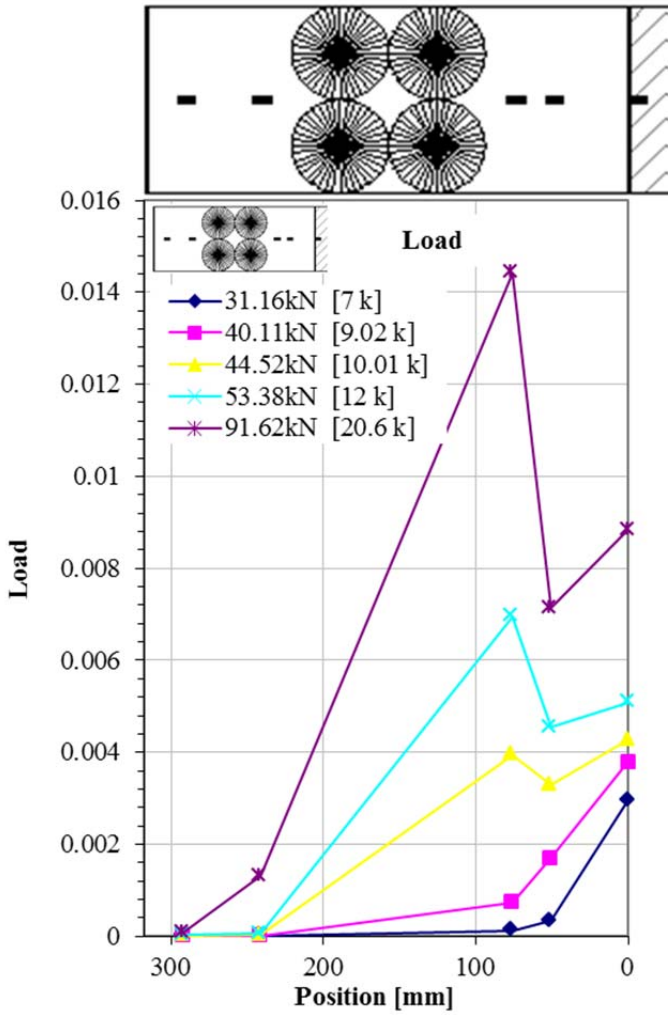

Figure 4.71 Longitudinal strain profile for specimen S1-4a-1-12.5

4.3.4.3.6 Specimen S1-4a-2-24

The longitudinal strain profile for specimen S1-4a-2-24 is presented in Figure 4.72. Specimens S1-4a-2-24 and F1-4a-2-24 differed from all other anchored specimens in that there was 125 mm [5 in.], or two splay diameters, between the two rows of anchors instead of 64 mm [2.5 in.], or one splay diameter. There were also two longitudinal strain gauges between the two rows of anchors, as shown in Figure 3.19.

From approximately 27 kN to 33 kN [6,000 lbs to 7,500 lbs] there was a rapid increase in strain in gauges G2 and G3B, indicating the initiation of debonding at both gauges. From approximately 33 kN to 53 kN [7,500 lbs to 12,000 lbs] gauges G1, G2 and G3B recorded a linear increases in strain. Around a load of 49 kN [11,000 lbs] the debonding front passed the front anchors, which is evident by a sudden increase in strain in gauge G4B. Around 53 kN [12,000 lbs], part of the right side of the sheet slipped from the loading plates, as discussed in section 4.2.2.4. Since part of the sheet was no longer resisting load, there was a sudden increase in strain in gauges G1, G2, G3B, G4B, and G5. There was also a noticeable increase in rate of strain in gauge G6B. Gauges G1, G2, G3B, and G4B recorded an approximately linear increase in strain until the max load of 62.9 kN [14,140 lbs]. After the peak load was reached a 20 mm [0.75 in.] width of fibers ruptured adjacent to the fibers that slipped on the plates, which caused the sheet to suddenly debond past the back row of anchors. This event is evident in Figure 4.72 by a sudden increase in strain in gauge G6B. Once there was debonding behind the trailing anchors the debonding front quickly progressed through the rest of the sheet. It is likely that if the right side of the sheet had not slipped from the loading grips prior to failure,

the specimen would have reached a higher peak load. Also the debonding front would likely not have passed the second row of anchors as early.

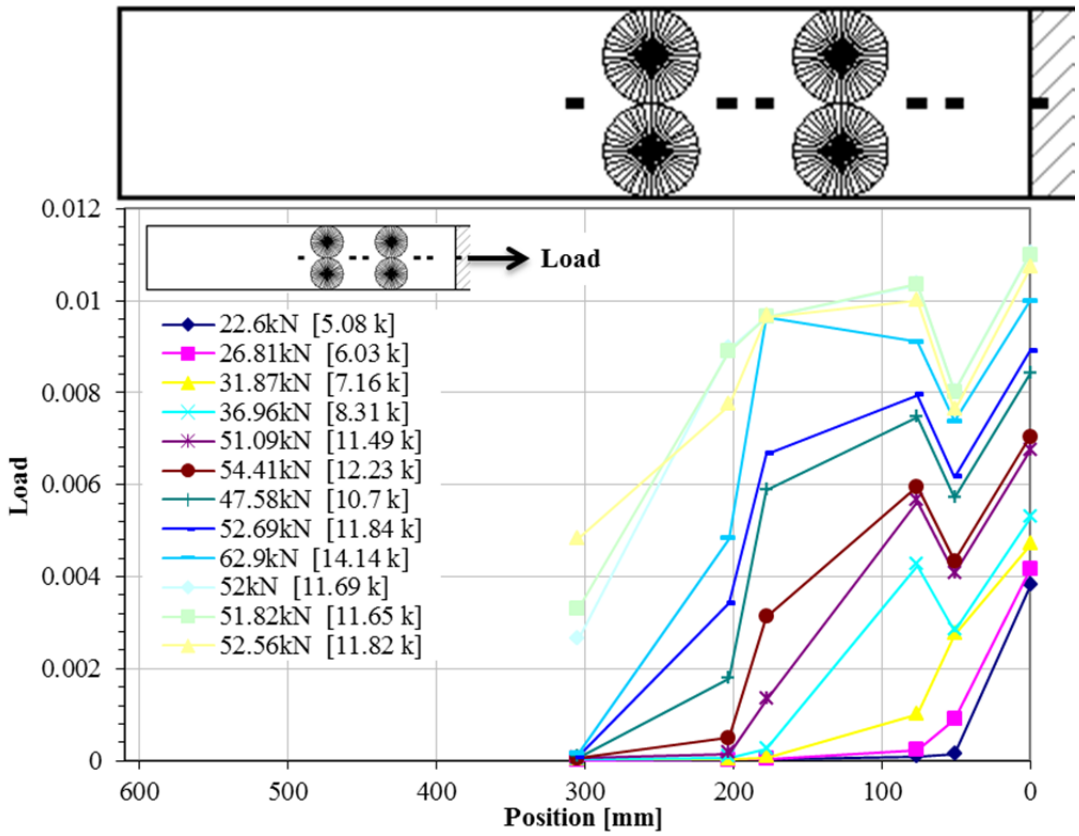

Figure 4.72 Longitudinal strain profile for specimen S1-4a-2-24

4.3.4.3.7 Specimen F1-4a-2-24

The longitudinal strain profile for specimen F1-4a-2-24 is presented in Figure 4.73. From loads of approximately 31 kN to 40 kN [7,000 lbs to 9,000 lbs] there was a rapid increase in strain in gauges G2 and G3B, indicating that the initiation of debonding at both gauges. Gauge 3B showed a significantly greater increase in strain during this load range compared to gauge G2. From 40 kN [9,000 lbs] to failure of the specimen, gauges G1, G2, and G3B recorded a linear increase in strain. Strain in gauges G1 and G3B increased at roughly the same rate, and G2 increased at a slightly lower rate.

Gauges G4B and G5, located in between the two rows of anchors, recorded negligible strain until 36 kN [8,000 lbs], around the load that debonding initiated in front of the anchors. From approximately 49 kN to 56 kN [11,000 lbs to 12,500] there is a rapid increase in strain in gauges G4B and G5 indicating that the debonding front passed these gauges and reached the trailing row of anchors. From 56 kN [12,500 lbs] to failure, both gauges showed roughly the same constant rate of strain increase.

Gauges G6B, located in behind the back row of anchors, recorded negligible strain until 36 kN [8,000 lbs], around the load that debonding initiated in front of the anchors. Strain increased slowly until approximately 58 kN [13,000 lbs], shortly after debonding initiated between the rows of anchors. From 58 kN to 107 kN [13,000 lbs to 24,000 lbs], the rate of strain increased slowly with increasing load. From 107 kN [24,000 lbs] until failure, there was a rapid increase in strain in gauge G6B, indicating that the initiation of debonding at this gauge prior to failure. Figure 4.16 (a), shows that debonding front only passed the anchors along the centerline and edges of the sheet.

As with most anchored specimens, after the debonding front passed gauge G3B the strain increased sharply between gauges G2 and G3B. The same is true for the trailing anchors; once the sheet debonded between the anchors, there was an increase in strain from gauge G4B to G5. At the peak load, there were a sharp decreases in strain from gauges G3B to G4B and from G5 to G6B, which indicates that the both rows of anchors resisted a significant amount of load.

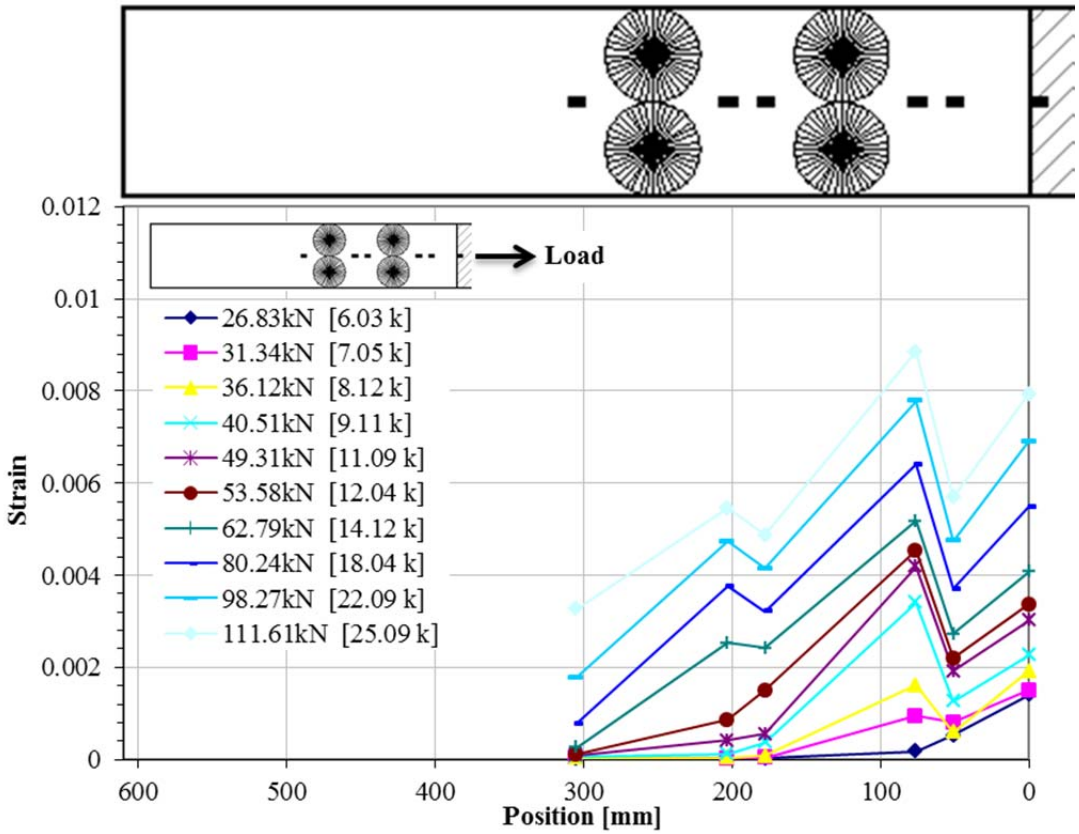

Figure 4.73 Longitudinal strain profile for specimen F1-4a-2-24

4.3.4.4 Double Ply Specimens

4.3.4.4.1 Specimen F2-0a-24

The longitudinal strain profile for specimen F2-0a-24 is presented in Figure 4.74. The strain profile is similar to that of the single ply unbonded specimens. The initial transfer length is somewhere between 100 mm [4 in.] and 230 mm [9 in.], judging by the shape of the strain profile shortly before debonding, at a load of 66.8 kN [15.02 k]. Gauge G5 recorded a small amount of strain prior to debonding, therefore technically the initial STZ would be at least 230 mm [9 in.], however prior to failure strain in gauge G5 was only 10% of the strain in gauge G4, and less than 3% of the strain in gauge G2.

From initial loading to a load of 69 kN [15,500 lbs] strain increased in the sheet within the STZ. At a load of 69 kN [15,500 lbs] there was a rapid increase in strain in gauges G2 and G3 until failure, indicating the initiation of debonding at these gauges. Shortly after, at the peak load of 70 kN [15,700 lbs], the debonding front reached gauge G4.

The maximum strain achieved along the centerline of the sheet was 0.00349, which is 84% of the max strain achieved by specimen F1-0a-24. The peak load of specimen F2-0a-24 was 40% higher than that of specimen F1-0a-24.

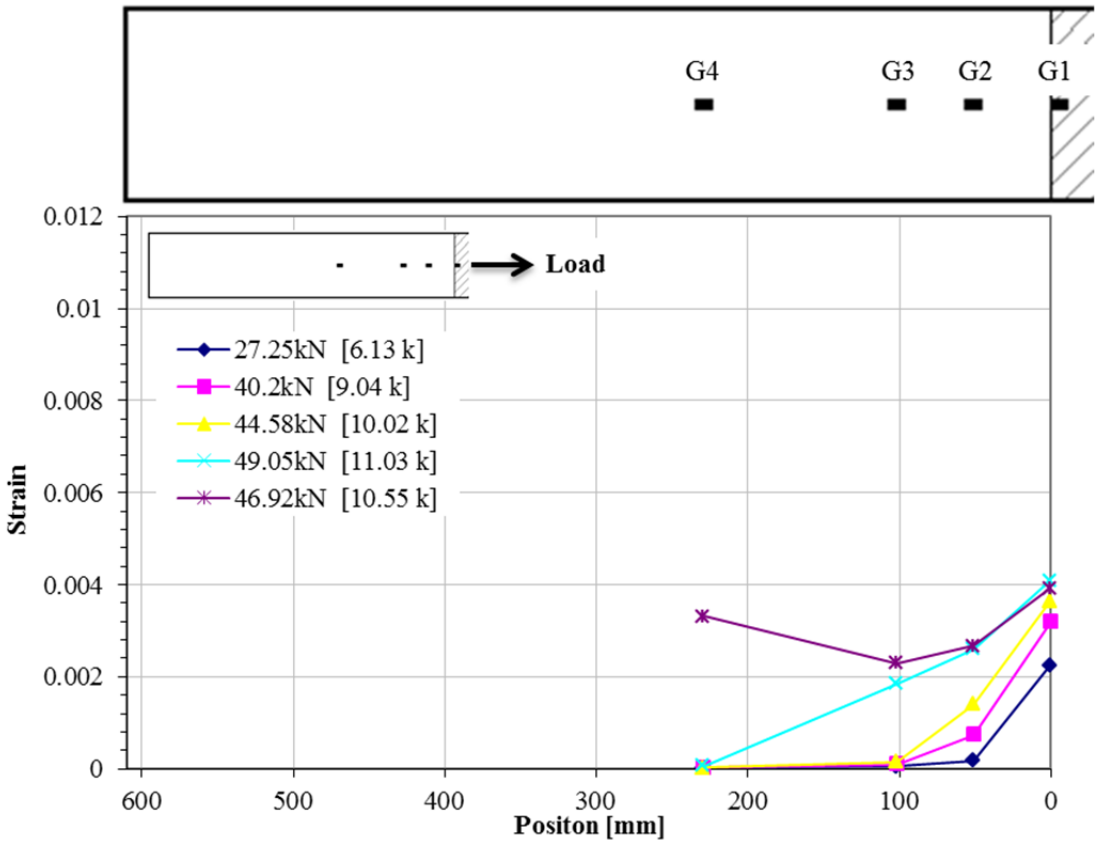

Figure 4.74 Longitudinal strain profile for specimen F2-0a-24

4.3.4.4.2 Specimen S2-2a-24

The longitudinal strain profile for specimen S2-2a-24 is presented in Figure 4.75. From loads of approximately 44 kN to 60 kN [12,000 lbs to 13,500lbs] there was a rapid increase in strain in gauges G2 and G3B, indicating the initiation of debonding at these gauges. From loads of 60 kN [13,500 lbs] to failure of the specimen, gauges G1 and G2 recorded approximately the same linear increase in strain. Gauge G3 recorded a higher rate of strain increase than gauges G1 and G2 until approximately 80kN [18,000 lbs], then recorded a lower rate of strain until failure.

At load of approximately 58 kN [13,000 lbs], when the debonding front passed the gauges in front of the anchors, there was a clear increase in the rate of strain in gauges G4B and G5. The test video showed that roughly five seconds prior to failure the anchor splays began to delaminate, as explained in section 4.2.3.4. This caused an increase in load behind the anchors, and accelerated debonding, which is evident by a rapid increase in strain in gauges G4B and G5. At the peak load the strain profile resembles that of the unanchored specimens, since there is less difference in strain from in front to behind the anchors compared to other anchored specimens. This indicates that the anchors were likely not resisting significant load at failure, which is likely due to the observed anchor splay delamination. The maximum strain achieved along the centerline of the sheet was 0.00593 in gauge G1, which is 70% of the maximum strain recorded for specimen S1-2a-24, although specimen S2-2a-24 reached a 50% higher peak load.

Like most other anchored specimens, after the debonding front passed gauge G3B the strain increased from G2 to G3B, however, unlike most anchored specimens, strain decreased from gauge G1 to G2.

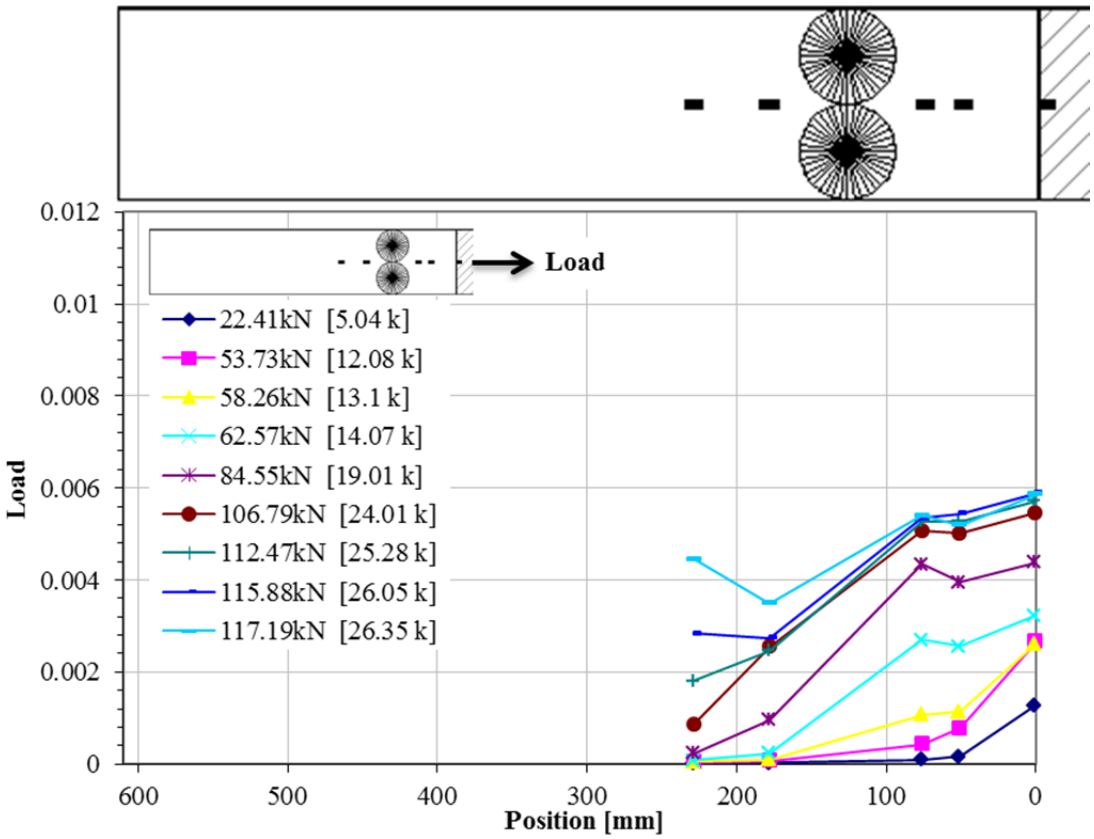

Figure 4.75 Longitudinal strain profile for specimen S2-2a-24

4.3.4.4.3 Specimen F2-2a-24

It took three test runs to fail specimen F2-2a-24, as discussed in section 4.2.3.2. The longitudinal strain profile for the first test run of specimen F-2a-24 is presented in Figure 4.76 (a) and the third test run is presented in Figure 4.76 (b). In the first test run, from loads of approximately 67 kN to 76 kN [15,000 to 17,000], there was a rapid increase in strain in gauges G2 and G3B, indicating the initiation of debonding at both gauges. From loads of approximately 80 kN [18,000 lbs] to failure of the specimen, gauges G1 and G2 recorded roughly the same linear increase in strain and gauge G3 recorded a higher rate of strain. As with most anchored specimens, there was an increased

rate of strain increase in gauges G4B and G5, at the same load that debonding initiated at the gauges in front of the anchors.

The longitudinal strain profile for the third test run is given in Figure 4.76 (b). The extent of debonding after the second attempt is given in Figure 4.18. From initial loading to approximately 138 kN [31,000 lbs], gauges G1, G2, G3B, located in front of the anchors, recorded a linear increases in strain. At a load of 138 kN [31,000 lbs] (the load at which there was damage to the left side of sheet, as discussed in section Figure 4.18), there was a small increase in strain in all three gauges, and then strain in all three gauges increased linearly until failure. Gauge G4B, located behind the anchors, recorded a constant rate of strain until 129 kN [29,000 lbs], then recorded a greater rate of strain until 138 kN [31,000 lbs], at which point it recorded erratic changes in strain due to the damage to the left side of the sheet. Gauge G5 recorded a lower rate of strain than gauge G4B until 116 kN [26,000 lbs], and then from 116 kN to 138 kN [26,000 lbs to 31,000 lbs] recorded a significantly higher rate of strain, that was higher than the rate recorded by gauge G4B. From 138 kN [31,000 lbs] until failure, gauge G4B and G5 recorded a constant increase in strain, at approximately the same rate as the other longitudinal gauges.

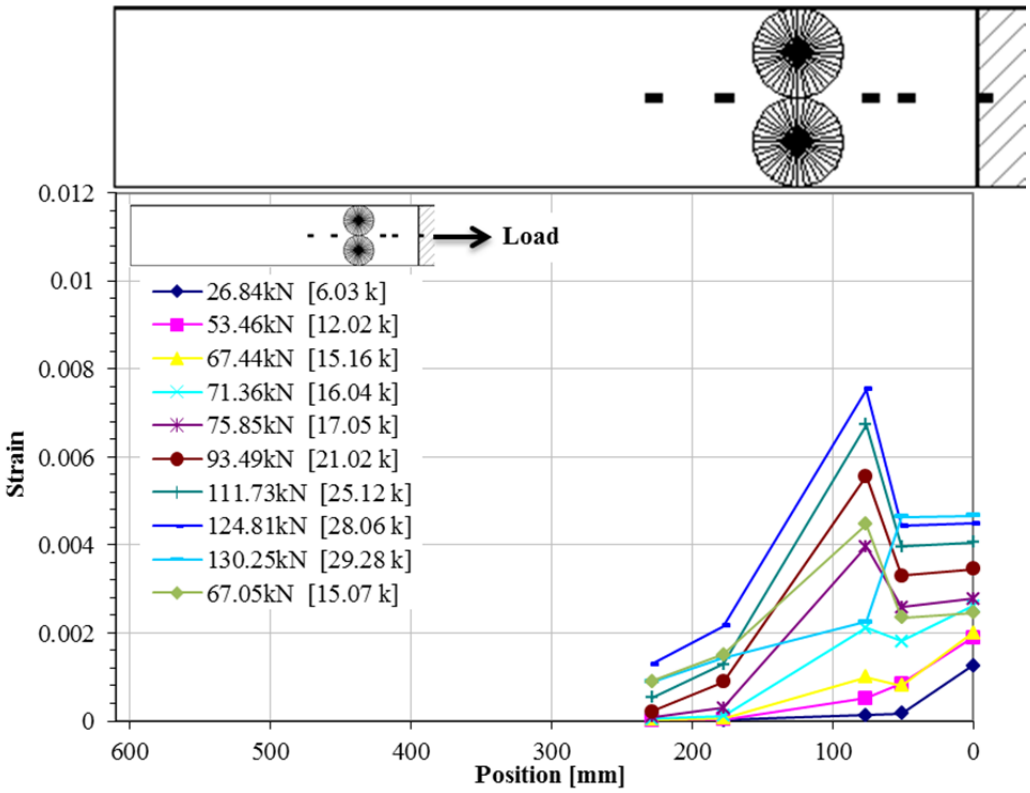

(a)

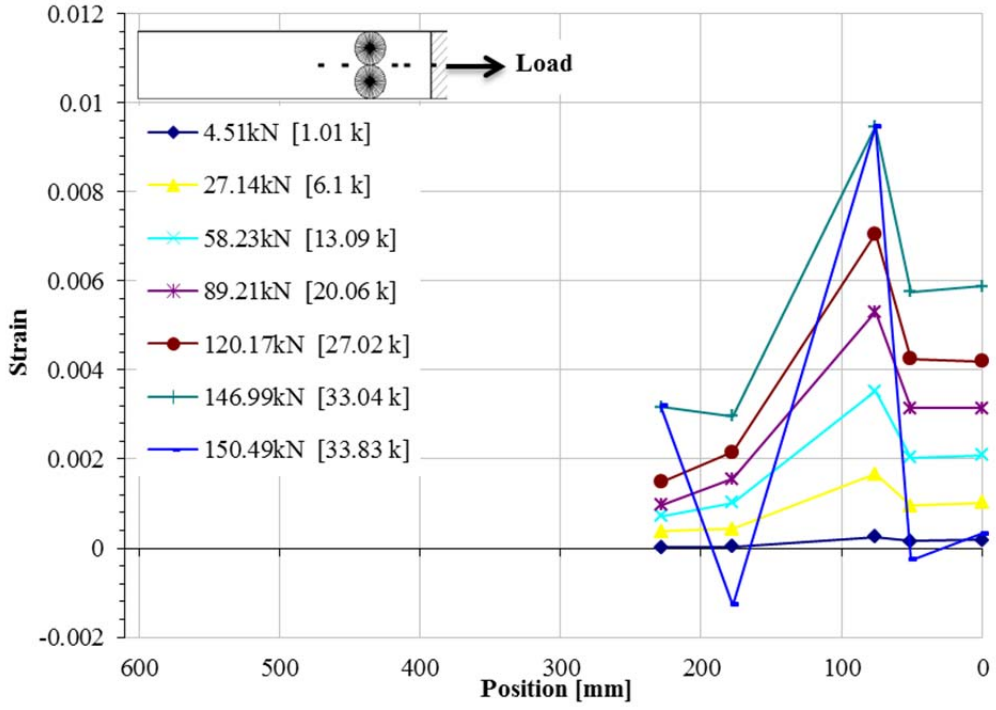

(b)

Figure 4.76 Longitudinal strain profile for specimen F2-2a-24 for the first test run (a) and the third test run (b). The negative strains indicate compression.

4.3.4.4.4 Specimen S2-4a-1-24

The longitudinal strain profile for specimen S2-4a-1-24 is presented in Figure 4.77. At a loads of approximately 53 kN to 76 kN [12,000 lbs to 17,000 lbs] gauge G2 recorded an overall decrease in strain, while all of the other gauges recorded an increase in strain. The reason for this is unknown. From loads of approximately 76 kN to 80 kN [17,000 lbs to 18,000 lbs] there was a rapid increase in strain in gauge G2, indicating that the initiation of debonding at this gauge. From 76 kN [17,000 lbs] to failure of the specimen, gauge G2 recorded a slightly nonlinear increase in strain, and the magnitude of the strain was 5%-10% greater than in gauge G1. Gauge G3B recorded an increase in rate of strain at a load of 38 kN [8,500 lbs] and then a decrease in rate of strain at a load of 80 kN [18,000 lbs], which is the load at which debonding initiated at gauge G2. Gauges G3A, G3B and G3C did not record a rapid increase in strain at the initiation of debonding, as was typical of other gauges located in front of the anchors in other specimens. Around a load of 80 kN [18,000 lbs] the strain recorded by gauge G2 went from approximately 50% less than to approximately 5% greater than the strain recorded by gauge G3. From 80 kN [18,000 lbs] until failure, gauge G2 continued to increase relative to gauge G3B.

Gauges G4B and G5 recorded very little strain until a load of approximately 80 kN [18,000 lbs], when the debonding front passed the gauges in front of the anchors, at which point there was a noticeable increase in rate of strain in these gauges. At a load of approximately 107 kN [24,000 lbs], there was another increase in rate of strain in gauge G4B and G5, that is believed to correspond to the initiation of debonding at these gauges. From 107 kN [24,000 lbs] until shortly before failure, strain increases approximately at a

constant rate in gauge G5. For an unknown reason gauge G4 shows little change in strain from 138 kN [31,000 lbs] to failure. From loads of approximately 80 kN [18,000 lbs] until failure, the strains actually decreased approaching the anchors from gauge G2 to G3. This is unlike most anchored specimens in which there was a large increase in strain from gauge G3 to G2. In specimen S2-2a-24 there was approximately equal strain in gauges G2 and G3 at failure.

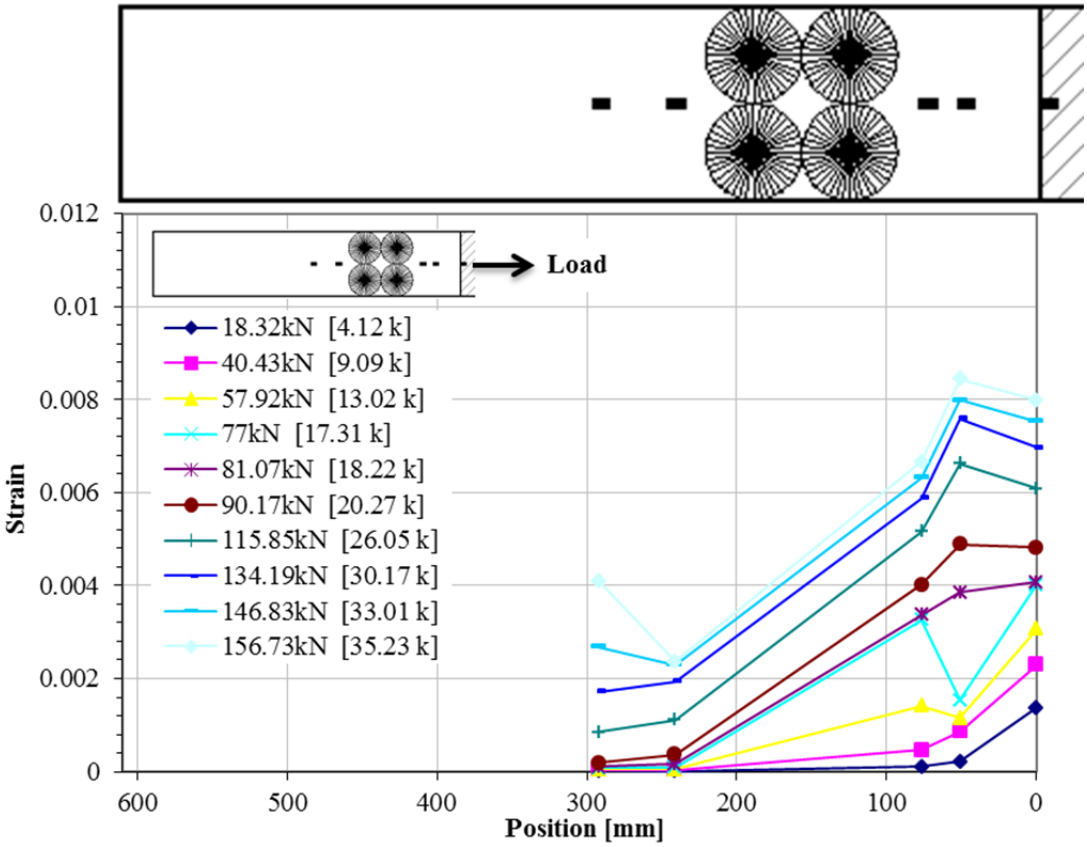

Figure 4.77 Longitudinal strain profile for specimen S2-4a-1-24

4.3.4.4.5 Specimen F2-4a-1-24

Longitudinal strain profiles for specimen F2-4a-1-24 are presented in Figure 4.78. Gauges G2 and G3B showed a rapid increase in strain at a load of approximately 62 kN [14,000 lbs], indicating that the debonding front passed these gauges at this load. Gauges G1, G2 and G3 then show approximately equal linear increase in strain until failure.

At a load of 58 kN [13,000 lbs], the same load that the debonding front passed gauges G2 and G3B, gauges G4B and G5 record an increase in rate of strain. Prior to this load both gauges showed negligible strain. The rate of strain in gauges G4B and G5 increased slowly until approximately 151 kN [34,000 lbs], when both gauges recorded a sudden increase in rate of strain, indicating that the debonding front passed these gauges. Gauges G4B and G5 then recorded an approximately linear increase in strain until failure. As in specimen S2-2a-24, there was approximately equal strain in gauges G2 and G3 after the debonding front passed gauge G3.

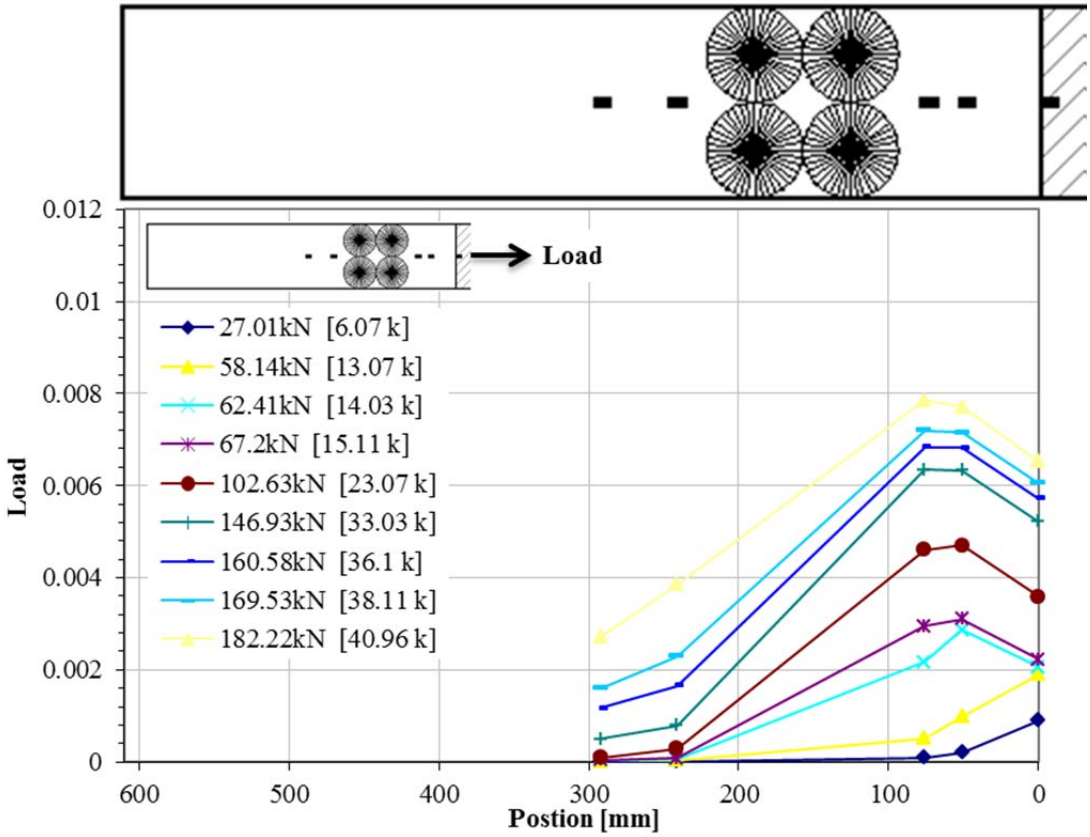

Figure 4.78 Longitudinal strain profile for specimen F2-4a-1-24

4.3.4.5 Unbonded Specimens

4.3.4.5.1 Specimen F1-2a-24U

The longitudinal strain profile for specimen F1-2a-24U is presented in Figure 4.79. Specimens F1-2a-24U and F1-4a-24U differed from the other anchored specimens in that they were unbonded, except for a 125 mm [5 in.] length at the back of the sheet. These tests are valuable because they isolate the behavior of the anchors. An additional strain gauge was placed between the anchor splays, as shown in Figure 3.20 and the attached drawing in Figure 4.79.

Gauges G1, G2, G3B recorded a linear increase in strain from initial loading until failure, except at a load of 43.6 kN [9,800 lbs], when all three gauges recorded a small sudden increase in strain. From initial loading to 40.06 kN [9,010 lbs] the rate of strain increased in gauges GC, G4B and G5B with increasing load. At a load of 40.06 kN [9,010 lbs] gauge GC recorded an irrational strain, indicating that there was damage to the anchor splays where the gauge was placed. Gauges G4B and G5B also recorded a sudden increase in rate of strain. Prior to a load of 40.06 kN [9,010 lbs] the strain decreased roughly linearly from the loaded end towards the unloaded end.

At a load of 43.6 kN [9,800 lbs], gauges G4B and G5B recorded a sudden large increase strain, which indicates that the anchors suddenly resisted less load, either because the anchors deflected, or more likely because the anchor splays lost hold of the sheet. From 3.6 kN [9,800 lbs] to failure of the specimen the strain behind the anchors was only slightly less than in front of the anchors, which further indicates that the anchors resisted little load during this load range. The large strain behind the sheets means that

the bonded area resisted load, which makes the data from that point on less useful, since the anchor behavior was not isolated.

There was a decrease in strain approaching the anchors from gauges G2 to G3B, which is unlike in most of the singly ply anchored specimens in which there was a large increase in strain from gauges G2 to G3B.

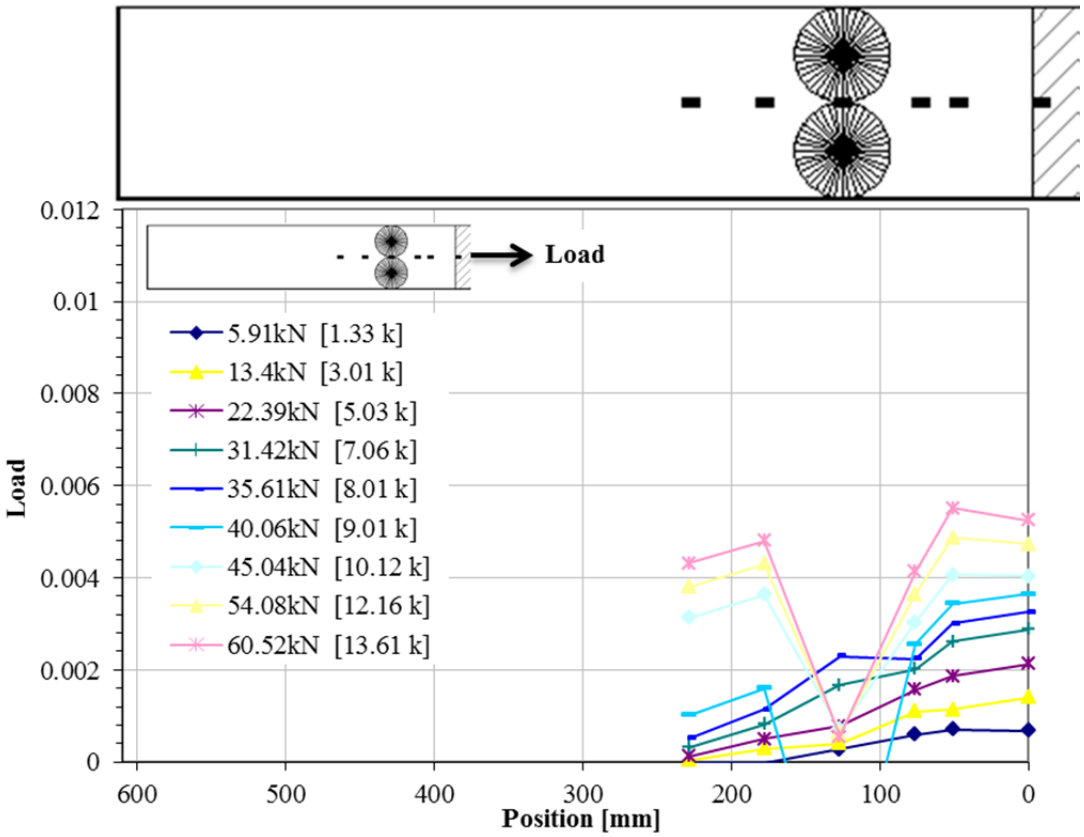

Figure 4.79 Longitudinal strain profile for specimen F1-2a-24U

4.3.4.5.2 Specimen F1-4a-1-24U

The longitudinal strain profile for specimen F1-4a-1-24U is presented in Figure 4.80. Specimens F1-2a-24U and F1-4a-24U differ from the other anchored specimens in that they are unbonded, except for a 125 mm [5 in.] length at the back of the sheet. An additional strain gauge was placed between each of the two columns of anchor splays, as shown in Figure 3.21 and the attached drawing in Figure 4.80.

Gauges G1, G2, and G3B, located in front of the anchors, recorded roughly linear strain increase from initial loading until failure. Gauge G2 recorded a slightly greater rate of strain increase than gauge G1, which recorded a slightly greater rate than gauge G3B. As with specimen F1-2a-24U, strains decrease approaching the anchors from gauges G2 to G3B.

The rate of strain in gauges G4 and G5, located behind the anchors, increased slightly with increasing load until failure. All three gauges show periods of approximately constant increase in strain, separated by sudden small jumps in strain. These small jumps in strain are likely due to the anchors suddenly resisting less load, either due to anchor deflection or anchor splay damage.

At a load of around 52 kN [11,700 lbs] gauge GC1 recorded a negative jump in strain and gauge GC2 recorded a positive jump in strain. This indicates that load from the front anchors was transferred to the back row, which was likely due to the anchor splays losing hold of the sheet. This is believed, because around a load of 49 kN [11,000 lbs] the edges of the right front anchor splay can be seen in the test video detaching from the FRP sheet, as discussed in section 4.2.4.2. It is interesting that at the peak load in specimen F1-4a-1-24U there is significantly more strain in gauge G4B than in G5. This indicates that the stress distribution is not constant in the unbonded region behind the anchors.

Figure 4.81 compares the longitudinal strain profiles for specimens F1-4a-1-24U and F1-4a-1-24. The two specimens were identical except specimen F1-4a-1-24U was unbonded. The strain profiles were different until the debonding front reached the anchors in specimen F1-4a-1-24. At a load of approximately 44.5 kN [10,000 lbs] both specimens had a close level of strain in gauge G3B. In specimen F1-4a-1-24U there is

less strain in G3B than in G2, unlike in specimen F1-4a-1-24 and almost all of the anchored-bonded specimens.

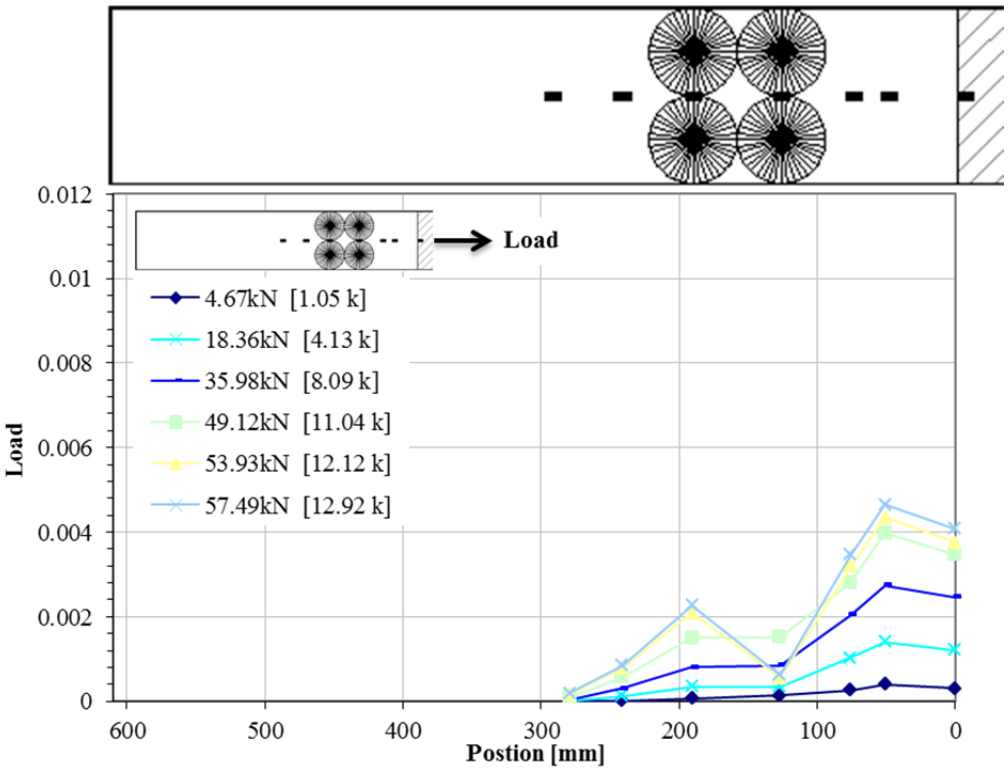

Figure 4.80 Longitudinal strain profile for specimen F1-4a-1-24U

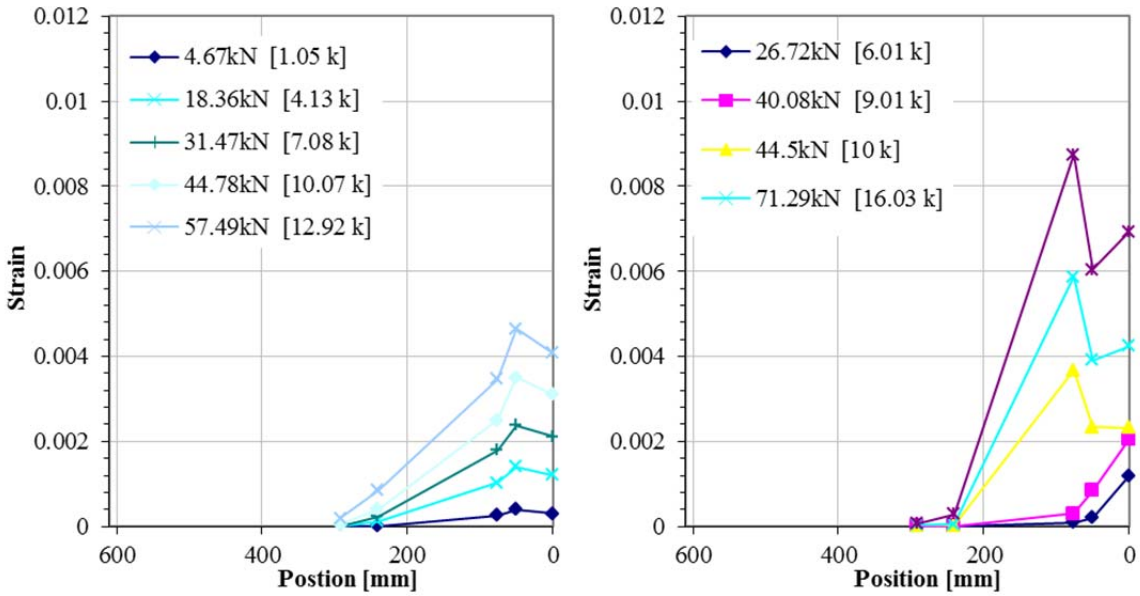

Figure 4.81 Longitudinal strain profile for specimens F1-4a-1-24U (left) compared to that of specimen F1-4a-1-24 (right)

4.3.5 Summary of Measured FRP Strains

This section summarizes and discusses the axial FRP strain results. Table 4-3 presents a summary of the strain results, including the peak recorded strain and the gauge that recorded it, the percent of the manufacturer published FRP strain ($\frac{\varepsilon_{test}}{\varepsilon_{ult}}$) and load capacities ($\frac{p_{test}}{p_{ult}}$) achieved and the failure mode of each specimen. P_{ult} is given by the manufacturer as a tensile strength per inch width of FRP sheet.

Figure 4.82 shows that the relationship between $\frac{\varepsilon_{test}}{\varepsilon_{ult}}$ and $\frac{p_{test}}{p_{ult}}$ is not linear, as one would anticipate for a linear-elastic material behavior. This is largely because of large variations in strain across the width and length of the FRP sheets (anchored and unanchored), due to local variations in bond strength, uneven loading and debonding, and localized FRP anchor effects.The maximum recorded strain (ε_{test}) was very sensitive to the location of the gauges.

Figure 4.82 shows that all three of the specimens that failed by FRP rupture had a peak recorded strain that was less than the manufacturer's published average strain capacity. This is not surprising for two main reasons. First it is difficult to capture the maximum strain in a sheet with a finite number of gauges, because of strain localization in anchored sheets as already mentioned. Second, the failure load of all of the specimens that failed by FRP rupture was lower than the load capacity given by the manufacturer. This is likely because the manufacturer capacity values are determined from unbonded coupon tests, which enable a more even distribution of stresses in the FRP, and therefore higher failure loads. Unanchored-bonded FRP sheets have uneven distribution of stresses across the width of the sheet. In addition, uneven debonding causes uneven loading of the

sheet. In anchored-bonded specimens the anchors cause local stress concentrations, as well as require the fibers to be bent around the anchor shaft, which may affect the strength of the fibers by introducing bending. This explains why FRP rupture usually occurred around the location of the anchors.

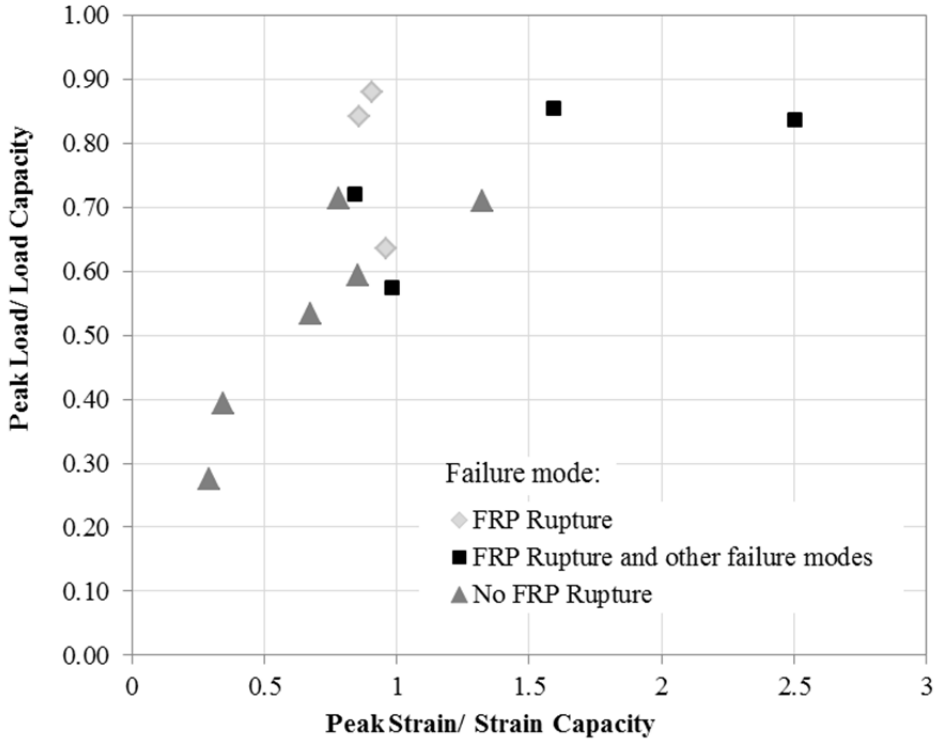

Figure 4.82 Ratio of peak load/ load capacity to peak strain/ strain capacity

For three specimens the peak recorded strain was higher than the published strain capacity. Specimens S1-2a-24, S1-4a-1-24, and S1-4a-1-12.5, recorded peak strains that were 33%, 59% and 151% higher than the strain capacity, respectively.

Table 4-3 shows that for the anchored specimens the peak strain usually occurred in front of and in line with the anchors. In every anchored specimen the peak strain was recorded in front of the anchors. In every anchored specimen, except specimens S1-4a-2-24 and F1-2a-1-24U, the peak strain occurred in either gauge G3A, G3B or G3C. Of the

anchored specimens that had a peak strain in gauges G3A, G3B or G3C, only specimen S1-4a-1-24 recorded a peak strain in gauge G3B, which was along the centerline of the sheet. This is consistent with previous findings by (Niemitz, 2008), who indicated the highest strains tend to occur in line with the anchors, even when the anchors are not along the centerline of the sheet.

Table 4-3 Specimen Strain Summary

Specimen	Max Strain Gauge	Max FRP Strain	Strain Capacity	$\varepsilon_{test}/\varepsilon_{ult}$	Peak Load P_{test}	P_{test}/P_{ult}	Failure Mode
S1-0a-24	-	-	0.0112	-	9,750	39.6%	Debonding
F1-0a-24	G1	0.004	0.012	34.7%	11,200	39.3%	Debonding
S1-2a-24	G3C	0.015	0.0112	132.6%	17,500	71.0%	Debonding,Anchor splay rupture and delamnination
F1-2a-24	G3C	0.012	0.012	96.2%	18,120	63.6%	FRP Rupture
S1-4a-1-24	G3B	0.018	0.0112	159.3%	21,060	85.5%	FRP debonding and rupture, and anchor splay rupture and delamination
F1-4a-1-24	G3A	0.010	0.012	86.1%	23,970	84.1%	FRP Rupture
S1-4a-2-24	G1	0.011	0.0112	98.4%	14,140	57.4%	FRP debonding, FRP rupture, splay delamination and splay rupture
F1-4a-2-24	G3A	0.011	0.012	90.8%	25100	88.1%	FRP Rupture, minor splay delamination
S1-4a-1-12.5	G3C	0.028	0.0112	250.7%	20,600	83.6%	Anchor splay delamination, FRP rupture and debonding
F2-0a-24	G3	0.003	0.012	29.1%	15,700	27.5%	FRP debonding
F2-2a-24	G3A	0.010	0.012	85.4%	33,830	59.4%	FRP debonding and splay delamination and rupture
S2-2a-24	G3C	0.008	0.0112	67.6%	26,300	53.4%	Debonding and anchor splay delamination
F2-4a-1-24	G3A	0.010	0.012	84.3%	41,000	71.9%	Debonding, FRP rupture and splay delamination
S2-4a-1-24	G3A	0.009	0.0112	78.2%	35,200	71.4%	Splay delamination, FRP debonding
F1-2a-24U	G2	0.006	0.012	45.9%	13,900	48.8%	Splay delamination
F1-4a-1-24U	G3A	0.007	0.012	59.8%	14,000	49.1%	Anchor splay delamination and FRP rupture

CHAPTER 5

EVALUATION OF TEST RESULTS

5.1 Introduction

In this chapter the results of the experimental program are discussed. Section 5.2 compares the performance of different manufacturers, including the Sika and Fyfe specimens tested in this research program, and the MBrace specimens tested by Niemitz (2008). Section 5.3 discusses the effects of fastening FRP sheets with anchors. Section 5.4 discusses the effects of adding a second row of anchors. Section 5.5 discusses the effect of the bonded length behind the anchors. Section 5.6 compares the performance of double and single ply specimens, and section 5.7 discusses the behavior of unbonded and anchored specimens.

5.2 Comparison of Different Manufacturers

This section compares the performance of CFRP systems from Sika (SikaWrap® Hex-103 C), Fyfe (Tyfo® SCH-41) and Mbrace (Wabo® Mbrace CF 130). All three systems were unidirectional carbon fiber sheets. Sika and Fyfe systems were tested in this experimental program and Niemitz (2008) tested Mbrace systems using a similar test setup.

Several of the Sika and Fyfe specimens were specifically designed to be companion specimens to specimens from Niemitz (2008) so that comparisons could be made between the three manufacturers. Specimens F1-0a-24 and S1-0a-24 are similar to specimen A-0-0-50 from Niemitz (2008) and specimens F1-2a-24 and S-2a-24 are similar to specimens B-Y-2-5-4 and B-X-2-5-4 from Niemitz (2008).

Table 5-1 compares the properties of the CFRP systems from the three manufacturers. The sheet dimensions and anchor locations for the Mbrace specimens are presented in

Figure 3.22 Specimen A-0-0-5-0 (Niemitz, 2008)

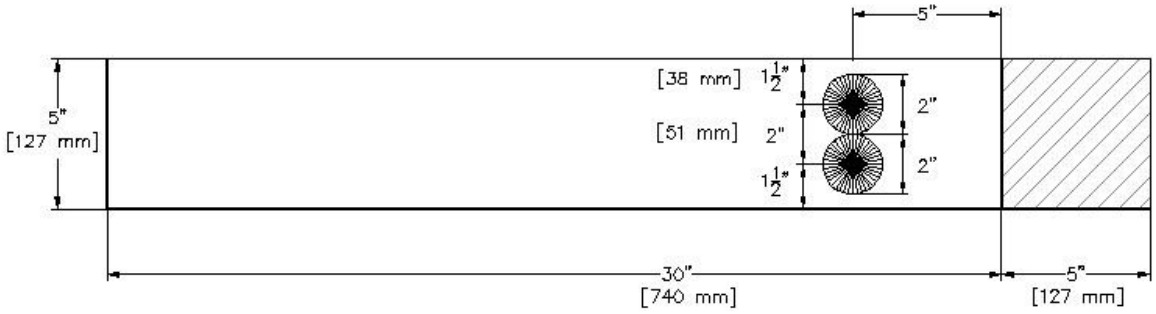

Figure 3.23 Specimen B-Y-2-5-4 (Niemitz, 2008)

through Figure 3.24.

The Sika and Mbrace anchors were fabricated by cutting an appropriately sized rectangular piece from the FRP sheet. The Sika anchors were then formed by applying epoxy to both sides of the FRP piece and then rolling the sheet into a cylinder. The Fyfe anchors (Tyfo® SCH Fibr™ Anchors) were provided by the manufacturer in bundles of individual carbon fibers. The anchors were cut to a desired length, and then saturated with epoxy by immersing the anchor in epoxy. The anchor properties and fabrication processes are discussed in greater detail in section 3.4.1.3. Before applying epoxy, the Fyfe and Sika anchors had masses of 8.2 grams and 5.2 grams [0.29 ounces and 0.18 ounces], respectively.

Figure 5.1 compares the performance of the three manufacturers based on the measured failure load, and the load ratio ($\frac{p_{test}}{p_{ult}}$). Similar specimens (same sheet dimensions and anchor arrangement) are positioned next to each other in Figure 5.1. The difference in $\frac{p_{test}}{p_{ult}}$ for identical Sika and Fyfe specimens was never more than 6%, except for specimens S1-4a-2-24 and F1-4a-2-24 because S1-4a-2-24 failed at a very low load. The Fyfe specimens failed at a higher load than the identical Sika specimens in every

case. It is believed that this is largely because the Fyfe anchors were stiffer and stronger than the handmade Sika anchors, since they had a significantly greater mass of fibers (approximately 58% more mass). The Fyfe specimens failed less by FRP debonding and more by FRP rupture compared to the anchored Sika specimens. This indicates that the Fyfe anchors were more effective than the Sika anchors. It is likely that Sika anchors could perform better if the amount of fibers was increased. In addition the Fyfe sheets had higher rupture strength, and the majority of the anchored specimens failed at least partially by FRP rupture. The companion Mbrace specimens from (Niemitz, 2008) performed similarly to the Sika and Fyfe specimens.

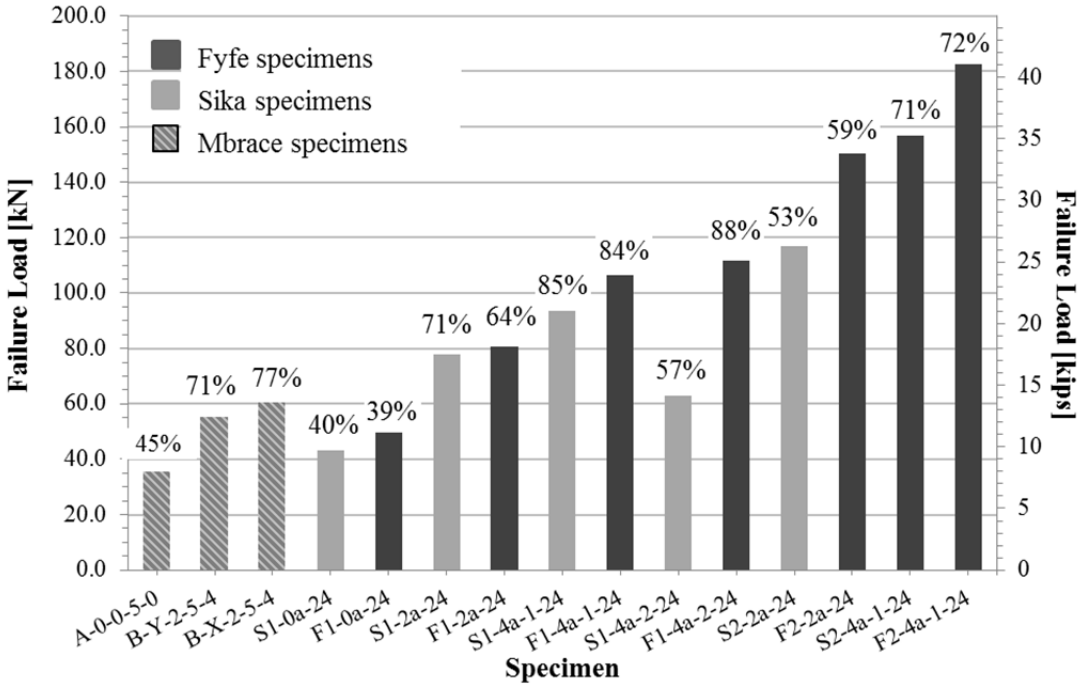

Figure 5.1 Comparison of the failure loads of the Sika, Fyfe and Mbrace (Niemitz, 2008) specimens

Table 5-1 Comparison of material properties of the different CFRP materials

	Sika Composite Gross Laminate				Fyfe Composite Gross Laminate				Mbrace Composite Gross Laminate Properties			
	Average Value*		Design Value**		Average Value*		Design Value**		Average Value*		Design Value**	
	Psi	GPa	Psi	GPa	Psi	GPa	Psi	GPa	Psi	GPa	Psi	GPa
Tensile Strength in primary fiber direction	123,200	0.849	104,000	0.651	127,000	0.876	107,950	0.745				
Tensile Strength per inch width	4,298 lbs	21.9 kN	4,160 lbs.	18.5 kN	5,100 lbs	-	4,300 lbs	-				
Tensile Modulus in primary fiber direction	10,239,800	70.552	9,446,600	65.087	10,500,000	72.4	8,900,000	61.5				
Tensile Elongation at break	1.12%	-	0.98%	-	1.20%	-	1.00%	-				
Laminate Thickness	0.04 in	1.016 mm	-	-	0.04 in	1.0 mm	-	-				

*ASTM test method D-3039

** Average value minus 2 stnd deviations as recommended by ACI 440

	Sikadur 300 (Fabric Saturant/ surface	Ffye (Fabric Saturant/ surface	Ffye (Fabric Saturant/
Tensile Strength	8,000 psi	10,500 psi	10,500 psi
Tensile Modulus	250,000psi	461,000 psi	461,000 psi
Elongation at Break	0.03	0.05	0.05
Flexural Strength	11,500 psi	17,900 psi	17,900 psi
Flexural Modulus	500,000psi	452,000 psi	452,000 psi

An important observation is that similar peak loads were obtained in Sika and Fyfe specimens designed using the same design parameters, with the exception of the outlier result of specimen S1-4a-2-24. In other words the peak loads achieved using different designs was similar for both manufacturers. Table 5-2 shows the percent increase in failure load achieved by anchored systems from the different manufacturers (Sika, Fyfe and Mbrace) relative to the respective single ply unanchored specimens.

Table 5-2 Percent increase in failure load relative to the single ply unanchored specimens (S1-0a-24 and F1-0a-24, A-0-0-5-0)

Design Change	**Specimens**	**Sika**	**Fyfe**	**Mbrace**
Two anchors	S1-2a-24, F1-2a-24, B-Y-2-5-4, B-X-2-5-4	+179%	+162%	+155%, +170%
Four anchors	S1-4a-1-24, F1-4a-1-24	+216%	+214%	-
Four anchors (with additional space between anchors)	S1-4a-2-24, F1-4a-2-24	+145%	+224%	-
Double ply, two anchors	S2-2a-24, F2-2a-24	+270%	+302%	-
Double ply, four anchors	S2-4a-1-24, F2-4a-1-24	+361%	+366%	-

Design Change	**Specimens**	**Sika**	**Fyfe**	**Mbrace**
Two anchors	S1-2a-24, F1-2a-24, B-Y-2-5-4*, B-X-2-5-4*	+179%	+162%	+155%*, +170%*
Four anchors	S1-4a-1-24, F1-4a-1-24	+216%	+214%	-
Four anchors (with additional space between anchors)	S1-4a-2-24, F1-4a-2-24	+145%	+224%	-
Double ply, two anchors	S2-2a-24, F2-2a-24	+270%	+302%	-
Double ply, four anchors	S2-4a-1-24, F2-4a-1-24	+361%	+366%	-

* Results from (Niemitz, 2008)

(a) **(b)** **(c)**

Figure 5.2 (a) Specimens S1-0a-24, (b) F1-0a-24 and (c) A-0-0-5-0 (Niemitz, 2008) after failure. Specimen F2-0a-24 after failure looked very similar to specimen F1-0a-24 as shown in (b).

All unanchored specimens from this research program (Sika and Fyfe specimens) and the unanchored Mbrace specimens from (Niemitz, 2008) failed by debonding. The debonding failures occurred almost entirely within a shallow layer of concrete in specimens F1-0a-24, F2-0a-24 and A-0-0-5-0. As explained in section 4.2.1.1, there was some failure within the epoxy layer of specimen S1-0a-24, as is evident by the randomly distributed patches where the adhesive is visible in Figure 5.2. However, in many of these places there are diagonal cracks that extend into the concrete several millimeters, indicating that failure occurred in both the adhesive layer and within a shallow layer of concrete. It is known that concrete strength is a governing factor in the load capacity of

unanchored sheets, which is why it appears in many bond strength models, including those presented by (Lu et al., 2005; Chen and Teng, 2001). Figure 5.3 (a) shows a positive correlation between concrete compressive strength and load capacity, however Figure 5.3 (b) shows little correlation between concrete tensile strength and load capacity. This is likely because of the inherent variability in determining tensile capacity of concrete experimentally. The tensile strength was determined using the split-cylinder test in conformance with AST C496.

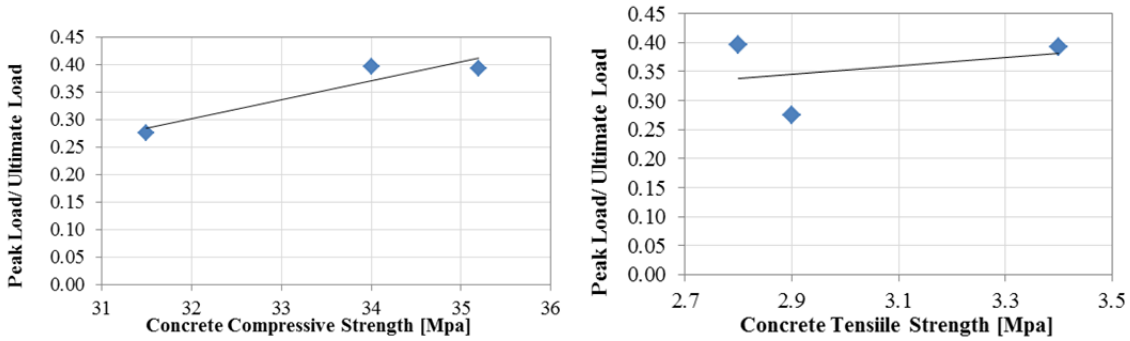

(a) **(b)**

Figure 5.3 Load ratio as a function of (a) compressive concrete strength and (b) tensile strength for the three unanchored specimens (S1-0a-24, F1-0a-24 and F2-0a-24)

The anchored Fyfe, Sika and Mbrace specimens generally had close values of $\frac{P_{test}}{P_{ult}}$ as shown in Figure 5.1, and had similar failure modes, which included combinations of FRP rupture, debonding, anchor splay delamination, and anchor splay rupture, as shown in Table 4-2. The longitudinal and transverse strain distributions were also similar, as discussed in sections 4.3.4 and 4.3.3, respectively. It is clear from Figure 5.4 that the effect of concrete strength was less apparent with the anchored specimens, than with the unanchored specimens.

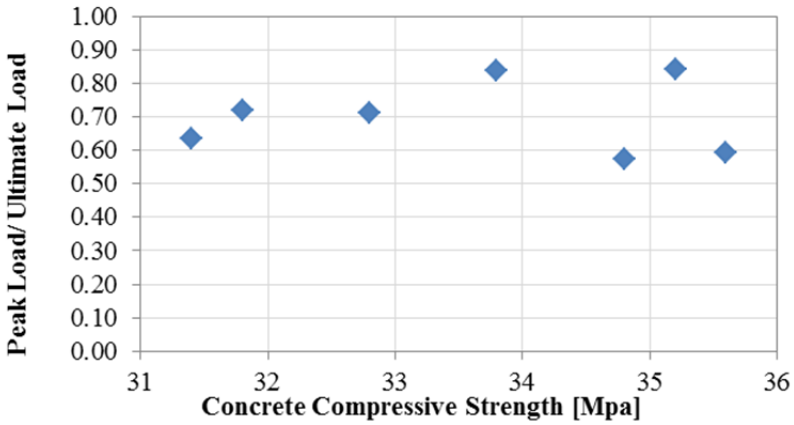

Figure 5.4 Load ratio as a function of concrete strength for all of the anchored-bonded specimens

5.3 Effect of Anchors:

As discussed in greater detail in the literature review, Niemitz, (2008) tested a variety of FRP anchor design parameters including anchor diameter and embedment depth, anchor splay diameter (relative to anchor diameter and relative to the width of the FRP sheet), and anchor arrangement (rows and columns). A 13 mm [0.5 in.] diameter anchor was determined to be strong enough for a 50 mm [2 in.] diameter anchor splay. Anchor embedment depth was determined to not be a governing failure mode when the depth was at least 50 mm [2 in.] and the anchor diameter was 13 mm [0.5 in]. It was determined that anchor splays are most effective when they engage the full width of the sheet.

Following these findings, and to minimize the number of design parameters in the tests conducted for this research, a single embedment depth, anchor diameter, and anchor splay diameter were used in all tests. In addition the sheet width was kept constant, and the sheet length was the same for every specimen except for specimen S1-4a-1-12.5. Instead, the following design parameters were investigated: manufacturer, unanchored

and anchored sheets, influence of number of anchor rows and spacing between rows, number of sheet plies (single or double), and length of bonded sheet behind the anchors.

It is clear from the experimental results that FRP sheets secured with FRP anchors can achieve significantly higher loads than identical unanchored sheets. This was discussed with reference to Table 4-2 and was illustrated graphically in Figure 4.3. Even a small number of anchors can greatly increase load capacity. For instance, specimen F2-2a-24 failed at more than double the load of specimen F2-0a-024, and the FRP material used to fabricate the two anchors in specimen F2-2a-24 was almost negligible compared to the amount used for the sheets.

All of the unanchored specimens failed by debonding well below the ultimate load capacity of the sheet. The average load ratio ($\frac{P_{test}}{P_{ult}}$) of the three unanchored specimens was just 35%. It is clear from experimental results that it is possible to prevent debonding failure by fastening the sheet with FRP anchors. Unfortunately all of the anchored specimens that failed by FRP rupture, failed prior to reaching the manufacturer published average load capacity. Of the anchored specimens that failed primarily by FRP rupture, the highest $\frac{P_{test}}{P_{ult}}$ reached was 88% (specimen F1-4a-2-24) and the lowest $\frac{P_{test}}{P_{ult}}$ was 64% (specimen F1-2a-24). Several phenomena may be attributable to the rupture of the FRP sheets prior to reaching full capacity of the sheets. In anchored specimens, higher strains develop in line with the anchors so force is not developed uniformly across the width of FRP sheet. Furthermore, the skewed propagation of the debonding crack front or non-uniform load application due to slight imperfections in the loading apparatus may tend to generate higher stresses in parts of the sheet. In addition local stress

concentrations develop around the location of anchors, and the sheet fibers must be worked around the anchor shaft, which compromises the strength of the fibers due to bending. This is may be the primary reason why FRP rupture usually occurred around the location of anchors. The manufacturer's published ultimate strengths are determined using FRP coupon tests so the influence of bond and stress concentrations are minimized.

As discussed in section 4.3.5, the anchored specimens reached higher loads than the identical unanchored sheets because they delayed or prevented the debonding front from progressing towards the unloaded end. Debonding was delayed because a portion of the load was transferred from the bond to the anchors. The increase in capacity of a sheet fastened with anchors compared with an identical unanchored specimen is related to the amount of load that the anchors resist. This is discussed further in section 5.7.

The maximum strains reached by the three unanchored specimens were well below the ultimate strain capacities of the FRP. ACI 440.2R-08 limits the maximum design strain of FRP sheets because of the potential for debonding, as discussed in greater detail in section **Error! Reference source not found.**. For shear strengthening applications, ACI 440.2R-08 states that the effective strain in FRP laminates should never exceed 0.004, or $0.75\varepsilon_{fu}$. For the Sika and Fyfe materials used in this research program, the 0.004 limit controls. This reduction accounts for the loss of aggregate interlock that occurs prior to the FRP reaching its ultimate strain. The design ultimate strain value recommended for use by the manufacturers of the FRP systems equals two standard deviations less than the average test ultimate strain, and is 0.0098 for the Sika FRP material and 0.01 for the Fyfe FRP material. Since FRP behaves as a linear elastic material when loaded axially, limiting the strain to 0.004 is equivalent to a strength limit

of 40% of the design strength. For u-wraps and bonded face plies ACI 440.2R-08 recommends additional strength reduction factors that account for debonding failures that occur prior to loss of aggregate interlock, as discussed in section **Error! Reference source not found.**. Figure 4.82 shows that the anchored specimens reached significantly higher loads than the ACI 440.2R-08 recommended limits. This discussion illustrates the motivation for modifying these recommendations to account for FRP sheets fastened with FRP anchors. It is sometimes not possible to have the FRP sheet even as long as the STZ, which further limits the capacity of unanchored sheets. Such cases can occur in shear strengthening applications, especially with T-shaped beams, or when using multiple ply specimens, which have a longer STZ.

Fastening sheets with anchors not only increases load capacity, but can also increase the displacement capacity of the anchored sheet. Unanchored sheets give little warning prior to failure. After the initiation debonding, the debonding front often quickly propagates along the sheet until the sheet completely debonds, with little change in force prior to failure. In contrast, the anchored specimens tested showed initial signs of damage long before failure. Debonding generally initiated around the same load for anchored and unanchored specimens. For the anchored specimens the debonding front either stopped at the anchors until failure, or passed the anchors and progressed towards the unloaded end of the sheet, but at a much slower rate than in the unanchored specimens. For all anchored specimens, after the initiation of debonding the load capacity increased significantly before failing, as the anchors resisted more load.

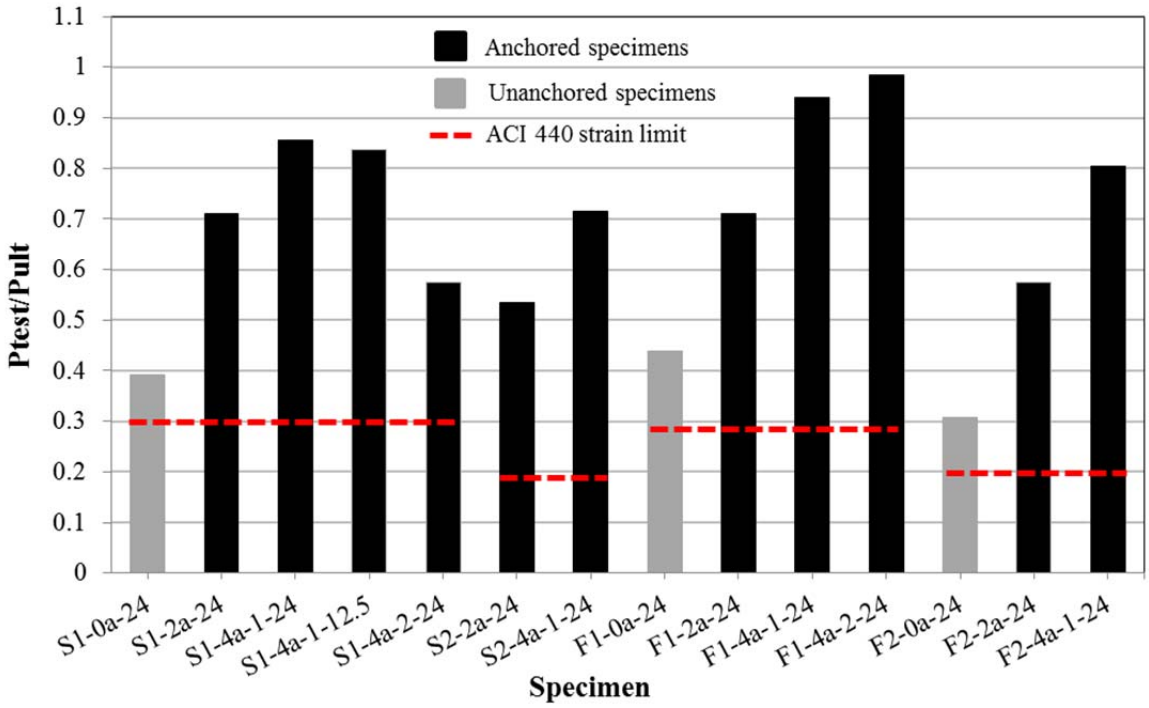

Figure 5.5 Load capacity compared to load calculated using ACI 440.2R-08 strain limits

5.4 Effect of multiple anchor rows

Table 4-2 and Figure 4.3 clearly show that it is possible to increase the ultimate load capacity by adding a second row of anchors. This is important because previous research Niemitz (2008) showed that when the anchor groups are spaced far apart 250 mm [10 in.] the trailing anchor appeared to add little capacity to the ultimate load. The distance between anchor rows that Niemitz (2008) used (250 mm [10 in.]) was longer than the stress transfer zone (STZ) for the specimen, so there was little strain in the sheet near the back row of anchors until the debonding front passed the first row of anchors. The back anchors appeared to only resist appreciable load until shortly before failure. For this research program there were several specimens with two rows of anchors spaced only 65 mm [2.5 in.] apart, which allowed the anchor splays to touch. Placing the two

rows of anchors at a smaller distance apart than the STZ length allowed the two rows of anchors to be engaged simultaneously in FRP stress development.

The specimens with four anchors performed significantly better than the specimens with two anchors, except for the outlier result of specimen S1-4a-2-24. As explained in section 4.2.2.4, specimen S1-4a-2-24 failed at a low load largely because a width of fibers on the right side of the sheet slipped from the loading grips prior to failure. In general, the specimens fastened with four anchors failed at significantly higher loads than the identical specimens fastened with only two anchors. In addition specimens fastened with four anchors had significantly lower strains behind the anchors than similar specimens fastened with two anchors. Figure 5.6 compares the strains recorded in gauges G4B and G5 (located 50 and 75 mm [2 and 3 in.] behind the anchors along the centerline of the sheet) for the Fyfe and Sika specimens with two and four anchors (specimens F1-2a-24 and F1-4a-1-24 and S1-2a-24 and S1-4a-1-24). This illustrates how the FRP stresses were being developed within the sheet region with FRP anchors, and the advantage of fastening sheets with two rows of anchors compared to one row.

Niemitz (2008) stated that the ability to achieve FRP rupture was dependent on the effectiveness of the leading FRP anchors. Results from this research program indicate that anchors behind the leading anchors can resist load too, and act as an anchor group with the leading anchors. For two of the three single ply specimens fastened with four anchors (specimens S1-4a-1-24 and S1-4a-1-12.5) the debonding front did not pass the anchors until failure, which consisted of a combination of debonding and FRP rupture. In specimen F1-4a-1-24 the debonding front was stopped at the anchors, and failure was due to FRP rupture. In contrast, the debonding front passed the anchors prior to failure in both

of the single ply specimens fastened with two anchors (specimens S1-2a-24 and F1-2a-24). Specimen F1-2a-24 failed by FRP rupture, however it is believed that the sheet strength was compromised by the loading apparatus. All double ply specimens failed primarily by debonding. However, specimens S2-4a-1-24 and F2-4a-1-24 failed at 34% and 40% higher loads than specimens S2-2a-24 and F2-2a-24, respectively, which indicates that the second row of anchors helped further delay debonding, although it was not sufficient to prevent it.

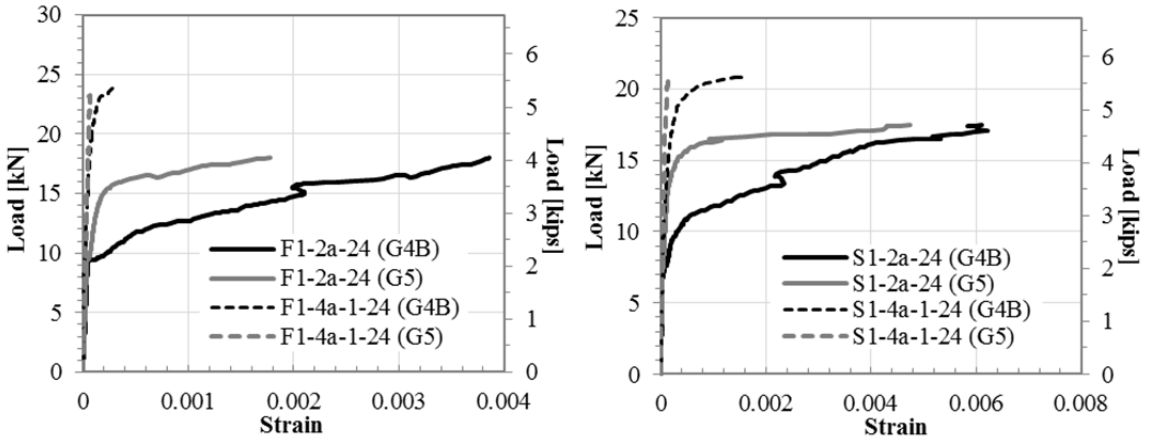

(a) **(b)**

Figure 5.6 Comparison of strain behind the anchors: (a) specimens F1-4a-1-24 and F1-2a-24 and (b) S1-4a-1-24 and S1-2a-24

In specimens S1-4a-2-24 and F1-4a-2-24 everything was identical to specimens S1-4a-1-24 and F1-4a-1-24 except that the spacing between the two rows of anchors was increased from 65 mm [2.5 in.]to 125 mm [5 in.], or equivalently, 1 anchor splay diameter to 2 splay diameters. The purpose of the two tests was to determine the effect of the longitudinal spacing of the anchors. Specimen S1-4a-2-24 failed at a significantly lower load than specimen S1-4a-1-24, and an even lower load than specimen S1-2a-24. However, specimen S1-4a-2-24 failed at a low load largely because a width of fibers on the right side of the sheet slipped from the loading grips prior to failure. In contrast, the

failure loads were very close for specimens F1-4a-2-24 and F1-4a-1-24. However, it appears that the anchors were not as effective at delaying the debonding front, as the closer spaced anchors did in specimen F1-4a-1-24. Strains behind the first row of anchors increased similarly to the strains behind the anchors in specimen F1-2a-24. The debonding front did not pass the anchors in specimen F1-4a-1-24. In specimen F1-4a-2-24 the debonding front passed both rows of anchors prior to failure, although the specimen still failed by FRP rupture. The specimen initially behaved more like specimen F1-2a-24, as the strain increased behind the first row of anchors at similar rate. This is believed to be because the back row of anchors initially resisted negligible load.

Figure 5.7 compares the longitudinal strain profile of specimens S1-4a-2-24 and S1-2a-24 from loads of approximately 27 kN to 49 kN [6,000 lbs to 11,000 lbs]. Specimen S1-4a-2-24 was identical to S1-2a-24, except there was an additional row of anchors placed 125 mm [5 in.] behind the front row of anchors. With the exception of gauge G1 the two specimens show very similar behavior. This is because during this load range there was negligible strain in the sheet near the trailing anchors, which means this row of anchors resisted little load, and therefore would expectedly have little impact on the behavior of the sheet.

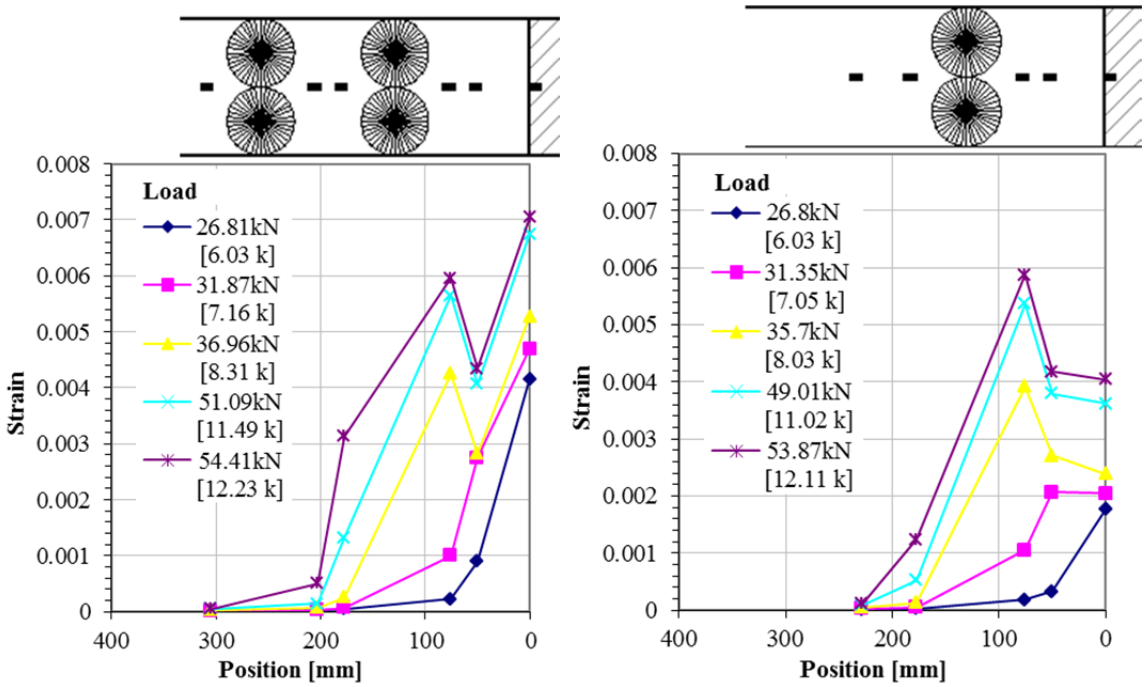

(a) **(b)**

Figure 5.7 Longitudinal strain profiles from loads of approximately 27 kN to 49 kN [6,000 lbs to 11,000 lbs]: for (a) specimen S1-4a-2-24 and (b) specimen S1-2a-24

To estimate the load that the front and back rows of anchors resisted, the drop in strain in the sheet from in-front-of-to-behind the first and second row of anchors was graphed versus applied load, as shown in Figure 5.8 and Figure 5.9. Since strain in the sheet is related to the load in the sheet, the difference in strain from in-front-of-to-behind each row of anchors, is related to the load that the anchors resist, minus the load that the bond resists. It is difficult to determine the amount of load that is resisted by the bond and the amount that is resisted by the anchors, however it is believed that Figure 5.8 and Figure 5.9 still give a good idea of the relative load assumed by the front and back rows of anchors.

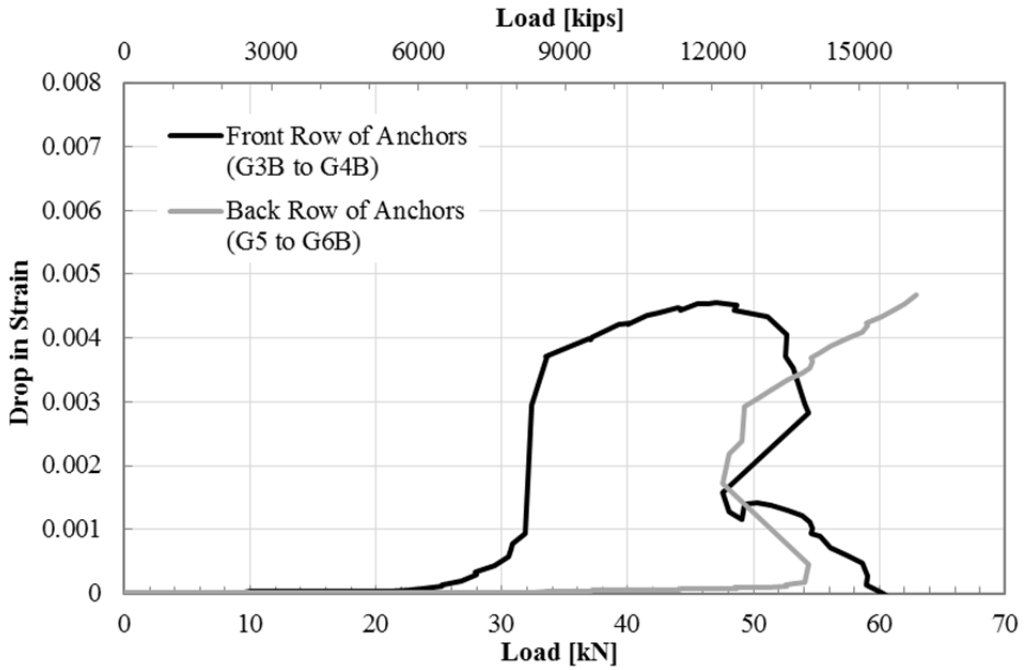

Figure 5.8 Difference in strain from in front of the given anchor to behind the anchor for Specimen S1-4a-2-24

The rapid increases in the graph in Figure 5.8 for the front and back row anchors occur at the same loads that the debonding front reached the respective row of anchors. Another important observation is that when the back row of anchors starts assuming significant load around 53 kN [12,000 lbs], there is a corresponding drop in load in the front row of anchors, which indicates that load was redistributed from the front row of anchors to the back row.

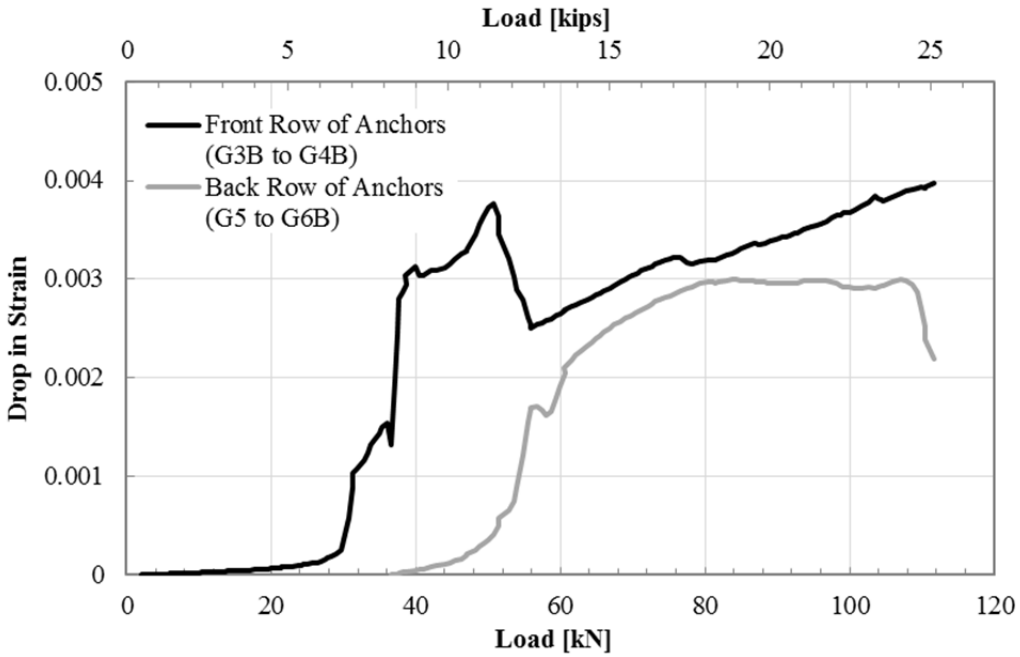

Figure 5.9 Difference in strain from in front of the given anchor to behind the anchor for Specimen F1-4a-2-24

Although Figure 5.8 and Figure 5.9 appear to look quite different at first glance, they do share important similarities. As with specimen S1-4a-2-24, the rapid increases in the graph for the front and back rows anchors occur at the same loads that the debonding front reached the respective row of anchors. Also, when the back row of anchors starts assuming significant load around 50 kN [11,000 lbs], there is a corresponding drop in load in the front row of anchors. Unlike specimen S1-4a-2-24, both anchors appear to assume significant load until failure, which could partly explain why specimen S1-4a-2-24 failed at a much lower load than F1-4a-2-24. It is likely that the drop in load in the front anchors in specimen S1-4a-2-24 was due to anchor damage such as splay delamination.

From the data it is believed that in general it is better to have the rows of anchors spaced as close as possible in order to have the highest load capacity. This will result in a more even distribution of load between the rows of anchors, since less load is taken by

the bond between the rows of anchors. If the space between the anchors is large compared to the length of the STZ, than the back row or rows of anchors may not assume appreciable load until after the debonding front has progressed passed the first row of anchors. If the front anchors are not ductile, then they may fail before the back row of anchors assumes load. In this case, the back rows of anchors may not increase the load capacity of the sheet, but could still increase the ductility of the sheet, as the back rows of anchors act as reserve strength after debonding passes the front row of anchors. Also, if the trailing anchors are close to the end of the sheet, then the sheet may suddenly debond before the anchors start resisting load. It is believed that in addition to the spacing of the rows of anchors, the distribution of forces to the front and back row of anchors depends on the relative stiffness of the sheet and the anchors. A very stiff sheet, for instance a multi-ply carbon fiber sheet, will more evenly engage the rows of anchors than a sheet with smaller stiffness, because will allow for less movement of one row relative to another row.

5.5 Effect of Bond Length Behind Anchors

It is clear from results from this research program and consistent with previous investigations (Chen and Teng, 2001; Subramaniam, et al., 2007) that increasing the length of sheet beyond the STZ causes negligible increase in ultimate load capacity, but can increase the ductility of failure. This observation is not always true for bonded sheets fastened with anchors.

The stronger and stiffer the anchors the more likely FRP rupture will occur across the width of the sheet prior to the debonding front passing them, since stiffer anchors assume more load, which results in lower strains behind the anchors. As expected, the

specimens that did not have debonding behind the anchors had little strain behind the anchors at failure. If there is negligible strain in the sheet behind the anchors from initial loading until failure, then the sheet behind the anchors has little effect on the performance and behavior of the specimen.

This theory was tested by comparing specimens S1-4a-1-24 and S1-4a-1-12.5. The specimens were identical, except in the latter specimen the sheet behind the anchors was shortened from 420 mm to 125 mm [16.5 in. to 5 in]. Both specimens had very low strains behind the anchors. The recorded strains, the failure load, and the failure modes were all similar. Had the anchors been less effective for both specimens, and allowed the debonding front to pass them, the increased bond length of specimen S1-4a-1-24 would likely have allowed for a more ductile failure. Also it is possible that the failure load would have been higher for specimen S1-4a-1-24 compared to S1-4a-12.5. Once the sheet debonds past the anchors, the anchors can still assume significantly more load, depending on the ductility and strength of the anchors. This is because as the sheet debonds behind the anchors the unbonded portion of the sheet elongates, and larger elongation will cause higher loads to be resisted by the anchors. A longer sheet will allow for more overall elongation prior to debonding failure. In several of the anchored specimens, including all four of the anchored double ply specimens (F2-2a-24, F2-4a-1-24, S2-2a-24, S2-4a-1-24), the load continued to increase after the initiation of debonding behind the anchors. This can be seen in the longitudinal strain distribution plots in section 4.3.4.

5.6 Effect of multiple FRP plies (single and double)

Table 4-2 and Figure 4.3 show that all double ply specimens failed at higher loads than the identical single ply specimens. However, Figure 5.10 shows that the double ply specimens always failed at a lower load ratio ($\frac{P_{test}}{P_{ult}}$) than the identical single ply specimens. This is likely because the same anchors were used for the single and double ply specimens; therefore the anchor capacity was lower relative to the sheet capacity for the double ply specimens. It appears that in general debonding initiated behind the anchors at around the same or higher load than in the single ply specimens. Since the double ply specimens had greater load capacity they were more likely to fail by debonding than the single ply specimens. The failure modes of all four of the anchored double ply specimens included debonding and anchor splay delamination. This indicates that the capacity of the anchors was being reached as more load demand was being placed on them. In contrast, in most anchored single ply specimens FRP rupture was either the primary or a secondary failure mode.

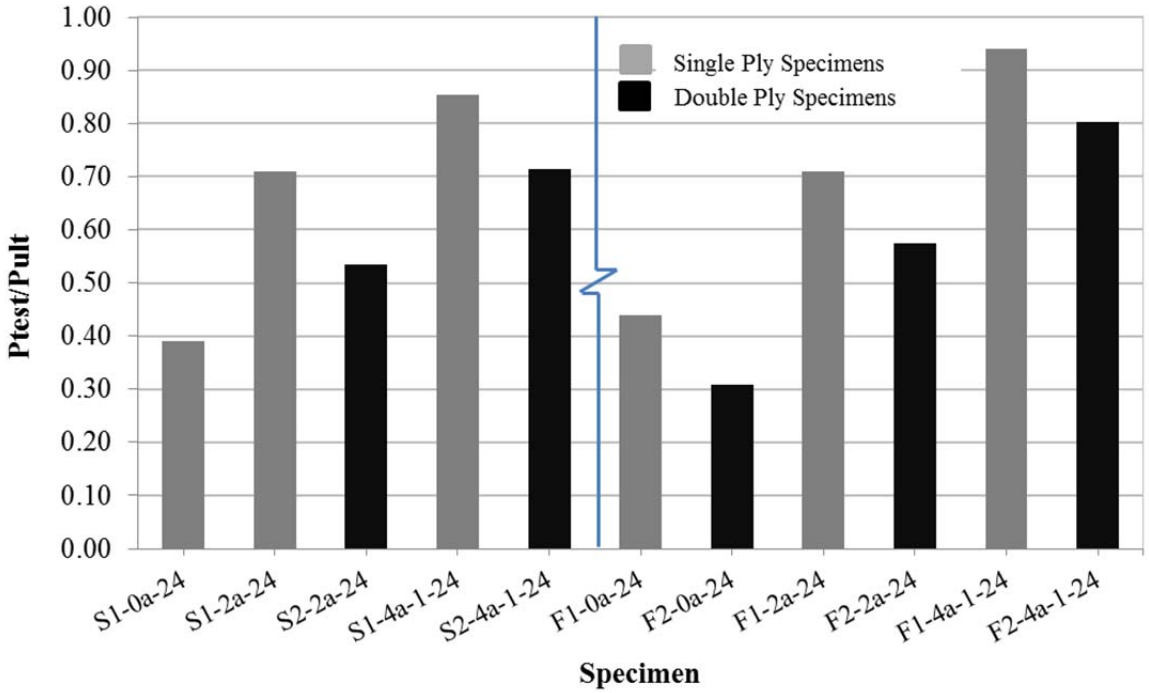

Figure 5.10 Comparison of single vs. double ply specimens

Single and double ply unanchored specimens exhibited the same behavior, as discussed in section 4.3.2.1The unanchored double ply specimens failed at higher loads than the unanchored single ply specimens, but at a lower $\frac{P_{test}}{P_{ult}}$. This indicates the advantage of using additional unanchored plies, but also the increased inefficiency of additional plies. Figure 5.11 compares the longitudinal strain profiles of the unanchored single and double ply Fyfe specimens (F1-0a-24 and F2-0a-24). The strain in gauge G1, located in the unbonded section, was roughly double for the singly ply specimen than for the single ply specimen. It can be seen that debonding initiated around 67 kN [15,000 lbs] for specimen F2-0a-24 and approximately 50% lower load for specimen F1-0a24 at around 44 kN [10,000 lbs].

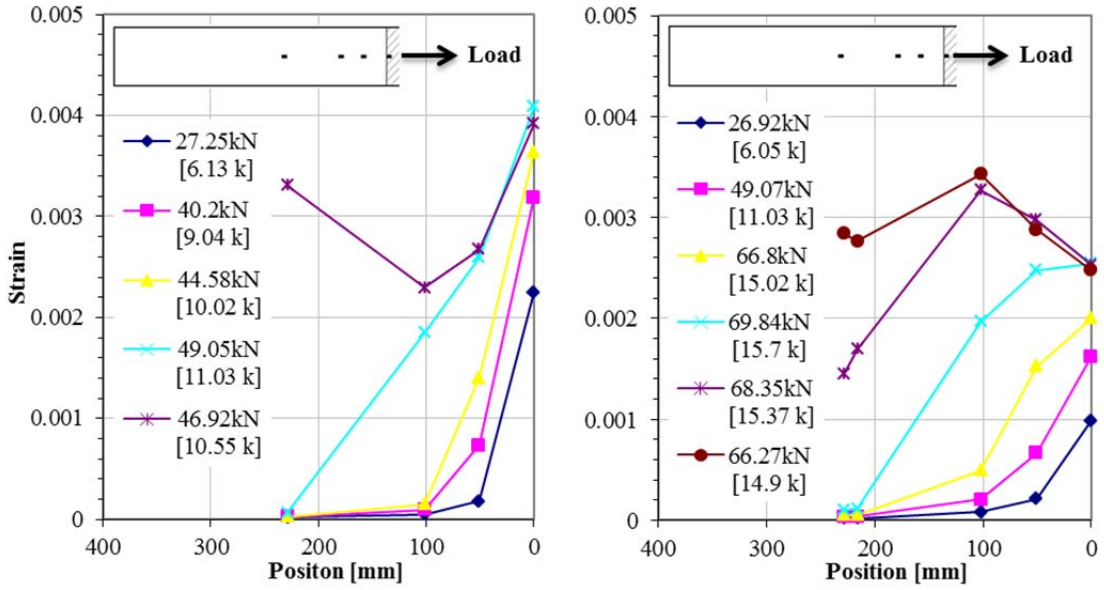

Figure 5.11 Comparison of longitudinal strain profiles in (a) specimen F1-0a-24 and (b) specimen F2-0a-24

The single ply and double ply specimens showed similar trends in load capacity from unanchored specimens to specimens fastened with two anchors to specimens fastened with four anchors. The double ply Sika and Fyfe specimens also showed similar trends in increase in load capacity. The advantage of FRP anchors was even more pronounced for the double ply Fyfe specimens than it was for the single ply specimens, in regards to load capacity. It is very likely that the same would have been true for the Sika specimens, although this cannot be verified because there was not an unanchored double ply Sika specimen. Double plys specimens F2-2a-24 and F2-4a-1-24 recorded peak loads that were 115% and 161% higher than F2-0a-24, respectively, while single ply specimens F1-2a-24 and F1-4a-1-24 recorded peak loads that were 62% and 114% higher than F1-0a-24.

5.7 Isolated anchor behavior in unbonded specimens

Two anchored-unbonded specimens were tested to better isolate the behavior of the anchors. The anchors were not completely isolated, however, since the bonded section behind the anchors resisted some load for both specimens. The bonded section prevented the sheet behind the anchors from bending upwards, which happens when there is no bonded section. It is believed that this happens because the anchors bend slightly under load causing the anchor splays and the attached sheet to bend upwards. To determine the ratio of the applied load that was resisted by the bonded section the sum of the strains recorded by the three gauges located across the width of the sheet in front of the anchors (gauges G3A, G3B, G3C) was divided by the sum of the strains in the three gauges located behind the anchors (gauges G4A, G4B, G4C). For specimen F1-4a-1-24, the average strain in the three transverse gauges located behind the anchors was approximately 12% of the strain in the three gauges in front of the anchors prior to failure, which means that the bonded section resisted approximately 12% of the load. It is believed that the load that is resisted by the anchors can be estimated closely by reducing the applied load by 12%. For specimen F1-2a-24, at a load of 40 kN [9,000 lbs], the average strain in the three transverse gauges located behind the anchors was 20% of the strain in front of the anchors. Around 45 kN [10,000 lbs] there was a large jump in strain behind the anchors, and shortly before failure the strain behind the anchors was approximately 75% of the strain in front of the anchors. Therefore from 45 kN [10,000 lbs] until failure the data is not useful as far as determining the isolated behavior of the anchors, and therefore data collected beyond 45 kN [10,000 lbs] is not discussed.

The transverse strain profiles in front of and behind the anchors are similar to the anchored and bonded specimens. For both specimens, in front of the anchors strain was significantly higher in line with the anchors than along the centerline of the sheet, and behind the anchors the opposite was true. This is further evidence that in front of the anchors the anchor splays most effectively engage the sheet in line with the anchors, which causes this part of the sheet to assume more load.

Figure 5.12 compares the load-displacement relationships for the anchors from specimen F1-2a-24U with the front row of anchors from specimen F1-4a-1-24U. Displacement was measured primarily to estimate the stiffness of the anchors. For specimen F1-4a-1-24U, the relative displacement of the front and back rows of anchors also gives an approximate idea of the relative force that the two rows of anchors resisted. In both specimens the left anchor deflected more than the right anchor. This is likely due to uneven loading.

Figure 5.12 shows that the anchors in specimen F1-2a-24U deflected more than the front anchors in specimen F1-4a-1-24U, even though the bonded section resisted more load in specimen F1-2a-24 than in F1-4a-1-24U. This indicates that both rows of anchors in specimen F1-4a-1-24U resisted load. Figure 5.13 shows that for specimen F1-4a-1-24 the displacement of the front anchors was significantly greater than the displacement of the back anchors, which indicates that the front anchors carried significantly more load than the back anchors. At a load of approximately 36 kN [8,000 lbs], the front left anchor gauge detached from the sheet. It is believed that this was due to deformation of the anchor splay, which caused a redistribution of forces to the other anchors, and the displacement gauges registered a sudden increase in displacement of the

back left and front right anchors. This demonstrates the added robustness of having more than one row of anchors.

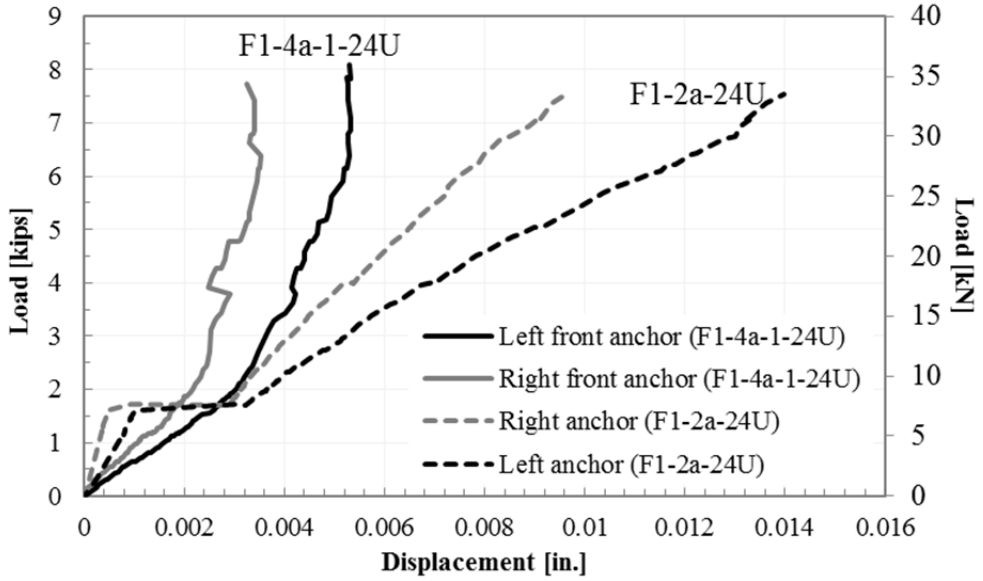

Figure 5.12 Comparison of load-displacement behavior for the front anchors of specimens F1-4a-1-24U and F1-2a-24U

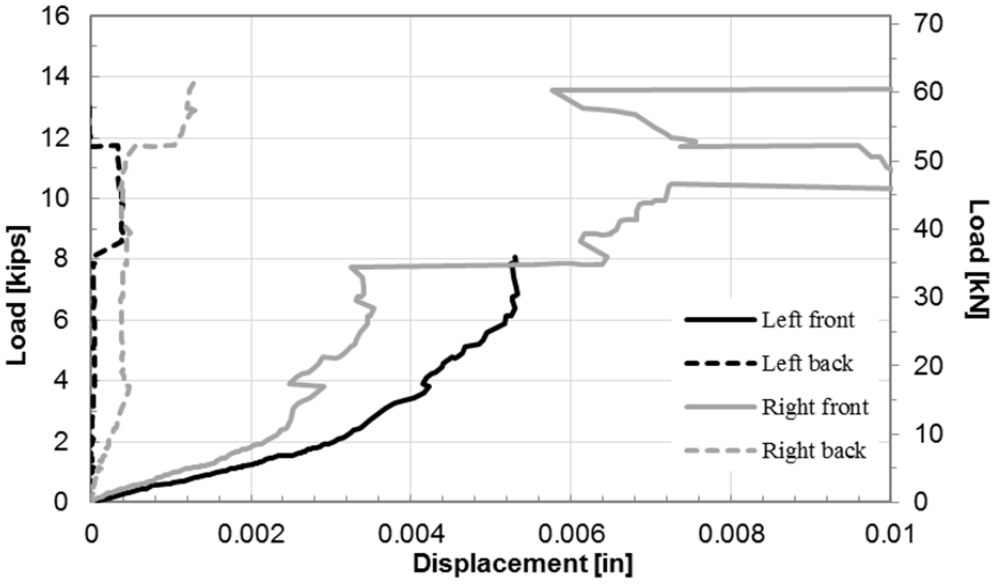

Figure 5.13 Load-displacement behavior of anchors in specimen F1-4a-1-24U

Figure 5.14 shows the load-displacement relationship for the left and right front anchors of specimen F1-4a-1-24U. Prior to a load of 36 kN [8,000 lbs], when there was

believed to be damage to the front left anchor gauge, there were two distinct linear regions, labeled (A) and (B). At a load of approximately 9 kN [2,000 lbs] the front anchors started displacing at a lower rate. It is believed that this is because the back anchors started assuming appreciable load. The average stiffness of the front two anchors in region (A) was 117 kN/mm (669 kip/in.) and in region (B) was 465 kN/mm (2,654 kip/in.). The stiffnesses were approximated as the slope of the lines shown in Figure 5.14 multiplied by 88% since it was estimated that 12% of the load was resitsed by the bonded section. Since very little displacement was recorded for the back anchors, the stiffness of the back anchors was not calculated.

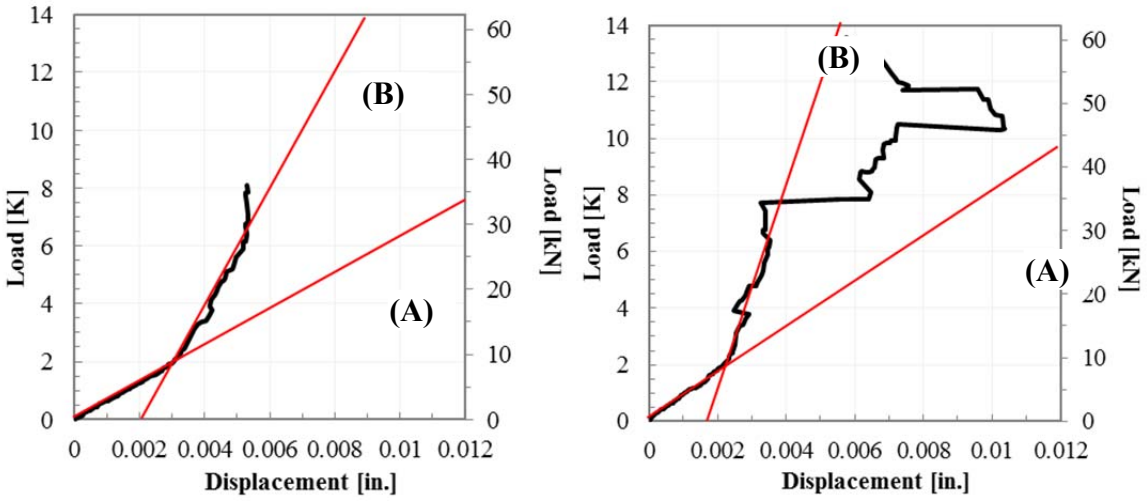

(a) (b)

Figure 5.14 Load-displacement behavior of (a) the left and (b) right front anchors for Specimen F1-4a-1-24U

Table 5-3 Stiffness of left and right front anchors for Specimen F1-4a-1-24U

	(A)	(B)
Anchor	kN/mm (kip/in.)	
Left Front	100 (572)	289 (1,650)
Right Front	134 (766)	640 (3,657)
Avg	117 (669)	465 (2,654)

Figure 5.15 shows the load-displacement relationships for the anchors of specimen F1-2a-24U. This load-displacement relationship is used to define the anchors in the finite element models presented in Chapter 6. As can be seen, there is a sudden change in the behavior of the anchors around 9 kN [2,000 lbs] like with specimen F1-4a-1-24U. However, the anchors were initially stiffer and then became less stiff, which is the opposite of what happened with specimen F1-4a-1-24U. The average stiffness during region (A) was 355 kN/mm [2,026 kip/in.] and in region (B) was 99 kN/mm [562 kip/in.]. The stiffnesses were approximated as the slope of the lines shown in Figure 5.15 multiplied by 80% since it was estimated that 20% of the load was resitsed by the bonded section.

It is believed that region (A) of specimen F1-4a-1-24U occurred when the first row of anchors resisted a large portion of the load, so that the front anchors behaved similarly to the anchors in F1-2a-24U. In region (A) of specimen F1-4a-124U the slope is approximately 20% higher than the slope in region (B) for the front anchors of specimen F1-2a-24U. This is a small difference given the precision of the instrumentation. It is likely that region (A) in specimen F1-2a-24U could be responsible for the sheet behavior under low loads, by the sheet aligning and slack being removed from the sheet. The recorded strains in front of the anchors increased slowly as well during the same load range of region (A). Therefore, it is believed that region (B) is more representative of the stiffness of the anchors from specimen F1-2a-24U.

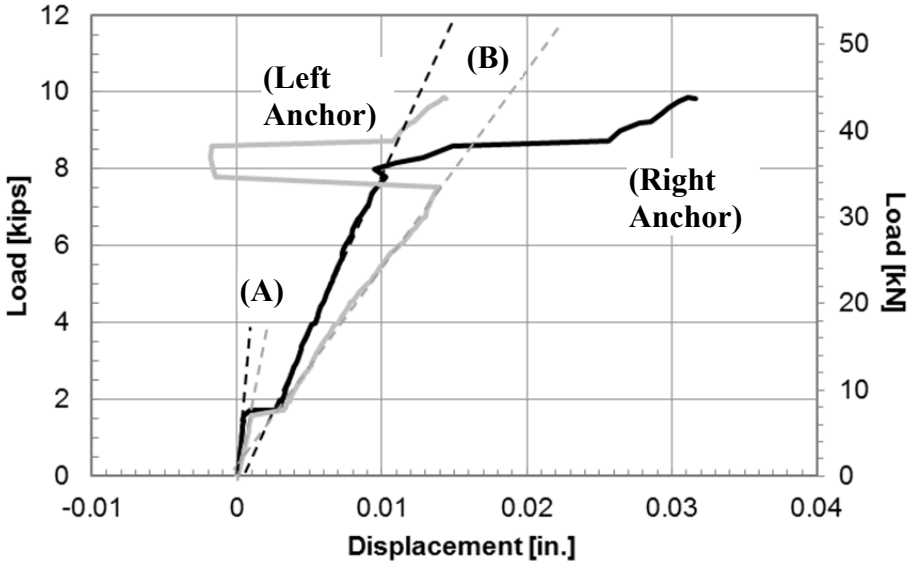

Figure 5.15 Load vs. Displacement for Specimen F1-2a-24U

Table 5-4 Stiffness of left and right front anchors for Specimen F1-2a-24U

	Region	
	(A)	(B)
Anchor	kN/mm (kip/in.)	
Left	500 (2,857)	72 (410)
Right	209 (1,194)	125 (714)
Avg.	355 (2,026)	99 (562)

The increase in capacity of a sheet fastened with anchors compared with an identical unanchored specimen is related to the amount of load that the anchors resist. An interesting observation is that the failure load of the bonded but unanchored specimen (F1-0a-24) added to the failure load of the anchored but unbonded specimen (F1-4a-24U) equals 112 kN [25,200 lbs], which is 5% greater than the failure load of the anchored and bonded specimen (F1-4a-1-24). In other words, the capacity of the bond alone plus the capacity of the anchors alone was close to the capacity of the bonded and anchored specimen.

Figure 5.17 compares the failure load of anchored Fyfe specimens with the summation of the failure load of the identical unanchored specimens and the estimated

load capacity of the anchors from Figure 5.16. The load capacity of the anchors was estimated as the load at which the anchors failed in the unbonded-anchored specimens minus the load that was resisted by the bonded section.

Specimen	Failure Load	Anchor Failure Load	% of Load Resisted by Bonded Area	Load Capacity of Anchors
F1-2a-24U	13,900	9800	20%	**7840**
F1-4a-1-24U	14,000	14,000	12%	**12320**

Figure 5.16 Estimation of the capacities of one row and two rows of anchors from experimental data collected from specimens F1-2a-24U and F1-4a-1-24U, respectively

Figure 5.17 shows that the failure load of the bonded-unanchored specimen F1-0a-24 added to the estimated capacity of two rows of anchors equals 112 kN [25,200 lbs], which is only 2% less than the failure load of the anchored and bonded specimen F1-4a-1-24. The failure load of the bonded-unanchored specimen F1-0a-24 added to the estimated capacity of one row of anchors equals 34.9 kN [7,840 lbs], which is only 5% more than the failure load of the anchored and bonded specimen F1-4a-1-24. Unfortunately the failure loads of the anchored double ply specimens (F2-2a-24 and F2-4a-1-24) are approximately 30% less than the summation of the unbonded specimen capacity and the estimated anchors capacities.

Specimen	Load [lb]	Ratio
2 anchors+F1-0a-24	19,040	1.05
F1-2a-24	18,120	
4 anchors +F1-0a-24	23,520	0.98
F1-4a-1-24	23,970	
2 anchors+F2-0a-24	23,540	0.70
F2-2a-24	33,830	
4 anchors +F1-0a-24	28,020	0.68
F2-4a-1-24	41,000	

Figure 5.17 Comparison of the failure load of anchored specimens with the summation of the failure load of the identical unanchored specimen and the estimated capacity of the anchors from Figure 5.16

CHAPTER 6

FINITE ELEMENT ANALYSIS

6.1 Introduction

This chapter discusses the development of preliminary finite element models of anchored and unanchored FRP sheets bonded to concrete using SAP2000. The models are validated by comparing to experimental results from this research program, including load capacity, extent of debonding, and strain distribution. The models are two dimensional (2D) models in the plane of the FRP sheet. There are many existing theoretical models of the bond behavior of FRP to concret joints; however, the only known theoretical model of anchored FRP sheets was presented by Niemitz (2008). Existing bond models include those that are based on fracture mechanics, finite element analysis, or empirically on experimental data.

6.2 Modeling Overview

There are many existing finite element models that successfully model bonded (unanchored) sheets to concrete. The adhesive layer is usually modeled with an extremely fine mesh. Another successful method, used by Niemitz (2008) and others, uses interface elements to model the entire bonding layer, including contributions from the sheet, the epoxy layer and a thin layer of concrete, where debonding failures typically occurr. The properties of these interface elements are based on bond-slip models which can be found in literature. Niemitz, (2008) developed a 2D finite element model of the plane perpendicular to the FRP sheet plane. The advantages of a 2D model include reduced

computational demand, which allows for a finer mesh, and in general are less complicated to develop. In reality stress varies across the width of bonded sheets, which is not captured by a 2D model of the profile of the FRP sheet. Capturing the transverse variation of stress is particularly important for accuratly modeling anchored sheets, since the stress can vary greatly across the width of the sheet. Also debonding often does not occur at the same rate across the width of anchored FRP sheets. For these reasons, it was decided to develop a 2D model in the plane of the sheet. Figure 6.1 compares element configurations for 2D models of FRP bonded to concrete oriented perpendicular to the FRP (a) and in the plane of the sheet (b).

6.3 Material Modeling

The proposed finite element model consists of three components; the CFRP sheet, the interface and anchors. This section presents a description of each component. The same interface and sheet element properties were used in all models, and the same anchor properties were used in the models of the unbonded-anchored and bonded-anchored specimens.

6.3.1 FRP Sheet

The CFRP sheet was modeled using thin shell elements with orthotropic properties. The material properties given by the manufacturer were used, which are based on average experimental values. CFRP sheets are very closely linear elastic and exhibit a sudden failure. The material was modeled as linear elastic in the three orthogonal directions. Elastic moduli of the FRP sheet in the direction and perpendicular to the direction of fiber was 72,400 MPa [10,500,000 psi] and 3,180 MPa [461,000 psi], respectively. The epoxy had an elastic modulus of 3,180 MPa [461,000 psi], so this value

was used in directions orthogonal to fibers. Poisson's ratio was assumed to be 0.15 for all orthogonal directions. The thickness of the shell elements was set to 1.02 mm [0.04 in.], which is the avergae thickness of a cured FRP sheet, as given by the manufacturer. A strength for the sheet elements was not defined in the models, so rupture of the sheets needed to be determined manually by inspecting the stress results.

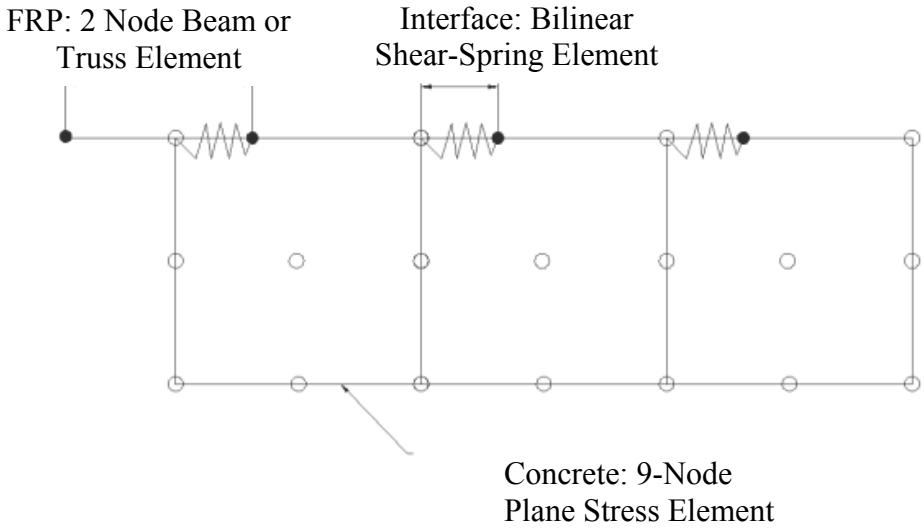

(a)

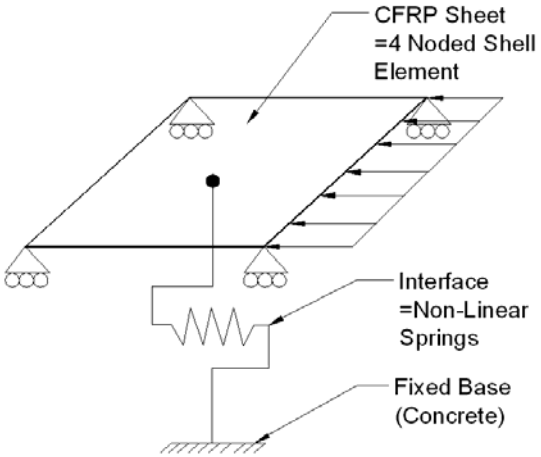

(b)

Figure 6.1 Element configuration for 2D models of FRP bonded to concrete oriented perpendicular to the FRP (a) and in the plane of the sheet (b)

6.3.2 FRP-Concrete Interface

The heart of the model is the interface. As mentioned earlier, the interface is modeled using separate interface elements, which model the entire interface, including contributions from the sheet, the epoxy layer and a thin layer of concrete, where debonding failures typically occur. The interface elements are defined by a force-displacement relationship, based on a bond-slip model presented by Lu et al. (2005) , which is regarded as one of the most accurate bond-slip models currently available. Lu et al. (2005) presents three similar bond-slip models of varying degrees of complexity and accuracy, which are shown in Figure 6.2. The interface elements are based on the bilinear model.

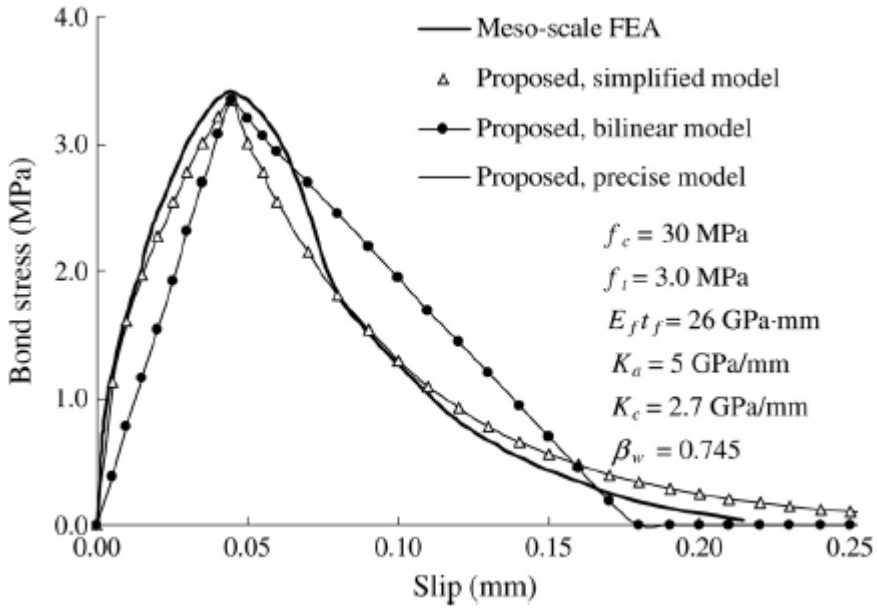

Figure 6.2 Bond-slip curves from meso-scale finite element simulation and the three proposed bond-slip models (Lu, et al., 2005)

The Lu et al. (2005) model accounts for the width of the concrete block, the width of the bonded FRP sheet, the stiffness of the adhesive, and properties of the concrete. Bond-slip relationships are commonly derived from experimental results in two ways;

from axial strains of the FRP measured at finite locations, or from the load-displacement relationship of the loaded end of the FRP sheet. With the first method the local slip can be estimated from the strain measurements, however strains can vary significantly within a short distance in the FRP sheet due to local variations in FRP and the concrete, including crack locations, and aggregate distribution. The problem with the second method is that different bond-slip relationships can result in similar load-displacement relationships. To avoid the deficiencies of these two methods, Lu et al. (2005) developed a bond-slip model based on results from a finite element simulation with a very small element size (0.25-0.50 mm), and which was calibrated to match experimental results. Table 6-1 shows the performance of the bond strength and bond-slip models found in literature and those proposed by Lu et al. (2005) based on the predicted bond strength compared to experimental results from 253 shear tests. It can be seen that the three proposed models all performed slightly better than the Chen and Teng (2001) model, and also the bilinear model behaves very closely to the precise model. All three proposed models also closely matched the experimental strain distributions in the FRP, so the bilnear model was used, since it is the simplest.

Table 6-1 Predicted-to-test bond strength ratios of (a) bond strength and (b) bond-slip models (Lu et al., 2005)

	Bond strength model	Average Predicted-to-test bond strength ratio	Coefficient of variation	Correlation coefficient
1	Tanaka [25]	4.470	0.975	0.481
2	Hiroyuki and Wu [26]	4.290	0.611	−0.028
3	Sato [32]	1.954	0.788	0.494
4	Chaallal et al. [31]	1.683	0.749	0.240
5	Khalifa et al. [30]	0.680	0.293	0.794
6	Neubauer and Rostasy [29]	1.316	0.168	0.885
7	Izumo [32]	1.266	0.506	0.656
8	van Gemert [27]	1.224	0.863	0.328
9	Maeda et al. [9]	1.094	0.202	0.773
10	Iso [32]	1.087	0.282	0.830
11	Yang et al. [33]	0.996	0.263	0.766
12	Chen and Teng [7]	1.001	0.163	0.903
13	Proposed strength formula (Eq. (4e))	1.001	0.156	0.908

	Bond–slip model	Average predicted-to-test bond strength ratio	Coefficient of variation	Correlation coefficient
1	Neubauer and Rostasy [34]	1.330	0.209	0.887
2	Nakaba et al. [12]	1.326	0.231	0.846
3	Savioa et al. [36]	1.209	0.199	0.847
4	Monti et al. [35]	1.575	0.164	0.888
5	Proposed, precise model	1.001	0.155	0.910
6	Proposed, simplified model	1.001	0.155	0.910
7	Proposed, bilinear model	1.001	0.156	0.908

The interface elements have stiffness in the direction of the loading only. In reality the interface provides stiffness parallel and perpendicular to the loading, but the model performed well when the stiffness perpendicular to the loading was ignored. The computational demand was also significantly reduced. To convert the stress-slip values from the Lu et al. (2005) bilinear bond-slip model to force-displacement values, the bond stress values were multiplied by the area of the bond that each interface element covers, which was 161.3 mm^2 [0.25 $in.^2$]. The bond-slip values according to Lu et al. (2005) are shown in Figure 6.3 and the corresponding force-displacement relationship for the interface elements is shown in Figure 6.4

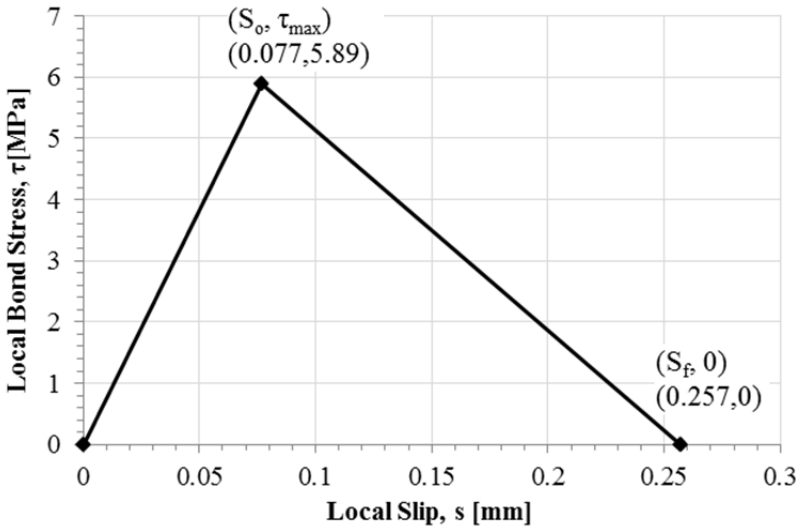

Figure 6.3 Bond-slip model according to (Lu et al., 2005)

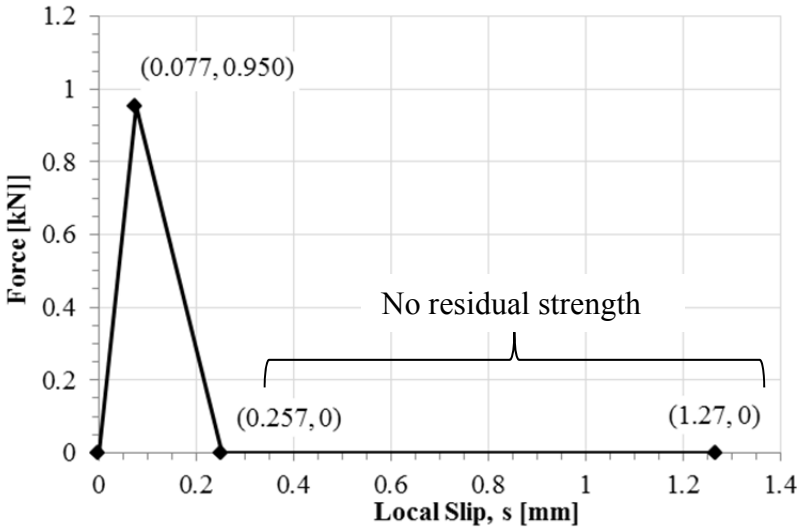

Figure 6.4 Force-displacement relationship for the interface elements derived from (Lu, et al., 2005) model. Relationship is mirrored in third quadrant.

6.3.3 FRP Anchors

The FRP anchors are modeled using the same type of spring elements as used for the interface elements. The anchor elements were assigned stiffness in both orthogonal directions. The force-displacement relationship of the anchor elements is based on experimental load-displacement measurements of the anchors from the anchored-

unbonded specimen F1-2a-24U. One difficulty in defining the force-displacement relationships of anchors is that the relationship is affected by the failure mode of the anchors; either by anchor shearing, anchor splay rupture, or anchor splay delamination. Specimen F1-2a-24U failed by anchor splay delamination, therefore the force-displacement relationship of the anchors is based on this failure mode. This was also the most common anchor failure mode for the specimens from this research program. Two force-displacement relationships were derived from the same experimental measurements from specimen F1-2a-24U, and are shown in Figure 6.6. Figure 6.6 shows how the force-displacement relationships were derived. To determine which anchor type to use, models were run using both anchor types and the results were compared to experimental results.

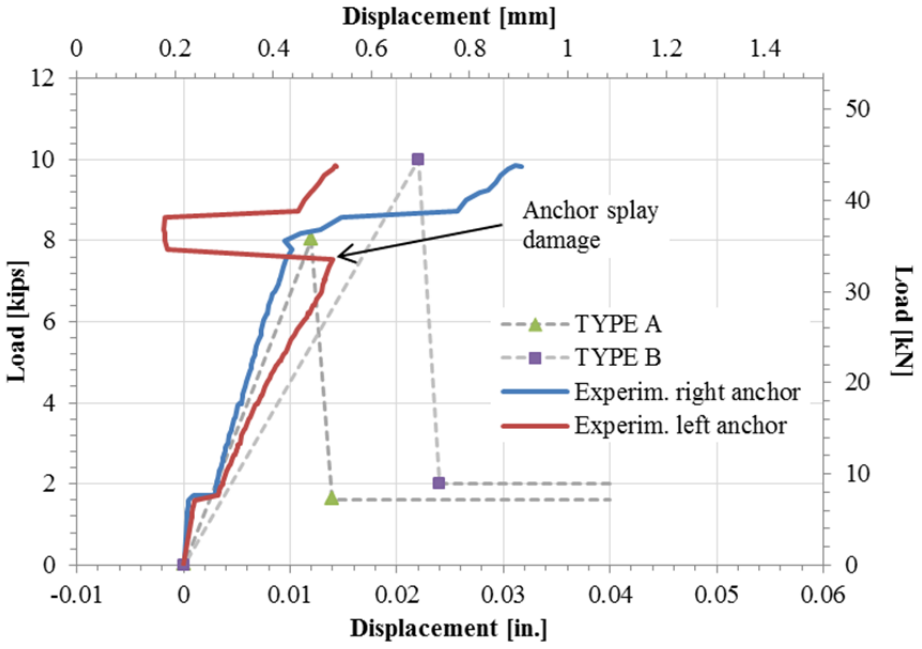

Figure 6.5 Anchor force-displacement relationships compared to experimental force-displacement measurements from specimen F1-2a-24U

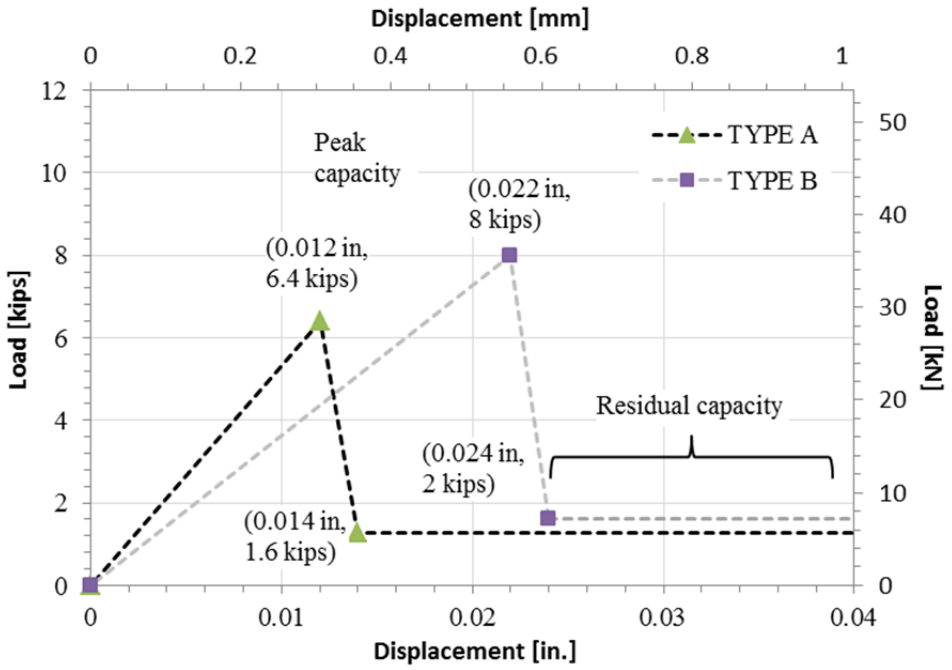

Figure 6.6 Comparison of the force-displacement relationships for type A and type B anchors

Both force-displacement relationships have a linear ascending branch, a sharp linear descending branch and then a constant residual force for infinite deflection. The peak load for the Type A anchors is based on the load and correpsonding deflection at which the anchor splays began to delaminate, at a load of 35.6kN [8.0 kips], as shown in Figure 6.5. The peak load for the Type B anchors is based on the approximate load and corresponding average displacement at which both anchor splays were assumed to have fully delaminated (43.6 kN [10.0 kips]), as shown in Figure 6.5. It is believed that the anchor shafts contiued to resist load beyond 43.6 kN [10.0 kips] only because the shafts bore against the sheet placed behind the anchors to avoid splitting of the FRP sheet. The peak forces from the two force-displacement relationships in Figure 6.5 were mutliplied by 80% because at the peak experimental load approximately 20% of the applied load was resisted by the bonded region and not the anchors, as discussed in section 5.7. The

resulting force-displacement values are shown in Figure 6.6. The loads from Figure 6.6 were then divided by eight, since there were two anchors, and each anchor was modeled with four equivalent spring elements, as discussed in section 6.4. The reserve strength of the anchors equals 20% of the peak capacity. This accounts for the load of the anchor shaft bearing against the sheet.

6.4 Model Geometry

A diagram of a typical model is shown in Figure 6.7. Shell elements were chosen to model the sheets since the sheets are thin and because most other models found in literature use shell elements to model FRP sheets. Only membrane action was captured. The shell elements were square shaped, 12.7 mm by 12.7 mm [0.5 in. by 0.5 in.]. Interface elements were applied at the corners of each shell element within the the bonded region. The first 127 mm [5 in.] of the sheet on the loaded end had no interface elements, since the experimental specimens were unbonded for the first 127 mm [5 in.] adjacent to the load application end. The model dimensions were the same as the FRP sheet dimensions used in the experiments: 610 mm [24 in.] long by 127 mm [5 in.] wide.

The anchors were modeled using spring elements, which were connected to the corners of the shell elements across the section where anchors were placed. Each anchor was modeled with four equivalent spring elements, aligned in a single row, as show in Figure 6.7.

Analyses were conducted by displacement control. All nodes on the loaded edge of the sheet were constrained to the center node, since in the experimental tests the end of the FRP sheet was fixed to the loading plates. A load was applied to the center node, and

displacement was monitored at the start of the bonded region in the middle of the sheet, as shown in Figure 6.7.

6.5 Results

The validity of the model was confirmed by comparing model results to experimental results. The primary experimental results used to verify the model were failure load, extent of debonding prior to failure, force-displacement curve and strain distribution.

The shell elements had infinite strength so failure due to FRP rupture needed to be determined manually by inspecting the sheet stress results, which can be difficult with anchored specimens due to stress concentrations. This also means that the model can not capture local FRP rupture and corresponding redistribution of forces. This was done to focus primarily on bond and anchor failures instead of FRP rupture

6.5.1 Convergence Study

Two parameters were investigated as part of the convergence study: (1) FRP shell element size, and (2) relative iteration convergence. The effect of these parameters is shown in Figure 6.8 and Figure 6.9, respectively, for the model of specimen F1-0a-24. As can be seen in Figure 6.8 element size had little effect on peak load, and the finer mesh model shows less variation in load after the initiation of debonding, which is represented by the plateau region. The stiffness of the FRP prior to debonding appears to be lower for the model with smaller elements, although this represents only a single load step. It is believed this is due to the magnitude of the first load step chosen by SAP2000. Based on the convergence study the FRP mesh selected was [0.5 in. by 0.5 in.] and the relative iteration convergence tolerance was 0.001.

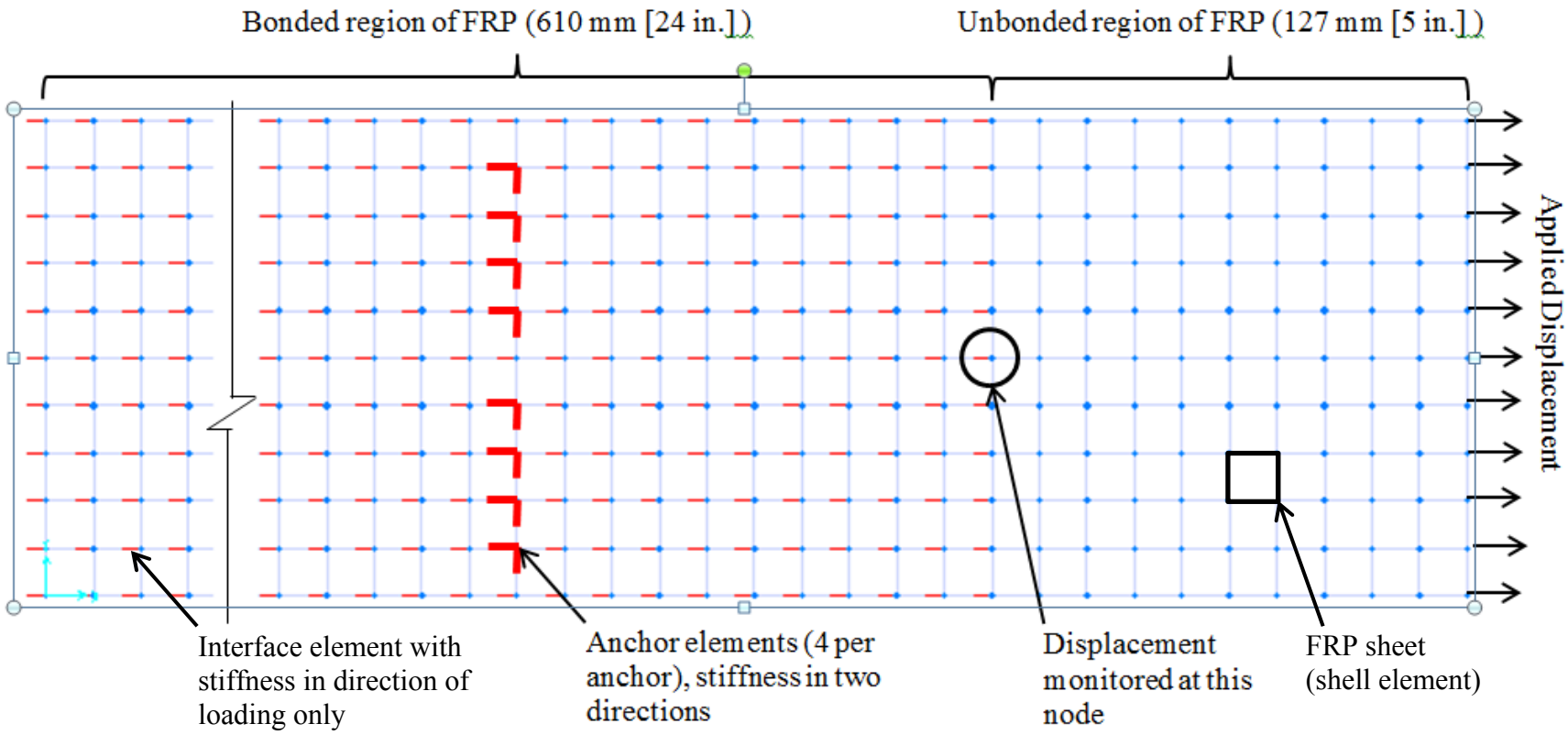

Figure 6.7 Diagram of a model (specimen F1-2a-24)

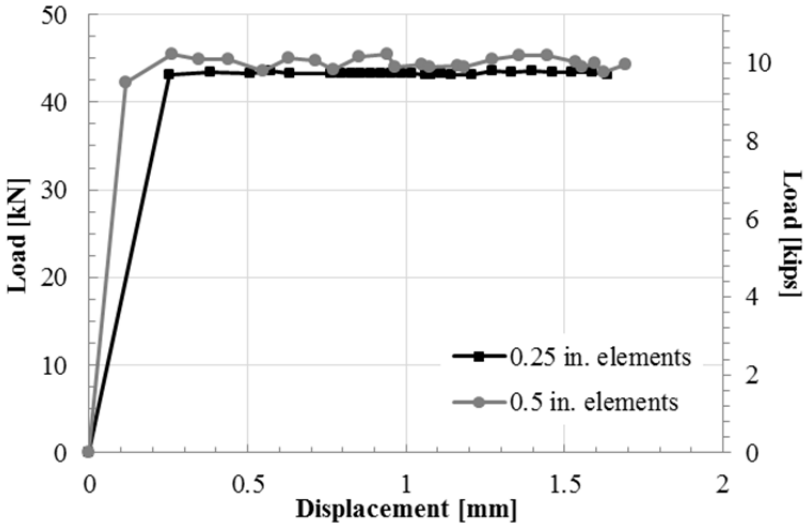

Figure 6.8 Element size

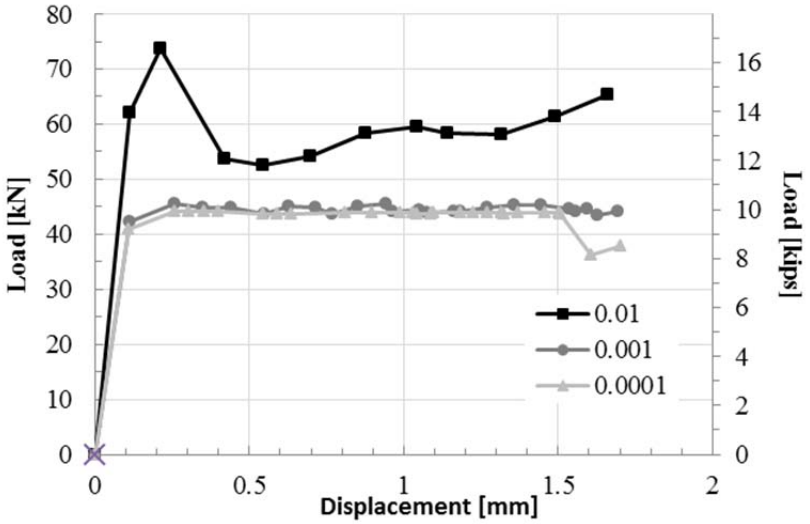

Figure 6.9 Relative iteration convergence tolerance

6.5.2 Comparison of different anchor models

The performance of type A and type B anchors (described in section 6.3.3) were compared by using both anchor types in the models of unbonded specimens F1-2a-24U and F1-4a-1-24U. Figure 6.10 (a) compares the load-displacement relationship predicted by the models of the two specimens using the two different anchor properties. Figure 6.10 (a) shows that the two different anchor properties resulted in a close peak load, but the

type A anchors caused the peak load to occur when the anchors reached peak capacity, while the type B anchors caused the peak load to occur after the anchor peak capacity had been surpassed. After the peak anchor capacities were reached both models predicted similar load capacities because the two anchor types had close residual capacities. The model with type A anchors better matched experimental results. In specimen F1-2a-24U the anchor splays failed around 44.5 kN [10.0 kips], which caused a loss in load and a shift of load to the bonded region, and the peak capacity exceeded the load at which the anchor splays debonded. Figure 6.10 (b) compares the effect of anchor properties on the load-displacement curve of the model of specimen F1-4a-1-24U. With both anchor properties the peak load occurred when the anchors reached peak capacity. The type A anchors underestimated the peak load by 18% and the type B anchors overestimated the peak load by 14%. It was decided to use Type A anchors since they gave better overall failure force prediction in the models of specimens F1-2a-24U and F1-4a-1-24U.

After defining the force-displacement relationship (Type A) of anchor elements the anchors were modeled with one, three, and four springs each. The models that used one, three and four springs per anchor predicted peak loads of 98%, 103% and 96% of the experimental load of specimen F1-2a-24. Although modeling the anchors with four springs resulted in the least accurate peak load, the anchors modeled with four springs best estimated the extent of debonding at the peak load, while the anchors modeled with one or two springs allowed the debonding front to pass the anchors earlier than in the experimental tests. Because peak load and the extent of debonding were the primary criteria for validating the model, the anchors were modeled using four springs. In reality it is believed the anchor splays most effectively restrain the region of FRP sheet closest to

the anchor shaft. Therefore it would likely be more accurate to have stiffer center springs compared to the two springs on the edges. However, for simplicity the properties of the anchor spring elements were kept identical.

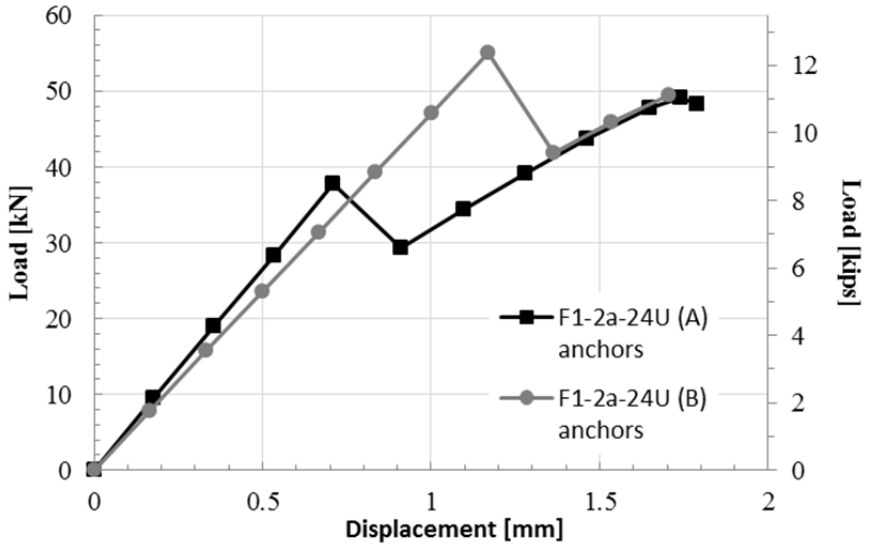

(a)

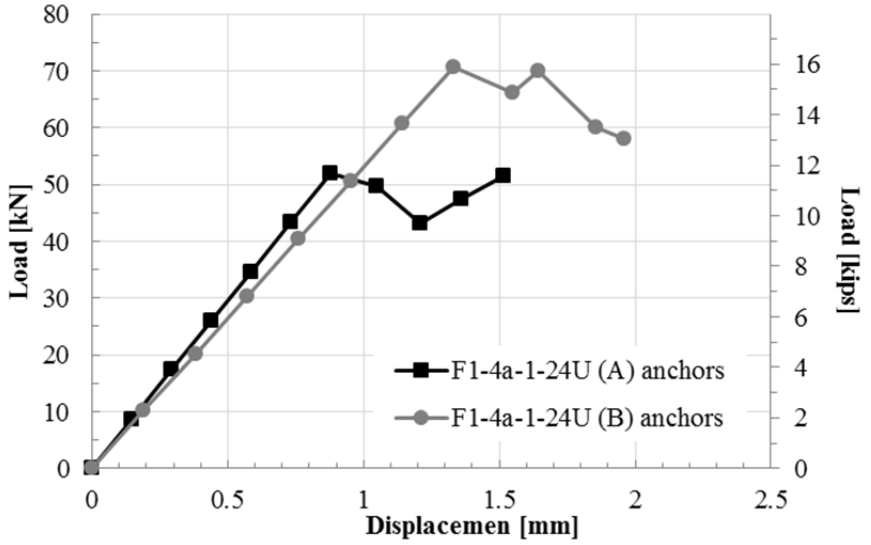

(b)

Figure 6.10 Load vs. Displacement for models of specimens F1-2a-24U (a) and F1-4a-1-24U (b) with anchor types A and B

6.5.3 Specimen F1-0a-24

Specimen F1-0a-24 consisted of unanchored singly ply Fyfe specimen, as shown in Figure 3.15. The peak load predicted by the model was 45.5 kN (10.2 kips), which is 91% of the failure load of specimen F1-0a-24 of 49.8 kN (11.2 kips). It is believed that a 9% discrepancy is small compared to the variation in experimental results. The model correctly captured the behavior of unanchored FRP sheets bonded to concrete. After the initiation of debonding the STZ propagated along the sheet and there was negligible change in load. The length of the STZ was approximately 100 mm [4 in.], as shown in Figure 6.14, which matches experimental results. The debonding front progressed to approximately 125 mm [5 in.] from the unloaded end, compared to an approximate length of 100 [4 in.] determined during the experiment. At this load step the FE model could no longer converge on a solution, indicating that sheet was close to the debonding failure load. This result is consistent with the length determined for the STZ.

6.5.4 Specimen F1-2a-24

Specimen F1-2a-24 was a singly ply Fyfe specimen with a single row of two anchors, as shown in Figure 3.16. Specimen F1-2a-24 failed by FRP rupture at a load of 80.6 kN [18.1 kips]. The peak load predicted by the model was 77.3 kN [17.4 kips], or 96% of the experimental failure load. The extent of debonding in the model at the peak load was very close to the extent of debonding in the experiment at failure. Experimentally measured longitudinal strains indicate that there was no debonding behind the anchors until approximately 4.5 kN [1.0 kips] prior to failure. Just prior to failure debonding had progressed approximately 50 mm [2 in.] behind the anchors in the center of the sheet and on the left edge. At the peak load of 77.3 kN [17.4 kips] the model

predicted that the debonding front was 25 mm [1 in.] behind the anchors in the center and on both sides.

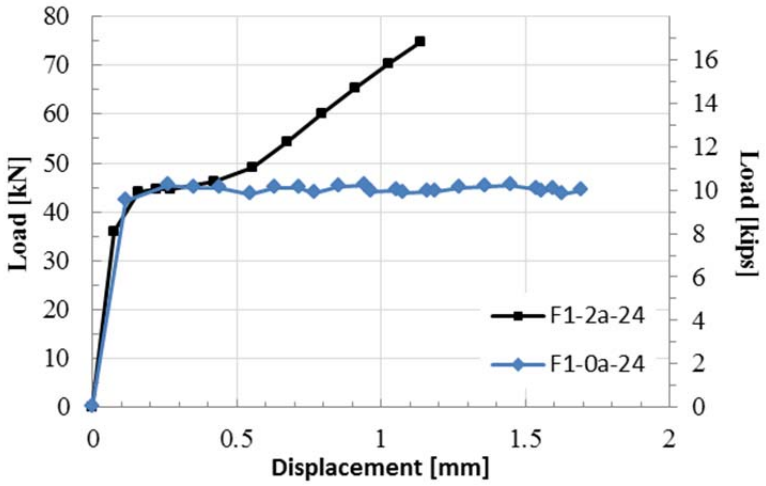

Figure 6.11 Comparison of the models of specimens F1-0a-24 and F1-2a-24

Figure 6.11 compares the force-displacement relationships calculated by FE models of specimens F1-0a-24 and F1-2a-24. It is clear that both specimens initially exhibit very similar behavior, prior to debonding, which agrees with experimental results as discussed in section 4.3.2.2. The reason for this result is believed to be caused by the anchor location, which lie outside of the STZ initially. Once the anchors are engaged as the debonding front travels toward the end of the FRP sheet the capacity of specimen F1-0-24 increased significantly relative to F1-0a-24. The load in specimen F1-0a-24 remains constant after debonding initiates.

6.5.5 Specimen F1-4a-1-24

Specimen F1-4a-1-24 was a singly ply Fyfe specimen with two rows of two anchors each, as shown in Figure 3.17. Specimen F1-4a-1-24 failed by FRP rupture at a load of 106.6 kN [24.0 kips]. Debonding progressed on the edges of the sheet to the

second row of anchors. The model predicted a peak load of 100 kN [22.5 kips], or 94% of the experimental failure load. At the peak load in the model, debonding had progressed 13 mm [0.5 in.] behind the first row of anchors in the center of the sheet and 25 mm [1 in.] behind the first row of anchors on both edges of the sheet. Figure 6.12 compares force-displacement curves calculated using the FE model for specimens F1-2a-24 and F1-4a-1-24. In the model of specimen F1-4a-1-24 the peak load occurred when the front row of anchors reached their peak capacity. In the next load step the front row of anchors failed and there was a corresponding increase in load in the back row of anchors. The load increased until the back row of anchors failed, after which the load remained constant as the sheet debonded, like the unanchored specimen. It is clear that the additional row of anchors in specimen F1-4a-1-24 increased the peak load and delayed debonding, which agrees with experimental results. The ultimate deformation capacity was also slightly higher in the model of specimen F1-4a-1-24 compared with the result of the model for F1-2a-24.

6.5.6 Specimen F1-2a-24U

Specimen F1-2a-24U was an unbonded singly ply Fyfe specimen with a single row of two anchors, as shown in Figure 3.20. The model predicted a peak load of 49.0 kN [11.0 kips], which corresponds to 79% of the failure load of 61.8 kN [13.9 kips] measured in the laboratory. In the model the anchors reached peak capacity at a load of 37.8 kN [8.5 kips]. At this load the bonded section resisted 31% of the load, compared to approximately 20% in the experiment. In the laboratory test of specimen F1-2a-24U it is believed that the right anchor splay delaminated at an approximate load of 33.5 kN [7.5 kips] and the left anchor splay at 44.5 kN [10.0 kips]. It is believed that the experimental

peak load was higher because the transverse sheet placed behind the sheet allowed the anchors to continue resisting significant load, while the model assumed a large loss in capacity after surpassing the peak anchor capacity (which is based on the experimental load at which the anchor splays delaminated). A further refinement of the FE model including FRP sheets placed transversely behind the anchors might improve the results, but this was not done in this research.

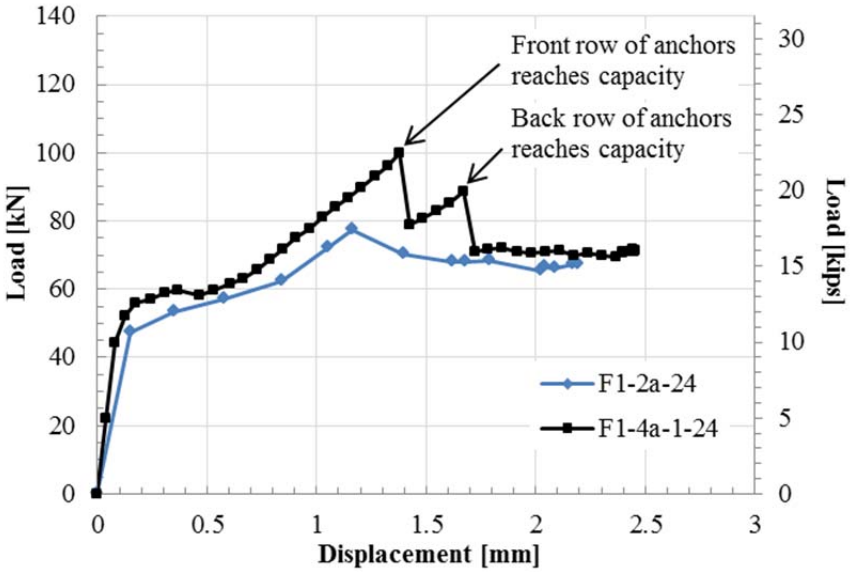

Figure 6.12 Comparison of model load-displacement relationships for specimens F1-2a-24 and F1-4a-1-24

6.5.7 Specimen F1-4a-1-24U

Specimen F1-4a-1-24U was an unbonded singly ply Fyfe specimen with two rows of two anchors, as shown in Figure 3.21. The model predicted a peak load of 51.0 kN [11.5 kips], which is 82% of the experimental failure load of 62.3 kN [14.0 kips]. At this load the bonded section resisted 18.8% of the load, compared to approximately 12% in specimen F1-4a-1-24U. The peak load determined through FE modeling occurred when the front row of anchors reached peak capacity. The applied load then dropped 4.20 kN

and then 6.83 kN [0.9 kips and 1.5 kips], when the capacities of the first and second rows of anchors were exceeded, respectively.

6.5.8 Strain Distribution

Strains were calculated by dividing the stresses in the sheet calculated by the models by the elastic modulus of the FRP sheet. Figure 6.13 shows the stress distribution of the model of specimen F1-0a-24. The propagation of the debonding front is clear from the stress distribution. The length of the STZ remains approximately constant as the sheet debonds, and there is negligible stress beyond the STZ. Stress varies across the width and length of the sheet in the unbonded region.

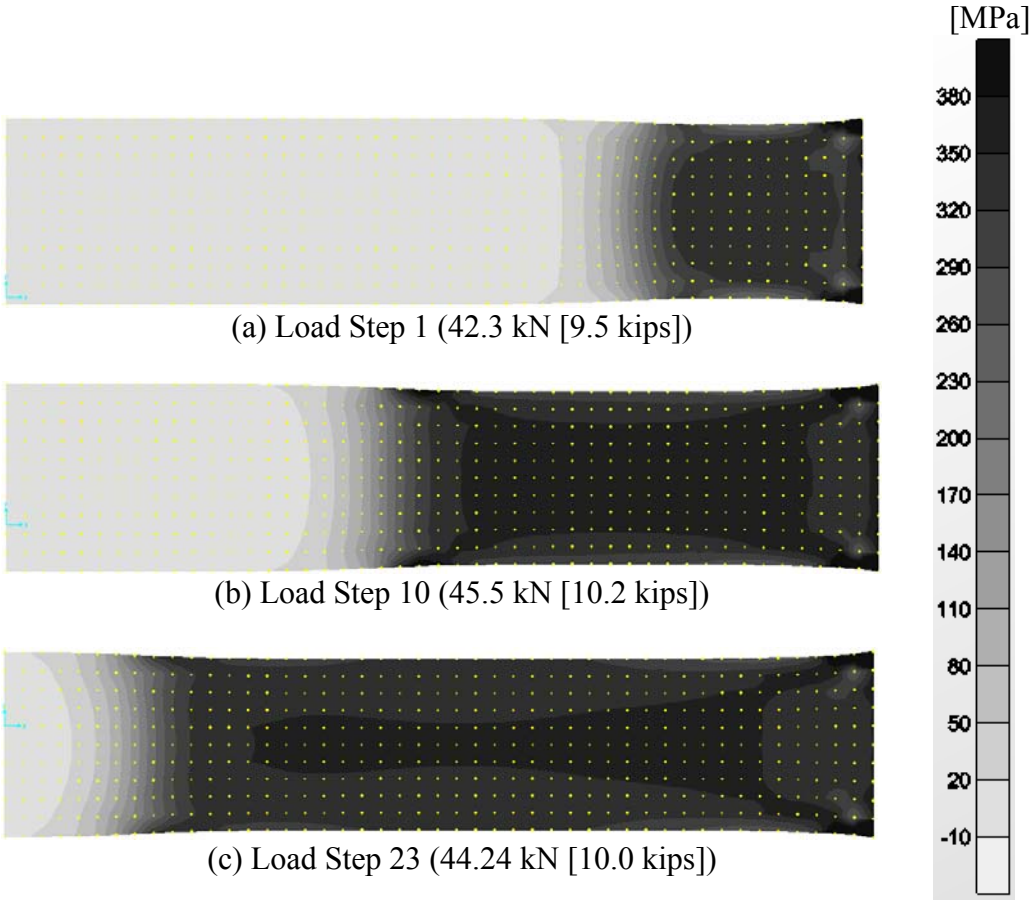

(a) Load Step 1 (42.3 kN [9.5 kips])

(b) Load Step 10 (45.5 kN [10.2 kips])

(c) Load Step 23 (44.24 kN [10.0 kips])

Figure 6.13 Stress distributions predicted by the model of specimen F1-0a-24

Figure 6.14 compares the longitudinal distribution of strain along the centerline of the sheet predicted by the model and measured experimentally in specimen F1-0a-24. The peak strain was higher in the model compared to the experimentally measured strain. The length of the STZ was approximately 100 mm [4 in.] for both. However, the overall shape of the strain longitudinal profile is reasonably accurate, considering the difficulty in capturing large strain variations within a short FRP sheet distance in the laboratory.

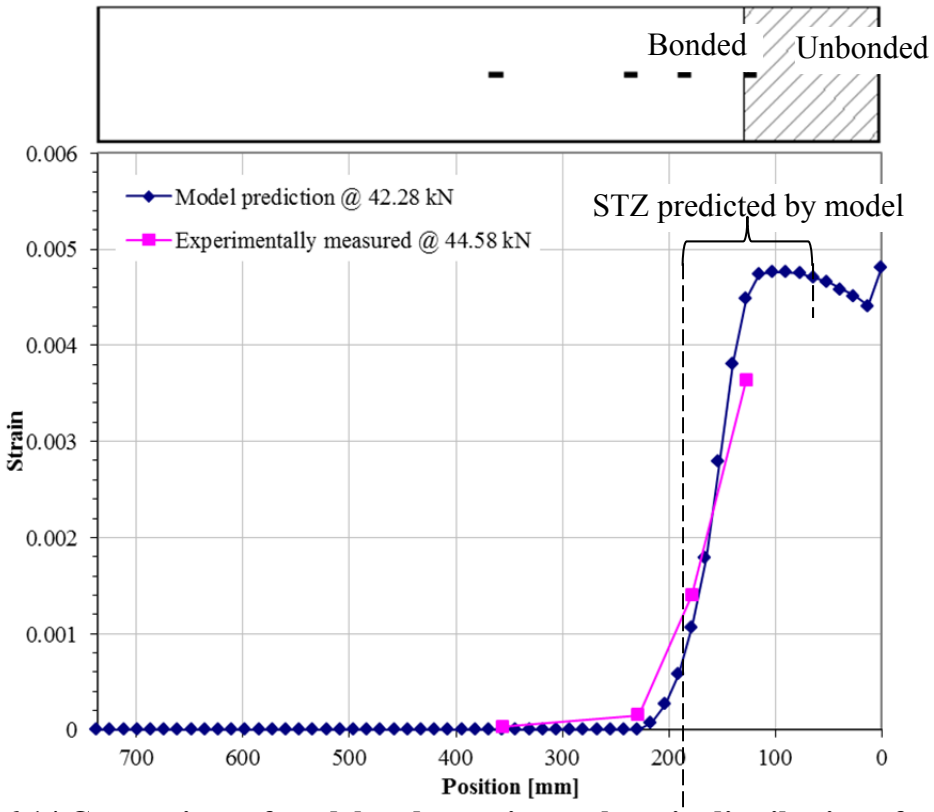

Figure 6.14 Comparison of model and experimental strain distribution of strain along the FRP sheet in specimen F1-0a-24

Figure 6.15 shows the stress distribution from the model of specimen F1-2a-24 at a number of key load steps in the progression of failure. The stress distribution is similar to the other anchored-bonded specimen F1-4a-1-24. **Figure 6.15** (a) shows the stress distribution prior to debonding. The stress distribution is similar to that of the unanchored specimen F1-0a-24 (shown in Figure 6.13 (a)) prior to debonding. This is because the

anchors lie initially outside the STZ, so they resisted negligible load prior to the initiation of debonding. After initiation of debonding the debonding front progressed to the anchors where it stopped until the peak load was reached. The stress distribution at the peak load is shown in **Figure 6.15** (b). As can be seen, there is a complex distribution of strain within the unbonded and bonded regions. There is also a visible flow of forces from the middle of the sheet toward each of the two anchor locations. After the peak capacity of the anchors are reached the debonding front progresses past the anchors towards the unloaded end, as shown in **Figure 6.15** (c) and (d).

Figure 6.16 and Figure 6.17 show a comparison of transverse distributions of strain in front and behind the anchors, respectively, determined using the FE model and during testing of specimen F1-2a-24 at approximately equal load. The debonding front had not reached the anchor locations in either the model or the test at these loads. The calculated transverse distributions of strain were similar in the other anchored-bonded model (specimen F1-4a-1-24). In front of the anchors the model predicts higher strain in line with the anchors than along the centerline of the sheet and the edges of the sheet. The experimental results also show higher strains in line with the anchors than along the centerline of the sheet, although the difference is more pronounced in the experimental results. It is believed that this is partially because the anchors were modeled using four springs which were given equal properties. In reality it is likely that anchor efficiency increases near the center of the anchor and that there are shear lag effects from the edge of the anchor splay to the center of the anchor. It is therefore likely that the two center anchor springs need to be stiffer than the outside two springs but there wasn't sufficient experimental data taken to support this type of modeling. In addition **Figure 6.15**(b)

shows that stresses vary significantly along the center of the sheet at sections located near the anchors, so the difference in strain from FRP sheet centerline to locations in line with anchors is very sensitive to the distance of each section to the anchor locations.

Behind the anchors there were higher strains along the centerline and edges of the sheet. The experimental results also show higher strains along the center of the sheet than in line with the anchors, although, unlike in front of the anchors, the model predicts a larger difference in strain than experimental results.

Figure 6.18 shows the strain distribution along the centerline of the FRP sheet from the FE model and from experimental strains from specimen F1-4a-1-24. The strain distribution 12.5 mm [0.5 in.] to the right or left of the centerline of the sheet is also given, to illustrate the change in strain distribution at different locations across the width of the sheet. This is an important observation when relying on a single line of strain gauges to determine the strain distribution of these systems, as most researchers have done in the past. The debonding front was in front of the anchors in both the model and in the experiment at the loads that are plotted. The strain distribution along the centerline of the other anchored-bonded model (specimen F1-4a-1-24) is similar. The models predict a sharp decrease in strain from a section in front to a section behind the anchors, which agrees with experimental data. All three plots show non-constant strain in front of the anchors, despite the sheet being debonded in front of the anchors. As can be seen there is a large difference between the strain profiles plotted along the centerline of the FRP sheet and profiles plotted 12.5 mm [0.5 in.] to the right and left of centerline. Along the centerline there is a sharp decrease in strain and then a sharp increase in strain

approaching the anchors. The decrease in strain in the model is caused by strain being drawn away from the center of the sheet towards the anchors, as seen in **Figure 6.15**(b).

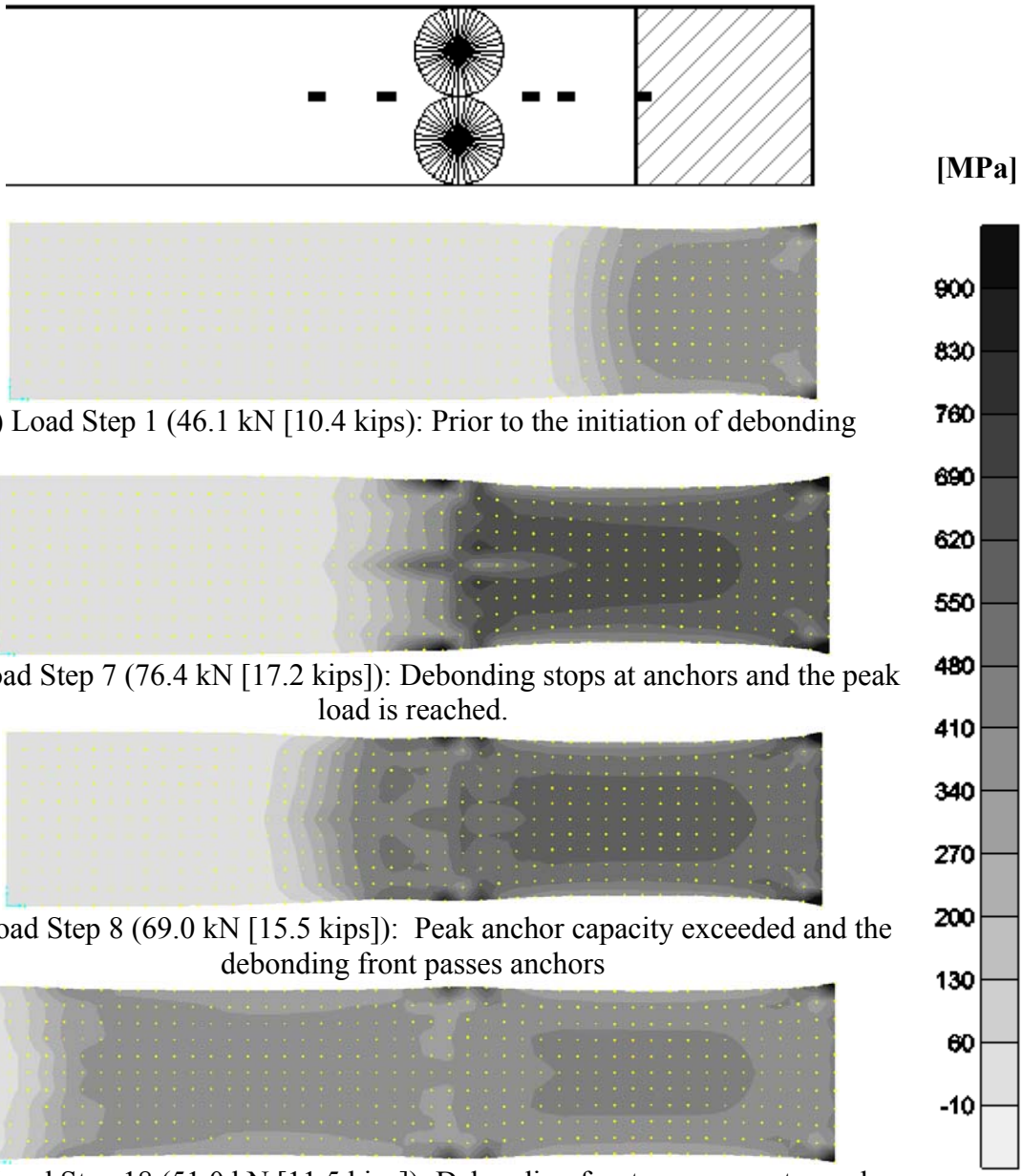

(a) Load Step 1 (46.1 kN [10.4 kips): Prior to the initiation of debonding

(b) Load Step 7 (76.4 kN [17.2 kips]): Debonding stops at anchors and the peak load is reached.

(c) Load Step 8 (69.0 kN [15.5 kips]): Peak anchor capacity exceeded and the debonding front passes anchors

(d) Load Step 18 (51.0 kN [11.5 kips]): Debonding front progresses towards unloaded end until the sheet fails by debonding.

Figure 6.15 Stress distribution predicted by the model of specimen F1-2a-24

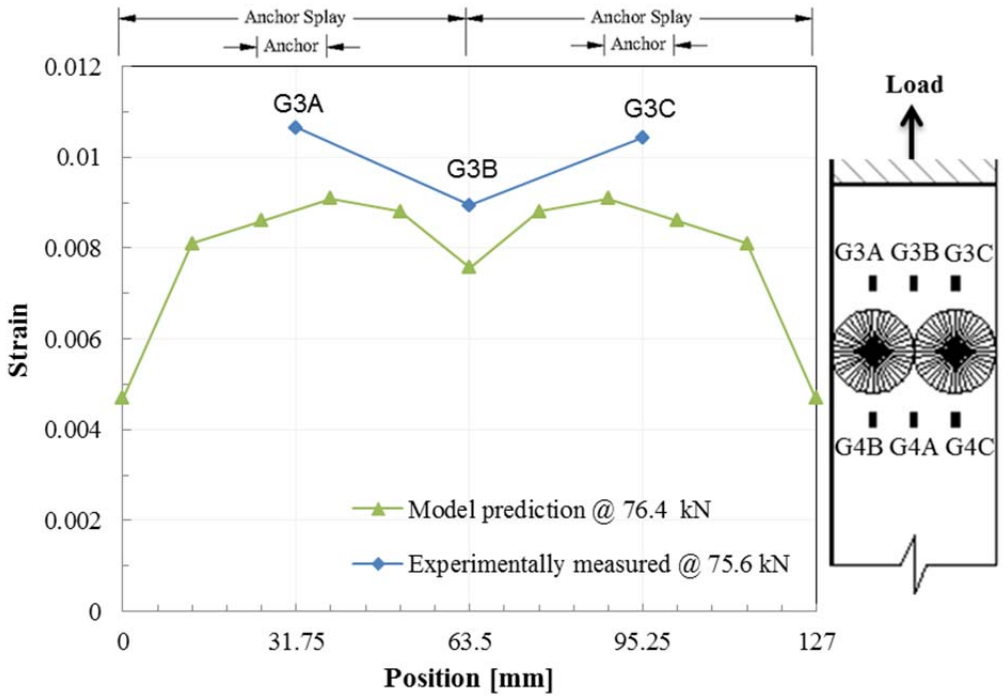

Figure 6.16 Experimentally measured and model prediction of transverse strain distribution in front of the anchors in specimen F1-2a-24

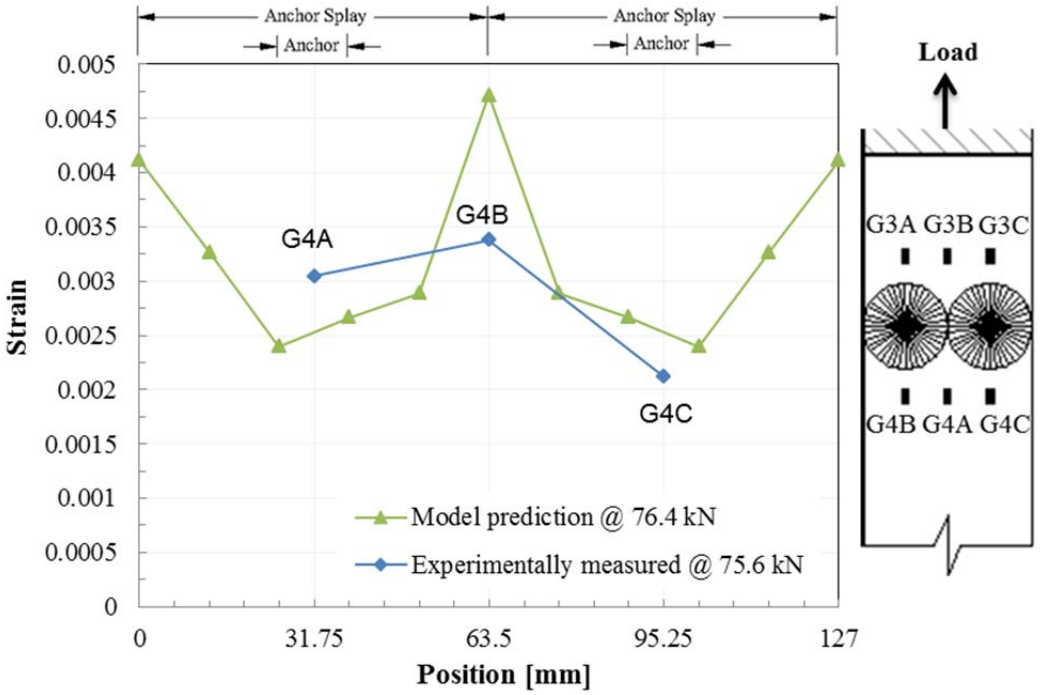

Figure 6.17 Experimentally measured and model prediction of transverse strain distribution behind the anchors in specimen F1-2a-24

The strain profile plotted at 12.5 mm [0.5 in.] off-center does not experience the decrease in strain at sections approaching the anchors. The experimentally measured strain peaked further from the anchors. It is believed that this is because in the model the anchor splays are modeled as a single line of springs, instead of a circle which extends 32 mm [1.25 in.] from the anchor center. Anchor stiffness calibration could correct this small discrepancy, but it is believed that more detailed experimental data are needed on unbonded specimens to allow this.

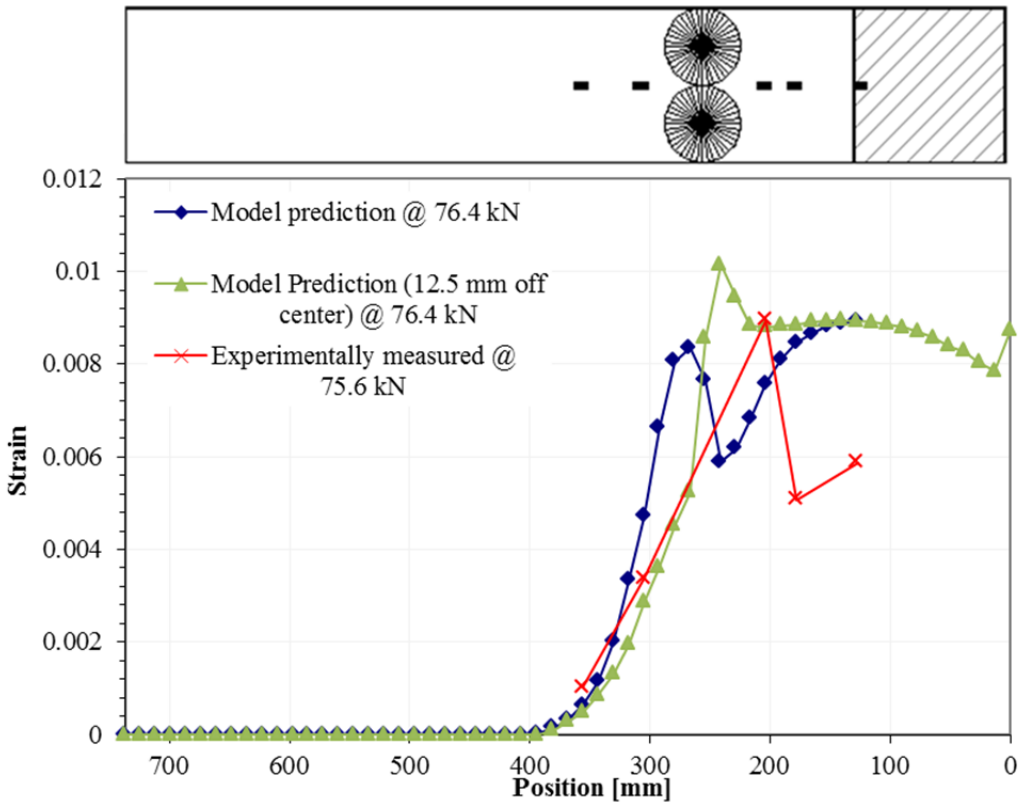

Figure 6.18 Experimentally measured and model prediction of longitudinal strain distribution in specimen F1-2a-24

Figure 6.19 shows the load-strain curve predicted by the model at the same location on the sheet as strain gauge G3B (along the centerline of the sheet, 50 mm [2 in.]

in front of the anchors) and the experimental load-strain curves of gauges G3A, G3B and G3C from specimen F1-4a-1-24. As with the experimentally measured strains, the model captures three distinct regions of behavior: (1) a nonlinear increase of strain prior to debonding, (2) a sudden increase in strain at the initiation of debonding, and (3) an approximately linear increase in strain until failure of the specimen. The model provides a reasonable prediction of measured strains given the large variations observed during testing. The strain behavior of anchored-bonded specimens is discussed further in section 4.3.2.2.

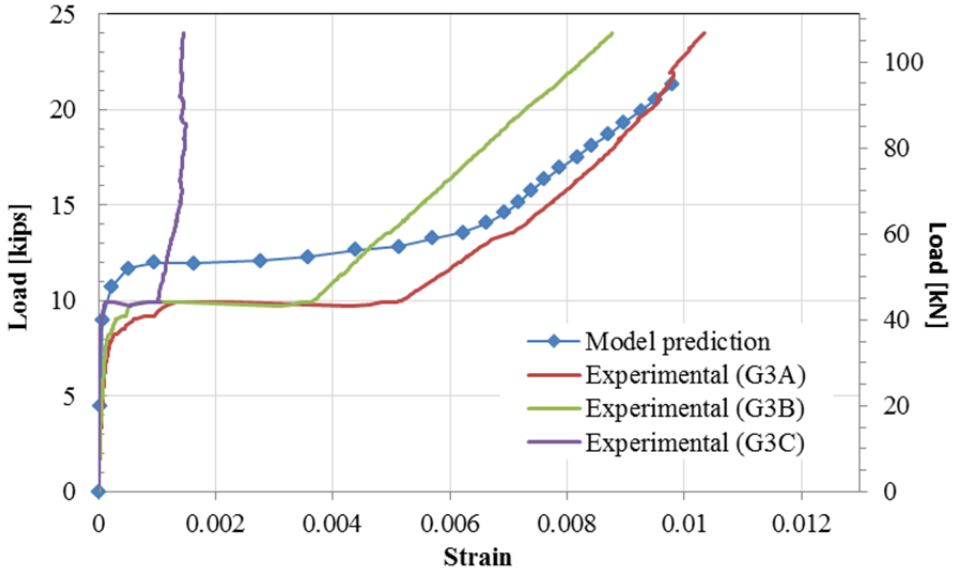

Figure 6.19 Load-strain plots for three gauges in front of the anchors (gauges G3A, G3B and G3C0 and the model prediction at the same location as G3B

6.5.9 Conclusion on the performance of the finite element models

The finite element models presented in this chapter predict, with different levels of accuracy, the failure load of the unanchored, anchored-bonded and anchored-unbonded specimens modeled from this research program. The model accurately predicted the propagation of the debonding front, in particular the load at which the debonding front passed the anchors in anchored specimens. The extent of debonding coupled with the

load at which the anchor capacity was exceeded, gives insight into the type of failure mode, whether the specimen will fail by debonding, FRP rupture or anchor splay delamination. The same interface and anchor properties were used in the different models of the unachored-bonded, anchored-bonded and anchored-unbonded specimens, which shows the versatility of the model.

A weakness of the model is that it was not able to accurately predict stress distributions in anchored specmimens. However, the model did agree approximately with experimental results as far as the overall shape of the transverse and longitudinal strain profiles, and the length of the STZ. It is believed that strain distribution results could be improved by improving modeling of anchors, particularly in the properties and placement of anchor springs, but more detailed experimenal measurements are needed to warrant this degree of refinement. The model captured the overall behavior of the anchored and unanchored specimens from initial loading to failure. Since anchored FRP sheets have a complicated transverse and longitudinal distribution of stresses it is believed that a 2D model in the plane of the sheet is prefered over a 2D model of the profile of the sheet.

An advantage of the model is its simplicity and basis in reality. It is very easy to manipulate parameters (such as sheet width and length of the FRP sheet, FRP sheet material properties, number of anchors and anchor location, anchor stiffness, etc.) and has a fast run time, which allows many designs to be analyzed quickly. The interface elements are based on a widely accepted bond-slip model (Lu et al., 2005), which is based on results from a finite element model that is calibrated to match experrimental results, and the anchor elements are based on experimental force-displacement measurements.

CHAPTER 7

SUMMARY AND CONCLUSIONS

7.1 Summary of the Research Program

The primary objective of this research program was to better understand the behavior of bonded FRP sheets that are secured with FRP anchors. Past research concluded that fastening FRP sheets with FRP anchors is an effective method for delaying or preventing debonding failures, which are the most common failure modes of FRP-strengthened reinforced concrete members. There is a clear lack of research pertaining to fastening FRP sheets with FRP anchors. ACI 440.2R-08 does not even mention the use of FRP anchors, which leaves engineers with little guidance if they choose to use FRP anchors in a design.

This research program consisted of a series of single shear tests on carbon fiber unidirectional sheets applied using the wet layup system. Single shear tests mimic the stress states found in FRP that fails due to intermediate crack induced debonding, which is the predominate debonding failure mode of members strengthened in flexure and shear using FRP. A total of sixteen specimens were tested including two single ply unanchored-bonded specimens, seven singly ply anchored-bonded specimens, five double ply specimens and two anchored-unbonded specimens.

Load was recorded using a load cell and strain distribution in the sheets was measured with transversely and longitudinally spaced strain gauges. Experimental results that were discussed included failure load and failure mode, load ratio ($\frac{P_{test}}{P_{ult}}$), longitudinal

and transverse strain distributions, load at the initiation of debonding and the extent of debonding.

The following design parameters were investigated: manufacturer, unanchored and anchored sheets, influence of number of anchor rows and spacing between rows, number of sheet plies (single or double), and length of bonded sheet behind the anchors. Several of the Sika and Fyfe specimens were specifically designed to be companion specimens to Mbrace specimens from Niemitz (2008) so that comparisons could be made between the three manufacturers.

7.2 Summary of Experimental Findings

It is clear from this research program that fastening FRP sheets with FRP anchors can delay or prevent debonding failures and significantly increase load capacity. The FRP material used to fabricate the anchors was almost negligible compared to the size of the FRP sheets, which is particularly important because high material costs are one of the primary drawbacks of using FRP systems. The increase in capacity of a sheet fastened with anchors compared with an identical unanchored specimen is related to the amount of load that the anchors resist. There are additional advantages to anchoring FRP sheets besides increasing load capacity. For instance the performances of anchored specimens are less affected by concrete strength than unanchored specimens. Also unanchored sheets give little warning prior to failure. After the initiation of debonding, the debonding front often quickly propagates along the sheet until the sheet completely debonds, with little change in force prior to failure. With anchored specimens the initiation of debonding often occurred at a load significantly below the peak load.

ACI 440.2R-08 limits the maximum design strain of FRP sheets because unanchored specimens often fail before the rupture strength of the FRP is reached. However, the anchored specimens reached significantly higher loads than the ACI 440.2R-08 recommended limits. Unfortunately all of the anchored specimens that failed by FRP rupture, failed prior to reaching the manufacturer published average load capacity. The specimens were not able to reach the full capacity of the FRP sheets because of non- uniform stress distributions in the sheet. Experimentally recorded strains and finite element modeling showed that there is a complex distribution of strain in anchored and unanchored sheets. For anchored specimens, in front of the anchors there tended to be higher strains in line with the anchors than along the centerline of the sheet. In addition, in anchored specimens sheet fibers must be worked around the anchor shaft, which compromises the strength of the fibers due to bending. Another weakness of the anchored specimens was that debonding initiated in anchored and unanchored specimens at approximately the same load in many cases. This is because prior to the initiation of debonding the anchors were either outside or near the end of the STZ, and therefor assumed little load. Therefore the anchors should be placed as close to the expected location of the initiation of debonding.

In general, the specimens fastened with four anchors failed at significantly higher loads than the identical specimens fastened with only two anchors. In addition specimens fastened with four anchors had significantly lower strains behind the anchors than similar specimens fastened with two anchors. Placing the two rows of anchors at a smaller distance apart than the STZ length allowed the two rows of anchors to be engaged simultaneously in FRP stress development. If the space between the anchors is large

compared to the length of the STZ, than the back row or rows of anchors may not assume appreciable load until after the debonding front has progressed passed the first row of anchors. Therefore, the back rows of anchors may not increase the load capacity of the sheet, but could still increase the ductility of the sheet

The identical Fyfe and Sika specimens, and the similar Mbrace specimens tested by Niemitz (2008), generally had close values of ($\frac{p_{test}}{p_{ult}}$), and had similar failure modes, which included combinations of FRP rupture, debonding, anchor splay delamination, and anchor splay rupture, as shown in Table 4 2. The Fyfe specimens performed slightly better than the Sika specimens in terms of peak load and prevention of debonding, which was attributed to the fact that the Fyfe anchors had a significantly greater mass of fibers. An important observation is that the peak loads of different anchorage designs (such as number of anchor rows and spacing between rows) relative to the respective single ply unanchored specimens increased closely for the three different manufacturers (Sika, Fyfe and Mbrace).

For unanchored specimens, a longer length of sheet behind the anchors can increase ductility and peak load. In several of the anchored specimens, including all four of the anchored double ply specimens (F2-2a-24, F2-4a-1-24, S2-2a-24, S2-4a-1-24), the load continued to increase after the initiation of debonding behind the anchors.

Single and double ply unanchored specimens exhibited similar behavior. The advantages of anchoring FRP sheets, in terms of increase in load capacity, was even more apparent with the double ply specimens, since unanchored double ply specimens tend to fail by debonding at lower load ratios ($\frac{P_{test}}{P_{ult}}$) compared to unanchored single ply

specimens. Double ply specimens always failed at a lower load ratio ($\frac{P_{test}}{P_{ult}}$) than the identical single ply specimens. The failure modes of all four of the anchored double ply specimens included debonding and anchor splay delamination. This indicates that the capacity of the anchors was being reached as more load demand was being placed on them. In contrast, in most anchored single ply specimens FRP rupture was either the primary or a secondary failure mode.

7.3 Summary of Finite Element Modeling

Finite element models were developed of anchored and unanchored FRP sheets bonded to concrete using SAP2000. Since anchored FRP sheets have a complicated transverse and longitudinal distribution of stresses it is believed that a 2D model in the plane of the sheet is prefered over a 2D model of the profile of the sheet.The models were two dimensional (2D) models in the plane of the FRP sheet. The interface was modeled with separate interface elements that were defined by a force-displacement relationship, based on a bond-slip model presented by Lu et al. (2005). The sheets were modeled using shell elements with orthotropic properties and the anchors were modeled using springs elements given a force-displacement relationship based on experimental measurements.

The finite element models were validated by comparing to experimental results from this research program, including load capacity, extent of debonding, and strain distribution. The model captured the general observed experimental behavior of the bonded-unanchored, bonded-anchored and unbonded-anchored specimens. The model accurately predicted the propagation of the debonding front, in particular the load at which the debonding front passed the anchors in anchored specimens.

APPENDIX A - MEASURED STRAINS

Specimen S1-0a-24

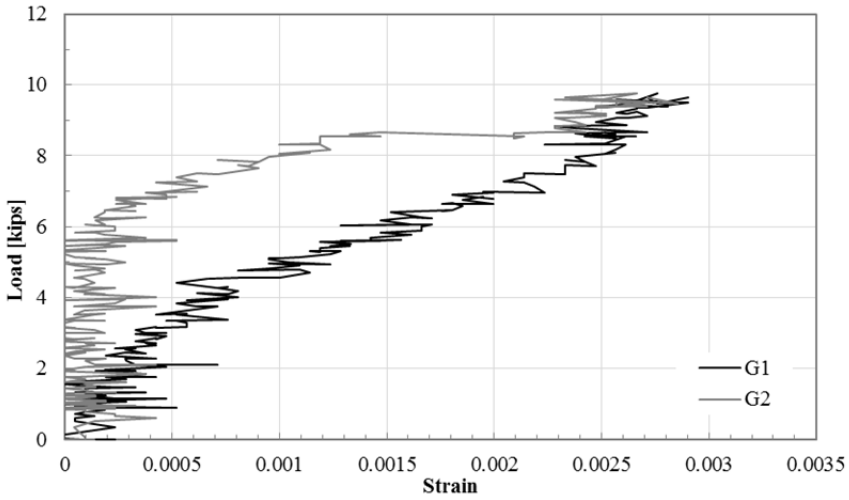

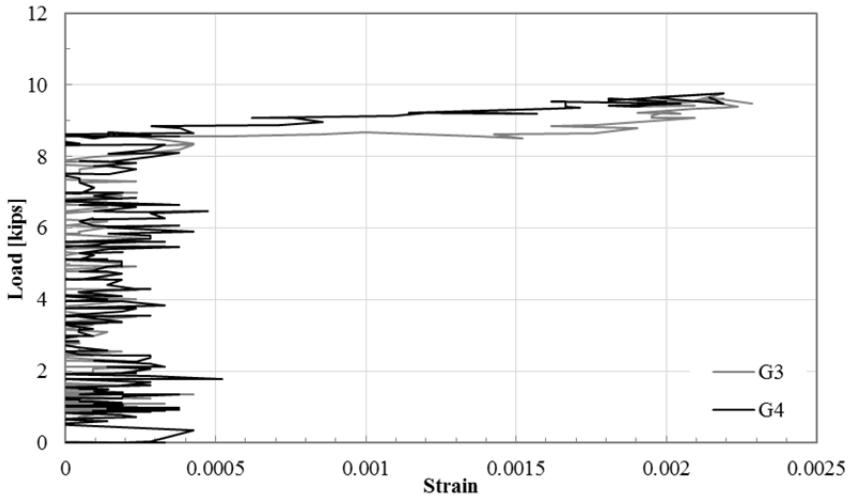

Specimen F1-0a-24

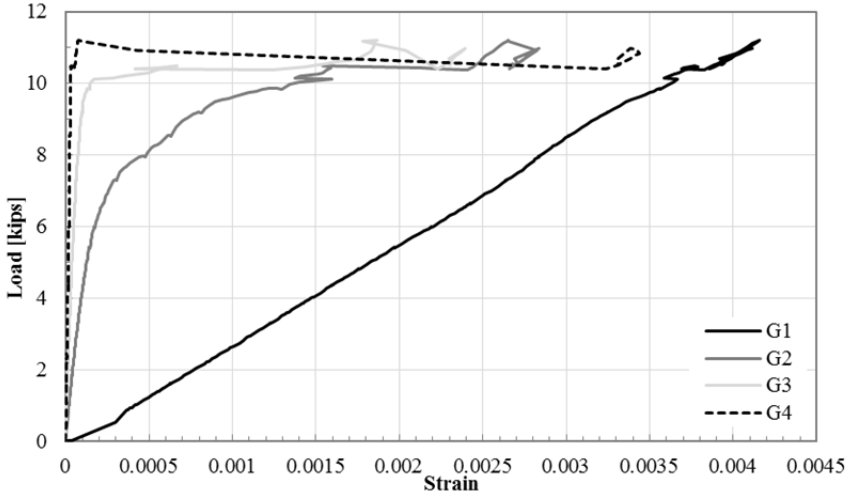

Specimen S1-2a-24

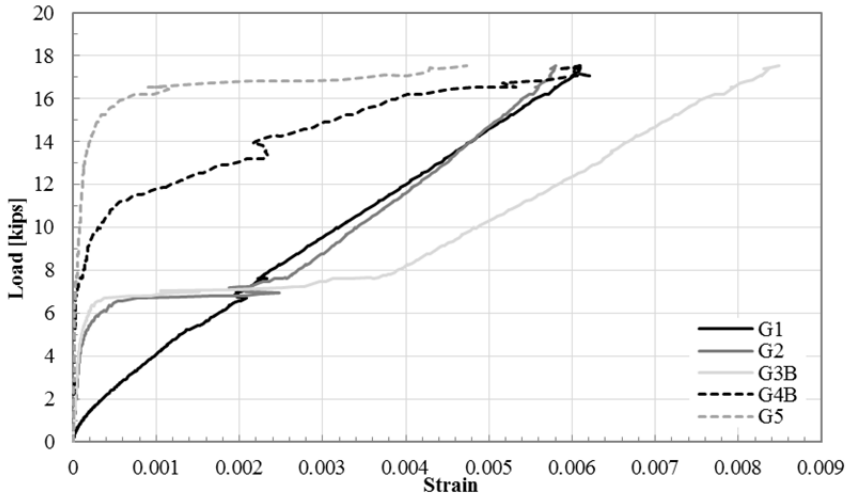

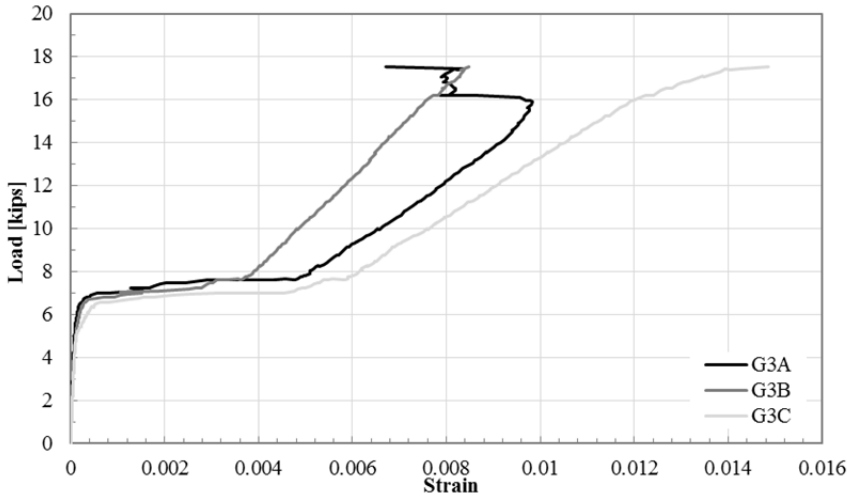

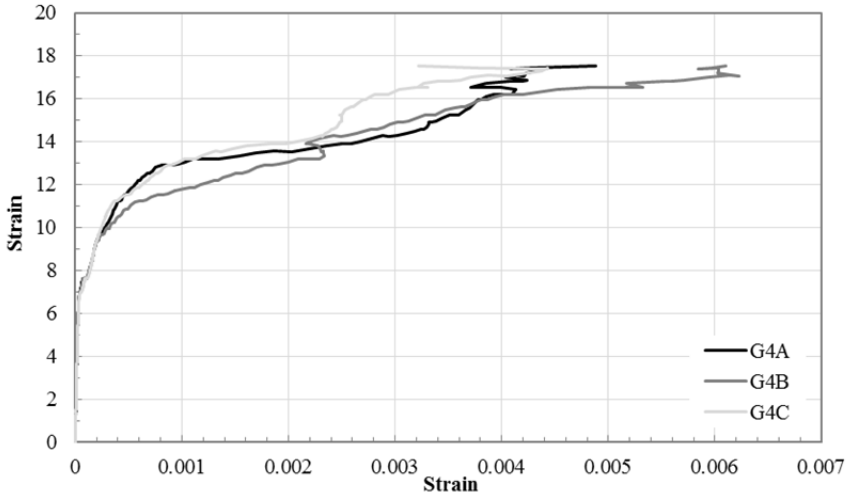

Specimen S1-4a-1-24

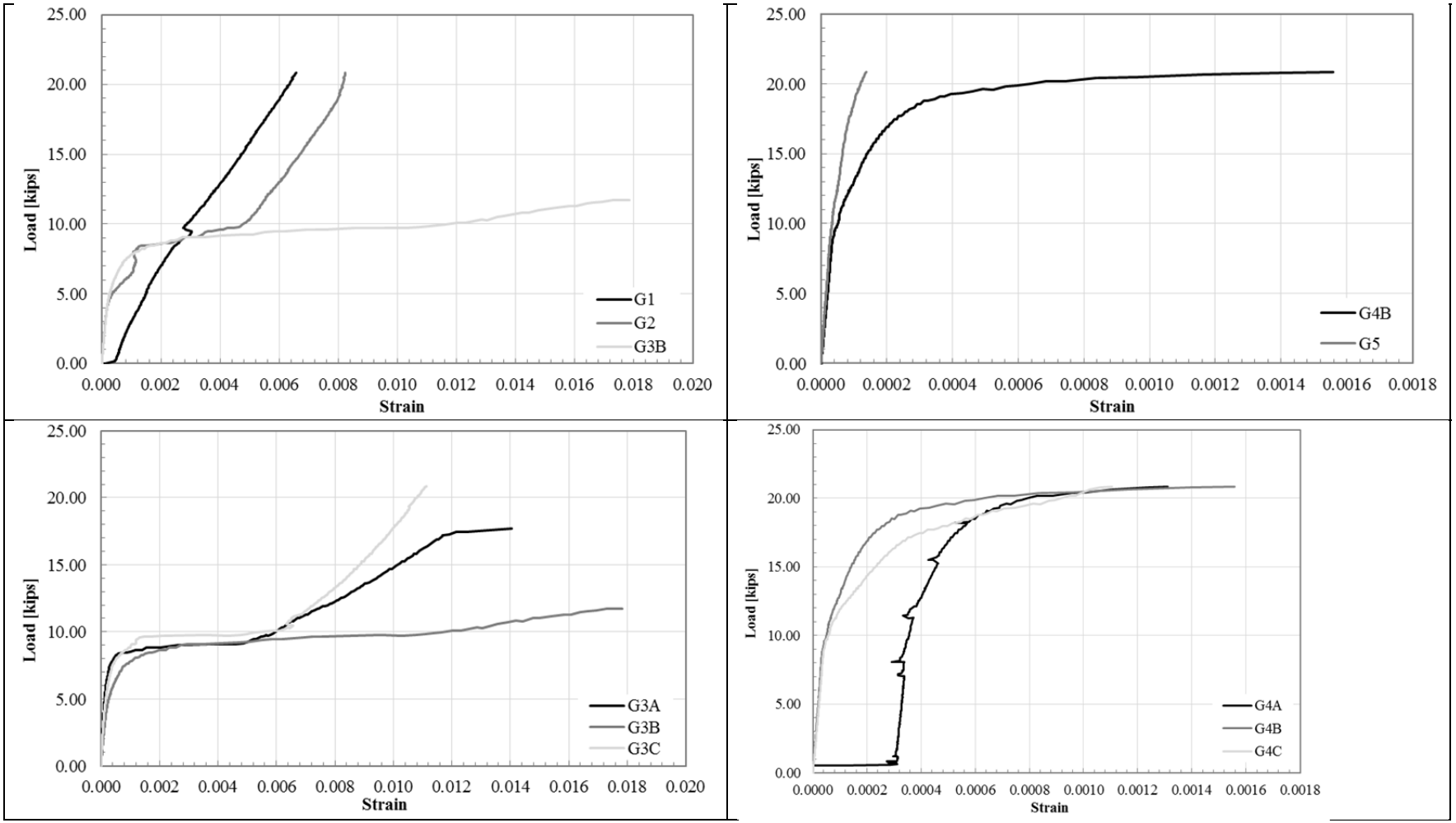

Specimen S1-4a-1-12.5

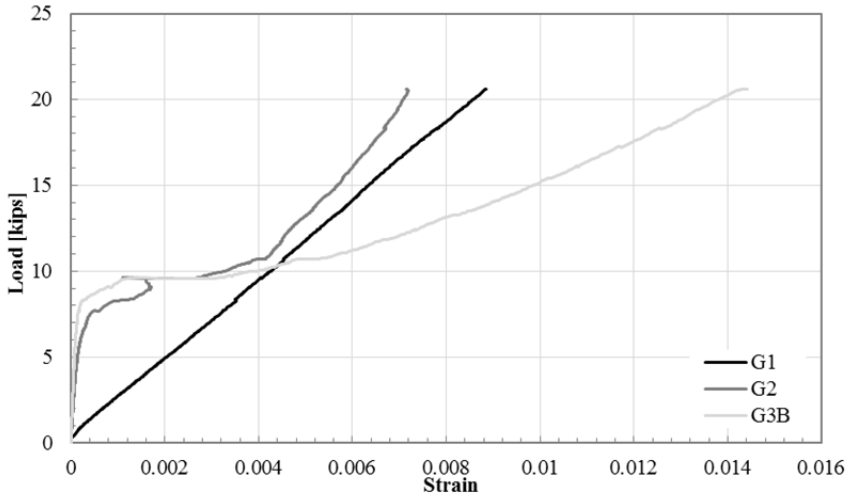

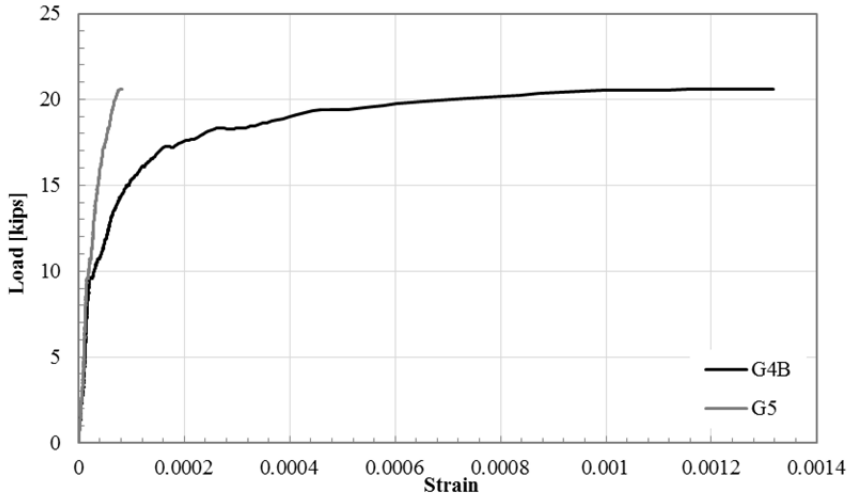

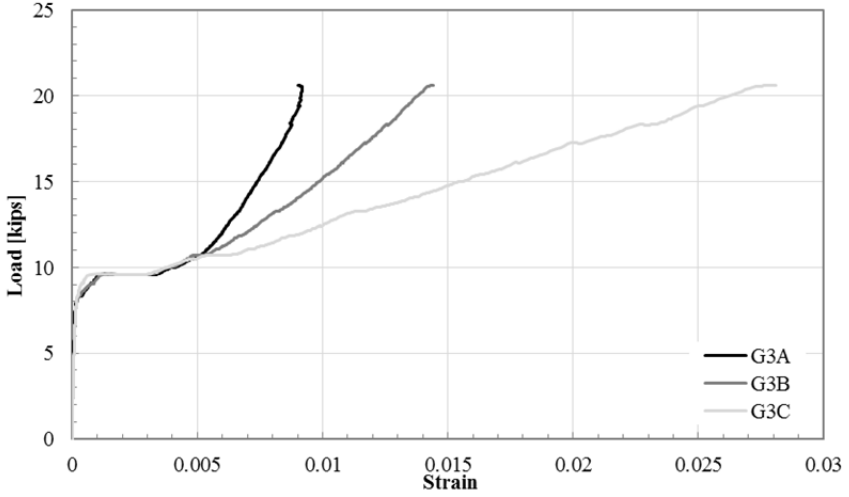

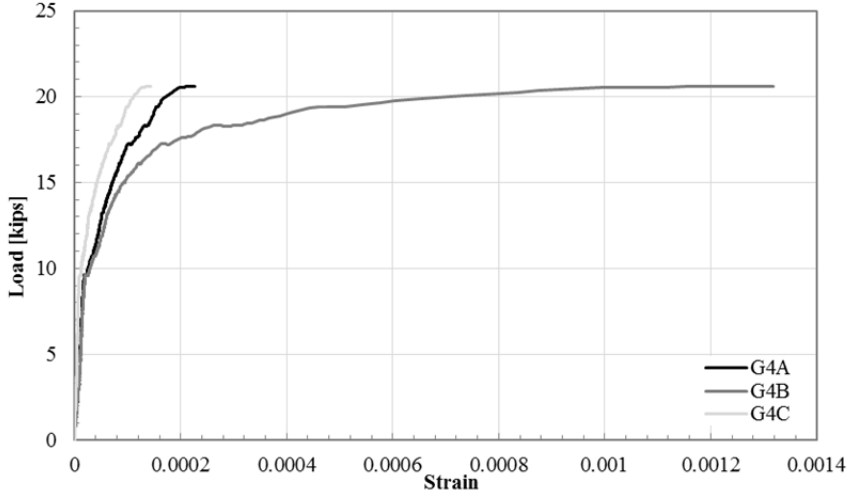

Specimen S1-4a-2-24

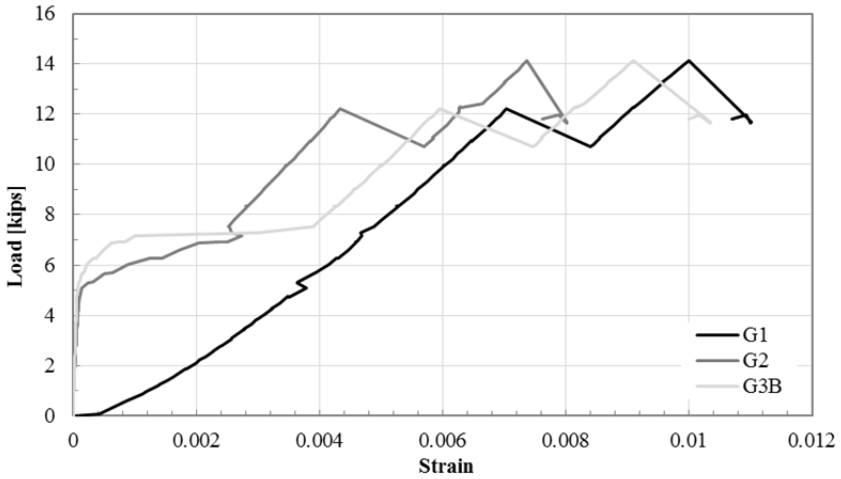

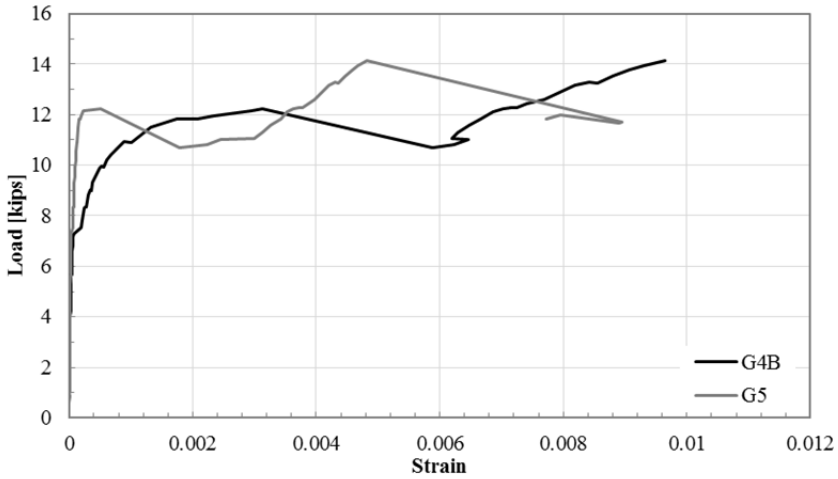

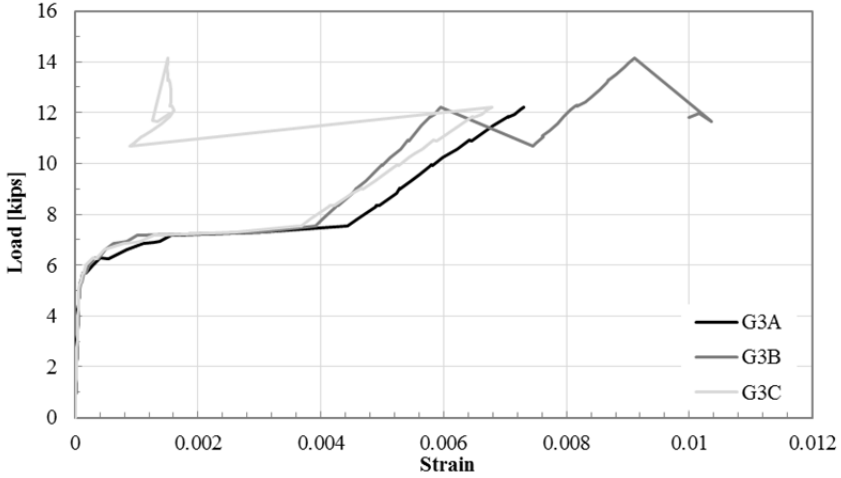

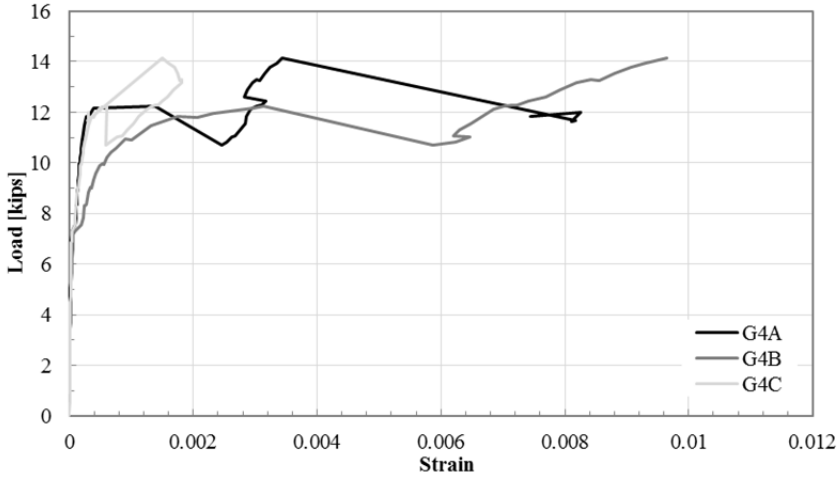

Specimen F1-2a-24

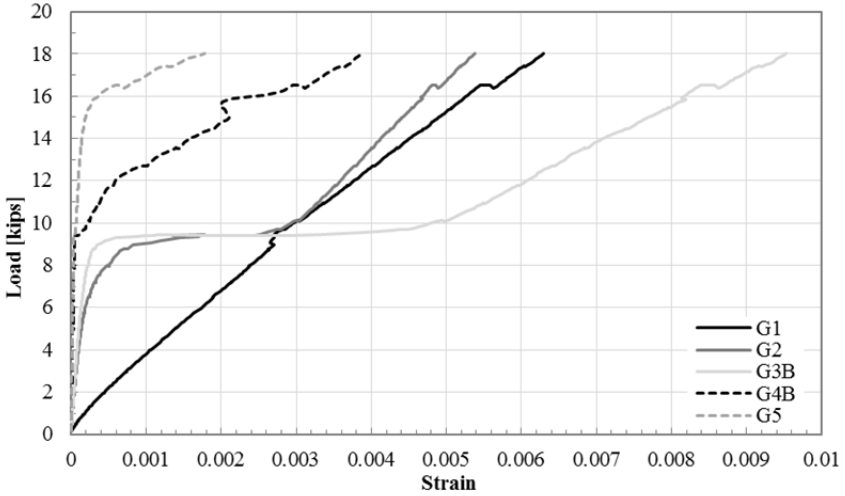

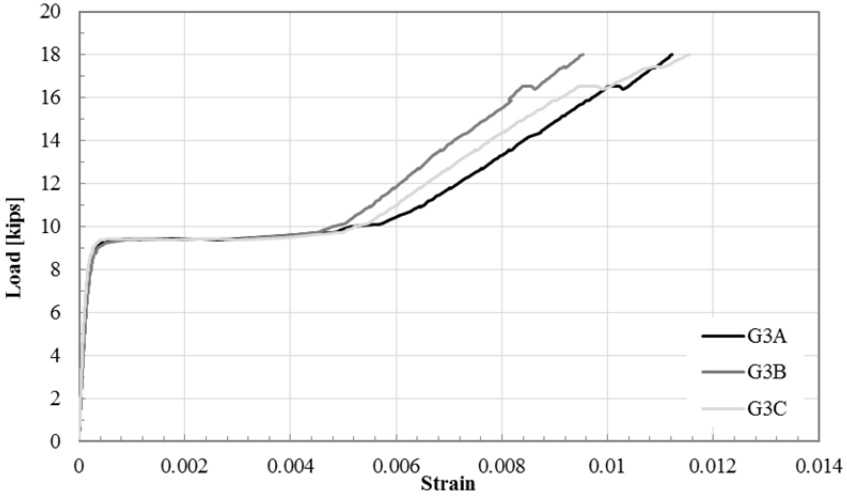

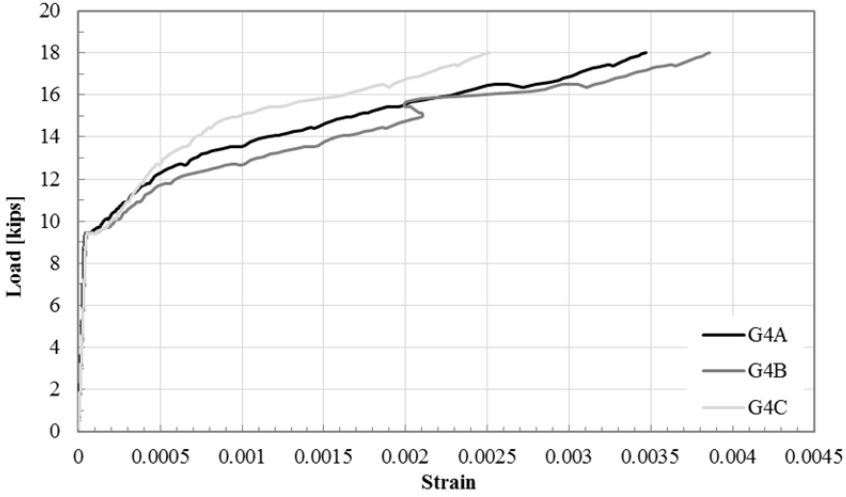

Specimen F1-4a-1-24

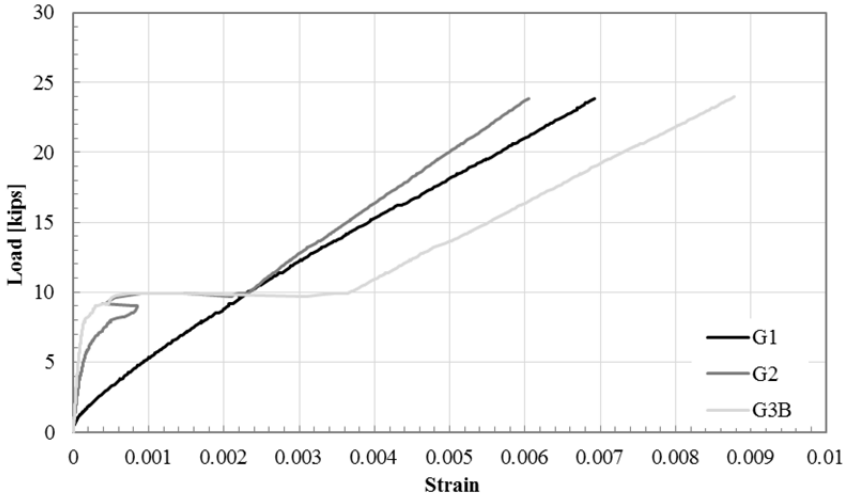

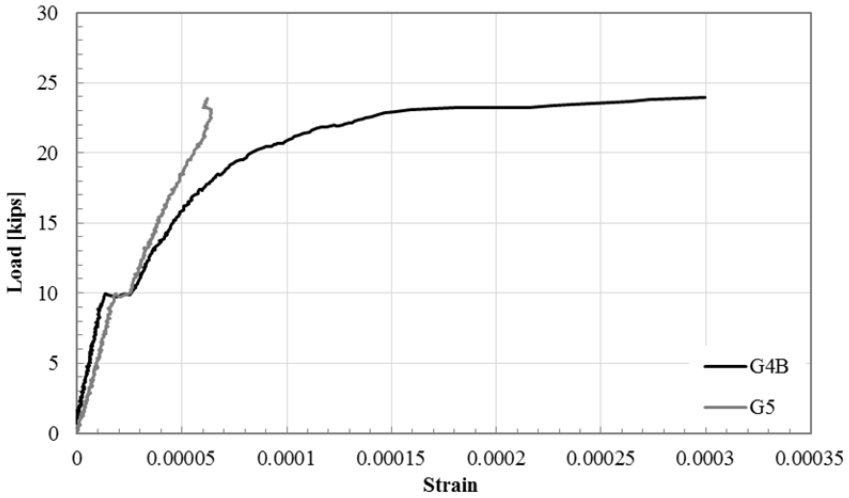

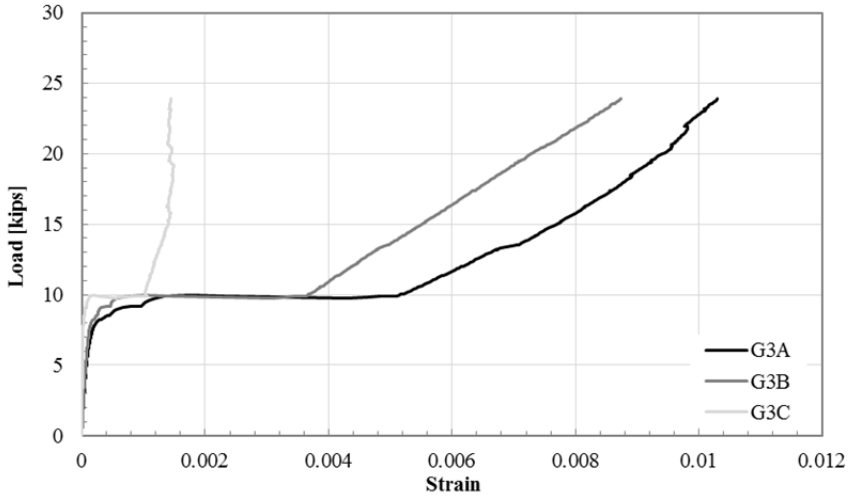

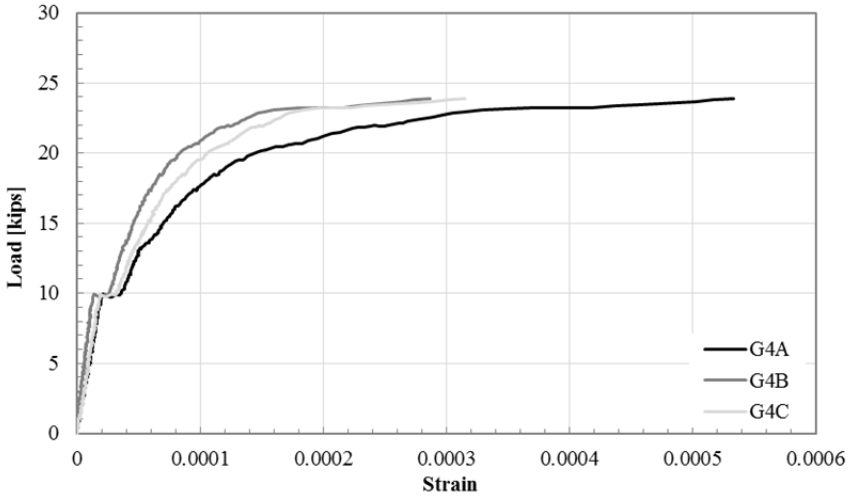

Specimen F1-4a-2-24

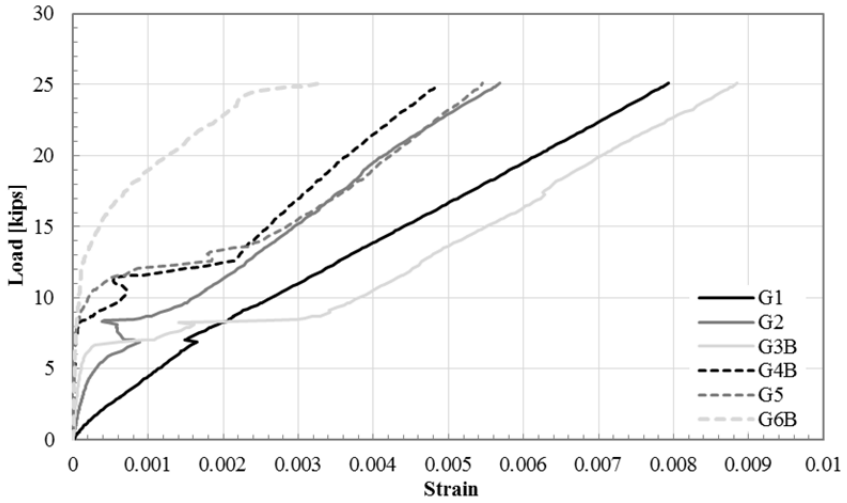

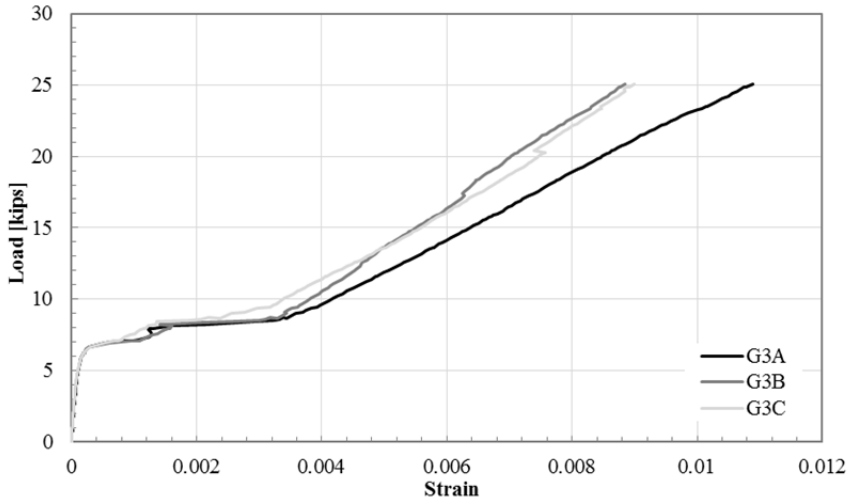

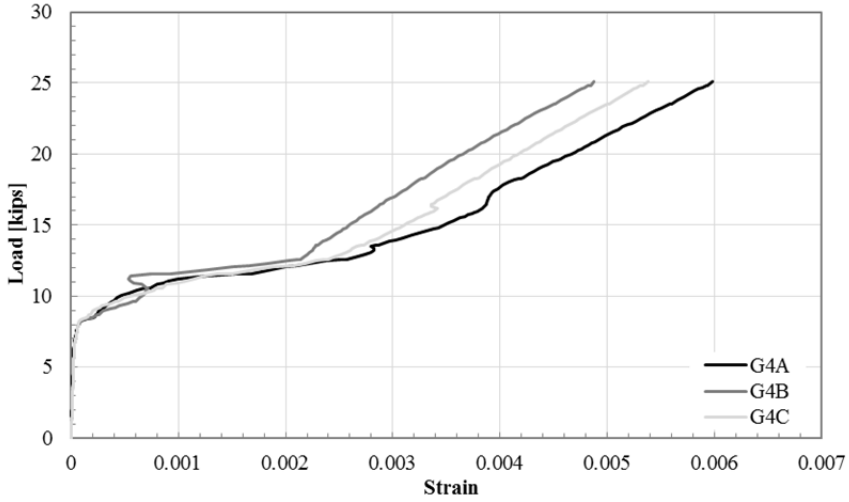

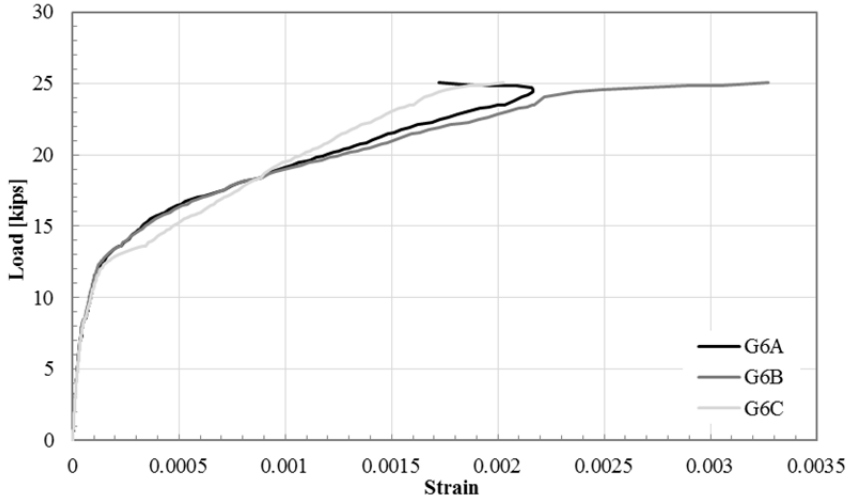

Specimen F2-0a-24

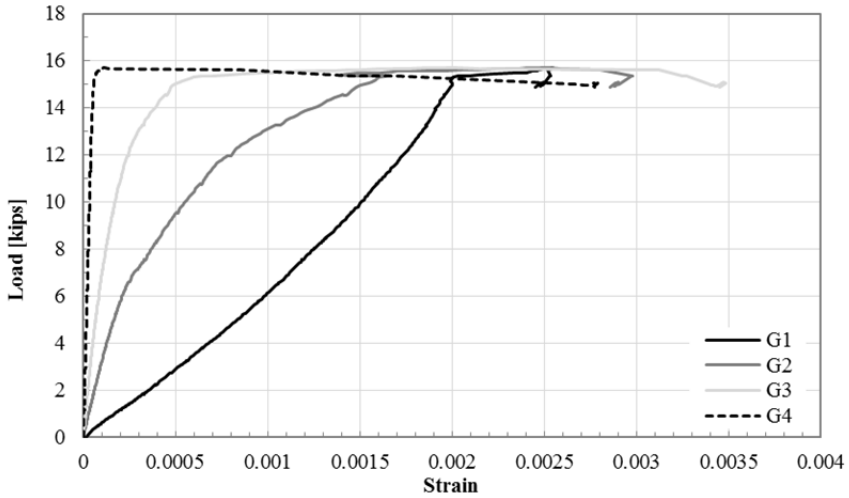

Specimen F2-2a-24

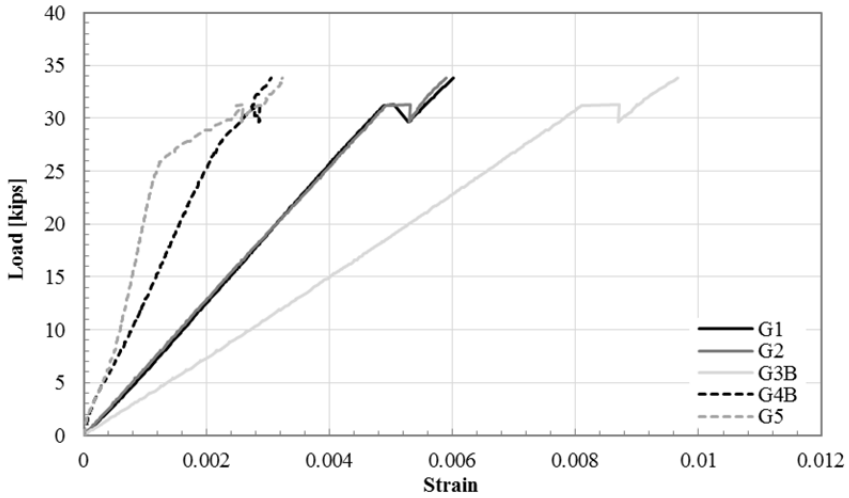

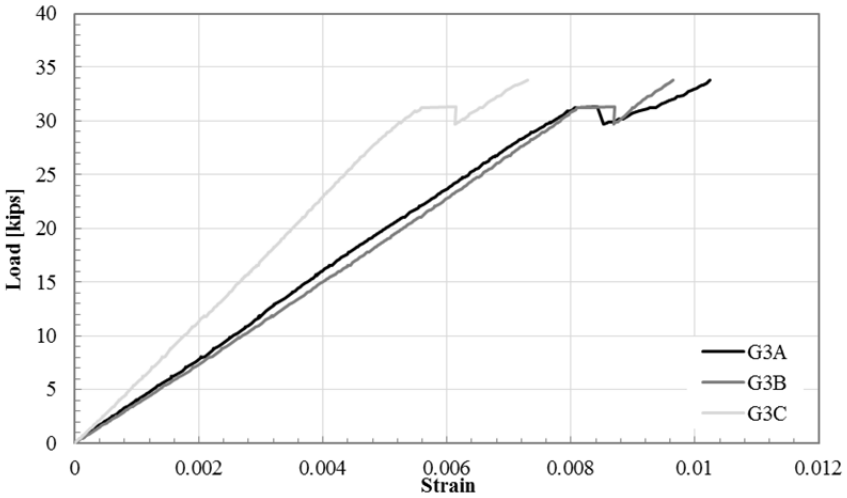

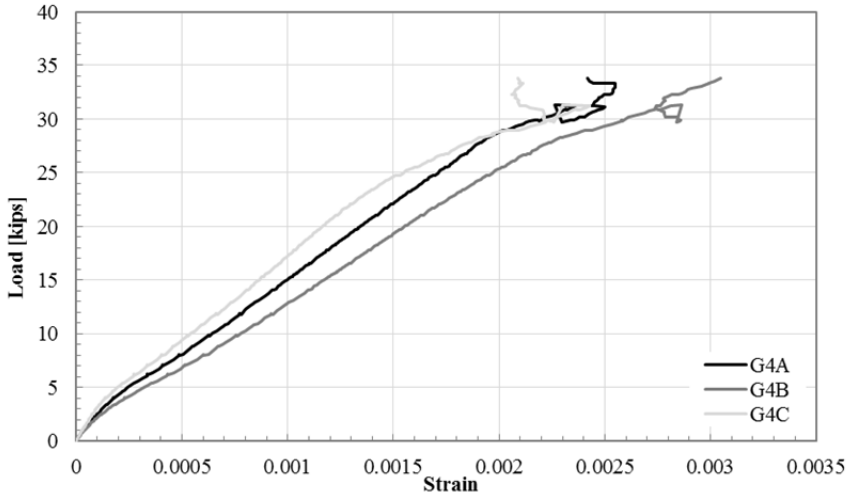

Specimen F2-4a-1-24

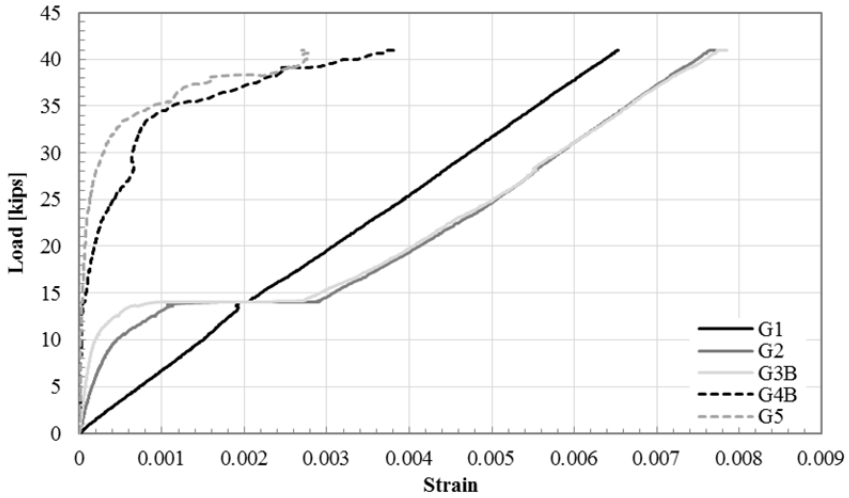

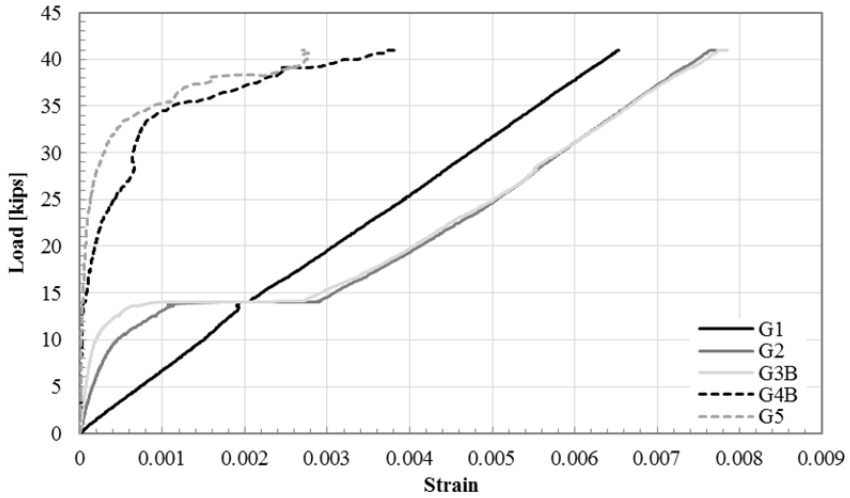

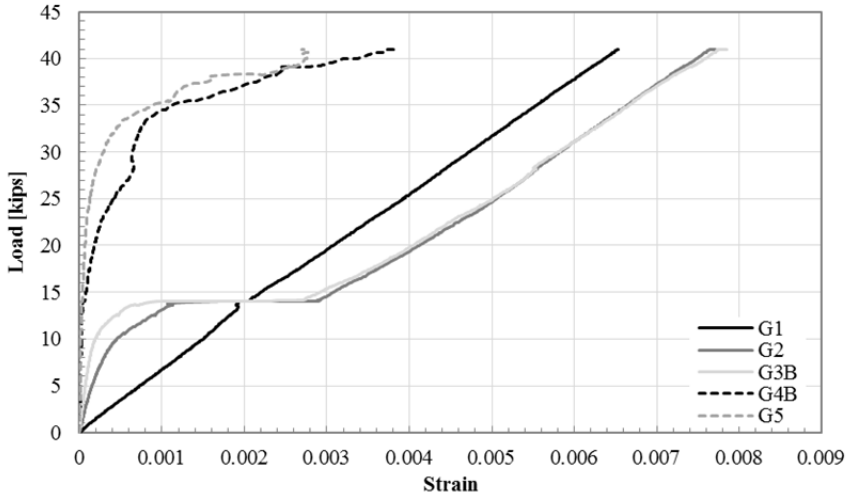

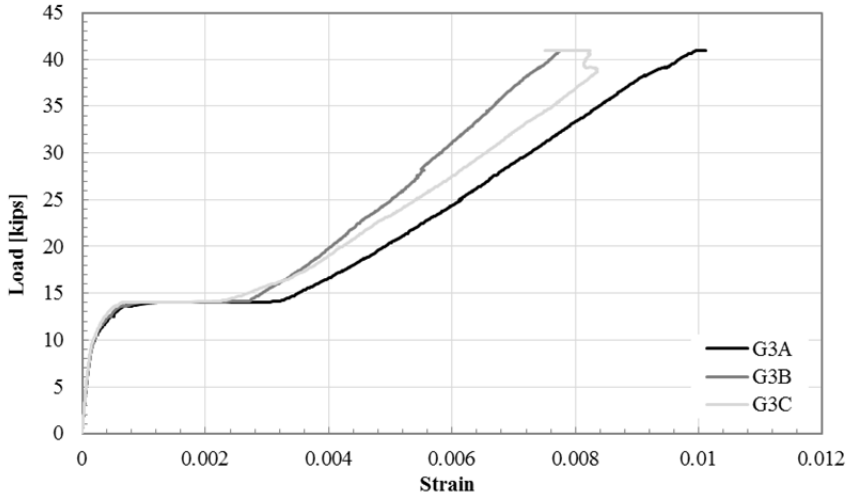

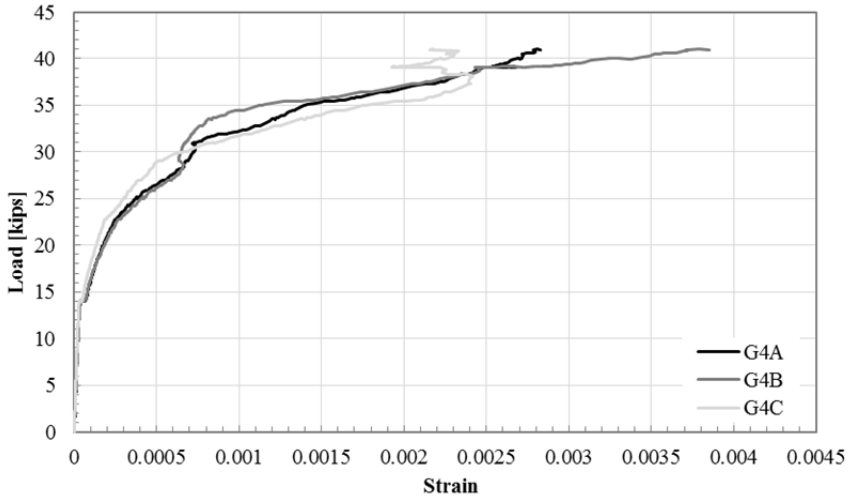
45
40
35
30
25
20
15
10
5
0
Load [kips]
0
0.0005
0.001
0.0015
0.002
0.0025
0.003
0.0035
0.004
0.0045
Strain
G4A
G4B
G4C

Specimen S2-2a-24

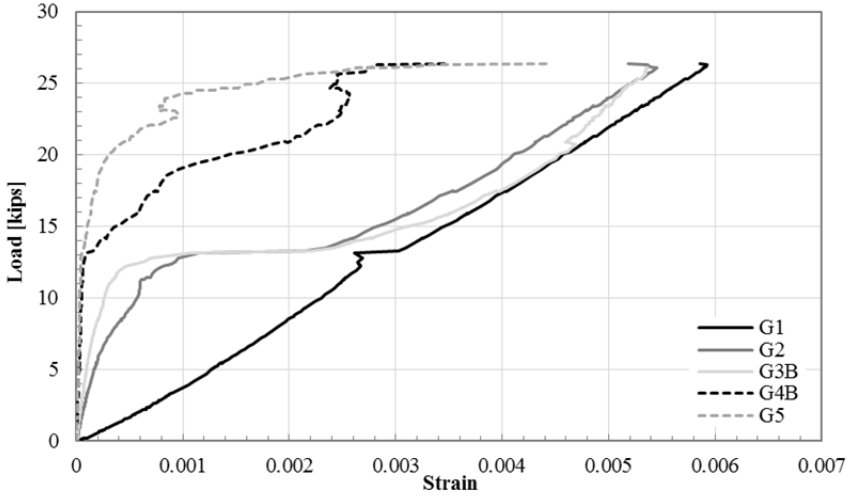

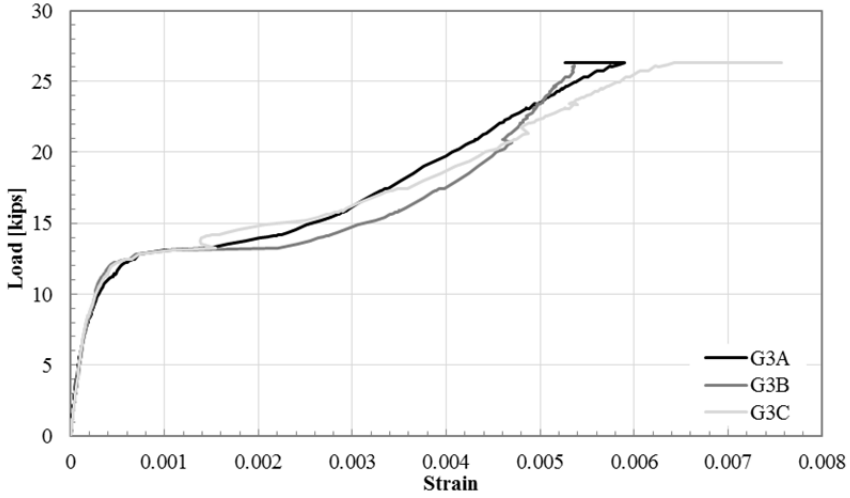

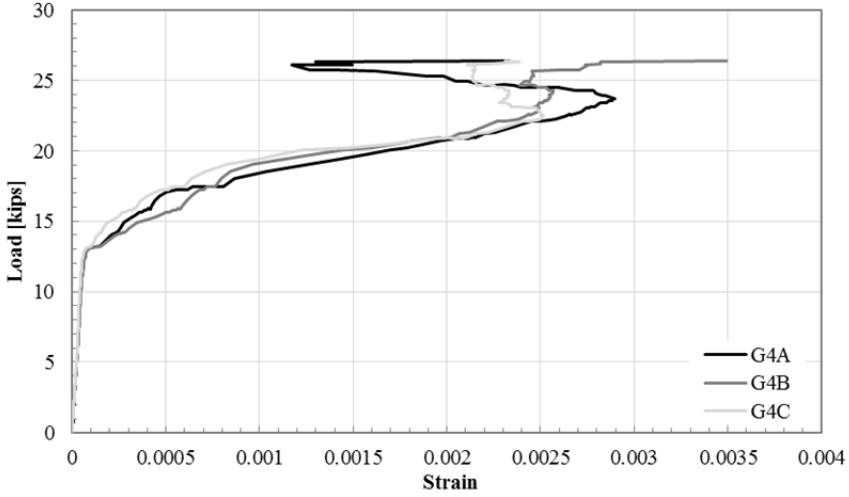

Specimen S2-4a-1-24

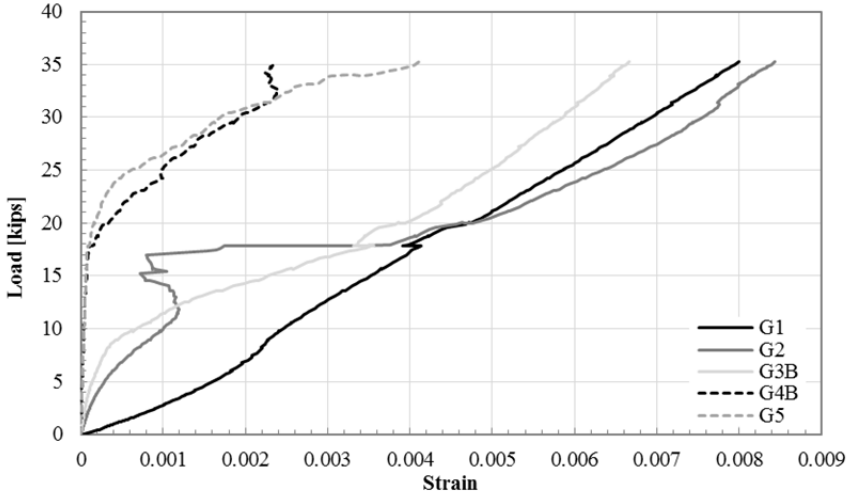

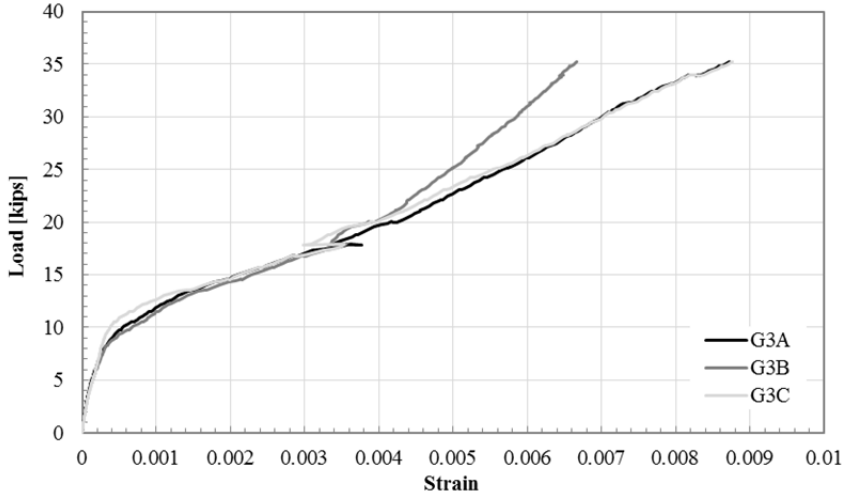

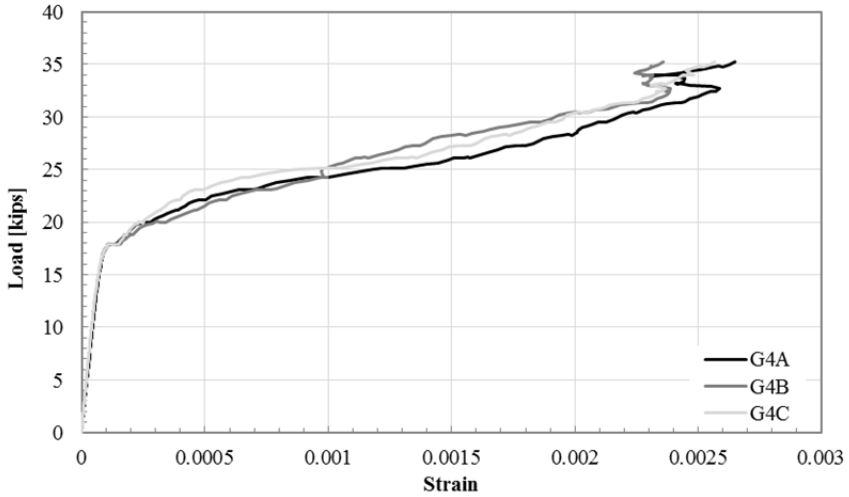

Specimen F1-2a-24U

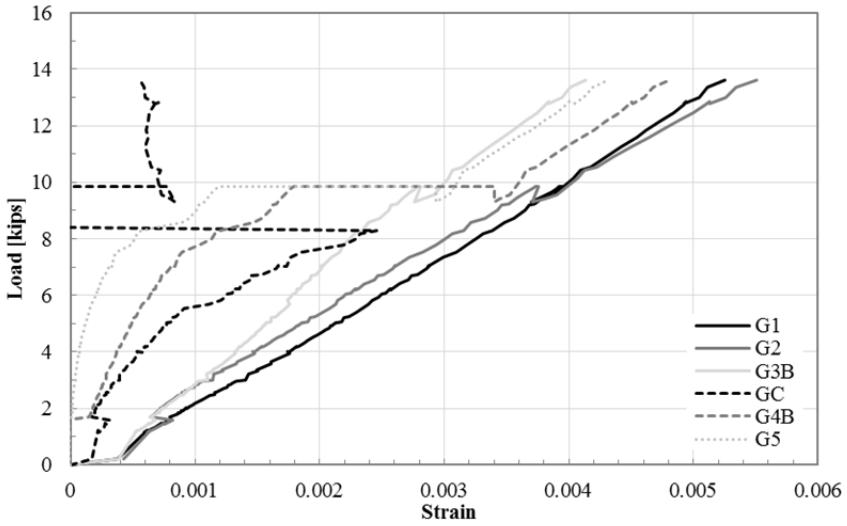

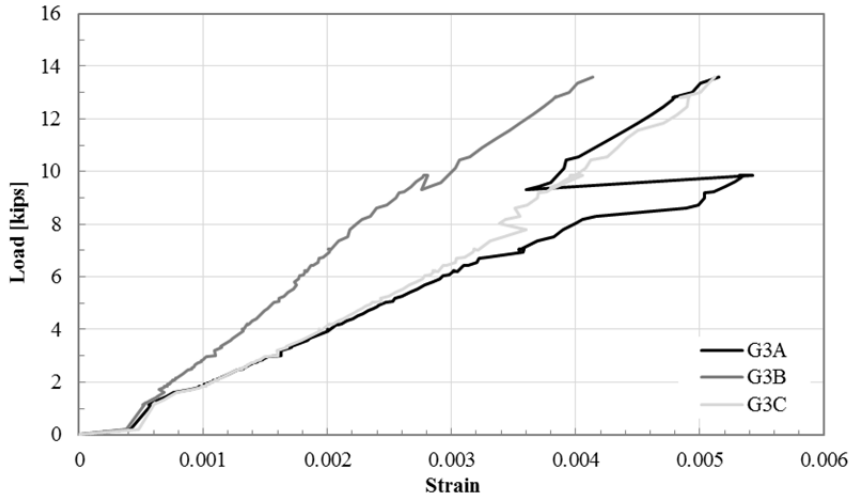

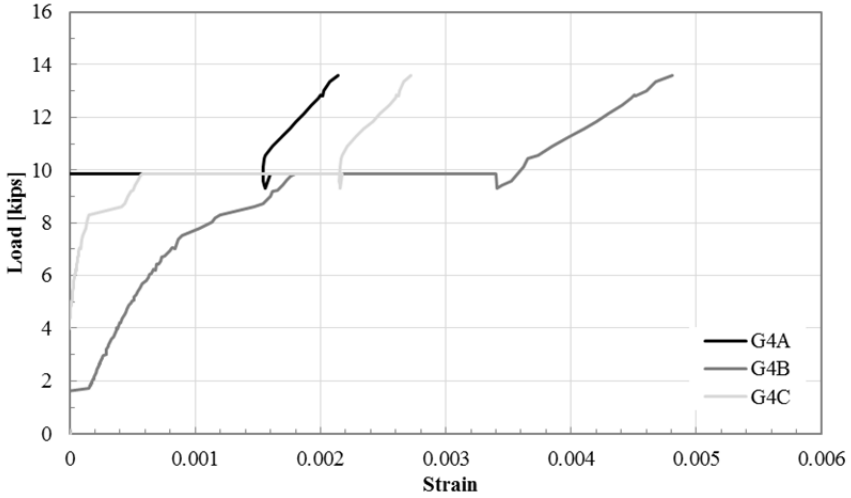

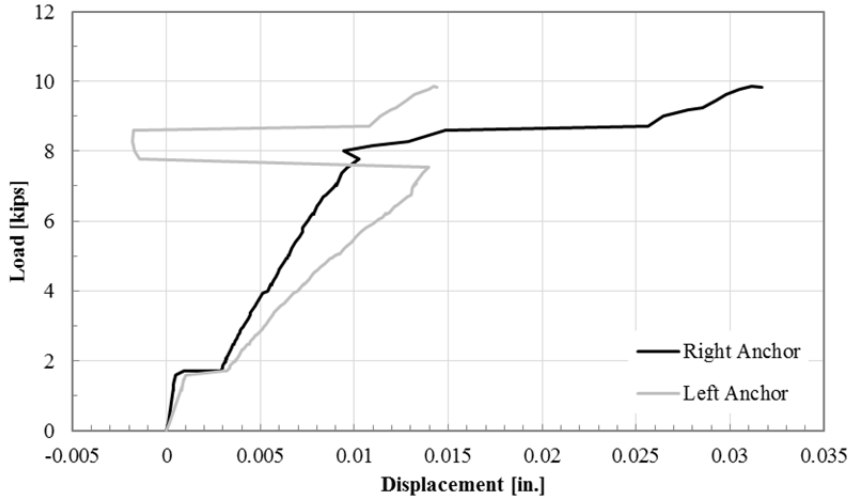

Specimen F1-4a-1-24U

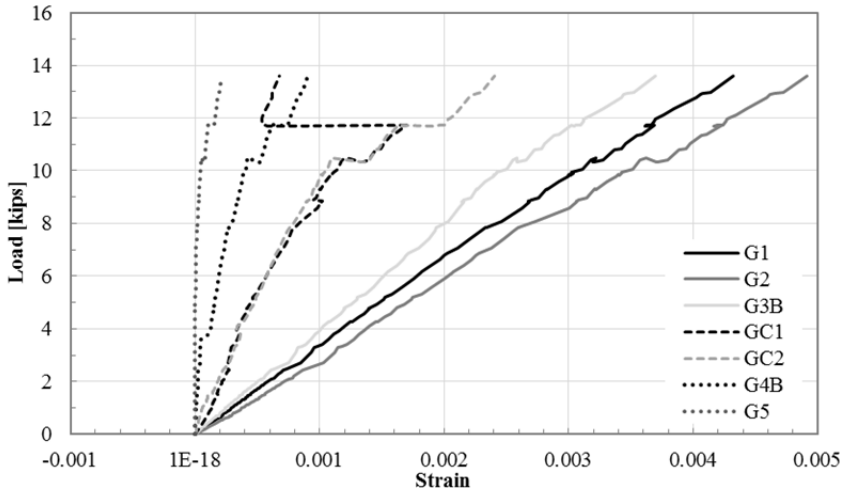

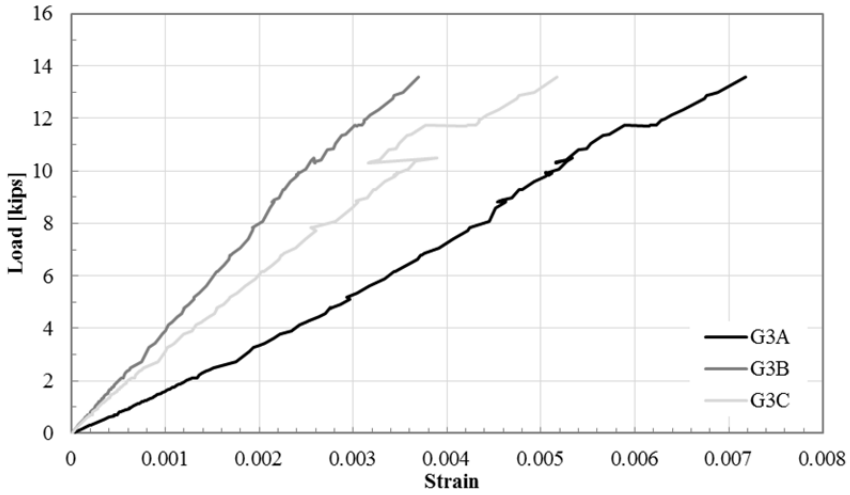

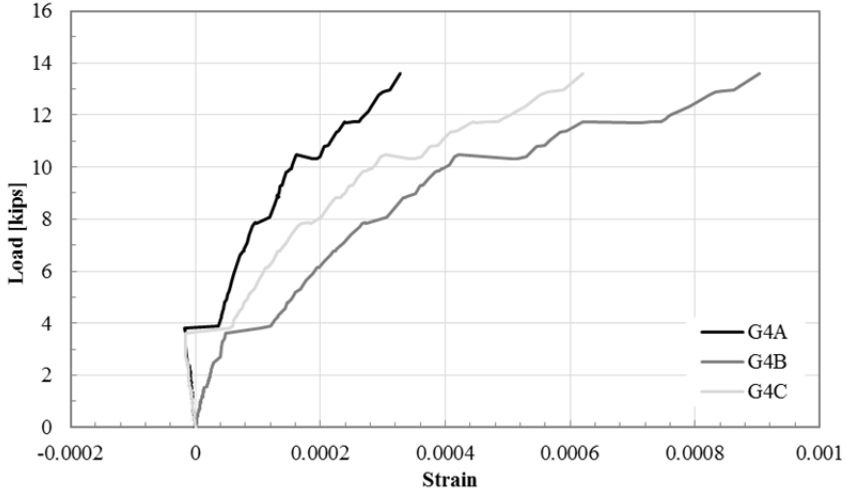

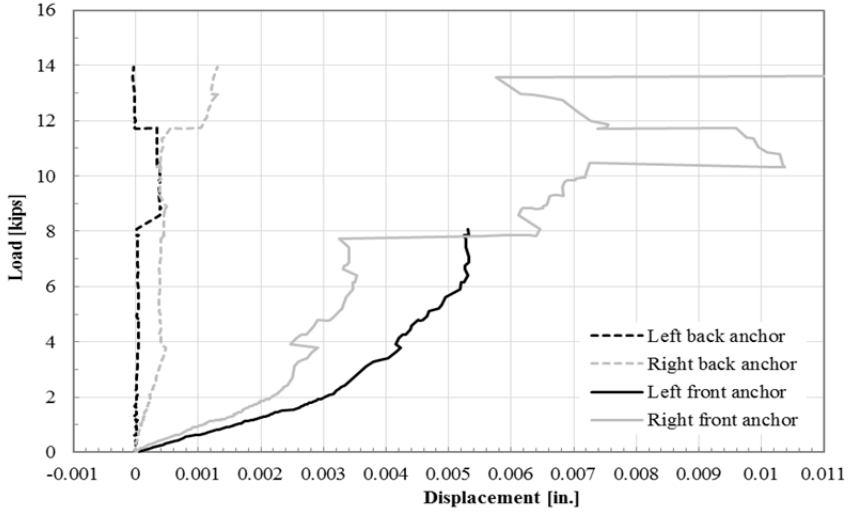

REFERENCES

ACI Committee 440 (2002). "Design and Construction of Externally Bonded FRP Systems for Strengthening Concrete Structures". ACI 440.2R-02, Farmington Hills, Michigan: American Concrete Institute.

Anil, Özgür and Belgin M., Çagåtay (2010). "Anchorages Effects on CFRP-to-concrete Bond Strength" *Journal of Reinforced Plastics and Composites*,

Antoniades et al., (2005). "Tests on Seismically Damaged Reinforced Concrete Walls Repaired and Strengthened Using Fiber-Reinforced Polymers." *Journal of Composites for Construction*, Vol. 9(3), pp. 236–246.

Aram, M. R, Christoph Czaderski and Masoud Motavalli (2008). "Debonding failure modes of flexural FRP-strengthened RC beams." *Composites: Part B,* Vol. 39, pp. 826–841.

Binici et al., (2007). "Analysis and design of FRP composites for seismic retrofit of infill walls in reinforced concrete frames*." Composites: Part B,* Vol. 38, pp. 575–583.

Ceroni, Francesca and Pecce, Marisa.(2009) "Performance of Anchorage System for Elements Strengthened with FRP Sheets." *9th International Symposium on Fiber Reinforced Polymer Reinforcement for Concrete Structures*.

Chen, J. F., and J. G. Teng (2001). "Anchorage Strength Models for FRP and Steel Plates Bonded to Concrete." *Journal of Structural Engineering,* Vol. 127(7), pp. 784-91.

Chen, J. F., Z. J. Yang, and G. D. Holt.(2001) "FRP Or Steel Plate-to-Concrete Bonded Joints: Effect of Test Methods on Experimental Bond Strength." *Steel and Composite Structures*, Vol. 1(2), pp. 231-44.

El Gawady et al., (2005). "In-Plane Seismic Response of URM Walls Upgraded with FRP." *Journal of Composites for Construction*, Nov-Dec., pp. 524-535.

El Maaddawy, Tamer and Soudki, Khaled (2008). "Strengthening of reinforced concrete slabs with mechanically-anchored unbonded FRP system." *Construction and Building Materials*, Vol. 22, pp. 444–455.

Eshwar, Nagaraj, et al.(2008) "Performance of Two Anchor Systems of Externally Bonded Fiber-Reinforced Polymer Laminates." *ACI Materials Journal*, January-February.

Huang, P.C, J.J Myers and A. Nanni (2000), "Dapped-End Strengthening in Precast Prestressed Concrete Double Tee Beams with FRP Composites," *Proc., 3rd Inter. Conf. on Advanced Composite Materials in Bridges and Structures*, Ottawa, Canada, J.Humar and A.G. Razaqpur, Editors, 15-18 Aug., pp. 545-552.

Khalifa, A., T. Alkhrdaji, A. Nanni, and S. Lansburg (1999), "Anchorage of Surface Mounted FRP Reinforcement," *Concrete International: Design and Construction*, Vol. 21(10), pp. 49-54.

Khalifa, Ahmed, and Antonio Nanni (2000). "Improving Shear Capacity of Existing RC TSection Beams using CFRP Composites." *Cement and Concrete Composites,* V.22(3), pp. 165-74.

Kim, I. S. (2006), "Use of CFRP to Provide Continuity in Existing Reinforced Concrete Members Subjected to Extreme Loads," Ph.d Dissertation, University of Texas at Austin, USA, 478 pp.

Kim, S.J., and Smith, S.T. (2009). "Shear Strength and Behavior of FRP Spike Anchors in Cracked Concrete." *9th International Symposium on Fiber Reinforced Polymer Reinforcement for Concrete Structures*, July.

Lu, X. Z., et al. (2005) "Bond-Slip Models for FRP sheets/plates Bonded to Concrete." *Engineering Structures*, Vol. 27, pp. 920-37.

Niemitz, Carl W. (2008). "Anchorage of Carbon Fiber Reinforced Polymers to Reinforced Concrete in Shear Applications." M.S. Report, University of Massachusetts Amherst, USA.

Orton, Sarah L. (2008) "Design Considerations of Carbon Fiber Anchors." *Journal of Composites for Construction*, Nov-Dec, pp. 608-616.

Salom, P. R., Janos Gergely and David T. Young (2004). "Torsional Strengthening of Spandrel Beams with Fiber-Reinforced Polymer Laminates." *Journal of Composites for Construction*, March-Apr., pp. 157-162.

Smith, ST, et al. (2011) "FRP-Strengthened RC slabs anchored with FRP anchors." *Engineering Structures*, doi: 10.1016/j.engstruct.2010.11.018.

Smith, ST and J.G. Teng. (2002) "FRP-strengthened RC beams. I: review of debonding strength models." *Engineering Structures*, Vol. 24, pp. 385–395.

Subramaniam, Kolluru V., Christian Carloni, and Lucio Nobile (2007). "Width Effect in the Interface Fracture during Shear Debonding of FRP Sheets from Concrete." *Engineering Fracture Mechanics*, Vol. 74(4), pp. 578-94.

Tan, Kiang Hwee (2002). "Strength Enhancement of Rectangular Reinforced Concrete Columns using Fiber-Reinforced Polymer." *Journal of Composites for Construction*, pp. 175-183.

Teng, J. G. (2002), *FRP-Strengthened RC Structures*. New York: Wiley, 2002.

Teng, J. G.; Lu, X. Z.; Ye, L. P.; and Jiang, J. J. (2004), "Recent Research on Intermediate Crack Induced Debonding in FRP Strengthened Beams," *Proceedings of the 4th International Conference on Advanced Composite Materials for Bridges and Structures*, Calgary, AB, Canada.

Teng, J. G.; Smith, S. T.; Yao, J.; and Chen, J. F.(2001), "Intermediate Crack Induced Debonding in RC Beams and Slabs." *Construction and Building Materials*, Vol. 17(6-7), pp. 447-462.

Yao, J, J.G. Teng and J.F. Chen (2005). "Experimental study on FRP-to-concrete bonded joints." *Composites: Part B,* Vol. 36, pp. 99–113.